

Semi-Analytical Solution to Buckling of Variable-Stiffness Composite Panels

Plates and Shallow Cylindrical Shells

Jinghua Tang

Master of Science Thesis

Semi-Analytical Solution to Buckling of Variable-Stiffness Composite Panels

Plates and Shallow Cylindrical Shells

MASTER OF SCIENCE THESIS

For the degree of Master of Science in Aerospace Structures at Delft
University of Technology

Jinghua Tang

May 12, 2015

DELFT UNIVERSITY OF TECHNOLOGY
DEPARTMENT OF
AEROSPACE STRUCTURES & COMPUTATIONAL MECHANICS

The undersigned hereby certify that they have read and recommend to the Faculty of
Aerospace Engineering for acceptance a thesis entitled

SEMI-ANALYTICAL SOLUTION TO BUCKLING OF VARIABLE-STIFFNESS COMPOSITE
PANELS

by

JINGHUA TANG

in partial fulfillment of the requirements for the degree of
MASTER OF SCIENCE AEROSPACE STRUCTURES

Dated: May 12, 2015

Supervisor:

Dr. ir. Roeland De Breuker, supervisor

Committee members:

Dr. Mostafa M. Abdalla, committee chair

Dr.ir. René C. Alderliesten, committee member

Dr. Juriij Sodja, supervisor

ir. Noud P.M. Werter, supervisor

Acknowledgements

Foremost, I would like to express my deepest thanks to my supervisor, Dr.ir. Roeland De Breuker, for offering this challenging but interesting topic to me and his continuous support throughout the research. I still remember I had spent nearly three month on selecting a challenging thesis topic until I met Roeland. Now I would say I would never regret immersing myself in the thesis for over ten months.

Secondly, I would like to thank my second and third supervisors, Dr. Jurij Sodja and ir. Noud.P.M.Werter for their expert guidance on the research and writing of this thesis. Their patience, encouragement, and immense knowledge became important motivations for my master study. I have learnt from them vital skills of critical thinking and English writing. Their work of constructive and detailed revision of my technical writing was invaluable and will benefit my writing style all my life. I cannot think of better supervisors to have.

Besides my supervisors, I wish to thank Prof.dr. Chiara Bisagni and Dr. Mostafa Abdalla. I started the thesis from reading Prof. Bisagni's papers. I still remember she replied us an email with detail explanations and examples regarding to the questions on her papers. It was her brilliant works inspired my initial ideals of the thesis. At the end of the thesis, I encountered several serious problems related to the foundational theory of buckling and numerical computational problems. It was Dr. Abdalla who always solved my problems precisely and patiently. His immense knowledge became important motivations for my further study and work.

Finally, I would like to thank all teachers and friends in the department of Aerospace Structures and Materials, TU Delft. Special thanks to Dr.ir. René.C. Alderliesten, ir. Jan Hol, Wang Zhengpei, Wang Dan, Liang Ke, Zheng Weilin, Guo Yujie, Hong Zhi, Wang Yang, Etana, Mario, Laurence, Laura and Miranda for their practical help.

Delft, University of Technology
May 12, 2015

Jinghua Tang

Abstract

Variable-stiffness panels have previously shown enhanced buckling performance compared to constant-stiffness panels, due to the beneficial load and stiffness redistribution. Two semi-analytical models based on the Galerkin method and the Ritz method have been developed in order to solve the buckling problem of variable-stiffness composite panels (plates and shallow cylindrical shells).

The laminates considered are assumed to be symmetric, which results in zero extension-bending couplings. However, the bending-twisting couplings, D_{16} and D_{26} , are retained in the model due to their dramatic influence on the convergence of the predicted buckling loads.

In the first model the governing equations for composite plates and shallow cylindrical shells with variable stiffness are derived and then solved using the Galerkin method. The variable stiffness in this model is approximated using two-dimensional Fourier series, which, however, appears to be less accurate and less efficient as compared to the Ritz method.

The Ritz method avoids using Fourier series to approximate the stiffness. Instead, the stiffness is exactly expressed in the integral of the energy functional. The detailed derivations of the energy functional which were rarely shown in literature have been presented. The buckling analysis of this model comprises two main steps. First, the in-plane loads are calculated by applying the principle of minimum complementary energy in pre-buckling state. Second, the critical buckling loads are determined from the stability equations which are obtained from the total energy functional through applying either adjacent equilibrium criterion or the principle of minimum potential energy. The total energy functional for stability analysis in this model is expressed in terms of out-of-plane displacement and the Airy stress function, which appears to be a combination of negative membrane complementary energy, bending strain energy and external work.

In order to ensure fast convergence, several shape functions used in Ritz method were investigated. The in-plane loads were approximated either using the beam characteristic function or polynomial function that were orthogonalized by the Gram-Schmidt process. In addition, the predictions of in-plane loads using sine and cosine function that do not satisfy the boundary conditions of in-plane loads were significantly improved by using Lagrange multiplier method. The out-of-plane displacement was approximated using either sine function or

orthogonalized polynomials. The influence of the shape functions on the convergence of the predicted buckling load was analysed and discussed for different examples. These examples included plates and shells with either constant-stiffness or variable stiffness, within which D_{16} and D_{26} were either zero or non-zero. The boundary conditions considered for these examples were four-edge simply-supported in current thesis. However, the developed model can be easily extended to consider other boundary conditions.

The model can solve the buckling problem of variable-stiffness panels under prescribed in-plane loads $(\bar{N}_x, \bar{N}_y, \bar{N}_{xy})$ or prescribed in-plane displacements (\bar{u}, \bar{v}) . In the current thesis, only the prescribed loads \bar{N}_x, \bar{N}_{xy} and the prescribed end-shortenings \bar{u} have been investigated and compared to Abaqus model; all the results satisfactorily match the results of Abaqus models.

In addition, the model have been proved to be able to predict the buckling loads of shallow cylindrical shells with variable curvatures.

Table of Contents

Acknowledgements	i
1 Introduction	1
1.1 Background and Motivation	1
1.2 Research Question and Objective	2
1.3 Thesis Outline	2
2 Literature Review	3
2.1 Basic Stability Theory	3
2.2 Buckling of Plates	5
2.2.1 Isotropic Plates	5
2.2.2 Composite Plate	6
2.3 Buckling of Shells	8
2.3.1 Isotropic Shells	8
2.3.2 Composite Shells	10
2.4 Various Boundary conditions and loads	12
2.5 Panels with Spatially Varying Stiffness	12
2.6 Conclusions	13
3 Governing Equations and Galerkin Method	15
3.1 Introduction	15
3.1.1 Plate	15
3.1.2 Shallow Cylindrical Shell	15
3.1.3 Assumptions	16
3.1.4 Classical Laminate Theory	17
3.2 Governing Equations for Plate	20
3.2.1 Equations for Prebuckling Analysis	20

3.2.2	Equations for Stability Analysis	21
3.2.3	Comparison with previous work	25
3.3	Governing Equations for Shallow Cylindrical Shell	26
3.3.1	Equations for Prebuckling Analysis	26
3.3.2	Equations for Stability Analysis	27
3.4	Galerkin method	30
3.4.1	Prebuckling Analysis	31
3.4.2	Stability Analysis	32
3.4.3	Approximation of Stiffness	34
3.4.4	Boundary Integral	35
3.5	Summary	37
4	Ritz Method	39
4.1	Introduction	39
4.2	Strain Energy in Bending and Stretching of Laminated Panels	40
4.3	Total Energy Functional for Prebuckling Analysis	41
4.3.1	Prescribed Loads and Displacements	42
4.3.2	Prescribed Loads	44
4.3.3	Prescribed Displacements	44
4.4	Total Energy Functional for Stability Analysis	45
4.4.1	Prescribed Loads and Displacements	46
4.4.2	Prescribed Loads	51
4.4.3	Prescribed Displacements	52
4.5	Plates	52
4.5.1	Prescribed Loads	52
4.5.2	Prescribed Displacements	56
4.6	Shallow Cylindrical Shells	59
4.6.1	Prescribed Loads	59
4.6.2	Prescribed Displacement	67
4.7	Summary	68
5	Prebuckling Analysis: in-plane loads distribution	71
5.1	Introduction	71
5.1.1	Material Property	71
5.1.2	Model	72
5.1.3	Verification	72
5.2	Prescribed Compression (\bar{N}_x)	73
5.2.1	Boundary Condition	73
5.2.2	Sine Function	74
5.2.3	Beam Characteristic Function	76
5.2.4	Polynomial Function	86

5.2.5	Sine Function with Lagrange Multiplier	91
5.2.6	Cosine Function with Lagrange Multiplier	95
5.3	Prescribed Shear (\bar{N}_{xy})	100
5.3.1	Pure Shear	100
5.3.2	Shear and Compression	101
5.4	Prescribed Displacement	103
5.4.1	Boundary Condition	103
5.4.2	Shape function	104
5.4.3	Verification	106
5.5	Summary	108
6	Stability Analysis	109
6.1	Introduction	109
6.1.1	Boundary Condition	109
6.1.2	Curvature	111
6.2	Stability Analysis: prescribed compression	112
6.2.1	Buckling of Specially Orthotropic Laminate ($D_{16} = D_{26} = 0$)	114
6.2.2	Buckling of General Symmetric Laminate ($D_{16}, D_{26} \neq 0$)	129
6.2.3	Buckling of Shallow Cylindrical Shells with Variable Curvature	138
6.3	Stability Analysis: prescribed shear	140
6.3.1	Pure Shear	140
6.3.2	Shear and Compression	142
6.4	Stability Analysis: prescribed displacement	145
6.4.1	Verification	146
6.5	Summary	150
7	Conclusion and Recommendation	153
7.1	Thesis Review and Conclusion	153
7.2	Recommendation	154
A	Total Potential Energy for Prebuckling Analysis	157
	Bibliography	163
	Glossary	167
	List of Acronyms	167
	List of Symbols	167

List of Figures

2.1 Buckling loads of Simply-Supported Plates (picture from literature [2])	7
2.2 Values of α_i and γ_i in Zhang's Paper [12]	11
3.1 Coordinate and dimensions of rectangular plate	16
3.2 Cylindrical shell displacements and forces (picture form Yoo and Lee [6])	16
3.3 Variable Stiffness: sections	34
3.4 Approximation of D_{11} of plate with 4 sections	35
4.1 Boundary of of a free body	42
5.1 Mesh Density (25×25 per section)	72
5.2 Layup 1	75
5.3 In-plane stress of Layup 1 (Mpa, $K=L=10$, $\bar{N}_x = 1$ N/mm)	75
5.4 In-plane Stress of Layup 1 (Mpa, $K=L=10$, $\bar{N}_x = 1$ N/mm)	79
5.5 In-plane Stress of Layup 1 (Mpa, $K=L=18$, $\bar{N}_x = 1$ N/mm)	80
5.6 In-plane Stress of Layup 1 (Mpa, $K=L=50$, $\bar{N}_x = 1$ N/mm)	80
5.7 Layup 2	81
5.8 In-plane Stress of Layup 2 (Mpa, $K=L=18$, $\bar{N}_x = 1$ N/mm)	81
5.9 Layup 3	82
5.10 In-plane Stress of Layup 3 (Mpa, $K=L=18$, $\bar{N}_x = 1$ N/mm)	82
5.11 Plot of X_k with Numerical Error as Increasing k ($\frac{x}{a} = 0 \dots 1$)	84
5.12 Plot of X_k as Increasing k ($\frac{x}{a} = 0 \dots 1$)	85
5.13 Numerical Error of In-plane Stress of Beam Characteristic Function (Mpa, $K=L=18$)	86
5.14 In-plane Stress of Layup 1 (Mpa, $K=L=18$, $\bar{N}_x = 1$ N/mm)	89

5.15 In-plane Stress of Layup 2 (Mpa, K=L=18, $\bar{N}_x = 1$ N/mm)	90
5.16 In-plane Stress of Layup 3 (Mpa, K=L=18, $\bar{N}_x = 1$ N/mm)	91
5.17 In-plane Stress of Layup 1 (Mpa, K=L=18, $\bar{N}_x = 1$ N/mm)	94
5.18 In-plane Stress of Layup 2 (Mpa, K=L=18, $\bar{N}_x = 1$ N/mm)	95
5.19 In-plane Stress of Layup 1 (Mpa, K=L=18, $\bar{N}_x = 1$ N/mm)	97
5.20 In-plane Stress of Layup 2 (Mpa, K=L=18, $\bar{N}_x = 1$ N/mm)	98
5.21 In-plane Stress of Layup 3 (Mpa, K=L=18, $\bar{N}_x = 1$ N/mm)	99
5.22 In-plane Stress of Layup 1 (Mpa, K=L=18, $\bar{N}_{xy} = 1$ N/mm)	100
5.23 In-plane Stress of Layup 2 (Mpa, K=L=18, $\bar{N}_{xy} = 1$ N/mm)	101
5.24 In-plane Stress of Layup 3 (Mpa, K=L=18, $\bar{N}_{xy} = 1$ N/mm)	102
5.25 In-plane Stress of Layup 1 (Mpa, K=L=18, $\bar{N}_x = \bar{N}_{xy} = 1$ N/mm)	102
5.26 In-plane Stress of Layup 2 (Mpa, K=L=18, $\bar{N}_x = \bar{N}_{xy} = 1$ N/mm)	103
5.27 In-plane Stress of Layup 1 (Mpa, K=L=18, $\Delta u_1 = 0.001$ mm, $\Delta u_2 = 0.001$ mm)	106
5.28 In-plane Stress of Layup 2 (Mpa, K=L=18, $\Delta u_1 = 0.001$ mm, $\Delta u_2 = 0.001$ mm)	107
5.29 In-plane Stress of Layup 3 (Mpa, K=L=18, $\Delta u_1 = 0.001$ mm, $\Delta u_2 = 0.001$ mm)	107
6.1 NACA 0012	111
6.2 Non-dimensional radius of NACA 0012	112
6.3 First Buckling Mode of Layup 4	118
6.4 Convergene study of Layup 4 in FEM	119
6.5 Buckling Load as incresing K_1 and L_1	120
6.6 Layup 7	121
6.7 First Buckling Mode of Layup 1	122
6.8 First Buckling Mode of Layup 7	123
6.9 Convergene study of Layup 4 in FEM	124
6.10 convergence of the buckling load (Layup 1)	125
6.11 Bending moment equilibrium on the boundary of sections	126
6.12 Plot of F_{kl} (Layup 1)	127
6.13 Comparasion of in-plane stresses of layup 1 before and after truncation (Mpa, K=L=18, $\bar{N}_x = 1$ N/mm)	128
6.14 First Buckling Mode of Layup 8	131
6.15 Layup 10	133
6.16 First Buckling Mode of Layup 2	134
6.17 First Buckling Mode of Layup 10	135
6.18 Layup 11	136
6.19 First Buckling Mode of Layup 3	137
6.20 First Buckling Mode of Layup 11	138

6.21 Shell with two different radii	138
6.22 First buckling mode of shells with variable curvature	140
6.23 First buckling mode of plates under shear	142
6.24 First buckling mode of shells under shear	143
6.25 First buckling mode of plates under shear and compression	144
6.26 First buckling mode of shells under shear and compression	145
6.27 First buckling mode of plates with constant stiffness (prescribed displacement)	147
6.28 First buckling mode of shells with constant stiffness (prescribed displacement)	147
6.29 First buckling mode of plates with variable stiffness (prescribed displacement)	150
6.30 First buckling mode of shells with variable stiffness (prescribed displacement)	151

List of Tables

5.1	Material Property of AS4/3501-6 graphite epoxy laminate obtained from literature [35]	71
5.2	The value of r_k and $r_k - 1$	83
6.1	Buckling load of Layup 4	116
6.2	Buckling load of Layup 5	117
6.3	Buckling load of Layup 6	117
6.4	Buckling Load of Layup 1	121
6.5	Buckling Load of Layup 7	122
6.6	Buckling load of Layup 1 after truncating the negligible parameters	128
6.7	Buckling load of Layup 7 after truncating the negligible parameters	129
6.8	Buckling load of Layup 8	130
6.9	Buckling load of Layup 9	131
6.10	Buckling Load of Layup 2	133
6.11	Buckling Load of Layup 10	133
6.12	Buckling load of Layup 2 after truncating the negligible parameters	135
6.13	Buckling load of Layup 10 after truncating the negligible parameters	136
6.14	Buckling Load of Layup 3	137
6.15	Buckling Load of Layup 11	137
6.16	Buckling load of shells with variable curvatures	139
6.17	Buckling load of plates under shear	141
6.18	Buckling load of shells under shear	141
6.19	Buckling load of plates under shear and compression	143
6.20	Buckling load of shells under shear and compression	144
6.21	Buckling factors of plates with constant stiffness (prescribed displacement)	146
6.22	Buckling factors of shells with constant stiffness (prescribed displacement)	146
6.23	Buckling factors of plates with variable stiffness (prescribed displacement)	149
6.24	Buckling factors of shells with variable stiffness (prescribed displacement)	149

Chapter 1

Introduction

1.1 Background and Motivation

Nowadays, composite material has been widely applied in aerospace industry due to its high strength-to-mass and stiffness-to-mass ratio. Especially the composite wing has drawn more and more research interests in the recently years. Since a composite wing box is comprised of thin-walled panels (plates and shallow cylindrical shells), buckling is considered to be one of the main failure constraints. Therefore, buckling is one of the most significant design criteria during wing box optimization and tailoring, which is the main research interest of the current thesis.

The research into buckling of plates and shells can date back to a hundred year ago [1]. Various buckling (or stability) theories have been introduced throughout these years. However, closed form analytical solutions to the buckling of composite plates and shells are limited to those with specially orthotropic layups exhibiting no membrane-bending and bending-twisting couplings [2–4]. However, most laminated panels encountered in practice do not fulfil the conditions. Therefore, closed form solutions are not available for most general mid-plane symmetric composite panels (to the best knowledge of the author).

Furthermore, composite panels with spatially varying stiffness have been a recently innovative topic. The variable stiffness is achieved by the steering of the fiber direction or tapering of the laminate thickness, resulting in beneficial load and stiffness distribution that improves the buckling resistance of laminated panels. For such kind of laminated panels, closed form analytical solutions to the buckling problems were barely introduced by previous researchers.

Therefore, the aim of the work reported in this thesis is to develop a semi-analytical method to predict the buckling load of variable-stiffness composite panels with general midplane symmetric layups. The model developed will provide engineers an efficient tool for the preliminary design of composite wing box. However, only a limited amount of research on the buckling of variable-stiffness composite plates (even less research on buckling of various-stiffness composite shells) which exhibit bending-twisting couplings using semi-analytical methods was done in the past. It is just this reason why this project is so promising and challenging.

1.2 Research Question and Objective

The key research questions addressed in this topic are:

- Is any closed form solution available? If not, what is the difference between the work in this thesis and the work done by previous researchers?
- If no closed form analytical solution is available, what semi-analytical methods can be used to predict the buckling load of this kind of panels?
- What is the accuracy of the developed semi-analytical method compared to the numerical solutions (for example, Abaqus)

To answer the research questions, the following steps were proposed.

- A literature review about the theory of buckling and the previous works.
- Derive and solve the governing equations for composite panels with variable stiffness
- Find a semi-analytical method and derive the corresponding equations
- Compare the accuracy of results from the semi-analytical solution with the results from numerical solution.

1.3 Thesis Outline

There are seven chapters in this thesis. A brief literature review is presented in Chapter 2, where the basic stability theory is reviewed as well as the previous works done by other researchers. The main part of the thesis starts from Chapter 3 to Chapter 6. In chapter 3, the basic assumptions are made and governing equations are derived. Then the Galerkin method is applied to solve the governing equations, which, however, appears to be not efficient. Then in Chapter 4, Ritz method is introduced. The total energy functionals are derived, and the equations equivalent to the governing equations in Chapter 3 are obtained using Ritz method. In chapter 5, the in-plane loads distributions in the prebuckling state are predicted using the equations derived in Chapter 4 and compared to the predictions of Abaqus. In Chapter 6, the buckling loads are predicted using the stability equations derived in Chapter 4 and in-plane loads obtained in prebuckling state (Chapter 5), and then compared to the prediction of Abaqus. Finally, conclusions and recommendations for future work are given in Chapter 7.

Chapter 2

Literature Review

This review covers fundamental buckling theories of isotropic and laminated composite plates and shells, and their corresponding differences and similarities. Recently published papers dealing with buckling problems of variable-stiffness panels and panels under various boundary conditions or various load conditions are also reviewed.

2.1 Basic Stability Theory

As indicated by Jones [5], buckling load is the load at which the current equilibrium state of a system suddenly changes from stable to unstable. The equilibrium state of a system is called stable if any 'small' disturbance of the system results only in a 'small' response and after which the system always returns to its original equilibrium state. While, the equilibrium state is called unstable if any 'small' disturbance results in a sudden change in deformation mode or displacement value after which the system cannot return to its original equilibrium state. From energy point of view [1, 5], the system is called stable at its equilibrium state when its potential energy is relatively minimum; it is called unstable (or neutral) when its potential energy ceases to be relatively minimum. The transition from stable to unstable (or neutral) is the main interest of the study of stability.

Jones [5] investigated buckling of isotropic, multiple fiber-reinforced layered plates and shells using the approach of variation of the potential energy. Starting from the total potential energy, the equilibrium equations, the stability equations and their corresponding boundary conditions can be derived using calculus of variations.

The total potential energy can be varied, or expanded in a Taylor's series, about an equilibrium state, as stated in Jones's book [5]:

$$V + \Delta V = V + \delta V + \frac{1}{2!}\delta^2 V + \frac{1}{3!}\delta^3 V + \dots \quad (2.1)$$

where, V is the total potential energy.

The equilibrium state is derived from the first variation of the potential energy, which is also known as the principle of stationary potential energy [5]:

$$\delta V = 0 \quad (2.2)$$

The stability of the equilibrium state is derived from the variation of the equilibrium state (or second variation of the total potential energy at the equilibrium state), also known as the principle of minimum potential energy [5]:

$$\bar{\delta}^2 V = \delta^2 V \Big|_{\delta V=0} > 0 \quad (2.3)$$

Since the potential energy is relatively minimum when the system is stable, every 'small' disturbance to the system will result in increasing the potential energy. Thus, if $\bar{\delta}^2 V$ is positive ($\delta V = 0$), the system is always stable. (However, when $\bar{\delta}^2 V = 0$, the stability should be determined by the rest terms. The reader is referred to the literature for more details [1,5].)

An alternative buckling criterion is based on the Trefftz buckling criterion, which is to make $\bar{\delta}^2 V$ stationary [1, 5, 6],

$$\delta(\bar{\delta}^2 V) = 0 \quad (2.4)$$

The Trefftz buckling criterion is derived from the principle of minimum potential energy as follows. According to the principle of minimum potential energy, when the applied load, for example P , is smaller than the critical buckling load $P_{critical}$, the potential energy is relative minimum because the system is stable. So all possible disturbances to the system will result in increase of the total potential energy, thus $\bar{\delta}^2 V > 0$ for all possible disturbances. When $P > P_{critical}$, the system is unstable. There exists at least one disturbance which results in decrease of the total potential energy, thus $\bar{\delta}^2 V < 0$ for that disturbance. As P increasing from zero to $P_{critical}$, only at $P = P_{critical}$ is it the first time there existing at least one disturbance which makes $\bar{\delta}^2 V = 0$. While, all other disturbances at $P = P_{critical}$ still make $\bar{\delta}^2 V > 0$. And all loads lower than $P_{critical}$ make $\bar{\delta}^2 V > 0$. So $\bar{\delta}^2 V = 0$ is a relative minimum for all disturbances at $P = P_{critical}$ and for all loads lower than or equal to $P_{critical}$. Therefore, $\delta(\bar{\delta}^2 V) = 0$ at $P = P_{critical}$.

Brush and Almroth [1] applied the adjacent-equilibrium approach to obtain the stability equations from the equilibrium equations. The equilibrium equations governing the equilibrium path are perturbed by small arbitrary and tentative increments of displacements. Let u_1, v_1, w_1 be the increments of displacements and u_0, v_0, w_0 the displacements in the primary equilibrium path, then the displacements in the equilibrium equations will be replaced by:

$$\begin{aligned} u_0 &\rightarrow u_0 + u_1 \\ v_0 &\rightarrow v_0 + v_1 \\ w_0 &\rightarrow w_0 + w_1 \end{aligned} \quad (2.5)$$

where, $u_0 + u_1$, $v_0 + v_1$ and $w_0 + w_1$ represent the possible adjacent equilibrium path (or secondary equilibrium path).

Substituting above displacements into the equilibrium equations and ignoring the higher order terms and subtracting the equilibrium equations written in u_0, v_0, w_0 , the buckling differential equations are obtained.

According to Ashton and Whitney [2], usually the second variation of total potential energy has not been explicitly considered when determining the buckling load. Instead, the onset of instability is determined by the existence of an equilibrium state with non-zero out-of-plate displacement. In other words, the stability is determined from the equilibrium equations by assuming a non-zero function for the displacement. This criterion has simplified the solutions to buckling problems. Jones [5] used variational principle to derive the stability differential equations from the second variation of total potential energy, which usually leads to lengthy derivations. With Ashton and Whitney's theory [2], the buckling load can be determined simply from the equilibrium equations by assuming proper buckling shapes function for the displacements. This approach was used in some literature when dealing with the buckling problems of plates and beams [2, 3, 7]. Moreover, this method makes the Ritz method, which determines the equilibrium state from minimizing total potential energy with respect to the undetermined parameters of the out-of-plane displacement, a practical and simplified way to solve the buckling problem for a complicated structure [2–4, 8–11]. However, this criterion has only been applied to linear system, such as beams and plates, in the literature [2, 3, 7].

2.2 Buckling of Plates

2.2.1 Isotropic Plates

According to Jones [5], the equilibrium equations of plates are derived from the first variation of the potential energy; the stability equations are derived from the second variation of the potential energy. Thus, the equilibrium and stability equations have fundamental differences. However, the equilibrium equations and stability equations of plates are similar to each other. For example, the out-of-plane equilibrium and stability differential equations are shown below, respectively.

$$D\nabla^4(w) - N_x w_{,xx} - N_y w_{,yy} - 2N_{xy} w_{,xy} = 0 \quad (2.6)$$

$$D\nabla^4(\delta w) - \bar{N}_x \delta w_{,xx} - \bar{N}_y \delta w_{,yy} - 2\bar{N}_{xy} \delta w_{,xy} = 0 \quad (2.7)$$

where, δw is the variation of w ; D is the bending stiffness for isotropic plates; ∇ is the Laplace operator in Cartesian coordinate; N_x, N_y, N_{xy} are the in-plane loads; $\bar{N}_x, \bar{N}_y, \bar{N}_{xy}$ are the in-plane loads applied on the edges of plates.

Jones [5] indicated that many authors are so overwhelmed by the similarity of these two equations that they overlook the essential differences of form and origin of the various terms, and state that they obtained the buckling equation from the equilibrium equation. Moreover, buckling is an eigenvalue problem and equilibrium is a boundary-value problem, which are the essential difference of the equilibrium and buckling equations. However, Ashton and Whitney [2] introduced a simplified theory where the onset of instability (or buckling) is determined by the existence of an equilibrium state with non-zero out-of-plate displacement, as mentioned in section 2.1.

The second interesting observation in Jones [5] refers to the potential energy. The second variation of the strain energy for a plate with a flat prebuckling shape is:

$$\bar{\delta}^2 V = \bar{\delta}^2 U_{m1} + \bar{\delta}^2 U_{m2} + \bar{\delta}^2 U_b \quad (2.8)$$

in which

$$\bar{\delta}^2 U_{m1} = A \iint [\delta u_x^2 + \delta v_y^2 + 2v\delta u_x \delta v_y + \frac{1}{2}(1-v)(\delta u_y + \delta v_x)^2] dx dy \quad (2.9)$$

$$\bar{\delta}^2 U_{m2} = - \iint [\bar{N}_x \delta w_x^2 + \bar{N}_y \delta w_y^2 + 2\bar{N}_{xy} \delta w_x \delta w_y] dx dy \quad (2.10)$$

$$\bar{\delta}^2 U_b = D \iint [\delta w_{xx}^2 + \delta w_{yy}^2 + 2(1-\nu)\delta w_{xy}^2] dx dy \quad (2.11)$$

where, A is the membrane stiffness; U_{m1} and U_{m2} are the membrane strain energies; ν is the Poisson's ratio for isotropic material; δu , δv and δw are the variations of u , v and w .

Because δu and δv are independent of δw , the equation 2.8 can be decoupled into two equations:

$$\bar{\delta}^2 U_{m1} = 0 \quad (2.12)$$

$$\bar{\delta}^2 U_{m2} + \bar{\delta}^2 U_b = 0 \quad (2.13)$$

These two decoupled equations are of significant importance since they indicate that the in-plane equation and the out-of-plane equation are essentially independent for plates (before buckling).

Another interesting statement by Jones is that the equation 2.9 is clearly derived from the strain energy and not from the potential energy of external forces *as so many authors erroneously state* [5]. Indeed, the equation 2.9 has the same expression as the potential energy of external work in other references [2, 7]. The reason for the similarity is that Jones [5] used the moderately large-deflection theory to derive the strain energy. For instance, the strain in x direction is expressed as :

$$\epsilon_x = u_{,x} + \frac{1}{2}w_{,x}^2 \quad (2.14)$$

where, ϵ_x is the strain in x direction.

The nonlinear term ($\frac{1}{2}w_{,x}^2$) in above equation led to the equation 2.9 in Jones' book. However, in other references [2, 7] the nonlinear term is not included in the strain, but considered in the derivation of the energy done by the external work. Therefore, Jones considered it as the second membrane energy due to the nonlinear term of moderately large-deflection; while, other researchers considered it as the external work done by the applied loads during buckling due to the same nonlinear term.

2.2.2 Composite Plate

Two kinds of laminated composite plates are of the main interests in this review, namely the specially orthotropic laminated plate and the general mid-plane symmetric laminated plate. The difference is that the bending-twisting couplings D_{16} and D_{26} are zero in the specially orthotropic laminated plates. The stability of specially orthotropic laminated plates under simply-support boundary condition has been analytically solved in closed form [2, 3, 5, 7]. However, closed form solution has not been presented in most literature for laminated plates with bending-twisting couplings.

One of the reasons are the natural boundary conditions for a four-edge simply-supported plate cannot be satisfied by any assumed function. As indicated in reference [3,5], the essential (geometry) and natural (moment) boundary conditions are

$$w = 0, M_x = -D_{11}w_{,xx} - D_{12}w_{,yy} - 2D_{16}w_{,xy} = 0 \quad (\text{on } x=0,a) \quad (2.15)$$

$$w = 0, M_y = -D_{12}w_{,xx} - D_{22}w_{,yy} - 2D_{26}w_{,xy} = 0 \quad (\text{on } y=0,b) \quad (2.16)$$

Normally, for simply-supported plates with specially orthotropic lamination, the out-of-plane displacement can be assumed as

$$w = \sum_m^M \sum_n^N \sin\left(\frac{m\pi x}{a}\right) \cos\left(\frac{n\pi y}{b}\right) \quad (2.17)$$

Obviously, this shape function does not satisfy the moment boundary conditions in equation 2.15 and 2.16.

The direct solution to this problem is to find an alternative set of series which can exactly satisfy the moment boundary condition. However, no such series are known. Ashton and Whitney [2] introduced additional terms to correct the unsatisfied natural boundary conditions in the solution of Galerkin method, in conjunction with a series which satisfies the essential boundary conditions. This series can take the form of equation 2.17, and the additional terms take the form of:

$$-\int_0^a 2D_{26}\left[\left(\frac{\partial^2 w}{\partial x \partial y}\right)_{y=b} - \left(\frac{\partial^2 w}{\partial x \partial y}\right)_{y=0}\right] \frac{l\pi}{b} \sin \frac{k\pi x}{a} dx - \int_0^b 2D_{16}\left[\left(\frac{\partial^2 w}{\partial x \partial y}\right)_{x=a} - \left(\frac{\partial^2 w}{\partial x \partial y}\right)_{x=0}\right] \frac{k\pi}{a} \sin \frac{l\pi y}{b} dy \quad (2.18)$$

The improvement of this additional term is clearly shown in this figure, where the lower solid curve corresponds to this result and the black dots correspond to the test results. So after adding the additional term, the prediction is quite closed to the test results. The additional terms were also applied by Zhang and Matthews [12–14], where the buckling of composite shell has been investigated, which indicates it as an acceptable solution to both plates and shells. However, this approach is valid for the Galerkin method, which is a semi-analytical method instead of closed form analytical solution.

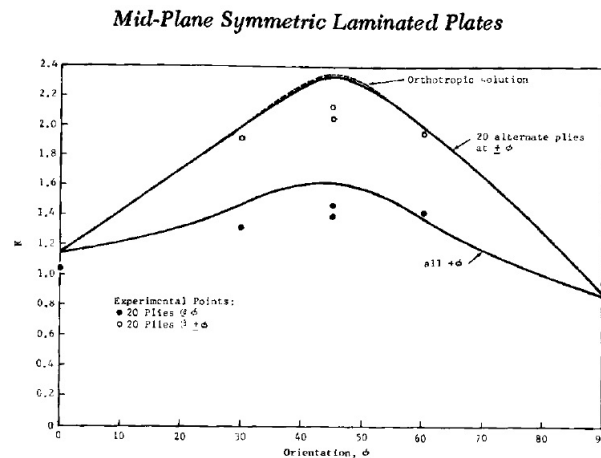


Figure 2.1: Buckling loads of Simply-Supported Plates (picture from literature [2])

2.3 Buckling of Shells

2.3.1 Isotropic Shells

The difference between plates and shells is that shells have initial curvatures in the unloaded state. Thus, the linear kinematics relation of the middle plane of a cylindrical shell will be

$$\epsilon_y = \frac{\partial v}{\partial y} - \frac{w}{R} \quad (2.19)$$

Clearly, the term $\frac{w}{R}$ will be zero for plates since the curvature of plates is zero.

Due to the initial curvatures of shells, some nice properties of plates discussed in previous section no longer exist that makes the buckling problems of shells more complicated. The first one is that the similarity of the governing equations for equilibrium state and buckling state disappeared. According to Chai [6], the equilibrium equations have the following form:

$$N_{x,x} + N_{xy,y} = 0 \quad (2.20)$$

$$N_{xy,x} + N_{y,y} = 0 \quad (2.21)$$

$$D(w_{,xxxx} + 2w_{,xxyy} + w_{,yyyy}) - \frac{N_y}{R} - [N_x w_{,xx} + 2N_{xy} w_{,xy} + N_y w_{,yy}] = 0 \quad (2.22)$$

However, the stability equations take the form of

$$N_{x1,x} + N_{xy1,y} = 0 \quad (2.23)$$

$$N_{xy1,x} + N_{y1,y} = 0 \quad (2.24)$$

$$D(w_{1,xxxx} + 2w_{1,xxyy} + w_{1,yyyy}) - \frac{N_{y1}}{R} - [N_x w_{1,xx} + 2N_{xy} w_{1,xy} + N_y w_{1,yy}] = 0 \quad (2.25)$$

where, N_x, N_y, N_{xy} are the in-plane loads; N_{x1}, N_{y1}, N_{xy1} are the variations (or increments) of the in-plane loads; w is the out-of-plane displacement in the equilibrium state, while w_1 is the variation of w when buckling occurs.

The same equations are also shown in other literature [1,5]. Clear the additional term $\frac{N_{y1}}{R}$ has been added to the out-of-plane stability differential equation (equation 2.25). Moreover, the in-plane equilibrium differential equations are expressed in terms of N_x, N_y, N_{xy} , while the in-plane stability differential equations are expressed in terms of variations of N_{x1}, N_{y1}, N_{xy1} . Thus, the buckling load cannot be simply solved from the equilibrium equations. What is worse, the out-of-plane buckling differential equation is coupled with the in-plane buckling differential equation through the additional term $\frac{N_{y1}}{R}$, which makes the solution to the stability of shells more complicated than plates.

A lot of attempts have been done to decouple the stability equations. Jones mentioned Donnell's method [5], which results in

$$r\nabla^4 \delta u = -v \frac{\partial^3 \delta w}{\partial x^3} + \frac{\partial^3 \delta w}{\partial x \partial y^2} \quad (2.26)$$

$$r\nabla^4 \delta v = -(2 + \nu) \frac{\partial^3 \delta w}{\partial x^2 \partial y} - \frac{\partial^3 \delta w}{\partial y^3} \quad (2.27)$$

$$D\nabla^8\delta w + \frac{Et}{r^2}\frac{\partial^4\delta w}{\partial x^4} - \nabla^4(N_x\delta w_{xx} + 2N_{xy}\delta w_{xy} + N_y\delta w_{yy}) = 0 \quad (2.28)$$

where, these equations are expressed in terms of the variations of the displacements.

Then Batdorf modified equation 2.28 as

$$D\nabla^4\delta w + \frac{Et}{r^2}\nabla^{-4}\frac{\partial^4\delta w}{\partial x^4} - (N_x\delta w_{xx} + 2N_{xy}\delta w_{xy} + N_y\delta w_{yy}) = 0 \quad (2.29)$$

which is known as Batdorf's modified Donnell Equation.

Bazant and Cedolin [15] introduced another method similar to Donnell's method where they used Airy stress function and its perturbation to decouple and simplify the stability differential equations. They firstly introduced Airy stress function to the in-plane loads as

$$N_{xx} = F_{,yy}, N_{yy} = F_{,xx}, N_{xy} = -F_{,xy} \quad (2.30)$$

These equations can be substituted into the equilibrium equations (equation 2.20 2.21 2.22) and compatibility equation. The in-plane equilibrium equations (equation 2.20 2.21) are automatically satisfied by the Airy stress function, then only the out-of-plane equilibrium equation and compatibility equation are left, which are shown as follows:

$$D\nabla^4w = p + F_{,yy}w_{,xx} - 2F_{,xy}w_{,xy} + F_{,xx}w_{,yy} - \frac{1}{R}F_{,xx} \quad (2.31)$$

$$\frac{1}{Eh}\nabla^4F = w_{,xy}^2 - w_{,xx}w_{,yy} + \frac{1}{R}w_{,xx} \quad (2.32)$$

The stability equations are obtained by using adjacent-equilibrium criterion where F and w are replaced by

$$w \rightarrow w^0 + w_1 \quad (2.33)$$

$$F \rightarrow F^0 + F_1 \quad (2.34)$$

where, w^0, F^0 present the initial states; w_1, F_1 present the small increments (or variations).

Then they can be substituted into the equilibrium equation 2.31 and compatibility equation 2.32. The initial equilibrium equation and comparability equation written in w^0 and F^0 can be subtracted. After ignoring all higher order terms and assuming the initial state of shells is membrane, the remaining equations become:

$$D\nabla^4w_1 = F_{,yy}^0w_{1,xx} - 2F_{,xy}^0w_{1,xy} + F_{,xx}^0w_{1,yy} - \frac{1}{R}F_{1,xx} \quad (2.35)$$

$$\frac{1}{Eh}\nabla^4F_1 = \frac{1}{R}w_{1,xx} \quad (2.36)$$

Then substituting the compatibility equation (equation 2.36) into equation 2.35 and applying the operator ∇^4 :

$$D\nabla^8w_1 - \nabla^4(N_{xx}^0w_{1,xx} + 2N_{xy}^0w_{1,xy} + N_{yy}^0w_{1,yy} + \frac{Eh}{R^2}w_{1,xxxx}) = 0 \quad (2.37)$$

Notice that the in-plane buckling equations 2.23 and 2.24 are automatically satisfied by the perturbed Airy stress function (F_1), so only one buckling equation 2.37 left, instead of three coupled stability differential equations (2.23, 2.24, 2.25).

Zhang, Matthews [12] and Geier, Zimmermann [16] also used the Airy stress function to decoupled the stability equations. But they directly started from the stability equations, instead of the equilibrium differential equations and applying the adjacent-equilibrium method to them. Moreover, the Airy stress function was introduced to the variations of in-plane loads, instead of the in-plane loads. Thus the in-plane stability differential equations are automatically satisfied by the Airy stress functions. Only the out-of-plane stability differential equation was left.

Zhang and Matthews [12–14] also introduced the characteristic beam function with approximate orthogonality property into the shape function of Airy stress function, which exactly satisfies the boundary conditions of in-plane stresses. The Airy stress function was expressed as:

$$F = \sum_{m=1}^{\infty} \sum_{n=1}^{\infty} F_{mn} X_m(\xi) Y_n(\eta) \quad (2.38)$$

in which

$$X_i(\xi) = \cosh \alpha_i \xi - \cos \alpha_i \xi - \gamma_i (\sinh \alpha_i \xi - \sin \alpha_i \xi) \quad (2.39)$$

$$Y_i(\eta) = \cosh \alpha_i \eta - \cos \alpha_i \eta - \gamma_i (\sinh \alpha_i \eta - \sin \alpha_i \eta) \quad (2.40)$$

The α_i and γ_i are constants which ensure the following boundary conditions are satisfied.

$$X_i(0) = X_i(1) = \left. \frac{dX_i}{d\xi} \right|_{\xi=0} = \left. \frac{dX_i}{d\xi} \right|_{\xi=1} = 0 \quad (2.41)$$

$$Y_i(0) = Y_i(1) = \left. \frac{dY_i}{d\eta} \right|_{\eta=0} = \left. \frac{dY_i}{d\eta} \right|_{\eta=1} = 0 \quad (2.42)$$

The values of α_i and γ_i are shown in Figure 2.2. The values on the left were from Chia and Prabhakara [17], where the same characteristic beam function was applied. Zhang indicated [12] that six significant figures are not enough to get the approximate orthogonality of the functions so that more significant figures were needed. Although Zhang did not explicitly indicate, the exactly analytical expression for α_i can be solved from the boundary conditions (equation 2.41–2.42), as

$$\alpha_i = \frac{2i + 1}{2} \pi \quad (2.43)$$

The analytical expression for γ_i can also be solved from the boundary conditions (equation 2.41, 2.42), like α_i . Reddy [3] studied the solutions to these constants (γ_i and α_i) under different boundary conditions and also showed the examples of solutions.

2.3.2 Composite Shells

Besides the couplings of the in-plane stability equations and the out-of-plane stability equation, another difficulty of composite shells is again the bending-twisting coupling D_{16} and D_{26} . These coupling terms make the closed form solution to shell buckling impossible. However, for specially orthotropic laminated shells, where $D_{16} = 0$ and $D_{26} = 0$, approximated closed form solutions still exists. For example, Geier and Zimmermann [16] presented a closed form solution for a simply-supported cylindrical shell as:

$$N_i = \frac{1}{\beta^2} D_{11} \beta^4 + 2(D_{12} + 2D_{33}) \beta^2 \eta^2 + D_2 2\eta^4 + \frac{[e_{21} \beta^4 + (e_{11} + e_{22} - 2e_{33}) \beta^2 \eta^2 + e_{12} \eta^4 + \beta^2 / R]^2}{a_{22} \beta^4 + (2a_{12} + a_{33}) \beta^2 \eta^2 + a_{11} \eta^4} \quad (2.44)$$

The Values of α_i and γ_i				
i	Values used in References 6 and 7		Values used in present work	
	α_i	γ_i	α_i	γ_i
1	4.730 04	0.982 502	4.730 040 744 862 70	0.982 502 214 576 238
2	7.853 20	1.000 78	7.853 204 624 095 84	1.000 777 311 907 269
3	10.995 6	0.999 967	10.995 607 838 001 6	0.999 966 450 125 409
4	14.137 2	1.000 00	14.137 165 491 257 5	1.000 001 449 897 656
5	$(11/2)\pi$	1.000 00	17.278 759 657 399 5	0.999 999 937 344 383
6	$(13/2)\pi$	1.000 00	20.420 352 245 626 0	1.000 000 002 707 595
7	$(15/2)\pi$	1.000 00	23.561 944 902 040 4	0.999 999 999 882 994
8	$(17/2)\pi$	1.000 00	26.703 537 555 508 2	1.000 000 000 005 056
9	$(19/2)\pi$	1.000 00	29.845 130 209 103 3	0.999 999 999 999 781

Figure 2.2: Values of α_i and γ_i in Zhang's Paper [12]

This closed form solution was obtained by assuming the displacement w and Airy stress function F as

$$w = C_1 \sin \beta x \cos \eta y \quad (2.45)$$

$$F = C_2 \sin \beta x \cos \eta y \quad (2.46)$$

Obviously, the shape function for Airy stress function might not satisfy the boundary condition of in-plane loads as shown in equation 2.41 and 2.42, since the shear load is not zero at the edge $x = 0$. Therefore, although a closed form solution has been obtained from this solution, it might sacrifice the accuracy of the predicted buckling load.

Vescovini and Bisagni [18] studied the buckling of stiffened composite flat and curved panels using Ritz method. The total energy functional was expressed as the sum of the total potential energy of each element of the stiffened panel plus a penalty term which described the compatibility conditions between the adjacent plates. The potential energy of each element was considered as the sum of the membrane energy, bending energy and work done by the external loads. It is noted that the membrane energy was expressed by Airy stress function which was directly solved from the compatibility equation after assuming a Fourier series for out-of-plane displacement. The advantage of their method is that additional series for Airy stress function are not required. Thus the total potential energy was only expressed by the series of displacement which would increase the efficiency of Ritz method.

Zhang and Matthews [12–14] studied the buckling of curved panels using Galerkin method, where they started from the stability differential equations of shells. Similarly the Airy stress function, instead of the in-plane loads, were used in the compatibility equation and stability equations. However, the Airy stress function and out-of-plane displacement were approximated by two different series each satisfying the own boundary conditions, where the Airy stress function used beam characteristic function while displacement used Fourier series. However, the Airy stress function shows its advantages in simplifying the analytical derivations and enhancing the computational efficiency.

2.4 Various Boundary conditions and loads

As indicated in by Reddy [3], the beam characteristic function can also be used for panels under clamped or free boundary condition . Actually Ashton and Waddoups [19] introduced the beam characteristic function earlier to the panels with simply-supported, clamped, or one-edge-free boundary conditions. A combination of different beam characteristic functions can easily describe various boundary conditions of panels. They also indicated that these functions are very nearly (or exactly) the natural model shapes for isotropic and orthotropic plates, and thus are reasonably accurate shapes for weakly anisotropic plates [19].

Closed form solutions to buckling of laminated orthotropic plates under general in-plane loading were investigated by Qiao [20]. Two cases of composite plates under combined linearly varying axial and in-plane shear loading, with two opposite edges simply supported while the other two edges either both rotationally restrained or one rotationally restrained and the other free, were considered. The out-of-plane displacement w was described by only one term of the shape function in the Ritz method thus an explicit closed form solution was obtained by minimization the total energy. However, the shape function had to be properly selected to approximate the buckling mode shape as exactly as possible. This solution also can only be applied to long plates. For more complicated problems, this closed form solution will not have enough accuracy.

2.5 Panels with Spatially Varying Stiffness

Spatially varying stiffness laminated panel has been a recently innovative topic. The variable stiffness is achieved by the steering of the fibre direction or tapering of the laminate thickness, resulting in beneficial load and stiffness distribution that improves the buckling resistance of laminated panels. IJsselmuiden, Abdalla and Gürdal [21, 22] investigated the buckling of variable-stiffness plates and shells using finite element method. Gürdal and Olmedo [11, 23, 24] studied the in-plane response of laminates with spatially varying fiber orientations. The fibre orientation was assumed to vary in one direction, where the varying fibre orientation can be formulated by a simple function of the in-plane coordinates, thus the stiffness is also a function of the in-plane coordinates. The displacement fields were solved from the two coupled elliptic partial differential equations (similar to the in-plane equilibrium differential equation 2.20 2.21) using the numerical solver ELLPACK [25]. The exact closed form solutions were only presented for the simplified cases. Then the buckling behaviour of panels with varying fibre orientations were studied in their papers [11, 26] using the Ritz method.

Wu, Raju and Weaver [27] investigated the buckling of variable angle tow plates using Ritz method in two steps. In the first step, they obtained the in-plane loads by minimizing the total complementary energy of the membrane behaviour. In the second step, the stability of the panel under these in-plane loads was determined by minimization the total potential energy considering the bending behaviour of the panel. The Legendre polynomial functions were applied to approximate the Airy stress function and out-of-plane displacement in the Ritz method. Both the prediction of in-plane loads and buckling loads were well captured by the Legendre polynomial functions. Similar works can be found in other papers [28–31], where they extended the Ritz method to consider blade stiffened panels.

2.6 Conclusions

Basic stability theories and equations governing the equilibrium and stability of plates and cylindrical shells are reviewed in this chapter, which paves the fundamental to this thesis. Following conclusions are summarized for this review.

Closed form solution to the problems considered in current thesis has not been obtained by any researcher (to the best knowledge of the author). However, Galerkin method and Ritz method have advantages in predicting either the in-plane loads or the buckling loads of variable stiffness panels. These methods can be applied to problems under any boundary conditions and any in-plane loads, as long as the assumed shape function satisfies the corresponding boundary conditions.

The introduction of Airy stress function also simplifies the solution. As Vescovini, Bisagni [18] and Zhang [12] did in their papers, the Airy stress function was used to describe the non-uniform distribution of membrane stresses, which simplified the formulation of compatibility equation and equilibrium equations. Moreover, Airy stress function provided a way to easily decouple the stability equations of shells, as shown by Bazant and Cedolin [15].

Governing Equations and Galerkin Method

3.1 Introduction

In this chapter the governing equations for composite plates and shallow cylindrical shells with variable stiffness are derived. Due to complexity of these governing equations, the exact closed form solutions introduced in literature [3, 7] cannot be applied to solve these equations. Therefore, Galerkin method has been used in order to solve the governing equations approximately.

In this section, a brief description of the plates and shells considered in the thesis is given, follows by the basic assumptions and equations in classic laminate theory. In Section 3.2 and 3.3, the governing differential equations (compatibility equations and stability equations) for composite plates and shallow cylindrical shells with variable stiffness are derived, respectively. In Section 3.4, the Galerkin method is introduced to solve these governing differential equations approximately.

3.1.1 Plate

Rectangular plates are considered in the thesis. The cartesian coordinate system is defined for plates, as shown in Figure 3.1. The z axis is defined as the out-of-plane direction. The length of the plate along x axis is defined as a ; the width of the plate along y axis is defined as b . If not explicitly indicated, the coordinate system used for plates in the thesis is always the same as shown in Figure 3.1.

3.1.2 Shallow Cylindrical Shell

The difference between plates and shells is that shells are initially curved in the unloaded state while plates are flat. This difference makes the equations for shells much more complicated

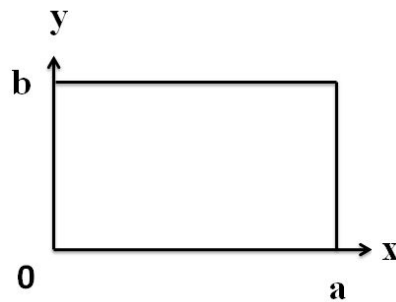


Figure 3.1: Coordinate and dimensions of rectangular plate

than plates. However, simplified equations introduced by Donnell are available when the shells are shallow or quasi-shallow. As defined by Bazant and Cedolin [15], a shallow shell is a shell whose rise with respect to any chord is small, as shown in Figure 3.2; a quasi-shallow shell is a shell which buckles in such a manner that each buckle alone represents a shallow shell, for instance, a complete cylindrical shell. This means the half wavelengths of the buckles of these shells are short compared to the radius. In this thesis shallow cylindrical shells are considered, so Donnell's simplified equations for shells are used which will be shown later in this chapter.

Normally cylindrical coordinate is used for cylindrical shells, however, for convenience the coordinate system is defined as a pointwise orthogonal rectangular coordinate system, as shown in Figure 3.2. The origin of the coordinate system is in the mid-plane of the shell. The x axis is parallel to the axis of the cylinder, the y axis is tangent to the circular arc, and the z axis is normal to the mid-plane of the shell directed toward the center of curvature.

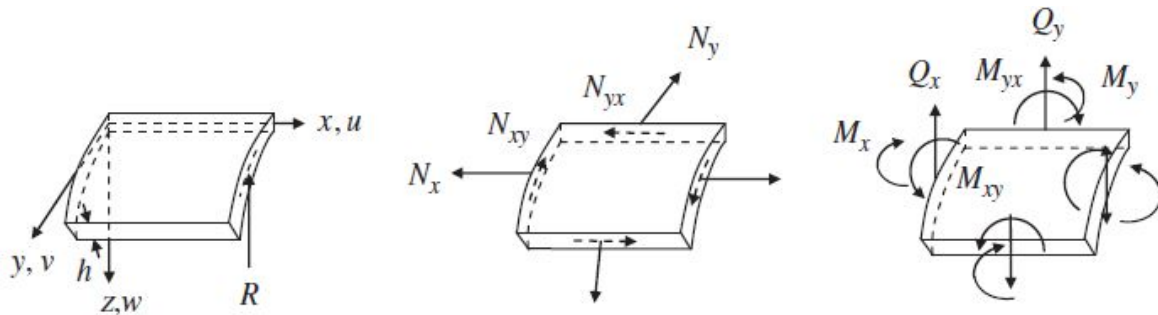


Figure 3.2: Cylindrical shell displacements and forces (picture form Yoo and Lee [6])

3.1.3 Assumptions

The following assumption have been mode for thin panels (plates and shallow shells),

- The panel is thin, the thickness is much smaller than other dimensions.
- No body forces and surface pressures are applied to the panels.
- Imperfections of the panels are ignored.

Since the panel has been assumed to be thin, the Kirchhoff hypothesis have to be hold [1,3],

- Straight lines perpendicular to the mid-surface before deformation remain straight after deformation.
- The transverse normal is inextensible.
- The transverse normal to the mid-plane is assumed to remain normal during deformation.
- The transverse normal stress σ_z is assumed to be small compared to other normal stresses.

The Kirchhoff hypothesis also implies the transverse normal and shearing strains are zero [1,3].

$$\epsilon_z = \gamma_{xz} = \gamma_{yz} = 0 \quad (3.1)$$

In addition, two important assumptions are made for the stability analysis of plates and shallow cylindrical shells which will be frequently used in the following chapters.

Assumption 1: The prebuckling deformation of a panel is membrane, if only in-plane loads or displacements have been applied to the edges. In other words, the slopes and curvatures of a panel in the prebuckling state are zero. So the derivatives of the out-of-plane displacement (w) with respect to x and y are zero.

Assumption 2: The out-of-plane displacement w is zero in the prebuckling equilibrium state.

For plates, it is easy to understand that the out-of-plane deflection is zero in the prebuckling state when only in-plane loads are applied. For cylindrical shells, this assumption is valid for shallow cylindrical shell panels, especially for these under the boundary conditions that the out-of-plane displacement is zero at the boundary (for instance, simply-support or clamping). However, for complete cylindrical shells (quasi-shallow shells) under axial compression load, it is noted that the shells will expand in the normal direction. So the out-of-plane displacement of complete cylindrical shells is uniform but non-zero thus assumption 2 is invalid.

Based on these two assumptions, the out-of-plane displacement w , rotations and curvatures of plates and shallow cylindrical shells in the prebuckling equilibrium state are all zero.

3.1.4 Classical Laminate Theory

The force resultants of plates are defined by integrating the stresses through the thickness of a laminate as [5, 7]

$$N_x = \int_{-\frac{h}{2}}^{\frac{h}{2}} \sigma_x dz \quad (3.2)$$

$$N_y = \int_{-\frac{h}{2}}^{\frac{h}{2}} \sigma_y dz \quad (3.3)$$

$$N_{xy} = \int_{-\frac{h}{2}}^{\frac{h}{2}} \gamma_{xy} dz \quad (3.4)$$

where, $\sigma_x, \sigma_y, \gamma_{xy}$ are the in-plane normal and shear stress; h is the thickness.

Similarly, the moment resultants of plates are defined as

$$M_x = \int_{-\frac{h}{2}}^{\frac{h}{2}} \sigma_x z dz \quad (3.5)$$

$$M_y = \int_{-\frac{h}{2}}^{\frac{h}{2}} \sigma_y z dz \quad (3.6)$$

$$M_{xy} = \int_{-\frac{h}{2}}^{\frac{h}{2}} \gamma_{xy} z dz \quad (3.7)$$

In shell theory, force resultants and moment resultants of cylindrical shells are defined as [1,6]

$$N_x = \int_{-\frac{h}{2}}^{\frac{h}{2}} \sigma_x \left(1 + \frac{z}{R}\right) dz \quad (3.8)$$

$$N_y = \int_{-\frac{h}{2}}^{\frac{h}{2}} \sigma_y \left(1 + \frac{z}{R}\right) dz \quad (3.9)$$

$$N_{xy} = \int_{-\frac{h}{2}}^{\frac{h}{2}} \gamma_{xy} \left(1 + \frac{z}{R}\right) dz \quad (3.10)$$

$$M_x = \int_{-\frac{h}{2}}^{\frac{h}{2}} \sigma_x \left(1 + \frac{z}{R}\right) z dz \quad (3.11)$$

$$M_y = \int_{-\frac{h}{2}}^{\frac{h}{2}} \sigma_y \left(1 + \frac{z}{R}\right) z dz \quad (3.12)$$

$$M_{xy} = \int_{-\frac{h}{2}}^{\frac{h}{2}} \gamma_{xy} \left(1 + \frac{z}{R}\right) z dz \quad (3.13)$$

$$(3.14)$$

where, R is the radius of cylindrical shell.

However, according to Donnell's shallow shell theory these accurate equations for shells can be approximated by the equations for plates (equation 3.2 - 3.7) since $\frac{z}{R}$ might be neglected for sufficiently thin shells [1, 5]. The positive directions of the force resultants and moment resultants are defined in Figure 3.2.

Furthermore, the force and moment resultants are related to the mid-plane strains for laminated panels (plates and shells) through the constitutive relations as [7]

$$\begin{pmatrix} N_x \\ N_y \\ N_{xy} \\ M_x \\ M_y \\ M_{xy} \end{pmatrix} = \begin{bmatrix} A_{11}(x, y) & A_{12}(x, y) & A_{16}(x, y) & B_{11}(x, y) & B_{12}(x, y) & B_{16}(x, y) \\ A_{12}(x, y) & A_{22}(x, y) & A_{26}(x, y) & B_{12}(x, y) & B_{22}(x, y) & B_{26}(x, y) \\ A_{16}(x, y) & A_{26}(x, y) & A_{66}(x, y) & B_{16}(x, y) & B_{26}(x, y) & B_{66}(x, y) \\ B_{11}(x, y) & B_{12}(x, y) & B_{16}(x, y) & D_{11}(x, y) & D_{12}(x, y) & D_{16}(x, y) \\ B_{12}(x, y) & B_{22}(x, y) & B_{26}(x, y) & D_{12}(x, y) & D_{22}(x, y) & D_{26}(x, y) \\ B_{16}(x, y) & B_{26}(x, y) & B_{66}(x, y) & D_{16}(x, y) & D_{26}(x, y) & D_{66}(x, y) \end{bmatrix} \begin{pmatrix} \epsilon_{xo} \\ \epsilon_{yo} \\ \gamma_{xyo} \\ \kappa_x \\ \kappa_y \\ \kappa_{xy} \end{pmatrix} \quad (3.15)$$

where, A_{ij}, B_{ij}, D_{ij} ($i, j = 1, 2, 6$) are functions of x and y due to the variable stiffness; $\epsilon_{xo}, \epsilon_{yo}, \gamma_{xyo}$ are mid-plane strains and $\kappa_x, \kappa_y, \kappa_{xy}$ are curvatures.

For convenience, these equations can be written in matrix form as

$$\begin{pmatrix} \mathbf{n} \\ \mathbf{m} \end{pmatrix} = \begin{bmatrix} \mathbf{A} & \mathbf{B} \\ \mathbf{B} & \mathbf{D} \end{bmatrix} \begin{pmatrix} \boldsymbol{\epsilon} \\ \boldsymbol{\kappa} \end{pmatrix} \quad (3.16)$$

where,

$$\mathbf{n} = \begin{pmatrix} N_x & N_y & N_{xy} \end{pmatrix}^T \quad (3.17)$$

$$\mathbf{m} = \begin{pmatrix} M_x & M_y & M_{xy} \end{pmatrix}^T \quad (3.18)$$

$$\mathbf{A} = \begin{bmatrix} A_{11}(x, y) & A_{12}(x, y) & A_{16}(x, y) \\ A_{12}(x, y) & A_{22}(x, y) & A_{26}(x, y) \\ A_{16}(x, y) & A_{26}(x, y) & A_{66}(x, y) \end{bmatrix} \quad (3.19)$$

$$\mathbf{B} = \begin{bmatrix} B_{11}(x, y) & B_{12}(x, y) & B_{16}(x, y) \\ B_{12}(x, y) & B_{22}(x, y) & B_{26}(x, y) \\ B_{16}(x, y) & B_{26}(x, y) & B_{66}(x, y) \end{bmatrix} \quad (3.20)$$

$$\mathbf{D} = \begin{bmatrix} D_{11}(x, y) & D_{12}(x, y) & D_{16}(x, y) \\ D_{12}(x, y) & D_{22}(x, y) & D_{26}(x, y) \\ D_{16}(x, y) & D_{26}(x, y) & D_{66}(x, y) \end{bmatrix} \quad (3.21)$$

$$\boldsymbol{\epsilon} = \begin{pmatrix} \epsilon_{xo} & \epsilon_{yo} & \gamma_{xyo} \end{pmatrix}^T \quad (3.22)$$

$$\boldsymbol{\kappa} = \begin{pmatrix} \kappa_x & \kappa_y & \kappa_{xy} \end{pmatrix}^T \quad (3.23)$$

For symmetric laminates, the membrane-bending couplings are zero [3, 7],

$$B_{ij} = 0 \quad (i, j = 1, 2, 6) \quad (3.24)$$

Then the constitutive relations reduce to

$$\begin{pmatrix} \mathbf{n} \\ \mathbf{m} \end{pmatrix} = \begin{bmatrix} \mathbf{A} & \mathbf{O} \\ \mathbf{O} & \mathbf{D} \end{bmatrix} \begin{pmatrix} \boldsymbol{\epsilon} \\ \boldsymbol{\kappa} \end{pmatrix} \quad (3.25)$$

where, \mathbf{O} is a zero matrix.

Then the mid-plane strains can be expressed in terms of the force resultants from above constitutive relations as

$$\begin{pmatrix} \epsilon_{xo} \\ \epsilon_{yo} \\ \gamma_{xyo} \end{pmatrix} = \begin{bmatrix} a_{11}(x, y) & a_{12}(x, y) & a_{16}(x, y) \\ a_{12}(x, y) & a_{22}(x, y) & a_{26}(x, y) \\ a_{16}(x, y) & a_{26}(x, y) & a_{66}(x, y) \end{bmatrix} \begin{pmatrix} N_x \\ N_y \\ N_{xy} \end{pmatrix} \quad (3.26)$$

where, a_{ij} ($i, j = 1, 2, 6$) are the compliance of the \mathbf{A} matrix.

$$\begin{bmatrix} a_{11}(x, y) & a_{12}(x, y) & a_{16}(x, y) \\ a_{12}(x, y) & a_{22}(x, y) & a_{26}(x, y) \\ a_{16}(x, y) & a_{26}(x, y) & a_{66}(x, y) \end{bmatrix} = \begin{bmatrix} A_{11}(x, y) & A_{12}(x, y) & A_{16}(x, y) \\ A_{12}(x, y) & A_{22}(x, y) & A_{26}(x, y) \\ A_{16}(x, y) & A_{26}(x, y) & A_{66}(x, y) \end{bmatrix}^{-1} \quad (3.27)$$

In addition, the moment resultants can be solved from the constitutive relation (equation 3.25) as

$$M_x = D_{11}(x, y)\kappa_x + D_{12}(x, y)\kappa_y + D_{16}(x, y)\kappa_{xy} \quad (3.28)$$

$$M_y = D_{12}(x, y)\kappa_x + D_{22}(x, y)\kappa_y + D_{26}(x, y)\kappa_{xy} \quad (3.29)$$

$$M_{xy} = D_{16}(x, y)\kappa_x + D_{26}(x, y)\kappa_y + D_{66}(x, y)\kappa_{xy} \quad (3.30)$$

where, the curvature-displacement relations are given as

$$\kappa_x = -w_{,xx} \quad (3.31)$$

$$\kappa_y = -w_{,yy} \quad (3.32)$$

$$\kappa_{xy} = -2w_{,xy} \quad (3.33)$$

3.2 Governing Equations for Plate

In this section, the linear compatibility equation is derived for prebuckling analysis, then the non-linear compatibility equation and stability equations are derived for stability analysis. In the end of this section, these governing equations are compared to the the governing equations in literature.

3.2.1 Equations for Prebuckling Analysis

For small deflections and rotations, the equations relating mid-plane strains to displacements are [7]

$$\epsilon_{xo} = u_{,x} \quad (3.34)$$

$$\epsilon_{yo} = v_{,y} \quad (3.35)$$

$$\gamma_{xyo} = u_{,y} + v_{,x} \quad (3.36)$$

where, u, v, w are the displacements along along x, y, z axis; a subscript x, y, z preceded by a comma indicates a partial derivative (with respect to coordinate x, y, z , respectively).

The linear compatibility equation for mid-plane strains can be derived from above relations as

$$\epsilon_{xo,yy} + \epsilon_{yo,xx} = \gamma_{xyo,xy} \quad (3.37)$$

Substituting equation 3.26 into above equation, the compatibility equation (equation 3.37) can be written in terms of in-plane loads as

$$\begin{aligned} & \frac{\partial^2}{\partial y^2} [a_{11}(x, y)N_x + a_{12}(x, y)N_y + a_{16}(x, y)N_{xy}] \\ & + \frac{\partial^2}{\partial x^2} [a_{12}(x, y)N_x + a_{22}(x, y)N_y + a_{26}(x, y)N_{xy}] \\ & = \frac{\partial^2}{\partial xy} [a_{16}(x, y)N_x + a_{26}(x, y)N_y + a_{66}(x, y)N_{xy}] \end{aligned} \quad (3.38)$$

Note that a_{ij} ($i, j = 1, 2, 6$) are functions of x and y , so the derivatives of them are not zero.

The linear equilibrium differential equations of plates are given in literature [1, 5, 7] as

$$N_{x,x} + N_{xy,y} = 0 \quad (3.39)$$

$$N_{xy,x} + N_{y,y} = 0 \quad (3.40)$$

$$M_{x,xx} + 2M_{xy,xy} + M_{y,yy} = 0 \quad (3.41)$$

The moment resultants can be solved from the constitutive relation and are given in equation 3.28, 3.29 and 3.30. According to assumption 1, the curvatures are zero before buckling occurs. So the out-of-plane equilibrium equation (equation 3.41) is satisfied by itself.

The in-plane equilibrium equations (equation 3.39, 3.40) can be automatically satisfied by introducing the Airy stress function to the in-plane loads as

$$N_x = F_{,yy}, \quad N_y = F_{,xx}, \quad N_{xy} = -F_{,xy} \quad (3.42)$$

where, F is the Airy stress function.

Then the compatibility equation 3.38 can be rewritten in terms of Airy stress function as

$$\begin{aligned} & \frac{\partial^2}{\partial y^2} [a_{11}(x, y)F_{,yy} + a_{12}(x, y)F_{,xx} - a_{16}(x, y)F_{,xy}] \\ & + \frac{\partial^2}{\partial x^2} [a_{12}(x, y)F_{,yy} + a_{22}(x, y)F_{,xx} - a_{26}(x, y)F_{,xy}] \\ & = \frac{\partial^2}{\partial xy} [a_{16}(x, y)F_{,yy} + a_{26}(x, y)F_{,xx} - a_{66}(x, y)F_{,xy}] \end{aligned} \quad (3.43)$$

The compatibility equation (equation 3.38 or 3.43) in the prebuckling state describes the membrane behavior of plates (relation of in-plane loads), hence it can be used to solve the in-plane loads distribution.

3.2.2 Equations for Stability Analysis

For moderate rotations, von Kármán's moderately large-deflection theory has to be applied. The equations relating mid-plane strains to displacements are [7]

$$\epsilon_{xo} = u_{,x} + \frac{1}{2}w_{,x}^2 \quad (3.44)$$

$$\epsilon_{yo} = v_{,y} + \frac{1}{2}w_{,y}^2 \quad (3.45)$$

$$\gamma_{xyo} = u_{,y} + v_{,x} + w_{,x}w_{,y} \quad (3.46)$$

Then the non-linear compatibility equation for mid-plane strains is derived from above equations as

$$\epsilon_{xo,yy} + \epsilon_{yo,xx} - \gamma_{xyo,xy} = w_{,xy}^2 - w_{,xx}w_{,yy} \quad (3.47)$$

The non-linear equilibrium differential equations of plates for moderate rotations are given in literature [1, 7] as

$$N_{x,x} + N_{xy,y} = 0 \quad (3.48)$$

$$N_{xy,x} + N_{y,y} = 0 \quad (3.49)$$

$$M_{x,xx} + 2M_{xy,xy} + M_{y,yy} + N_x w_{,xx} + 2N_{xy} w_{,xy} + N_y w_{,yy} = 0 \quad (3.50)$$

The moments can be written in terms of curvatures (equation 3.28 3.29 3.30) and the curvatures can be written in terms of displacement (equation 3.31 3.32 3.33). So the out-of-plane equilibrium equation (equation 3.50) can be written in terms of w as

$$\begin{aligned} & \frac{\partial^2}{\partial x^2} [D_{11}(x, y)w_{,xx} + D_{12}(x, y)w_{,yy} + 2D_{16}(x, y)w_{,xy}] \\ & + 2\frac{\partial^2}{\partial xy} [D_{16}(x, y)w_{,xx} + D_{26}(x, y)w_{,yy} + 2D_{66}(x, y)w_{,xy}] \\ & + \frac{\partial^2}{\partial y^2} [D_{12}(x, y)w_{,xx} + D_{22}(x, y)w_{,yy} + 2D_{26}(x, y)w_{,xy}] \\ & = N_x w_{,xx} + 2N_{xy} w_{,xy} + N_y w_{,yy} \end{aligned} \quad (3.51)$$

The in-plane equilibrium equations (equation 3.48 3.49) can still be automatically satisfied by introducing the Airy stress function (equation 3.42) to the in-plane loads.

Although the out-of-plane equilibrium differential equation (equation 3.50) was used in some literature [2–4, 7] to solve the buckling load, it is not theoretically correct as indicated by Jones [5] since the equilibrium equation is essentially different from the stability equation. So for stability analysis, the stability differential equations should be derived.

The stability differential equations can be derived applying either adjacent-equilibrium criterion to the equilibrium differential equations or minimum potential energy criterion. A brief example is shown for the adjacent-equilibrium criterion. However, the reader is referred to the literature [1, 5] for the details regarding this criteria.

In adjacent-equilibrium criterion, small perturbations are applied to the system. Normally, these perturbations result in infinitesimal increments of the displacements u , v , w , as follows

$$u \rightarrow u + u_1 \quad (3.52)$$

$$v \rightarrow v + v_1 \quad (3.53)$$

$$w \rightarrow w + w_1 \quad (3.54)$$

where, the arrows are read 'be replaced by'. u , v , w represent the displacements on the primary equilibrium path; u_1 , v_1 , w_1 represent the infinitesimal increments of u , v , w . So $u + u_1$, $v + v_1$, $w + w_1$ represent the possible adjacent equilibrium path (or secondary equilibrium path). Since the increments are small, the second order and any higher order terms in u_1, v_1, w_1 can be neglected. Moreover, according to assumption 1 and 2, the out-of-plane displacement w and its derivatives are zero.

The increments in u , v , w cause a corresponding change in the mid-plane strains as

$$\epsilon_{xo} \rightarrow \epsilon_{xo} + \Delta\epsilon_{xo} \quad (3.55)$$

$$\epsilon_{yo} \rightarrow \epsilon_{yo} + \Delta\epsilon_{yo} \quad (3.56)$$

$$\gamma_{xyo} \rightarrow \gamma_{xyo} + \Delta\gamma_{xyo} \quad (3.57)$$

where,

$$\Delta\epsilon_{xo} = u_{1,x} + w_{1,x}w_{,x} + \frac{1}{2}w_{1,x}^2 \quad (3.58)$$

$$\Delta\epsilon_{yo} = v_{1,y} + w_{1,y}w_{,y} + \frac{1}{2}w_{1,y}^2 \quad (3.59)$$

$$\Delta\gamma_{xyo} = u_{1,y} + v_{1,x} + 2w_{,x}w_{1,y} + w_{1,x}w_{1,y} \quad (3.60)$$

After ignoring the higher order terms in u_1, v_1, w_1 , the parts of $\Delta\epsilon_{xo}, \Delta\epsilon_{yo}, \Delta\gamma_{xyo}$ which are linear in u_1, v_1, w_1 become

$$\epsilon_{xo1} = u_{1,x} + w_{1,x}w_{,x} \quad (3.61)$$

$$\epsilon_{yo1} = v_{1,y} + w_{1,y}w_{,y} \quad (3.62)$$

$$\gamma_{xyo1} = u_{1,y} + v_{1,x} + 2w_{,x}w_{1,y} \quad (3.63)$$

According to the assumption 1 and 2, the out-of-plane displacement w and its derivatives are zero. So

$$\epsilon_{xo1} = u_{1,x} \quad (3.64)$$

$$\epsilon_{yo1} = v_{1,y} \quad (3.65)$$

$$\gamma_{xyo1} = u_{1,y} + v_{1,x} \quad (3.66)$$

Therefore, $\epsilon_{xo}, \epsilon_{yo}, \gamma_{xyo}$ can be replaced as

$$\epsilon_{xo} \rightarrow \epsilon_{xo} + \epsilon_{xo1} \quad (3.67)$$

$$\epsilon_{yo} \rightarrow \epsilon_{yo} + \epsilon_{yo1} \quad (3.68)$$

$$\gamma_{xyo} \rightarrow \gamma_{xyo} + \gamma_{xyo1} \quad (3.69)$$

Similarly, the in-plane loads and moments are replaced by (after ignoring the higher order terms in u_1, v_1, w_1 and applying assumption 1 and 2)

$$N_x \rightarrow N_x + N_{x1} \quad (3.70)$$

$$N_y \rightarrow N_y + N_{y1} \quad (3.71)$$

$$N_{xy} \rightarrow N_{xy} + N_{xy1} \quad (3.72)$$

and

$$M_x \rightarrow M_x + M_{x1} \quad (3.73)$$

$$M_y \rightarrow M_y + M_{y1} \quad (3.74)$$

$$M_{xy} \rightarrow M_{xy} + M_{xy1} \quad (3.75)$$

where, N_{x1}, N_{y1}, N_{xy1} are the parts of the increments of N_x, N_y, N_{xy} which are linear in u_1, v_1, w_1 ,

$$\begin{pmatrix} N_{x1} \\ N_{y1} \\ N_{xy1} \end{pmatrix} = \begin{bmatrix} A_{11}(x, y) & A_{12}(x, y) & A_{16}(x, y) \\ A_{12}(x, y) & A_{22}(x, y) & A_{26}(x, y) \\ A_{16}(x, y) & A_{26}(x, y) & A_{66}(x, y) \end{bmatrix} \begin{pmatrix} \epsilon_{xo1} \\ \epsilon_{yo1} \\ \gamma_{xyo1} \end{pmatrix} \quad (3.76)$$

and M_{x1}, M_{y1}, M_{xy1} are the parts of the increments of M_x, M_y, M_{xy} which are linear in u_1, v_1, w_1 ,

$$M_{x1} = -D_{11}(x, y)w_{1,xx} - D_{12}(x, y)w_{1,yy} - 2D_{16}(x, y)w_{1,xy} \quad (3.77)$$

$$M_{y1} = -D_{12}(x, y)w_{1,xx} - D_{22}(x, y)w_{1,yy} - 2D_{26}(x, y)w_{1,xy} \quad (3.78)$$

$$M_{xy1} = -D_{16}(x, y)w_{1,xx} - D_{26}(x, y)w_{1,yy} - 2D_{66}(x, y)w_{1,xy} \quad (3.79)$$

Then replacing the in-plane loads, moments and out-of-plane displacement in the equilibrium equations (equation 3.48, 3.49, 3.50) (then truncating the original equilibrium equations, neglecting the higher order terms and applying assumption 1 and 2), the stability differential equations become:

$$N_{x1,x} + N_{xy1,y} = 0 \quad (3.80)$$

$$N_{xy1,x} + N_{y1,y} = 0 \quad (3.81)$$

$$M_{x1,xx} + 2M_{xy1,xy} + M_{y1,yy} + N_x w_{1,xx} + 2N_{xy} w_{1,xy} + N_y w_{1,yy} = 0 \quad (3.82)$$

Clearly, these equations are similar to the non-linear equilibrium equations (equation 3.48, 3.49 and 3.50). This is why the equilibrium equations were used by some researchers [2–4, 7] to solve the buckling loads. However, as indicated by Jones [5], the stability equations are essentially different from the equilibrium equations, because buckling is an eigenvalue problem while equilibrium is a boundary-value problem.

The out-of-plane stability equation can be written in terms of w_1 as

$$\begin{aligned} & \frac{\partial^2}{\partial x^2} [D_{11}(x, y)w_{1,xx} + D_{12}(x, y)w_{1,yy} + 2D_{16}(x, y)w_{1,xy}] \\ & + 2 \frac{\partial^2}{\partial xy} [D_{16}(x, y)w_{1,xx} + D_{26}(x, y)w_{1,yy} + 2D_{66}(x, y)w_{1,xy}] \\ & + \frac{\partial^2}{\partial y^2} [D_{12}(x, y)w_{1,xx} + D_{22}(x, y)w_{1,yy} + 2D_{26}(x, y)w_{1,xy}] \\ & = N_x w_{1,xx} + 2N_{xy} w_{1,xy} + N_y w_{1,yy} \end{aligned} \quad (3.83)$$

Since $\epsilon_{xo1}, \epsilon_{yo1}, \gamma_{xyo1}$ are linear in u_1, v_1, w_1 as shown in equations 3.64, 3.65 and 3.66, a compatibility equation can be obtained as

$$\epsilon_{xo1,yy} + \epsilon_{yo1,xx} - \gamma_{xyo1,xy} = 0 \quad (3.84)$$

which is called the compatibility equation for stability analysis in this thesis and is different from the compatibility equation (equation 3.37) for the prebuckling analysis. This equation describes the non-uniform membrane behavior during buckling.

This compatibility equation can be rewritten in terms of N_{x1}, N_{y1}, N_{xy1} through equation 3.76 as

$$\begin{aligned} & \frac{\partial^2}{\partial y^2} [a_{11}(x, y)N_{x1} + a_{12}(x, y)N_{y1} + a_{16}(x, y)N_{xy1}] \\ & + \frac{\partial^2}{\partial x^2} [a_{12}(x, y)N_{x1} + a_{22}(x, y)N_{y1} + a_{26}(x, y)N_{xy1}] \\ & = \frac{\partial^2}{\partial xy} [a_{16}(x, y)N_{x1} + a_{26}(x, y)N_{y1} + a_{66}(x, y)N_{xy1}] \end{aligned} \quad (3.85)$$

Introduce the increment of Airy stress function to N_{x1}, N_{y1}, N_{xy1} as

$$N_{x1} = F_{1,yy}, N_{y1} = F_{1,xx}, N_{xy1} = -F_{1,xy} \quad (3.86)$$

where, F_1 is the increment of F .

Clearly, these equations automatically satisfy the in-plane stability differential equations (equation 3.80 and 3.81) as the Airy stress function (equation 3.42) automatically satisfy the in-plane equilibrium differential equations.

Then the out-of-plane stability differential equation (equation 3.83) can be written in terms of Airy stress function as

$$\begin{aligned} & \frac{\partial^2}{\partial x^2} [D_{11}(x, y)w_{1,xx} + D_{12}(x, y)w_{1,yy} + 2D_{16}(x, y)w_{1,xy}] \\ & + 2\frac{\partial^2}{\partial xy} [D_{16}(x, y)w_{1,xx} + D_{26}(x, y)w_{1,yy} + 2D_{66}(x, y)w_{1,xy}] \\ & + \frac{\partial^2}{\partial y^2} [D_{12}(x, y)w_{1,xx} + D_{22}(x, y)w_{1,yy} + 2D_{26}(x, y)w_{1,xy}] \\ & = F_{,xx}w_{1,xx} - 2F_{,xy}w_{1,xy} + F_{,yy}w_{1,yy} \end{aligned} \quad (3.87)$$

The compatibility equation (equation 3.85) for stability analysis can be written in terms of the increment of Airy stress function as

$$\begin{aligned} & \frac{\partial^2}{\partial y^2} [a_{11}(x, y)F_{1,yy} + a_{12}(x, y)F_{1,xx} - a_{16}(x, y)F_{1,xy}] \\ & + \frac{\partial^2}{\partial x^2} [a_{12}(x, y)F_{1,yy} + a_{22}(x, y)F_{1,xx} - a_{26}(x, y)F_{1,xy}] \\ & = \frac{\partial^2}{\partial xy} [a_{16}(x, y)F_{1,yy} + a_{26}(x, y)F_{1,xx} - a_{66}(x, y)F_{1,xy}] \end{aligned} \quad (3.88)$$

Clearly, the compatibility equation for stability analysis derived here is independent of the out-of-plane stability equation 3.87. So the buckling load of plates can be solved from the out-of-plane stability equation alone. Later in Section 3.3, similar compatibility equation and out-of-plane stability equations will be derived for shells where the two equations are coupled and have to be solved together. This is one of the differences between plates and cylindrical shells.

3.2.3 Comparison with previous work

If the stiffness of the plate is constant, A_{ij} and D_{ij} are no longer functions of x and y . Then the out-of-plane equilibrium equation (equation 3.50) will reduce to

$$\begin{aligned} & D_{11}\frac{\partial^4 w}{\partial x^4} + 2(D_{12} + 2D_{66})\frac{\partial^4 w}{\partial x^2 \partial y^2} + D_{22}\frac{\partial^4 w}{\partial y^4} - 4D_{16}\frac{\partial^4 w}{\partial x^3 \partial y} - 4D_{26}\frac{\partial^4 w}{\partial x \partial y^3} \\ & = N_x \frac{\partial^2 w}{\partial x^2} + N_y \frac{\partial^2 w}{\partial y^2} + 2N_{xy} \frac{\partial^2 w}{\partial xy} \end{aligned} \quad (3.89)$$

and the out-of-plane stability equation (equation 3.83) will reduce to

$$\begin{aligned} & D_{11} \frac{\partial^4 w_1}{\partial x^4} + 2(D_{12} + 2D_{66}) \frac{\partial^4 w_1}{\partial x^2 \partial y^2} + D_{22} \frac{\partial^4 w_1}{\partial y^4} - 4D_{16} \frac{\partial^4 w_1}{\partial x^3 y} - 4D_{26} \frac{\partial^4 w_1}{\partial x y^3} \\ & = N_x \frac{\partial^2 w_1}{\partial x^2} + N_y \frac{\partial^2 w_1}{\partial y^2} + 2N_{xy} \frac{\partial^2 w_1}{\partial x y} \end{aligned} \quad (3.90)$$

which are exactly the same equations derived in literature [3, 4] for composite plates with constant stiffness.

If the bending-twisting couplings (D_{16}, D_{26}) are zero, the above two equations can further reduce into

$$D_{11} \frac{\partial^4 w}{\partial x^4} + 2(D_{12} + 2D_{66}) \frac{\partial^4 w}{\partial x^2 \partial y^2} + D_{22} \frac{\partial^4 w}{\partial y^4} = N_x \frac{\partial^2 w}{\partial x^2} + N_y \frac{\partial^2 w}{\partial y^2} + 2N_{xy} \frac{\partial^2 w}{\partial x y} \quad (3.91)$$

and

$$D_{11} \frac{\partial^4 w_1}{\partial x^4} + 2(D_{12} + 2D_{66}) \frac{\partial^4 w_1}{\partial x^2 \partial y^2} + D_{22} \frac{\partial^4 w_1}{\partial y^4} = N_x \frac{\partial^2 w_1}{\partial x^2} + N_y \frac{\partial^2 w_1}{\partial y^2} + 2N_{xy} \frac{\partial^2 w_1}{\partial x y} \quad (3.92)$$

If the loads applied on the panel are only N_x and N_y , the exact closed form solution, for instance Navier solution, to the buckling load of simply-supported plate can be obtained, as shown in many literature [2–5, 7]. If shear load is applied to the plate, Navier solution does not exist [3]. Approximated closed form solution only exists in some special cases [3, 7, 32], for instance long plate.

If the bending-twisting couplings are not zero and no shear load applied, the exact closed form solution (for instance, Navier solution) is still not available (to the best knowledge of the author). Then the approximation solutions, such as Galerkin method, Ritz method and Finite element method, are used to solve the buckling loads [3, 7].

In current thesis, A_{ij} and D_{ij} are functions of x and y , the bending-twisting couplings are retained and shear load might be applied, the equilibrium equation and stability equation are thus more complicated than these in literature. No closed form solutions have been obtained (to the best knowledge of the author). So the approximation solution, such as Galerkin method, is a more practical method to solve these equations.

3.3 Governing Equations for Shallow Cylindrical Shell

Similar to the previous section, the linear compatibility equation for shells is derived for prebuckling analysis, then the non-linear compatibility equation and stability equations for shells are derived for stability analysis in this section .

3.3.1 Equations for Prebuckling Analysis

For cylindrical shells, the strain-displacement relations are given as [5]

$$\epsilon_{xo} = u_{,x} \quad (3.93)$$

$$\epsilon_{yo} = v_{,y} - \frac{w}{R} \quad (3.94)$$

$$\gamma_{xyo} = u_{,y} + v_{,x} \quad (3.95)$$

where, the a new term $\frac{w}{R}$ is added to ϵ_{yo} due to the initial curvature of cylindrical shells.

Consequently the linear compatibility equation of shell derived from above relations contains one more term which related to the curvature as [5, 12]:

$$\epsilon_{xo,yy} + \epsilon_{yo,xx} - \gamma_{xyo,xy} = -\frac{1}{R}w_{,xx} \quad (3.96)$$

Similarly to plates, the compatibility equation can be written in terms of in-plane loads as

$$\begin{aligned} & \frac{\partial^2}{\partial y^2} [a_{11}(x, y)N_x + a_{12}(x, y)N_y + a_{16}(x, y)N_{xy}] \\ & + \frac{\partial^2}{\partial x^2} [a_{12}(x, y)N_x + a_{22}(x, y)N_y + a_{26}(x, y)N_{xy}] \\ & - \frac{\partial^2}{\partial xy} [a_{16}(x, y)N_x + a_{26}(x, y)N_y + a_{66}(x, y)N_{xy}] \\ & = -\frac{1}{R}w_{,xx} \end{aligned} \quad (3.97)$$

According to the assumption 1, the derivatives of w before buckling occurs are zero. Thus, above equation reduces into

$$\begin{aligned} & \frac{\partial^2}{\partial y^2} [a_{11}(x, y)N_x + a_{12}(x, y)N_y + a_{16}(x, y)N_{xy}] \\ & + \frac{\partial^2}{\partial x^2} [a_{12}(x, y)N_x + a_{22}(x, y)N_y + a_{26}(x, y)N_{xy}] \\ & - \frac{\partial^2}{\partial xy} [a_{16}(x, y)N_x + a_{26}(x, y)N_y + a_{66}(x, y)N_{xy}] \\ & = 0 \end{aligned} \quad (3.98)$$

which is exactly the same as the compatibility equation (equation 3.38) for plates.

The in-plane loads distribution can be solved from the compatibility equation (equation 3.98) derived here. It implies the in-plane loads distribution of shallow cylindrical shell panels is the same as plates with the same stiffness and under the same in-plane loads.

3.3.2 Equations for Stability Analysis

For moderate rotations, the equations relating mid-plane strains to displacements for cylindrical shells are [1, 5]

$$\epsilon_{xo} = u_{,x} + \frac{1}{2}w_{,x}^2 \quad (3.99)$$

$$\epsilon_{yo} = v_{,y} - \frac{w}{R} + \frac{1}{2}w_{,y}^2 \quad (3.100)$$

$$\gamma_{xyo} = u_{,y} + v_{,x} + w_{,x}w_{,y} \quad (3.101)$$

Then the non-linear compatibility equation for mid-plane strains is derived from above equations as

$$\epsilon_{xo,yy} + \epsilon_{yo,xx} - \gamma_{xyo,xy} = w_{,xy}^2 - w_{,xx}w_{,yy} - \frac{1}{R}w_{,xx} \quad (3.102)$$

The non-linear equilibrium differential equations of shells for moderate rotations are given in literature as [1, 5]

$$N_{x,x} + N_{xy,y} = 0 \quad (3.103)$$

$$N_{xy,x} + N_{y,y} = 0 \quad (3.104)$$

$$M_{x,xx} + 2M_{xy,xy} + M_{y,yy} + N_x w_{,xx} + 2N_{xy} w_{,xy} + N_y w_{,yy} + \frac{N_y}{R} = 0 \quad (3.105)$$

The out-of-plane equilibrium equation (equation 3.105) can be written in terms of w as

$$\begin{aligned} & \frac{\partial^2}{\partial x^2} [D_{11}(x, y)w_{,xx} + D_{12}(x, y)w_{,yy} + 2D_{16}(x, y)w_{,xy}] \\ & + 2\frac{\partial^2}{\partial xy} [D_{16}(x, y)w_{,xx} + D_{26}(x, y)w_{,yy} + 2D_{66}(x, y)w_{,xy}] \\ & + \frac{\partial^2}{\partial y^2} [D_{12}(x, y)w_{,xx} + D_{22}(x, y)w_{,yy} + 2D_{26}(x, y)w_{,xy}] \\ & = N_x w_{,xx} + 2N_{xy} w_{,xy} + N_y w_{,yy} + \frac{N_y}{R} \end{aligned} \quad (3.106)$$

The in-plane equilibrium equations (equation 3.103 3.104) can still be automatically satisfied by introducing the Airy stress function (equation 3.42) to the in-plane loads.

Similarly to plates, the stability differential equations can be derived by either applying adjacent-equilibrium criterion to the equilibrium differential equations or using minimum potential energy criterion. The reader is referred to the literature [1, 5] for the details of these criteria.

By applying the adjacent-equilibrium criterion to obtain the stability equations and compatibility equation (like the compatibility equation 3.84 for plates), similar derivations will be obtained as those for plates in section 3.2.2. Hence the derivations are not repeated again in this section. However, due to the additional term $\frac{w}{R}$ added to ϵ_{y0} , the derivations are slightly different. The corresponding stability and compatibility equation will have one more term resulting from the additional term $\frac{w}{R}$.

The stability equations are then obtained as

$$N_{x1,x} + N_{xy1,y} = 0 \quad (3.107)$$

$$N_{xy1,x} + N_{y1,y} = 0 \quad (3.108)$$

$$M_{x1,xx} + 2M_{xy1,xy} + M_{y1,yy} + N_x w_{1,xx} + 2N_{xy} w_{1,xy} + N_y w_{1,yy} + \frac{N_{y1}}{R} = 0 \quad (3.109)$$

Clearly, for shells the out-of-plane stability equation is different from the out-of-plane equilibrium equation (equation 3.105), because not only the equation is written in terms of the increments of moments and out-of-plane displacement but also the term related to curvature is written in term of the increment of in-plane load (N_{y1}) which was written in term of the in-plane load (N_y) in the equilibrium equation. This curvature term makes the buckling load of shell can only be solved from the stability equation. However, the buckling for plates can be solved from the equilibrium equation as what did by some researchers [2, 4] (while, it is not theoretically correct as indicated by Jones [5]).

The out-of-plane stability equation can be written in terms of w_1 as

$$\begin{aligned}
& \frac{\partial^2}{\partial x^2} [D_{11}(x, y)w_{1,xx} + D_{12}(x, y)w_{1,yy} + 2D_{16}(x, y)w_{1,xy}] \\
& + 2\frac{\partial^2}{\partial xy} [D_{16}(x, y)w_{1,xx} + D_{26}(x, y)w_{1,yy} + 2D_{66}(x, y)w_{1,xy}] \\
& + \frac{\partial^2}{\partial y^2} [D_{12}(x, y)w_{1,xx} + D_{22}(x, y)w_{1,yy} + 2D_{26}(x, y)w_{1,xy}] \\
& = N_x w_{1,xx} + 2N_{xy} w_{1,xy} + N_y w_{1,yy} + \frac{N_{y1}}{R}
\end{aligned} \tag{3.110}$$

The compatibility equation for stability analysis (corresponds to the equation 3.84 for plates) is obtained as

$$\epsilon_{xo1,yy} + \epsilon_{yo1,xx} - \gamma_{xyo1,xy} = -\frac{1}{R}w_{1,xx} \tag{3.111}$$

It can be rewritten in terms of N_{x1} , N_{y1} , N_{xy1} as

$$\begin{aligned}
& \frac{\partial^2}{\partial y^2} [a_{11}(x, y)N_{x1} + a_{12}(x, y)N_{y1} + a_{16}(x, y)N_{xy1}] \\
& + \frac{\partial^2}{\partial x^2} [a_{12}(x, y)N_{x1} + a_{22}(x, y)N_{y1} + a_{26}(x, y)N_{xy1}] \\
& - \frac{\partial^2}{\partial xy} [a_{16}(x, y)N_{x1} + a_{26}(x, y)N_{y1} + a_{66}(x, y)N_{xy1}] \\
& = -\frac{1}{R}w_{1,xx}
\end{aligned} \tag{3.112}$$

If introducing the increments of Airy stress function (equation 3.86) to N_{x1} , N_{y1} , N_{xy1} , the in-plane stability differential equations (equation 3.107 and 3.108) are automatically satisfied.

Then the out-of-plane stability differential equation (equation 3.110) can be written in terms of Airy stress function and its increment as

$$\begin{aligned}
& \frac{\partial^2}{\partial x^2} [D_{11}(x, y)w_{1,xx} + D_{12}(x, y)w_{1,yy} + 2D_{16}(x, y)w_{1,xy}] \\
& + 2\frac{\partial^2}{\partial xy} [D_{16}(x, y)w_{1,xx} + D_{26}(x, y)w_{1,yy} + 2D_{66}(x, y)w_{1,xy}] \\
& + \frac{\partial^2}{\partial y^2} [D_{12}(x, y)w_{1,xx} + D_{22}(x, y)w_{1,yy} + 2D_{26}(x, y)w_{1,xy}] \\
& = F_{,yy}w_{1,xx} - 2F_{,xy}w_{1,xy} + F_{,xx}w_{1,yy} + \frac{F_{1,xx}}{R}
\end{aligned} \tag{3.113}$$

The compatibility equation (equation 3.112) for stability analysis can be written in terms of the increment of Airy stress function as

$$\begin{aligned}
& \frac{\partial^2}{\partial y^2} [a_{11}(x, y)F_{1,yy} + a_{12}(x, y)F_{1,xx} - a_{16}(x, y)F_{1,xy}] \\
& + \frac{\partial^2}{\partial x^2} [a_{12}(x, y)F_{1,yy} + a_{22}(x, y)F_{1,xx} - a_{26}(x, y)F_{1,xy}] \\
& - \frac{\partial^2}{\partial xy} [a_{16}(x, y)F_{1,yy} + a_{26}(x, y)F_{1,xx} - a_{66}(x, y)F_{1,xy}] \\
& = -\frac{1}{R}w_{1,xx}
\end{aligned} \tag{3.114}$$

The compatibility equation (equation 3.112 or 3.114) for stability analysis is of significant importance for shells, since it shows the increment of in-plane loads (or Airy stress function) is related to the increment of displacement. So this equation have to be solved together with the out-of-plane stability equation to obtain the buckling load. However, for plates the increment of in-plane loads (or Airy stress function) is not related to the increment of displacement since the terms with curvature vanish as shown in equation 3.85 and 3.88.

If the radius of shells is infinite large ($\frac{1}{R} = 0$), all the equations derived for shells will reduce to the equations derived for plates.

As mentioned in section 3.2.3, closed form solutions are barely developed to solve these governing differential equations. Therefore, the Galerkin method is introduced to solve these equations approximately.

3.4 Galerkin method

In mathematics, the Galerkin method is one of the weighted-residual methods which are used to solve a differential equation by converting it into a set of discrete equations [3]. Consider a differential equation as

$$L[w(x)] = f \quad (3.115)$$

where, L is the differential operator, $w(x)$ is the unknown function which needs to be determined.

The w is approximated by a set of linear independent functions as

$$w \approx W_N = \sum_{i=1}^N c_i \varphi_i + \varphi_0 \quad (3.116)$$

where, W_N is the approximation of w , c_i is the undetermined parameter, φ_i and φ_0 are the shape functions, N is the number of terms used for approximating the exact solution w .

The approximation is only exact when N is infinite. Since the solution W_N is an approximation to the exact solution w , a certain residual of the approximation exists after substituting the approximation back to the differential equation.

$$R_N = L \left[\sum_{i=1}^N c_i \varphi_i + \varphi_0 \right] - f \quad (3.117)$$

where, R_N is the residual when N terms are used.

The residual is required to be orthogonal to each of the shape functions φ_i ,

$$\int R_N \varphi_i dx = 0 \quad (i = 1, 2, \dots, N) \quad (3.118)$$

The undetermined parameter c_i can be solved from above N equations. Since the shape functions are known beforehand, the approximated solution W_N is obtained. As the number of terms increases, the approximation will be increasingly closer to the exact solution. When N is infinite, the approximation is exact and the differential equation is solved exactly. The mathematical explanation and demonstration will not be shown here, however, they can be found in literature [3, 15].

In Galerkin method, the assumed shape functions should have the following properties [3]:

- 1 φ_0 should satisfy the specified essential and natural boundary conditions; it plays the role of particular solution to the differential equation.
- 2 φ_i plays the role of homogeneous solution to the differential equation:
 - It satisfies the homogeneous form of essential and natural boundary conditions
 - The set of φ_i should be linearly independent and complete.

The completeness property is defined mathematically in literature [3] as follows. Given a function w and a real number $\epsilon > 0$, the set of φ_i is complete if there exists an integer N (which depends on ϵ) and scalar parameters c_i such that

$$\| w - \sum_1^N c_i \varphi_i \| < \epsilon \quad (3.119)$$

where, $\| \cdot \|$ denotes a norm.

3.4.1 Prebuckling Analysis

In this section, the Galerkin method is applied to solve the in-plane loads distribution from the compatibility equation (equation 3.43 and 3.98). Since the compatibility equations for plates and shells are the same, either of them can be applied here.

Considering a panel with variable stiffness under a constant applied load \bar{N}_x , the Airy stress function can be assumed as

$$F(x, y) = \frac{1}{2} \bar{N}_x y^2 + \sum_{k=1}^K \sum_{l=1}^L F_{kl} X_k(x) Y_l(y) \quad (3.120)$$

F_{kl} is the undetermined parameter. X_k and Y_l are the shape functions used in x and y direction, respectively. K and L are the numbers of shape functions used in x and y direction, respectively. For simplicity, above equation is written as

$$F(x, y) = \frac{1}{2} \bar{N}_x y^2 + \sum_{kl}^{KL} F_{kl} X_k(x) Y_l(y) \quad (3.121)$$

In the following chapters, similar simplifications are used.

Clearly, the first term $\frac{1}{2} \bar{N}_x y^2$ plays the role of φ_0 as the particular solution in equation 3.116 and X_k (and Y_l) plays the role of φ_i as the homogeneous solution.

Applying the Galerkin method to the compatibility equation (equation 3.43 or 3.98), a set of equations are obtained as follows.

$$\begin{aligned} & \int_0^a \int_0^b \left\{ \frac{\partial^2}{\partial y^2} [a_{11}(x, y) F_{,yy} + a_{12}(x, y) F_{,xx} - a_{16}(x, y) F_{,xy}] \right. \\ & + \frac{\partial^2}{\partial x^2} [a_{12}(x, y) F_{,yy} + a_{22}(x, y) F_{,xx} - a_{26}(x, y) F_{,xy}] \\ & \left. - \frac{\partial^2}{\partial xy} [a_{16}(x, y) F_{,yy} + a_{26}(x, y) F_{,xx} - a_{66}(x, y) F_{,xy}] \right\} X_k(x) Y_l(y) dx dy = 0 \\ & (k = 1, 2, \dots, K \text{ and } l = 1, 2, \dots, L) \end{aligned} \quad (3.122)$$

If the applied load (\bar{N}_x) and shape functions (X_k and Y_l) are assigned to the Airy stress function (F), above equations form $K \times L$ linear equations in $K \times L$ unknown parameters (F_{kl}). Then the $K \times L$ unknown parameters can be directly solved from the $K \times L$ linear equations. Then the approximated solution of Airy stress function will be obtained.

3.4.2 Stability Analysis

To determine buckling initiation, it is convenient to introduce the buckling factor to the Airy stress function as

$$F(x, y) = \lambda \left[\frac{1}{2} \bar{N}_x y^2 + \sum_{kl} F_{kl} X_k(x) Y_l(y) \right] \quad (3.123)$$

where, λ is the buckling factor.

The critical buckling factor determines the stability of panels under a certain applied load \bar{N}_x . In other words, the buckling load of the panel is $\lambda \bar{N}_x$.

The increment of the out-of-plane displacement is approximated as

$$w_1 = \sum_{pq} W_{pq}^1 X_p(x) Y_q(y) \quad (3.124)$$

W_{pq}^1 is the undetermined parameter. X_p and Y_q are the shape functions used in x and y direction, respectively. P and Q are the numbers of shape functions used in x and y direction, respectively.

Clearly, the φ_0 in equation 3.116 as the particular solution does not exist in above equation and X_k (and Y_l) plays the role of φ_i as the homogeneous solution. The reason is the initial out-of-plane deflection is zero.

For plates, Applying Galerkin method to the out-of-plane stability equation (equation 3.87) and introducing the buckling factor to the Airy stress function (as shown in equation 3.123), a set of linear equations are obtained as

$$\begin{aligned} & \int_0^a \int_0^b \left\{ \frac{\partial^2}{\partial x^2} [D_{11}(x, y)w_{1,xx} + D_{12}(x, y)w_{1,yy} + 2D_{16}(x, y)w_{1,xy}] \right. \\ & + 2 \frac{\partial^2}{\partial xy} [D_{16}(x, y)w_{1,xx} + D_{26}(x, y)w_{1,yy} + 2D_{66}(x, y)w_{1,xy}] \\ & + \frac{\partial^2}{\partial y^2} [D_{12}(x, y)w_{1,xx} + D_{22}(x, y)w_{1,yy} + 2D_{26}(x, y)w_{1,xy}] \\ & \left. - \lambda [F_{,xx}w_{1,xx} - 2F_{,xy}w_{1,xy} + F_{,yy}w_{1,yy}] \right\} X_p(x) Y_q(y) dx dy = 0 \\ & (p = 1, 2, \dots, P \text{ and } q = 1, 2, \dots, Q) \end{aligned} \quad (3.125)$$

where, the Airy stress function F is solved from the compatibility equation (equation 3.122) in prebuckling analysis.

If the shape functions (X_p and Y_q) are assigned to the increment of displacement (w_1), above equations form $P \times Q$ homogeneous equations which have $P \times Q$ unknown parameters W_{pq}^1 and the unknown buckling factor λ . These equations can be written in the form of matrix, where

a set of W_{pq}^1 play the role of eigenvector and λ plays the role of eigenvalue. Then λ is solved from the matrix as a set of eigenvalues, where the lowest one determines the most critical buckling load. While, the eigenvectors determine the buckling mode shape corresponding to each buckling factor.

For shells, if applying the Galerkin method to the stability equation (equation 3.113) and introducing the buckling factor to Airy stress function (as shown in equation 3.123), a set of linear equations are obtained as

$$\begin{aligned}
& \int_0^a \int_0^b \left\{ \frac{\partial^2}{\partial x^2} [D_{11}(x, y)w_{1,xx} + D_{12}(x, y)w_{1,yy} + 2D_{16}(x, y)w_{1,xy}] \right. \\
& + 2 \frac{\partial^2}{\partial xy} [D_{16}(x, y)w_{1,xx} + D_{26}(x, y)w_{1,yy} + 2D_{66}(x, y)w_{1,xy}] \\
& + \frac{\partial^2}{\partial y^2} [D_{12}(x, y)w_{1,xx} + D_{22}(x, y)w_{1,yy} + 2D_{26}(x, y)w_{1,xy}] \\
& \left. - \lambda [F_{,yy}w_{1,xx} - 2F_{,xy}w_{1,xy} + F_{,xx}w_{1,yy}] - \frac{F_{1,xx}}{R} \right\} X_p(x)Y_q(y)dx dy = 0 \\
& (p = 1, 2, \dots, P \text{ and } q = 1, 2, \dots, Q)
\end{aligned} \tag{3.126}$$

where, the Airy stress function F is solved from the compatibility equation (equation 3.122) in the prebuckling analysis.

However, due to the presence of the $\frac{F_{1,xx}}{R}$ term an additional compatibility equation for the Airy stress function F_1 has to be solved along with the out-of-plane stability equation. As mentioned in the end of section 3.3.2, the increment of Airy stress function (F_1) of shells is connected to the increment of out-of-plane displacement (w_1) through the compatibility equation for stability analysis (equation 3.114). So to get rid of the additional term ($\frac{F_{1,xx}}{R}$) in above equation, the compatibility equation for stability analysis (equation 3.114) should be utilized.

Similarly to Airy stress function (F), the increment of Airy stress function (F_1) is approximated as

$$F_1(x, y) = \sum_{kl}^{K_1 L_1} F_{kl}^1 X_k(x) Y_l(y) \tag{3.127}$$

F_{kl}^1 is the undetermined parameter. K_1 and L_1 are the numbers of shape functions used in x and y direction, respectively.

Applying Galerkin method to the compatibility equation for stability analysis (equation 3.114), a set of equations are obtained as

$$\begin{aligned}
& \int_0^a \int_0^b \left\{ \frac{\partial^2}{\partial y^2} [a_{11}(x, y)F_{1,yy} + a_{12}(x, y)F_{1,xx} - a_{16}(x, y)F_{1,xy}] \right. \\
& + \frac{\partial^2}{\partial x^2} [a_{12}(x, y)F_{1,yy} + a_{22}(x, y)F_{1,xx} - a_{26}(x, y)F_{1,xy}] \\
& - \frac{\partial^2}{\partial xy} [a_{16}(x, y)F_{1,yy} + a_{26}(x, y)F_{1,xx} - a_{66}(x, y)F_{1,xy}] \\
& \left. + \frac{1}{R} w_{1,xx} \right\} X_k(x) Y_l(y) dx dy = 0 \\
& (k = 1, 2, \dots, K_1 \text{ and } l = 1, 2, \dots, L_1)
\end{aligned} \tag{3.128}$$

Above equations form $K_1 \times L_1$ linear equations, which have $K_1 \times L_1$ unknown parameters F_{kl}^1 and $P \times Q$ unknown parameters W_{pq}^1 . The unknown parameters F_{kl}^1 can be solved in terms of W_{pq}^1 from above equations. Then substituting them back to the stability equations (equation 3.126), the stability equations completely get rid of the increment of Airy stress function (F_1) in the additional term ($\frac{F_{1,xx}}{R}$). Therefore, the buckling factor can be solved as the eigenvalue of the matrix form of the stability equations.

3.4.3 Approximation of Stiffness

The task was to analyze panels with variable stiffness, however the stiffness can assume arbitrary value across the plate (continuously varying through steering the fiber orientation or piece-wise constant, etc.). However, the variation of stiffness in this thesis is simplified to a few sections each having their own constant stiffness defined by fiber direction. Examples are shown in Figure 3.3, where the panel is divided into 4 and 16 sections, respectively. The reason for the simplicity is that the steering of fiber orientation is not easy to be assigned to the model in Abaqus, especially to the models of shells. Due to the limitation of time, this simplification has been adopted.

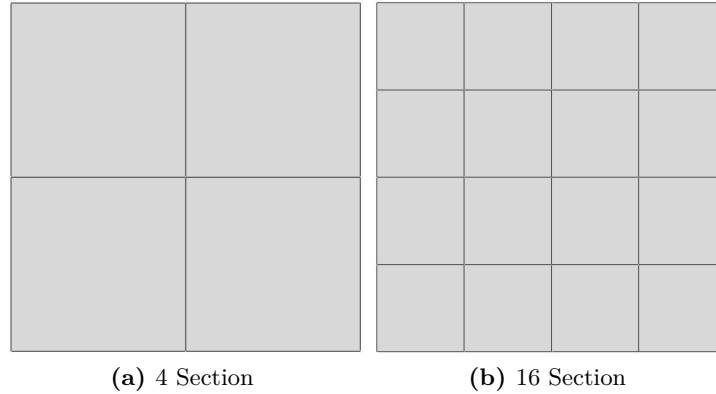


Figure 3.3: Variable Stiffness: sections

Therefore, the stiffness is a piecewise function instead of a continuous function. The governing equations require the derivatives of the stiffness across the panel. In the case of a piece-wise constant stiffness panels, the derivatives are zero inside of each section but infinity at the boundaries of neighboring sections which cause many numerical problems when evaluating the Galerkin integrals. To solve this problem, a set of series can be applied to approximate the stiffness. One example is the Fourier series, where the membrane and bending stiffness are approximated by double Fourier series as

$$\bar{a}_{ij}(x, y) = \sum_m^M \sum_n^N \bar{a}_{ij}(m, n) \sin \frac{m\pi x}{a} \sin \frac{n\pi y}{b} \quad (3.129)$$

$$\bar{D}_{ij}(x, y) = \sum_m^M \sum_n^N \bar{D}_{ij}(m, n) \sin \frac{m\pi x}{a} \sin \frac{n\pi y}{b} \quad (3.130)$$

where, the index $i, j = 1, 2, 6$, \bar{a}_{ij} and \bar{D}_{ij} are the approximations of a_{ij} and D_{ij} , M, N are the number of Fourier series used in x and y direction, and $\bar{a}_{ij}(m, n), \bar{D}_{ij}(m, n)$ are expressed as

$$\bar{a}_{ij}(m, n) = \frac{4}{ab} \int_0^a \int_0^b a_{ij}(x, y) \sin \frac{m\pi x}{a} \sin \frac{n\pi y}{b} dx dy \quad (3.131)$$

$$\bar{D}_{ij}(m, n) = \frac{4}{ab} \int_0^a \int_0^b D_{ij}(x, y) \sin \frac{m\pi x}{a} \sin \frac{n\pi y}{b} dx dy \quad (3.132)$$

Besides the sine functions, cosine functions can also be applied in Fourier series. An example of the approximation using sine function is given in Figure 3.4 when $M = N = 50$ terms of series are used to approximate the bending stiffness D_{11} of a plate with four section. Clearly, the approximation is very close to the exact stiffness.

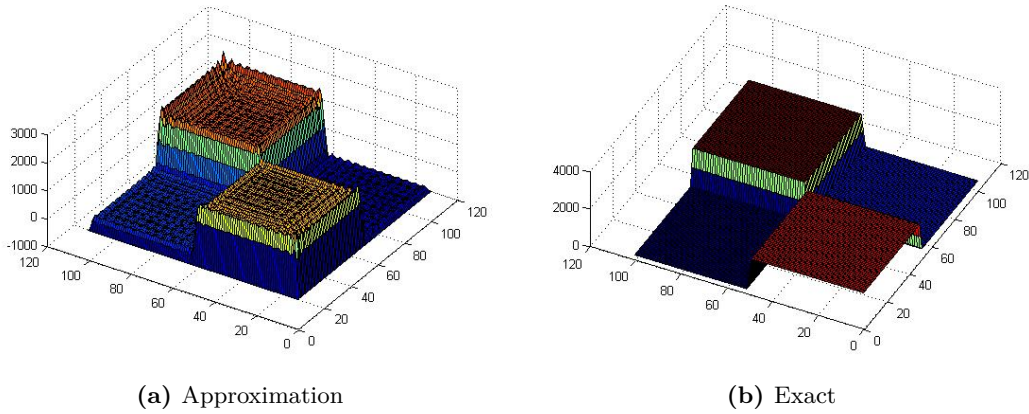


Figure 3.4: Approximation of D_{11} of plate with 4 sections

Since the stiffness is approximately expressed by Fourier series, the derivatives of the stiffness will never be vanish. Substituting the Fourier series back to the compatibility and stability equations, the in-plane loads and buckling factors can be solved.

However, a large number of terms in Fourier series are required to better approximate the stiffness, the efficiency of Galerkin method is reduced. Even a large number of series are used, the approximation of stiffness is still not exact which reduces the accuracy of the in-plane loads and buckling factor.

However, if the stiffness is continuous and can be described exactly by a continuous function, the approximation using series is not necessary.

3.4.4 Boundary Integral

One of the requirements of the Galerkin method is that the shape functions should satisfy both essential and natural boundary conditions. However, it is not always easy to find a shape function which can satisfy the natural boundary conditions of composite panels.

For example, for simply-supported panels the natural boundary condition is that the moments are zero at the boundaries, namely

$$M_x = -D_{11}w_{,xx} - D_{12}w_{,yy} - 2D_{16}w_{,xy} = 0 \quad (\text{on } x = 0, a) \quad (3.133)$$

$$M_y = -D_{12}w_{,xx} - D_{22}w_{,yy} - 2D_{26}w_{,xy} = 0 \quad (\text{on } y = 0, b) \quad (3.134)$$

When $D_{16} = 0$ and $D_{26} = 0$, the displacement w can be assumed as

$$w = \sum_{pq}^{PQ} W_{pq} \sin \frac{p\pi x}{a} \sin \frac{q\pi y}{b} \quad (3.135)$$

which can exactly satisfy the natural boundary condition.

However, when $D_{16} \neq 0$ and $D_{26} \neq 0$, it is difficulty to find a shape function which satisfies the natural boundary condition. Hence the accuracy of the buckling load prediction is decreased.

The solution to this problem is to add an additional boundary integral, which includes the natural boundary conditions, into the stability equation [2, 12] as

$$\begin{aligned} & \int_0^b [M_x \frac{\partial X_p(x)}{\partial x} Y_q(y)]_{x=a} - [M_x \frac{\partial X_p(x)}{\partial x} Y_q(y)]_{x=0} dy \\ & + \int_0^a [M_y X_p(x) \frac{\partial Y_q(y)}{\partial y}]_{y=b} - [M_y X_p(x) \frac{\partial Y_q(y)}{\partial y}]_{y=0} dx \end{aligned} \quad (3.136)$$

This boundary integral is the result of integration by parts in the derivation of the governing differential equations using the energy approach (virtual work principle or variational principle) [2, 13, 33].

A brief example is given by Zhang and Matthews [13] for the derivation of equilibrium equation using the virtual displacement principle,

$$\begin{aligned} & \int_0^a \int_0^b [M_{x,xx} + M_{y,yy} + 2M_{xy,xy} + \frac{N_y}{R} + N_x w_{,xx} + N_y w_{,yy} + 2N_{xy} w_{,xy}] \delta w dx dy \\ & + \int_0^b [M_x \delta w_x]_{x=a} - [M_x \delta w_x]_{x=0} dy + \int_0^a [M_y \delta w_y]_{y=b} - [M_y \delta w_y]_{y=0} dx = 0 \end{aligned} \quad (3.137)$$

Since the virtual displacement δw (which is called the variation of w in variational principle) and the virtual slopes (δw_x , δw_y) are arbitrary, to satisfy above equation the expressions in the brackets have to be zero individually. In other words,

$$M_{x,xx} + M_{y,yy} + 2M_{xy,xy} + \frac{N_y}{R} + N_x w_{,xx} + N_y w_{,yy} + 2N_{xy} w_{,xy} = 0 \quad (3.138)$$

$$M_x(x = a) = M_x(x = 0) = M_y(y = b) = M_y(y = 0) = 0 \quad (3.139)$$

The first equation obtained is exactly the out-of-plane equilibrium equation of shells (the same as equation 3.105). The rest equations are exactly the natural boundary conditions.

When applying the Galerkin method to solve the above equilibrium equation, the natural boundary conditions are satisfied by the assumed shape function of displacement (w). So the boundary integral does not have to be included in the equation. However, when the natural boundary conditions cannot be satisfied by the assumed shape function, the complete equation (equation 3.137) which includes the boundary integral must be used in order to satisfy the natural boundary conditions.

For stability analysis, similar derivations will be shown and the boundary integral (3.136) has to be added into the stability equation to satisfy the natural boundary conditions.

3.5 Summary

In this chapter, the governing differential equations for plates and shallow cylindrical shells have been derived based on the assumptions made in section 3.1.3. Due to the difficulty in solving these governing differential equations analytically, Galerkin method is introduced to achieve the approximated solutions. In principle, Galerkin method is a suitable choice. However, due to the discontinuity in the stiffness of the panels considered, the discontinuous stiffness has to be approximated by continuous functions, such as Fourier series. Since a lot of terms of series are required to approximate the stiffness, the efficiency of the model will be reduced while the stiffness is still not exact unless infinite number of series are used. Therefore, a similar approximation method, Ritz method, is introduced in the next chapter where the stiffness are expressed exactly as they are. The assumptions made in this chapter and the basic equations are still valid in the following chapters.

Ritz Method

4.1 Introduction

Ritz method bypasses the derivation of the governing differential equations, and goes directly from the variational statements of the problem, such as the principle of minimum potential energy, which are equivalent to the governing differential equations and the corresponding natural boundary conditions [3].

Similar to Galerkin method, in Ritz method the unknown variable (for example, the displacement w) is approximated by a finite linear combination of the shape functions with undetermined parameters [3]

$$w \approx W_N = \sum_{j=1}^N c_j \varphi_j + \varphi_0 \quad (4.1)$$

where, c_j denotes the undetermined parameters, φ_j and φ_0 are the selected shape functions.

The selected shape functions have to meet the following requirements [3]

- φ_0 should satisfy the specified essential (or geometric) boundary conditions, which plays the role of particular solution.
- φ_j should satisfy the homogeneous form of the essential boundary conditions. In addition,
 - φ_j should be linearly independent.
 - φ_j should form a complete system of functions.

Compared to Galerkin method, Ritz method has several advantages

- Only the essential boundary condition should be satisfied by the shape function in Ritz method [3]. The natural boundary condition is not required to be satisfied by the shape function in Ritz method [19].

- It avoids using Fourier series to approximate the stiffness variation, thus increasing the efficiency and accuracy.
- The extra boundary integral (equation 3.136) is automatically included in the variational statements using the Ritz method.

Although the selected shape functions in Ritz method do not have to satisfy the natural boundary conditions, however, if they do the approximations are better, usually substantially better [15]. Moreover, the shape functions are not required to be orthogonal to each other in Ritz method. But for computational accuracy and convenience, it is advantageous to choose orthogonal shape functions [15].

Before applying Ritz method, the first step is to derive the total complementary energy of the panels in the prebuckling state, from which the in-plane loads will be solved, and the total energy functional for buckling analysis, from which the buckling are determined. The terminology 'total energy functional' has been used here because it is a mixture of complementary energy and strain energy. The detailed derivation of the total energy functional will be shown in this chapter.

As indicated in the literature review (section 2.2.1), there is an argument indicated by Jones [5], that whether the energy done by the in-plane loads during buckling should be regarded as the work done by the external loads or part of the membrane strain energy. Jones clearly indicated that this energy was derived from the membrane strain and was a part of the membrane strain energy. However, in other literature this energy term was still regarded as the work done by the external loads [2, 4, 7, 11, 28]. In this chapter, this energy term will be derived and proved to be a part of the membrane energy, not the external work.

In the section of Galerkin method, the panels are considered as only under the prescribed loads. However, the constant loads applied on the edges of the panels with variable stiffness, will result in variable deformations on the edges. In experiments, the edges of the panels are normally restrained as straight and rather the prescribed displacements are applied since the constant prescribed loads are very difficult to be applied to the panels. Therefore, in this chapter, buckling of panels under prescribed displacements (end-shortening) on the edges is also considered. The corresponding energy functional (for both prebuckling analysis and stability analysis) will be derived considering these two load cases in section 4.3 and 4.4 of this chapter.

Ritz method will be applied to the derived energy functionals for plates and shells in section 4.5 and 4.6, respectively. The equations equivalent to the governing differential equations in previous chapter will be derived, among which the stability equations are obtained by applying the adjacent-equilibrium criterion or the principle of minimum potential energy (second variation of total energy functional or Trefftz buckling criterion).

4.2 Strain Energy in Bending and Stretching of Laminated Panels

The strain energy of an elastic body is given as [2, 4]

$$U = \frac{1}{2} \int \int \int (\sigma_x \epsilon_x + \sigma_y \epsilon_y + \sigma_z \epsilon_z + \tau_{xz} \gamma_{xz} + \tau_{yz} \gamma_{yz} + \tau_{xy} \gamma_{xy}) dx dy dz \quad (4.2)$$

The strain energy for thin panels can be simplified according to the Kirchhoff assumptions (section 3.1.3) since ϵ_z , γ_{xz} and γ_{yz} are zero.

$$U = \frac{1}{2} \int \int \int (\sigma_x \epsilon_x + \sigma_y \epsilon_y + \tau_{xy} \gamma_{xy}) dx dy dz \quad (4.3)$$

For symmetric laminated plates, where the stretching-bending couplings are zero ($\mathbf{B} = \mathbf{O}$), the strain energy becomes [7]

$$\begin{aligned} U = & \frac{1}{2} \int \int [A_{11}(\epsilon_{xo})^2 + 2A_{12}(\epsilon_{xo})(\epsilon_{yo}) + 2A_{16}(\epsilon_{xo})(\gamma_{xyo}) + A_{22}(\epsilon_{yo})^2 \\ & + 2A_{26}(\epsilon_{yo})(\gamma_{xyo}) + A_{66}(\gamma_{xyo})^2] dx dy \\ & + \frac{1}{2} \int \int [D_{11}\kappa_x^2 + 2D_{12}\kappa_x\kappa_y + 4D_{16}\kappa_x\kappa_{xy} + D_{22}\kappa_y^2 + 4D_{26}\kappa_y\kappa_{xy} + 4D_{66}\kappa_{xy}^2] dx dy \end{aligned} \quad (4.4)$$

where, the first term is the membrane strain energy

$$\begin{aligned} U_m = & \frac{1}{2} \int \int [A_{11}(\epsilon_{xo})^2 + 2A_{12}(\epsilon_{xo})(\epsilon_{yo}) + 2A_{16}(\epsilon_{xo})(\gamma_{xyo}) + A_{22}(\epsilon_{yo})^2 \\ & + 2A_{26}(\epsilon_{yo})(\gamma_{xyo}) + A_{66}(\gamma_{xyo})^2] dx dy \end{aligned} \quad (4.5)$$

and the second term is the bending strain energy

$$U_b = \frac{1}{2} \int \int [D_{11}\kappa_x^2 + 2D_{12}\kappa_x\kappa_y + 4D_{16}\kappa_x\kappa_{xy} + D_{22}\kappa_y^2 + 4D_{26}\kappa_y\kappa_{xy} + 4D_{66}\kappa_{xy}^2] dx dy \quad (4.6)$$

The reader is referred to the literature [2, 4, 7] for detailed derivation of these equations.

4.3 Total Energy Functional for Prebuckling Analysis

In this section, the total complementary energy of a panel in prebuckling state is derived. In Section 4.3.1, the panel is considered under a general load case where both external loads and displacements are prescribed. Then in Section 4.3.2 and 4.3.3, the panel is considered only under prescribed loads and displacements, respectively.

Based on the assumption 2 in Chapter 3, the out-of-plane displacements w of both plates and shallow cylindrical shell are zero in the prebuckling state. So the strain-displacement relations of cylindrical shells (equation 3.93, 3.94 and 3.95) reduce

$$\epsilon_{xo} = u_{,x}, \epsilon_{yo} = v_{,y}, \gamma_{xyo} = v_{,x} + u_{,y} \quad (4.7)$$

which are the same as those of plates.

Therefore, the membrane behaviors of plates and shells are the same in the prebuckling state. The total energy functional derived in this section is suitable for both plates and shells.

Moreover, a panel only deforms in stretching in the pre-buckling state. The strain energy comprises the membrane strain energy (equation 4.5) which can be expressed in terms of displacements (u, v, w) through the strain-displacement relations as

$$\begin{aligned} U_m = & \frac{1}{2} \int \int [A_{11}u_{,x}^2 + 2A_{12}u_{,x}v_{,y} + 2A_{16}u_{,x}(v_{,x} + u_{,y}) + A_{22}v_{,y}^2 \\ & + 2A_{26}v_{,y}(v_{,x} + u_{,y}) + A_{66}(v_{,x} + u_{,y})^2] dx dy \end{aligned} \quad (4.8)$$

4.3.1 Prescribed Loads and Displacements

In this section, a general load case, where a panel is under both the prescribed external loads and prescribed displacements on the boundaries, has been considered. The boundary of the panel can be divided into two parts from the viewpoint of the boundary conditions. The part over which boundary conditions are prescribed in terms of external loads is defined as $S1$; the part over which boundary conditions are prescribed in terms of displacements is defined as $S2$. The sum of them, $S = S1 + S2$, is the total boundary of the panels, as shown in Figure 4.1. For a rectangular plate, the total boundary is comprised of the four straight edges. The equations derived for this general load case can be reduced to the equations for the case of only prescribed loads or displacements, respectively, in the following two sections.

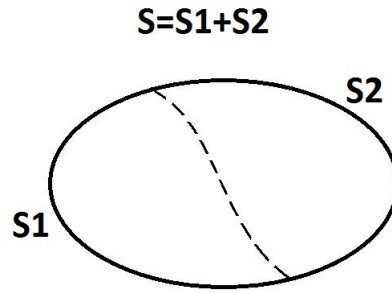


Figure 4.1: Boundary of of a free body

Consider a panel under prescribed loads $\bar{N}_x, \bar{N}_y, \bar{N}_{xy}$ on the boundary $S1$ and prescribed displacements \bar{u}, \bar{v} on the boundary $S2$.

The mechanical boundary conditions are

$$N_x = \bar{N}_x, N_y = \bar{N}_y, N_{xy} = \bar{N}_{xy} \text{ (on } S1) \quad (4.9)$$

The geometrical boundary conditions are

$$u = \bar{u}, v = \bar{v} \text{ (on } S2) \quad (4.10)$$

The total potential energy of the panel in stretching is given as [33]

$$\Pi_{pre} = U_m + V_{S1} \quad (4.11)$$

where, Π_{pre} is the total potential energy in prebuckling state, V_{S1} is the work done by the prescribed loads on boundary $S1$ in stretching.

Note that the work done by the prescribed displacements on boundary $S2$ is a complementary work, so it does not contribute to the total potential energy.

The membrane strain energy U_m is given as (equation 4.8)

$$U_m = \frac{1}{2} \int \int [(A_{11}(u,x)^2 + 2A_{12}(u,x)(v,y) + 2A_{16}(u,x)(v_x + u_y) + A_{22}(v,y)^2 + 2A_{26}(v,y)(v_x + u_y) + A_{66}(v_x + u_y)^2] dx dy \quad (4.12)$$

and the external work done on the boundary $S1$ is given in literature [5] as

$$V_{S1} = + \oint_{C_y} (\bar{N}_y v + \bar{N}_{xy} u) dx - \oint_{C_x} (\bar{N}_x u + \bar{N}_{xy} v) dy \quad (4.13)$$

For rectangular plates or cylindrical shells (as shown in Figure 3.1 and 3.2), the external work can be written as

$$V_{S1} = - \int_{S1} [(\bar{N}_y v + \bar{N}_{xy} u)_{y=b} - (\bar{N}_y v + \bar{N}_{xy} u)_{y=0}] dx - \int_{S1} [(\bar{N}_x u + \bar{N}_{xy} v)_{x=a} - (\bar{N}_x u + \bar{N}_{xy} v)_{x=0}] dy \quad (4.14)$$

Instead of total potential energy, the total complementary energy of the panel can be introduced, which is given as [28, 29, 33]

$$\Pi_{pre}^c = U_m^c + V_{S2} \quad (4.15)$$

where, Π_{pre}^c is the total complementary energy, U_m^c is the membrane complementary energy and V_{S2} is the complementary work done by the prescribed displacements on boundary $S2$.

Note that the work done by the prescribed loads on boundary $S1$ is a potential work, which does not contribute to the total complementary energy.

The membrane complementary energy U_m^c is given as [7, 28]

$$U_m^c = \frac{1}{2} \int \int a_{11} N_x^2 + 2a_{12} N_x N_y + 2a_{16} N_x N_y + a_{22} N_y^2 + 2a_{26} N_y N_{xy} + a_{66} N_{xy}^2 dx dy \quad (4.16)$$

The complementary work done on boundary $S2$ is [28, 33]

$$V_{S2} = - \int_{S2} (N_y \bar{v} + N_{xy} \bar{u})_{y=b} - (N_y \bar{v} + N_{xy} \bar{u})_{y=0} dx - \int_{S2} (N_x \bar{u} + N_{xy} \bar{v})_{x=a} - (N_x \bar{u} + N_{xy} \bar{v})_{x=0} dy \quad (4.17)$$

Moreover, it is noted that the total potential energy Π_{pre} (equation 4.11) can be transformed into

$$\Pi_{pre} = -U_m^c - V_{S2} = -\Pi_{pre}^c \quad (4.18)$$

The detail of the derivations is shown in Appendix A.

Above equation indicates that even if the total potential energy was utilized in the beginning, it can be transformed into the negative of total complementary energy where the in-plane loads are the variables instead of displacements or strains. As just mentioned that the work V_{S2} done by the prescribed displacements is complementary work, so it only appears in the expression for total complementary energy, as shown in equation 4.15 and 4.18. Similarly, the external work V_{S1} done by the prescribed loads is only shown in the total potential energy (equation 4.11) and is disappeared when the total potential energy transforms into the negative of total complementary energy (equation 4.18).

If making these two energy functionals, Π_{pre} (equation 4.18) and Π_{pre}^c (equation 4.15), stationary with respect to the unknown variables (in this case they are N_x , N_y and N_{xy}), the total complementary energy Π_{pre}^c will be minimized with respect to the unknown variables, however, the total potential energy Π_{pre} will be maximized since it is the negative of Π_{pre}^c .

However, both of Π_{pre} and Π_{pre}^c can be used to solve the in-plane loads distribution in Ritz method, as long as they are stationary with respect to the unknowns loads.

To reduce the number of unknowns (N_x , N_y and N_{xy}) and satisfy the in-plane equilibrium equations (equation 3.39 3.40 or equation A.21 A.22), the Airy stress function (equation 3.42) is introduced as

$$N_x = F_{,yy}, \quad N_y = F_{,xx}, \quad N_{xy} = -F_{,xy} \quad (4.19)$$

Then the total complementary energy (equation 4.15) can be rewritten as (in the form of matrix)

$$\begin{aligned} \Pi_{pre}^c = & \frac{1}{2} \int \int (\mathbf{f}^T \mathbf{A}^{-1} \mathbf{f}) dx dy \\ & - \int_{S_2} (F_{,xx} \bar{v} - F_{,xy} \bar{u})_{y=b} - (F_{,xx} \bar{v} - F_{,xy} \bar{u})_{y=0} dx \\ & - \int_{S_2} (F_{,yy} \bar{u} - F_{,xy} \bar{v})_{x=a} - (F_{,yy} \bar{u} - F_{,xy} \bar{v})_{x=0} dy \end{aligned} \quad (4.20)$$

where,

$$\mathbf{f} = (F_{,yy} \quad F_{,xx} \quad -F_{,xy})^T \quad (4.21)$$

Equation 4.15 and 4.20 are the generalized total complementary energies where both the external loads and geometry displacements conditions have been prescribed to the panels. In the following two sections, the specific expressions of total complementary energy for panels only under prescribed loads or displacements will be derived based on these equations.

4.3.2 Prescribed Loads

For the panel under only prescribed loads, the total potential energy is still the same as equation 4.11.

However, the total complementary energy (equation 4.15) reduces into

$$\Pi_{pre}^c = U_m^c = \frac{1}{2} \int \int a_{11} N_x^2 + 2a_{12} N_x N_y + 2a_{16} N_x N_y + a_{22} N_y^2 + 2a_{26} N_y N_{xy} + a_{66} N_{xy}^2 dx dy \quad (4.22)$$

Since no displacements are prescribed on the panel, the complementary energy term V_{S_2} is not involved in above equation.

After introducing the Airy stress function, above equation becomes

$$\Pi_{pre}^c = \frac{1}{2} \int \int (\mathbf{f}^T \mathbf{A}^{-1} \mathbf{f}) dx dy \quad (4.23)$$

4.3.3 Prescribed Displacements

For the panel under only prescribed displacements, the total potential energy (equation 4.11) reduces to

$$\begin{aligned} \Pi_{pre} = U_m = & \frac{1}{2} \int \int [(A_{11}(u_{,x})^2 + 2A_{12}(u_{,x})(v_{,y}) + 2A_{16}(u_{,x})(v_{,x} + u_{,y}) \\ & + A_{22}(v_{,y})^2 + 2A_{26}(v_{,y})(v_{,x} + u_{,y}) + A_{66}(v_{,x} + u_{,y})^2] dx dy \end{aligned} \quad (4.24)$$

Since no loads are prescribed on the panel, the external work V_{S1} is not involved in above equation.

However, the total complementary energy (equation 4.15) is still the same.

$$\Pi_{pre}^c = U_m^c + V_{S2} \quad (4.25)$$

After introducing the Airy stress function, the total complementary energy become

$$\begin{aligned} \Pi_{pre}^c = & \frac{1}{2} \int \int (\mathbf{f}^T \mathbf{A}^{-1} \mathbf{f}) dx dy \\ & - \int_{S2} (F_{,xx} \bar{v} - F_{,xy} \bar{u})_{y=b} - (F_{,xx} \bar{v} - F_{,xy} \bar{u})_{y=0} dx \\ & - \int_{S2} (F_{,yy} \bar{u} - F_{,xy} \bar{v})_{x=a} - (F_{,yy} \bar{u} - F_{,xy} \bar{v})_{x=0} dy \end{aligned} \quad (4.26)$$

which is the same as equation 4.20.

4.4 Total Energy Functional for Stability Analysis

In this section, the total energy functional of a panel for stability analysis is derived. In Section 4.4.1, the panel is considered under a general load case where both external loads and displacements are prescribed. Then in Section 4.4.2 and 4.4.3, the panel is considered only under prescribed loads and displacements, respectively.

Once buckling occurs, the panel will have bending deformation, thus the bending strain energy needs to be added into the total potential energy. Moreover, the assumption of small deflection will not be hold, von Kármán's moderately large-deflection theory has to be applied for stability (and post-buckling) analysis. Then the strain-displacement relations are replace by [5, 7]

$$\epsilon_{xo} = u_{,x} + \frac{1}{2} w_{,x}^2 \quad (4.27)$$

$$\epsilon_{yo} = v_{,y} + \frac{1}{2} w_{,y}^2 \quad (4.28)$$

$$\gamma_{xyo} = v_{,x} + u_{,y} + w_{,x} w_{,y} \quad (4.29)$$

for plates;

$$\epsilon_{xo} = u_{,x} + \frac{1}{2} w_{,x}^2 \quad (4.30)$$

$$\epsilon_{yo} = v_{,y} - \frac{w}{R} + \frac{1}{2} w_{,y}^2 \quad (4.31)$$

$$\gamma_{xyo} = v_{,x} + u_{,y} + w_{,x} w_{,y} \quad (4.32)$$

for cylindrical shells.

For simplicity, the strain vector has been introduced as

$$\mathbf{e} = \mathbf{e}_l + \mathbf{e}_n = \begin{pmatrix} \epsilon_{xo} \\ \epsilon_{yo} \\ \gamma_{xyo} \end{pmatrix} \quad (4.33)$$

where, the first part (\mathbf{e}_l) of \mathbf{e} relates to the in-plane displacements as

$$\mathbf{e}_l = \begin{pmatrix} u_{,x} \\ v_{,y} \\ u_{,y} + v_{,x} \end{pmatrix} \quad (4.34)$$

and second part (\mathbf{e}_n) of \mathbf{e} relates to the out-of-plane displacement as

$$\mathbf{e}_n = \begin{pmatrix} \frac{1}{2}w_{,x}^2 \\ \frac{1}{2}w_{,y}^2 \\ w_{,x}w_{,y} \end{pmatrix} \quad (4.35)$$

for plates,

$$\mathbf{e}_n = \begin{pmatrix} \frac{1}{2}w_{,x}^2 \\ -\frac{w}{R} + \frac{1}{2}w_{,y}^2 \\ w_{,x}w_{,y} \end{pmatrix} \quad (4.36)$$

for cylindrical shells.

4.4.1 Prescribed Loads and Displacements

Similar to the prebuckling analysis, first the total energy functional for a general load case will be derived, where the external loads \bar{N}_x , \bar{N}_y , \bar{N}_{xy} are prescribed on boundary $S1$ and geometry displacement conditions are prescribed on boundary $S2$.

So the mechanical boundary conditions are

$$N_x = \bar{N}_x, N_y = \bar{N}_y, N_{xy} = \bar{N}_{xy} \text{ on } S1 \quad (4.37)$$

The geometrical boundary conditions are

$$u = \bar{u}, v = \bar{v} \text{ on } S2 \quad (4.38)$$

For symmetric composite panels, the total strain energy (equation 4.4) is given as [7]

$$U = U_m + U_b \quad (4.39)$$

where, the membrane strain energy is the same as equation 4.5 which can be written in form of matrix as

$$U_m = \frac{1}{2} \int \int \mathbf{e}^T \mathbf{A} \mathbf{e} dx dy \quad (4.40)$$

and the bending strain energy is the same as equation 4.6 which can be written in form of matrix as

$$U_b = \frac{1}{2} \int \int \boldsymbol{\kappa}^T \mathbf{D} \boldsymbol{\kappa} dx dy \quad (4.41)$$

where, the vector $\boldsymbol{\kappa}$ contains the curvatures

$$\boldsymbol{\kappa} = \begin{pmatrix} -w_{,xx} \\ -w_{,yy} \\ -2w_{,xy} \end{pmatrix} \quad (4.42)$$

After applying the prescribed loads on the boundary S1, the panel is slightly deformed (pre-buckling). The potential work done by the prescribed loads on S1 is given as [5]

$$V_{S1} = + \oint_{C_y} (\bar{N}_y v + \bar{N}_{xy} u) dx - \oint_{C_x} (\bar{N}_x u + \bar{N}_{xy} v) dy \quad (4.43)$$

For rectangular plates or cylindrical shells where the edges are parallel to the x and y coordinates (as shown in Figure 3.1 and 3.2), the external work can be written as

$$V_{S1} = - \int_{S1} [(\bar{N}_y v + \bar{N}_{xy} u)_{y=b} - (\bar{N}_y v + \bar{N}_{xy} u)_{y=0}] dx - \int_{S1} [(\bar{N}_x u + \bar{N}_{xy} v)_{x=a} - (\bar{N}_x u + \bar{N}_{xy} v)_{x=0}] dy \quad (4.44)$$

Therefore, the total potential energy is given as

$$\begin{aligned} \Pi = U + V_{S1} &= \frac{1}{2} \int \int \mathbf{e}^T \mathbf{A} \mathbf{e} dx dy + \frac{1}{2} \int \int \boldsymbol{\kappa}^T \mathbf{D} \boldsymbol{\kappa} dx dy \\ &\quad - \int_{S1} [(\bar{N}_y v + \bar{N}_{xy} u)_{y=b} - (\bar{N}_y v + \bar{N}_{xy} u)_{y=0}] dx - \int_{S1} [(\bar{N}_x u + \bar{N}_{xy} v)_{x=a} - (\bar{N}_x u + \bar{N}_{xy} v)_{x=0}] dy \end{aligned} \quad (4.45)$$

Note that the work done by the prescribed displacements on boundary S2 is a complementary energy, so it does not contribute to the total potential energy.

For cylindrical shells, the total potential energy (equation 4.45) can be rewritten in terms of displacements as

$$\begin{aligned} \Pi &= \frac{1}{2} \int \int \begin{pmatrix} u_{,x} + \frac{1}{2} w_{,x}^2 \\ v_{,y} - \frac{w}{R} + \frac{1}{2} w_{,y}^2 \\ u_{,y} + v_{,x} + w_{,x} w_{,y} \end{pmatrix}^T \mathbf{A} \begin{pmatrix} u_{,x} + \frac{1}{2} w_{,x}^2 \\ v_{,y} - \frac{w}{R} + \frac{1}{2} w_{,y}^2 \\ u_{,y} + v_{,x} + w_{,x} w_{,y} \end{pmatrix} dx dy \\ &\quad + \frac{1}{2} \int \int \begin{pmatrix} -w_{,xx} \\ -w_{,yy} \\ -2w_{,xy} \end{pmatrix}^T \mathbf{D} \begin{pmatrix} -w_{,xx} \\ -w_{,yy} \\ -2w_{,xy} \end{pmatrix} dx dy \\ &\quad - \int_{S1} [(\bar{N}_y v + \bar{N}_{xy} u)_{y=b} - (\bar{N}_y v + \bar{N}_{xy} u)_{y=0}] dx \\ &\quad - \int_{S1} [(\bar{N}_x u + \bar{N}_{xy} v)_{x=a} - (\bar{N}_x u + \bar{N}_{xy} v)_{x=0}] dy \end{aligned} \quad (4.46)$$

For plates, the term $\frac{w}{R}$ will disappear from above equation since the curvature of plates is zero ($\frac{1}{R} = 0$). For convenience, the derivations in this section will only be given for shells. The derivations can be simply reduced to these for plates by making $\frac{1}{R} = 0$.

To get the equilibrium equations, normally the total potential energy can be minimized with respect to the displacements u , v , w . Alternately, the total potential energy can be minimized with respect to \mathbf{e} and w since the total potential energy can be a functional of \mathbf{e} and w (equation 4.45, if the curvatures are written in terms of w). However, during the minimization with respect to \mathbf{e} , the strain-displacement relations (equation 4.30, 4.31 and 4.32) must be hold. These strain-displacement relations can be treated as the subsidiary conditions during the minimization process. Therefore, the Lagrange multipliers are used in order to enforce

the strain-displacement relations. Then the total potential energy can be rewritten as

$$\begin{aligned}
\Pi &= U + V_{S1} - \int \boldsymbol{\lambda}^T \left[\mathbf{e} - \begin{pmatrix} u_{,x} + \frac{1}{2}w_{,x}^2 \\ v_{,y} - \frac{w}{R} + \frac{1}{2}w_{,y}^2 \\ u_{,y} + v_{,x} + w_{,x}w_{,y} \end{pmatrix} \right] dxdy \\
&= \frac{1}{2} \int \int \mathbf{e}^T \mathbf{A} \mathbf{e} dxdy + \frac{1}{2} \int \int \begin{pmatrix} -w_{,xx} \\ -w_{,yy} \\ -2w_{,xy} \end{pmatrix}^T \mathbf{D} \begin{pmatrix} -w_{,xx} \\ -w_{,yy} \\ -2w_{,xy} \end{pmatrix} dxdy \\
&\quad - \int \boldsymbol{\lambda}^T \left[\mathbf{e} - \begin{pmatrix} u_{,x} + \frac{1}{2}w_{,x}^2 \\ v_{,y} - \frac{w}{R} + \frac{1}{2}w_{,y}^2 \\ u_{,y} + v_{,x} + w_{,x}w_{,y} \end{pmatrix} \right] dxdy + V_{S1}
\end{aligned} \tag{4.47}$$

where, the Lagrange multipliers are

$$\boldsymbol{\lambda}^T = (\Lambda_x \quad \Lambda_y \quad \Lambda_{xy}) \tag{4.48}$$

If minimizing the total potential energy with respect to \mathbf{e} ,

$$\frac{\partial \Pi}{\partial \mathbf{e}} = \int \int (\mathbf{A} \mathbf{e} - \boldsymbol{\lambda}) dxdy = \mathbf{0} \tag{4.49}$$

which implies

$$\boldsymbol{\lambda} = \mathbf{A} \mathbf{e} \tag{4.50}$$

Moreover, notice that the membrane stress resultants are given as

$$\mathbf{n} = \begin{pmatrix} N_x \\ N_y \\ N_{xy} \end{pmatrix} = \begin{pmatrix} A_{11}\epsilon_{xo} + A_{12}\epsilon_{yo} + A_{16}\gamma_{xyo} \\ A_{12}\epsilon_{xo} + A_{22}\epsilon_{yo} + A_{26}\gamma_{xyo} \\ A_{16}\epsilon_{xo} + A_{26}\epsilon_{yo} + A_{66}\gamma_{xyo} \end{pmatrix} = \mathbf{A} \mathbf{e} \tag{4.51}$$

where, \mathbf{n} is the vector of in-plane loads.

Thus

$$\mathbf{n} = \mathbf{A} \mathbf{e} = \boldsymbol{\lambda} \tag{4.52}$$

so the physical meanings of Lagrange multipliers applied above are actually the membrane force resultants. Thus,

$$\mathbf{e} = \mathbf{A}^{-1} \boldsymbol{\lambda} = \mathbf{A}^{-1} \mathbf{n} \tag{4.53}$$

Then, substituting the equation 4.52 4.53 back to the total potential energy (equation 4.47), following equation is obtained

$$\begin{aligned}
\Pi &= -\frac{1}{2} \int \int (\mathbf{n}^T \mathbf{A}^{-1} \mathbf{n}) dxdy + \frac{1}{2} \int \int \begin{pmatrix} -w_{,xx} \\ -w_{,yy} \\ -2w_{,xy} \end{pmatrix}^T \mathbf{D} \begin{pmatrix} -w_{,xx} \\ -w_{,yy} \\ -2w_{,xy} \end{pmatrix} dxdy \\
&\quad + \int \int \mathbf{n}^T \begin{pmatrix} u_{,x} + \frac{1}{2}w_{,x}^2 \\ v_{,y} - \frac{w}{R} + \frac{1}{2}w_{,y}^2 \\ u_{,y} + v_{,x} + w_{,x}w_{,y} \end{pmatrix} dxdy + V_{S1} \\
&= -\frac{1}{2} \int \int (\mathbf{n}^T \mathbf{A}^{-1} \mathbf{n}) dxdy + \frac{1}{2} \int \int (\boldsymbol{\kappa}^T \mathbf{D} \boldsymbol{\kappa}) dxdy + \int \int \mathbf{n}^T (\mathbf{e}_l + \mathbf{e}_n) dxdy + V_{S1}
\end{aligned} \tag{4.54}$$

Furthermore, the third term on the right of above equation is

$$\int \int (\mathbf{n}^T \mathbf{e}_l) dx dy = \int \int [N_x u_{,x} + N_y v_{,y} + N_{xy}(v_{,x} + u_{,y})] dx dy \quad (4.55)$$

After integration by parts,

$$\begin{aligned} \int \int (\mathbf{n}^T \mathbf{e}_l) dx dy &= \oint_{C_x} (N_x u + N_{xy} v) dy - \oint_{C_y} (N_{xy} u + N_y v) dx \\ &\quad - \int \int [(N_{x,x} + N_{xy,y})u + (N_{xy,x} + N_{y,y})v] dx dy \end{aligned} \quad (4.56)$$

For rectangular plates or cylindrical shells,

$$\begin{aligned} \int \int (\mathbf{n}^T \mathbf{e}_l) dx dy &= \int_S (N_y v + N_{xy} u)_{y=b} - (N_y v + N_{xy} u)_{y=0} dx \\ &\quad + \int_S (N_x u + N_{xy} v)_{x=a} - (N_x u + N_{xy} v)_{x=0} dy \\ &\quad - \int \int [(N_{x,x} + N_{xy,y})u + (N_{xy,x} + N_{y,y})v] dx dy \end{aligned} \quad (4.57)$$

Note that, on the boundary S_1 ,

$$N_x = \bar{N}_x, N_y = \bar{N}_y, N_{xy} = \bar{N}_{xy} \quad (4.58)$$

on boundary S_2 ,

$$u = \bar{u}, v = \bar{v} \quad (4.59)$$

So

$$\begin{aligned} \int \int (\mathbf{n}^T \mathbf{e}_l) dx dy &= \int_{S_1} (\bar{N}_y v + \bar{N}_{xy} u)_{y=b} - (\bar{N}_y v + \bar{N}_{xy} u)_{y=0} dx \\ &\quad + \int_{S_1} (\bar{N}_x u + \bar{N}_{xy} v)_{x=a} - (\bar{N}_x u + \bar{N}_{xy} v)_{x=0} dy \\ &\quad + \int_{S_2} (N_y \bar{v} + N_{xy} \bar{u})_{y=b} - (N_y \bar{v} + N_{xy} \bar{u})_{y=0} dx \\ &\quad + \int_{S_2} (N_x \bar{u} + N_{xy} \bar{v})_{x=a} - (N_x \bar{u} + N_{xy} \bar{v})_{x=0} dy \\ &\quad - \int \int [(N_{x,x} + N_{xy,y})u + (N_{xy,x} + N_{y,y})v] dx dy \end{aligned} \quad (4.60)$$

In addition, according to the in-plane equilibrium equations (equation 3.103, 3.104),

$$N_{x,x} + N_{xy,y} = 0 \quad (4.61)$$

$$N_{xy,x} + N_{y,y} = 0 \quad (4.62)$$

Therefore,

$$\begin{aligned} \int \int (\mathbf{n}^T \mathbf{e}_l) dx dy &= \int_{S_1} (\bar{N}_y v + \bar{N}_{xy} u)_{y=b} - (\bar{N}_y v + \bar{N}_{xy} u)_{y=0} dx \\ &\quad + \int_{S_1} (\bar{N}_x u + \bar{N}_{xy} v)_{x=a} - (\bar{N}_x u + \bar{N}_{xy} v)_{x=0} dy \\ &\quad + \int_{S_2} (N_y \bar{v} + N_{xy} \bar{u})_{y=b} - (N_y \bar{v} + N_{xy} \bar{u})_{y=0} dx \\ &\quad + \int_{S_2} (N_x \bar{u} + N_{xy} \bar{v})_{x=a} - (N_x \bar{u} + N_{xy} \bar{v})_{x=0} dy \end{aligned} \quad (4.63)$$

It is noted that the first two terms on the right of the above equation are canceled with V_{S1} (equation 4.44),

$$\begin{aligned} \int \int (\mathbf{n}^T \mathbf{e}_l) dx dy + V_{S1} &= \int_{S2} (N_y \bar{v} + N_{xy} \bar{u})_{y=b} - (N_y \bar{v} + N_{xy} \bar{u})_{y=0} dx \\ &+ \int_{S2} (N_x \bar{u} + N_{xy} \bar{v})_{x=a} - (N_x \bar{u} + N_{xy} \bar{v})_{x=0} dy \end{aligned} \quad (4.64)$$

Hence, the total potential energy will become

$$\begin{aligned} \Pi &= -\frac{1}{2} \int \int (\mathbf{n}^T \mathbf{A}^{-1} \mathbf{n}) dx dy + \frac{1}{2} \int \int \begin{pmatrix} -w_{,xx} \\ -w_{,yy} \\ -2w_{,xy} \end{pmatrix}^T \mathbf{D} \begin{pmatrix} -w_{,xx} \\ -w_{,yy} \\ -2w_{,xy} \end{pmatrix} dx dy + \int \int \mathbf{n}^T \mathbf{e}_n dx dy \\ &+ \int_{S2} (N_y \bar{v} + N_{xy} \bar{u})_{y=b} - (N_y \bar{v} + N_{xy} \bar{u})_{y=0} dx \\ &+ \int_{S2} (N_x \bar{u} + N_{xy} \bar{v})_{x=a} - (N_x \bar{u} + N_{xy} \bar{v})_{x=0} dy \end{aligned} \quad (4.65)$$

It is noted that the first part of the total energy functional is the membrane complementary energy, while the second part is the bending strain energy. So the total energy functional is a mixture of complementary energy and strain energy. This is why it is mentioned in the introduction to this chapter that the final energy functional cannot be called total potential energy. Moreover, it is interesting to observed that the membrane complementary energy has a minus sign in front of it, while the bending strain energy does not. This formulation has also been shown in other literature [9, 10, 33, 34]. Since both the membrane complementary energy (if ignore the minus sign) and bending strain energy are quadratic forms, when making them stationary with respect to their own variables (for membrane energy the variables are in-plane loads; for bending energy the variables are out-of-plane displacement w) they will be minimized. However, if considering the minus sign in front of the membrane complementary energy, the negative of the membrane complementary energy will be maximized. So if making the total energy functional stationary with respect to the in-plane loads, the total energy functional will be maximized due to the negative of the membrane complementary energy (the bending energy is independent of the in-plane loads). While, if making the total energy functional stationary with respect to the out-of-plane displacement w , the total energy functional will be minimized since the membrane complementary energy is independent of w .

Last but not least, the third part of the total energy functional can be written in detail as

$$\int \int \mathbf{n}^T \mathbf{e}_n dx dy = \frac{1}{2} \int \int (N_x w_{,x}^2 + N_y w_{,y}^2 + 2N_{xy} w_{,x} w_{,y}) dx dy - \int \int N_y \frac{w}{R} dx dy \quad (4.66)$$

For plates, it reduces into

$$\int \int \mathbf{n}^T \mathbf{e}_n dx dy = \frac{1}{2} \int \int (N_x w_{,x}^2 + N_y w_{,y}^2 + 2N_{xy} w_{,x} w_{,y}) dx dy \quad (4.67)$$

which is what was called as 'work done by in-plane loads' or 'external work' by many researchers [2, 4, 7]. However, clearly this energy term is derived from the membrane strain energy through the introduction of the Lagrange multipliers, while the external work done by the applied loads is actually V_{S1} .

In addition, since the in-plane equilibrium equations (equation 4.61 and 4.62) were introduced during the derivation, they must be the subsidiary conditions for the equation 4.65. In other words, only when the in-plane equilibrium equations are hold, the total potential energy (equation 4.45) can be derived as the total energy functional (equation 4.65). These in-plane equilibrium equations can simply be fulfilled by introducing the Airy stress function into the in-plane loads as

$$N_x = F_{,yy}, \quad N_y = F_{,xx}, \quad N_{xy} = -F_{,xy} \quad (4.68)$$

Then the total energy functional can be written as

$$\begin{aligned} \Pi = & -\frac{1}{2} \int \int (\mathbf{f}^T \mathbf{A}^{-1} \mathbf{f}) dx dy + \frac{1}{2} \int \int \begin{pmatrix} -w_{,xx} \\ -w_{,yy} \\ -2w_{,xy} \end{pmatrix}^T \mathbf{D} \begin{pmatrix} -w_{,xx} \\ -w_{,yy} \\ -2w_{,xy} \end{pmatrix} dx dy + \int \int \mathbf{f}^T \mathbf{e}_n dx dy \\ & + \int_{S_2} (F_{,xx} \bar{v} - F_{,xy} \bar{u})_{y=b} - (F_{,xx} \bar{v} - F_{,xy} \bar{u})_{y=0} dx \\ & + \int_{S_2} (F_{,yy} \bar{u} - F_{,xy} \bar{v})_{x=a} - (F_{,yy} \bar{u} - F_{,xy} \bar{v})_{x=0} dy \end{aligned} \quad (4.69)$$

where,

$$\mathbf{f} = \begin{pmatrix} F_{,yy} \\ F_{,xx} \\ -F_{,xy} \end{pmatrix} \quad (4.70)$$

4.4.2 Prescribed Loads

In this case, only the external loads N_x , N_y , N_{xy} are prescribed on the boundary S_1 . The mechanical boundary conditions on S_1 are

$$N_x = \bar{N}_x, N_y = \bar{N}_y, N_{xy} = \bar{N}_{xy} \text{ on } S_1 \quad (4.71)$$

Since no displacements prescribed in S_2 , the total energy functional (equation 4.65) reduces to

$$\Pi = -\frac{1}{2} \int \int (\mathbf{n}^T \mathbf{A}^{-1} \mathbf{n}) dx dy + \frac{1}{2} \int \int \begin{pmatrix} -w_{,xx} \\ -w_{,yy} \\ -2w_{,xy} \end{pmatrix}^T \mathbf{D} \begin{pmatrix} -w_{,xx} \\ -w_{,yy} \\ -2w_{,xy} \end{pmatrix} dx dy + \int \int \mathbf{n}^T \mathbf{e}_n dx dy \quad (4.72)$$

which if written in terms of Airy stress function is

$$\Pi = -\frac{1}{2} \int \int (\mathbf{f}^T \mathbf{A}^{-1} \mathbf{f}) dx dy + \frac{1}{2} \int \int \begin{pmatrix} -w_{,xx} \\ -w_{,yy} \\ -2w_{,xy} \end{pmatrix}^T \mathbf{D} \begin{pmatrix} -w_{,xx} \\ -w_{,yy} \\ -2w_{,xy} \end{pmatrix} dx dy + \int \int \mathbf{f}^T \mathbf{e}_n dx dy \quad (4.73)$$

4.4.3 Prescribed Displacements

Only the displacements \bar{u}, \bar{v} are prescribed on the boundary S_2 . The geometrical boundary conditions are

$$u = \bar{u}, v = \bar{v} \text{ on } S_2 \quad (4.74)$$

Then the total energy functional is still the same as equation 4.65

$$\begin{aligned} \Pi = & -\frac{1}{2} \int \int (\mathbf{n}^T \mathbf{A}^{-1} \mathbf{n}) dx dy + \frac{1}{2} \int \int \begin{pmatrix} -w,_{xx} \\ -w,_{yy} \\ -2w,_{xy} \end{pmatrix}^T \mathbf{D} \begin{pmatrix} -w,_{xx} \\ -w,_{yy} \\ -2w,_{xy} \end{pmatrix} dx dy + \int \int \mathbf{n}^T \mathbf{e}_n dx dy \\ & + \int_{S_2} (N_y \bar{v} + N_{xy} \bar{u})_{y=b} - (N_y \bar{v} + N_{xy} \bar{u})_{y=0} dx \\ & + \int_{S_2} (N_x \bar{u} + N_{xy} \bar{v})_{x=a} - (N_x \bar{u} + N_{xy} \bar{v})_{x=0} dy \end{aligned} \quad (4.75)$$

which if written in terms of Airy stress function is (the same as equation 4.69)

$$\begin{aligned} \Pi = & -\frac{1}{2} \int \int (\mathbf{f}^T \mathbf{A}^{-1} \mathbf{f}) dx dy + \frac{1}{2} \int \int \begin{pmatrix} -w,_{xx} \\ -w,_{yy} \\ -2w,_{xy} \end{pmatrix}^T \mathbf{D} \begin{pmatrix} -w,_{xx} \\ -w,_{yy} \\ -2w,_{xy} \end{pmatrix} dx dy + \int \int \mathbf{f}^T \mathbf{e}_n dx dy \\ & + \int_{S_2} (F,_{xx} \bar{v} - F,_{xy} \bar{u})_{y=b} - (F,_{xx} \bar{v} - F,_{xy} \bar{u})_{y=0} dx \\ & + \int_{S_2} (F,_{yy} \bar{u} - F,_{xy} \bar{v})_{x=a} - (F,_{yy} \bar{u} - F,_{xy} \bar{v})_{x=0} dy \end{aligned} \quad (4.76)$$

4.5 Plates

The Ritz method will be applied to the derived energy functionals Π_{pre}^c and Π of plates to obtain the equations for solving the in-plane loads in prebuckling analysis and the stability equations for predicting the buckling loads. The two load cases, namely, prescribed loads and prescribed displacements, will be discussed separately.

4.5.1 Prescribed Loads

For simplicity, only the compression load \bar{N}_x is prescribed on the edges $x = 0, a$. The same derivations showing below can be easily extended to these considering the prescribed loads \bar{N}_y and \bar{N}_{xy} .

Prebuckling Analysis

The first step is to calculate the in-plane loads redistribution after prescribed external load \bar{N}_x on the edges $x = 0, a$. Due to the variation of stiffness the in-plane loads are not uniform over the plates. The distribution of the in-plane loads will affect the buckling resistance of

the plates. So the in-plane loads should be obtained before determining the stability of the plates.

The total complementary energy (equation 4.23) for prebuckling analysis can be applied here, which is shown below for convenience.

$$\Pi_{pre}^c = \frac{1}{2} \int \int (\mathbf{f}^T \mathbf{A}^{-1} \mathbf{f}) dx dy \quad (4.77)$$

Since only the external load \bar{N}_x is prescribed, the boundary conditions of the in-plane loads are

$$N_x = \bar{N}_x, N_{xy} = 0 \text{ on } x = 0, a \quad (4.78)$$

$$N_y = 0, N_{xy} = 0 \text{ on } y = 0, b \quad (4.79)$$

So the Airy stress function can be assumed as

$$F(x, y) = \frac{1}{2} \bar{N}_x y^2 + \sum_{kl}^{KL} F_{kl} X_k(x) Y_l''(y) \quad (4.80)$$

F_{kl} is the undetermined parameter. X_k and Y_l are the shape functions used in x and y direction, respectively. K and L are the numbers of shape functions used in x and y direction, respectively.

Clearly, the first term $\frac{1}{2} \bar{N}_x y^2$ plays the role of φ_0 as the particular solution in equation 4.1 and X_k (and Y_l) of the second term plays the role of φ_i as the homogeneous solution. So the first term $\frac{1}{2} \bar{N}_x y^2$ ensures that the in-plane load N_x on the edge $x = 0, a$ is exactly the same as the prescribed load \bar{N}_x .

Correspondingly, the second term should satisfy the stress-free condition which is the homogeneous form of solution. However, the detail of this condition will be discussed in the next chapter.

Substituting the Airy stress function into the total complementary energy,

$$\begin{aligned} \Pi_{pre}^c = \frac{1}{2} \int \int [& a_{11} \bar{N}_x^2 + 2 \bar{N}_x \sum_{kl}^{KL} F_{kl} \begin{pmatrix} a_{11} \\ a_{12} \\ a_{16} \end{pmatrix}^T \begin{pmatrix} X_k Y_l'' \\ X_k'' Y_l \\ -X_k' Y_l' \end{pmatrix} \\ & + \sum_{klk_2l_2}^{KLLK} F_{kl} F_{k_2l_2} \begin{pmatrix} X_k Y_l'' \\ X_k'' Y_l \\ -X_k' Y_l' \end{pmatrix}^T \mathbf{A}^{-1} \begin{pmatrix} X_{k_2} Y_{l_2}'' \\ X_{k_2}'' Y_{l_2} \\ -X_{k_2}' Y_{l_2}' \end{pmatrix}] dx dy \end{aligned} \quad (4.81)$$

X_k' and X_k'' indicate the first and second derivative of X_k with respect to x ; Y_l' and Y_l'' indicate the first and second derivative of Y_l with respect to y . And $k_2, l_2, F_{k_2l_2}, X_{k_2}, Y_{l_2}$ are the counterparts of k, l, F_{kl}, X_k, Y_l in the quadruple summation.

By making the total complementary energy stationary with respect to the undetermined parameters F_{kl} , a set of linear equations will be obtained, from which the unknown parameters can be determined.

$$\frac{\partial \Pi_{pre}}{\partial F_{kl}} = 0 \quad (k = 1 \dots K, l = 1 \dots L) \quad (4.82)$$

These linear equations can be written in matrix form as

$$\bar{N}_x \mathbf{c}_{kl} + \mathbf{C}_a \mathbf{f}_{kl} = \mathbf{0} \quad (4.83)$$

where, \mathbf{f}_{kl} is the vector of F_{kl} of length $K \times L$,

$$\mathbf{f}_{kl} = (F_{11}, F_{12}, \dots, F_{1L}, F_{21}, \dots, F_{kl}, \dots, F_{KL})^T \quad (4.84)$$

\mathbf{c}_{kl} is a vector of length $K \times L$, each element of which is

$$\int \int \begin{pmatrix} a_{11} \\ a_{12} \\ a_{16} \end{pmatrix}^T \begin{pmatrix} X_k Y_l'' \\ X_k'' Y_l \\ -X_k' Y_l' \end{pmatrix} dx dy \quad (k = 1 \dots K, l = 1 \dots L) \quad (4.85)$$

\mathbf{C}_a is a $K \times L$ by $K \times L$ matrix, each element of which is

$$\int \int \begin{pmatrix} X_k Y_l'' \\ X_k'' Y_l \\ -X_k' Y_l' \end{pmatrix}^T \mathbf{A}^{-1} \begin{pmatrix} X_{k_2} Y_{l_2}'' \\ X_{k_2}'' Y_{l_2} \\ -X_{k_2}' Y_{l_2}' \end{pmatrix} dx dy \quad (k = 1 \dots K, l = 1 \dots L) \quad (4.86)$$

The equations written in matrix form in equation 4.83 are equivalent to the linear compatibility equations 3.122 used in Galerkin method.

The undetermined parameter vector \mathbf{f}_{kl} can be solved as

$$\mathbf{f}_{kl} = -\bar{N}_x \mathbf{C}_a^{-1} \mathbf{c}_{kl} \quad (4.87)$$

Then the in-plane loads distribution can be easily obtained from the Airy stress function. Clearly, the in-plane loads are linearly related to the prescribed load \bar{N}_x , as implied by above equation. So buckling initiation can be determined by introducing the buckling factor λ to the prescribed load as

$$\bar{N}_x^{critical} = \lambda \bar{N}_x \quad (4.88)$$

If λ is larger than 1, the prescribed load \bar{N}_x is lower than the most critical buckling load. If the prescribed load $\bar{N}_x = 1$, the buckling factor is exactly the buckling load. So in the next section, the stability equations will be derived to solve the buckling factor λ based on the in-plane loads (Airy stress function) solved in current section.

Stability Analysis

For plates under prescribed load \bar{N}_x , the total energy functional is given in equation 4.73, which is shown below for convenience.

$$\begin{aligned} \Pi = & -\frac{1}{2} \int \int (\mathbf{f}^T \mathbf{A}^{-1} \mathbf{f}) dx dy + \frac{1}{2} \int \int \begin{pmatrix} -w_{,xx} \\ -w_{,yy} \\ -2w_{,xy} \end{pmatrix}^T \mathbf{D} \begin{pmatrix} -w_{,xx} \\ -w_{,yy} \\ -2w_{,xy} \end{pmatrix} dx dy \\ & + \frac{1}{2} \int \int (F_{,yy} w_{,x}^2 + F_{,xx} w_{,y}^2 - 2F_{,xy} w_{,x} w_{,y}) dx dy \end{aligned} \quad (4.89)$$

In to Ritz method, the out-of-plane displacement is approximated using a finite set of linear independent series, as

$$w = \sum_{pq}^{PQ} W_{pq} X_p(x) Y_q(y) \quad (4.90)$$

W_{pq} is the undetermined parameter. X_p and Y_q are the shape functions used for w in x and y direction, respectively, which are in general different from the shape functions X_k and Y_l used for Airy stress function F .

Clearly, the φ_0 in equation 4.1 as the particular solution does not exist in above equation and X_k (and Y_l) plays the role of φ_i as the homogeneous solution. The reason is that the initial out-of-plane deflection, which represents the particular solution, is zero.

To determined initiation of buckling , the buckling factor is introduced as

$$F(x, y) = \lambda \left[\frac{1}{2} \bar{N}_x y^2 + \sum_{kl}^{KL} F_{kl} X_k(x) Y_l(y) \right] \quad (4.91)$$

where, the parameter F_{kl} is solved from equation 4.87 in the prebuckling analysis.

After substituting above two equations back to equation 4.89 , the total energy functional becomes

$$\begin{aligned} \Pi = & -\frac{1}{2} \lambda^2 \int \int [a_{11} \bar{N}_x^2 + 2 \bar{N}_x \sum_{kl}^{KL} F_{kl} \begin{pmatrix} a_{11} \\ a_{12} \\ a_{16} \end{pmatrix}^T \begin{pmatrix} X_k Y_l'' \\ X_k'' Y_l \\ -X_k' Y_l' \end{pmatrix} \\ & + \sum_{klk_2l_2}^{K L K L} F_{kl} F_{k_2l_2} \begin{pmatrix} X_k Y_l'' \\ X_k'' Y_l \\ -X_k' Y_l' \end{pmatrix}^T \mathbf{A}^{-1} \begin{pmatrix} X_{k_2} Y_{l_2}'' \\ X_{k_2}'' Y_{l_2} \\ -X_{k_2}' Y_{l_2}' \end{pmatrix}] dx dy \\ & + \sum_{pq p_2 q_2}^{P Q P Q} W_{pq} W_{p_2 q_2} \int \int \frac{1}{2} \begin{pmatrix} X_p'' Y_q \\ X_p Y_q'' \\ 2 X_p' Y_q' \end{pmatrix}^T \mathbf{D} \begin{pmatrix} X_{p_2}'' Y_{q_2} \\ X_{p_2} Y_{q_2}'' \\ 2 X_{p_2}' Y_{q_2}' \end{pmatrix} dx dy \\ & + \lambda \bar{N}_x \sum_{pq}^{P Q} W_{pq} W_{p_2 q_2} \int \int \frac{1}{2} X_p' Y_q X_{p_2}' Y_{q_2} dx dy \\ & + \lambda \sum_{kl p q p_2 q_2}^{K L P Q P Q} W_{pq} W_{p_2 q_2} F_{kl} \int \int \frac{1}{2} \begin{pmatrix} X_k Y_l'' \\ X_k'' Y_l \\ -X_k' Y_l' \end{pmatrix}^T \begin{pmatrix} X_p' X_{p_2}' Y_q Y_{q_2} \\ X_p X_{p_2} Y_q' Y_{q_2}' \\ X_p' Y_q X_{p_2} Y_{q_2}' + X_p Y_q' X_{p_2}' Y_{q_2} \end{pmatrix} dx dy \end{aligned} \quad (4.92)$$

Making total energy functional stationary with respect to the unknown parameter W_{pq} , as

$$\frac{\partial \Pi}{\partial W_{pq}} = 0 \quad (p = 1 \dots P, q = 1 \dots Q) \quad (4.93)$$

a set of linear equations will be obtained, which can be expressed in matrix form as

$$[\mathbf{C}_D + \lambda (\mathbf{C}_N + \mathbf{C}_F)] \mathbf{w}_{pq} = \mathbf{0} \quad (4.94)$$

where, \mathbf{w}_{pq} is the vector of W_{pq} of length $P \times Q$,

$$\mathbf{w}_{pq} = (W_{11}, W_{12}, \dots, W_{1Q}, W_{21}, \dots, W_{pQ}, \dots, W_{PQ})^T \quad (4.95)$$

\mathbf{C}_D is a $P \times Q$ by $P \times Q$ matrix, each element of which is

$$\iint \begin{pmatrix} X_p'' Y_q \\ X_p Y_q'' \\ 2X_p' Y_q' \end{pmatrix}^T \mathbf{D} \begin{pmatrix} X_{p_2}'' Y_{q_2} \\ X_{p_2} Y_{q_2}'' \\ 2X_{p_2}' Y_{q_2}' \end{pmatrix} dx dy \quad (4.96)$$

\mathbf{C}_N is a $P \times Q$ by $P \times Q$ matrix, each element of which is

$$\bar{N}_x \iint X_p' Y_q X_{p_2}' Y_{q_2} dx dy \quad (4.97)$$

\mathbf{C}_F is a $P \times Q$ by $P \times Q$ matrix, each element of which is

$$\sum_{kl}^{KL} F_{kl} \iint \begin{pmatrix} X_k Y_l'' \\ X_k'' Y_l \\ -X_k' Y_l' \end{pmatrix}^T \begin{pmatrix} X_p' X_{p_2}' Y_q Y_{q_2} \\ X_p X_{p_2} Y_q' Y_{q_2}' \\ X_p' Y_q X_{p_2} Y_{q_2}' + X_p Y_q' X_{p_2}' Y_{q_2} \end{pmatrix} dx dy \quad (4.98)$$

The equation 4.94 is obtained from making the total energy functional stationary, so in principle it is an equilibrium equation. For stability analysis, the stability equation should be obtained from the second variation of the total energy functional, or from the equilibrium equation by applying adjacent-equilibrium criterion. However, since the equilibrium equation is similar to the stability equation for plates, many researchers directly used the equilibrium equation to predict the buckling initiation [2, 7, 11, 19, 28]. But strictly speaking, the equilibrium equation is essentially different from the stability equation even though they are so similar to each other for the case of plates. Later in the section for shells, the stability equation will be derived, in which case it is no longer similar to the equilibrium equation. However, from equation 4.94, the value of λ can still be solved as the generalized eigenvalue of the matrix \mathbf{C}_D and $[\mathbf{C}_N + \mathbf{C}_F]$, if the vector \mathbf{w}_{pq} of displacement w is not zero. So the stability equation for plates will not be derived in current section. The detail derivation for the stability equation of shells will be shown in next section. The same derivations can be applied here to derive the stability equation of plates by just assuming the curvature is zero.

4.5.2 Prescribed Displacements

For simplicity, only the end-shortening Δu is prescribed on the edges of $x = 0, a$. The same derivations showing below can be easily extended into that considered prescribed displacement \bar{v} on the edges of $y = 0, b$.

If the end-shortenings prescribed on the two edge are Δu_1 and Δu_2 , respectively, the geometrical boundary conditions are

$$u = \bar{u} = \Delta u_1 \text{ on } x = 0 \quad (4.99)$$

$$u = \bar{u} = -\Delta u_2 \text{ on } x = a \quad (4.100)$$

Since the plate is free to move in y direction, there is no load acting on the edges of $y = 0, b$ and no shear load acting on the four edges. The mechanical boundary conditions will be

$$N_x \neq 0, N_{xy} = 0 \text{ on } x = 0, a \quad (4.101)$$

$$N_y = 0, N_{xy} = 0 \text{ on } y = 0, b \quad (4.102)$$

Moreover, the in-plane load N_x is not constant on the edge $x = 0, a$, instead it is a variable due to the stiffness variation on edges, and in general N_x on the two edges are not necessarily the same. Therefore, the Airy stress function is assumed as

$$F(x, y) = \sum_e^E F_e \int \int Y_e(y) dy dy + \sum_{kl}^{KL} F_{kl} X_k(x) Y_l(y) \quad (4.103)$$

where, Y_e is the shape function to describe the stress variation on the edges ($x = 0, a$), F_e is the undetermined parameter for shape function Y_e , E is the number of terms. The second derivative of the first term with respect to y is exactly Y_e which represents part of the compression loads acting on the edges since the second derivative of F with respect to y represents the load N_x .

The first term expresses the stress variation in y direction on the edge under the prescribed displacements, which is constant through the plate in x direction. The second term expresses the stress variation inside of the plate due to the variation of the stiffness. Compared to the case of prescribed loads, the first term is actually similarly to the prescribed load \bar{N}_x in equation 4.80.

Then the in-plane loads are

$$N_x = F_{,yy} = \sum_e^E F_e Y_e + \sum_{kl}^{KL} F_{kl} X_k Y_l'' \quad (4.104)$$

$$N_y = F_{,xx} = \sum_{kl}^{KL} F_{kl} X_k'' Y_l \quad (4.105)$$

$$N_{xy} = -F_{,xy} = -\sum_{kl}^{KL} F_{kl} X_k' Y_l' \quad (4.106)$$

The shape functions selected for Y_e , X_k and Y_l will be discussed in next chapter.

Prebuckling Analysis

The first step is to calculate the in-plane loads redistribution after prescribed end-shortening Δu_1 and Δu_2 on the edges $x = 0, a$ of the rectangular plate. The total energy functional (equation 4.26) for prebuckling analysis can be applied here, which is reduced to the following equation considering only the prescribed end-shortening Δu_1 and Δu_2 .

$$\Pi_{pre}^c = \frac{1}{2} \int \int (\mathbf{f}^T \mathbf{A}^{-1} \mathbf{f}) dx dy - \int_{S_2} F_{,yy} (-\Delta u_2)_{x=a} - F_{,yy} (\Delta u_1)_{x=0} dy \quad (4.107)$$

After substituting the expression for Airy stress function (equation 4.103) into the total complementary energy and making it stationary with respect to the undetermined parameters

F_e and F_{kl} , respectively, two sets of linear equations can be obtained, which are expressed in matrix form as

$$\begin{bmatrix} \mathbf{C}_a & \mathbf{E}_1 \\ \mathbf{E}_1^T & \mathbf{E}_3 \end{bmatrix} \begin{pmatrix} \mathbf{f}_{kl} \\ \mathbf{f}_e \end{pmatrix} = \Delta u_1 \begin{pmatrix} \mathbf{i}_{kl_1} \\ \mathbf{i}_{e_1} \end{pmatrix} + \Delta u_2 \begin{pmatrix} \mathbf{i}_{kl_2} \\ \mathbf{i}_{e_2} \end{pmatrix} \quad (4.108)$$

where, \mathbf{f}_e is the vector of F_e of dimension E ,

$$\mathbf{f}_e = (F_1 \ F_2 \ \cdots \ F_e \ \cdots \ F_E)^T \quad (4.109)$$

\mathbf{E}_1 is a $K \times L$ by E matrix, \mathbf{E}_3 is a E by E matrix, \mathbf{i}_{kl_1} and \mathbf{i}_{kl_2} are vectors of dimension $K \times L$, \mathbf{i}_{e_1} and \mathbf{i}_{e_2} are vectors of dimension E . \mathbf{C}_a is given in equation 4.86.

The unknown parameter vectors \mathbf{f}_e and \mathbf{f}_{kl} can be solved from the above matrix equation. Clearly, these parameter vectors are linearly related to the prescribed end-shortening Δu_1 and Δu_2 . So to determine buckling initiation, buckling factor can be introduced as

$$\Delta u_1^{critical} = \lambda \Delta u_1 \quad (4.110)$$

$$\Delta u_2^{critical} = \lambda \Delta u_2 \quad (4.111)$$

Then the Airy stress function at the critical point can be assumed as

$$F(x, y) = \lambda \left[\sum_e^E F_e \int \int Y_e(y) dy dy + \sum_{kl}^{KL} F_{kl} X_k(x) Y_l(y) \right] \quad (4.112)$$

Stability Analysis

If only the end-shortening Δu_1 and Δu_2 are prescribed on the edges ($x = 0, a$), the total energy functional (equation 4.76) reduces into

$$\begin{aligned} \Pi = & -\frac{1}{2} \int \int (\mathbf{f}^T \mathbf{A}^{-1} \mathbf{f}) dx dy + \frac{1}{2} \int \int \begin{pmatrix} -w,_{xx} \\ -w,_{yy} \\ -2w,_{xy} \end{pmatrix}^T \mathbf{D} \begin{pmatrix} -w,_{xx} \\ -w,_{yy} \\ -2w,_{xy} \end{pmatrix} dx dy + \int \int \mathbf{f}^T \mathbf{e}_n dx dy \\ & + \int_{S_2} F,_{yy} (-\Delta u_2)_{x=a} - F,_{yy} (\Delta u_1)_{x=0} dy \end{aligned} \quad (4.113)$$

After introducing the buckling factor, the Airy stress function becomes,

$$F(x, y) = \lambda \left[\sum_e^E F_e \int \int Y_e(y) dy dy + \sum_{kl}^{KL} F_{kl} X_k(x) Y_l(y) \right] \quad (4.114)$$

where the parameters (F_e and F_{kl}) are solved in equation 4.108 in the prebuckling analysis, except the buckling factor λ which will be solved in this section.

The out-of-plane displacement is approximated using a finite set of linear independent series (the same as equation 4.90), as

$$w = \sum_{pq}^{PQ} W_{pq} X_p(x) Y_q(y) \quad (4.115)$$

Substituting above two equations back to equation 4.113, and making it stationary with respect to the undetermined parameters W_{pq} , a set of linear equations can be obtained, which are expressed in matrix form as

$$[\mathbf{C}_D + \lambda(\mathbf{C}_e + \mathbf{C}_F)] \mathbf{w}_{pq} = \mathbf{0} \quad (4.116)$$

\mathbf{C}_e is a $P \times Q$ by $P \times Q$ matrix, each element of which is

$$\sum_e^E F_e \int \int X'_p Y_q X'_{p_2} Y_{q_2} Y_e dx dy \quad (4.117)$$

Similar to the case of prescribing loads, this matrix equation is still the equilibrium equation, which, however, is similar to the stability equation for plates. From equation 4.116, the value of λ can still be solved as the generalized eigenvalue of the matrix \mathbf{C}_D and $[\mathbf{C}_e + \mathbf{C}_F]$, if the vector \mathbf{w}_{pq} of displacement w is not zero.

The stability equation for plates will not be derived in current section. The detail derivation for the stability equation of shells will be shown in next section. The same derivations of plates can be applied here to derive the stability equation by just assuming the curvature is zero.

4.6 Shallow Cylindrical Shells

Similar to plates, the buckling of shells under prescribed loads and prescribed displacements will be discussed separately. The stability equations are derived by using adjacent-equilibrium criterion and minimum potential energy approach (second variational of the total energy functional and Trefftz criterion), respectively.

4.6.1 Prescribed Loads

In this section a shell under prescribed load \bar{N}_x on edges $x = 0, a$ will be discussed. The derivations can be easily extended to these considered prescribed load \bar{N}_y and \bar{N}_{xy} .

Prebuckling Analysis

Based on the assumption 2 in Chapter 3, the out-of-plane displacement of shallow cylindrical shell panel is zero in the prebuckling state. So the strain-displacement relations for plates and shells should be the same, as shown in equation 4.7. Then, the prebuckling analysis for plates and shells should be the same. For convenience, the same equations as these for plates are shown as follows.

The total complementary energy (equation 4.23) for prebuckling analysis,

$$\Pi_{pre}^c = \frac{1}{2} \int \int (\mathbf{f}^T \mathbf{A}^{-1} \mathbf{f}) dx dy \quad (4.118)$$

The Airy stress function is,

$$F(x, y) = \frac{1}{2}\bar{N}_x y^2 + \sum_{kl}^{KL} F_{kl} X_k(x) Y_l(y) \quad (4.119)$$

The same equilibrium equations as plates (equation 4.83) are obtained as

$$\bar{N}_x \mathbf{c}_{kl} + \mathbf{C}_a \mathbf{f}_{kl} = \mathbf{0} \quad (4.120)$$

The undetermined parameters F_{kl} can be solved from the above equation, from which the in-plane loads will be obtained.

Stability Analysis

The total energy functional of shells is given in equation 4.73, which is shown as follows.

$$\Pi = -\frac{1}{2} \int \int (\mathbf{f}^T \mathbf{A}^{-1} \mathbf{f}) dx dy + \frac{1}{2} \int \int \begin{pmatrix} -w_{,xx} \\ -w_{,yy} \\ -2w_{,xy} \end{pmatrix}^T \mathbf{D} \begin{pmatrix} -w_{,xx} \\ -w_{,yy} \\ -2w_{,xy} \end{pmatrix} dx dy + \int \int \mathbf{f}^T \mathbf{e}_n dx dy \quad (4.121)$$

However, the strain \mathbf{e}_n for shells is not the same as plates, which is

$$\mathbf{e}_n = \begin{pmatrix} \frac{1}{2}w_{,x}^2 \\ -\frac{w}{R} + \frac{1}{2}w_{,y}^2 \\ w_{,x}w_{,y} \end{pmatrix} \quad (4.122)$$

So the total energy functional can be rewritten as

$$\begin{aligned} \Pi = & -\frac{1}{2} \int \int (\mathbf{f}^T \mathbf{A}^{-1} \mathbf{f}) dx dy + \frac{1}{2} \int \int \begin{pmatrix} -w_{,xx} \\ -w_{,yy} \\ -2w_{,xy} \end{pmatrix}^T \mathbf{D} \begin{pmatrix} -w_{,xx} \\ -w_{,yy} \\ -2w_{,xy} \end{pmatrix} dx dy \\ & + \frac{1}{2} \int \int (F_{,yy} w_{,x}^2 + F_{,xx} w_{,y}^2 - 2F_{,xy} w_{,x} w_{,y}) dx dy \\ & - \int \int F_{,xx} \frac{w}{R} dx dy \end{aligned} \quad (4.123)$$

Compared to plates, the last energy term with $\frac{w}{R}$ is added to the total energy functional of shells.

The displacement w is approximated using the same series as plates (equation 4.90).

$$w = \sum_{pq}^{PQ} W_{pq} X_p(x) Y_q(y) \quad (4.124)$$

The buckling factor is introduced to the Airy stress function as the same as for plates,

$$F(x, y) = \lambda \left[\frac{1}{2} \bar{N}_x y^2 + \sum_{kl}^{KL} F_{kl} X_k(x) Y_l(y) \right] \quad (4.125)$$

Substituting the expressions for displacement w and Airy stress function F in to the equation of the total energy functional, following equation is obtained.

$$\begin{aligned}
\Pi = & -\frac{1}{2}\lambda^2 \int \int [a_{11}\bar{N}_x^2 + 2\bar{N}_x \sum_{kl}^{KL} F_{kl} \begin{pmatrix} a_{11} \\ a_{12} \\ a_{16} \end{pmatrix}^T \begin{pmatrix} X_k Y_l'' \\ X_k'' Y_l \\ -X_k' Y_l' \end{pmatrix} \\
& + \sum_{klk_2l_2}^{K L K L} F_{kl} F_{k_2l_2} \begin{pmatrix} X_k Y_l'' \\ X_k'' Y_l \\ -X_k' Y_l' \end{pmatrix}^T \mathbf{A}^{-1} \begin{pmatrix} X_{k_2} Y_{l_2}'' \\ X_{k_2}'' Y_{l_2} \\ -X_{k_2}' Y_{l_2}' \end{pmatrix}] dx dy \\
& + \sum_{pq p_2 q_2}^{P Q P Q} W_{pq} W_{p_2 q_2} \int \int \frac{1}{2} \begin{pmatrix} X_p'' Y_q \\ X_p Y_q'' \\ 2X_p' Y_q' \end{pmatrix}^T \mathbf{D} \begin{pmatrix} X_{p_2}'' Y_{q_2} \\ X_{p_2} Y_{q_2}'' \\ 2X_{p_2}' Y_{q_2}' \end{pmatrix} dx dy \\
& + \lambda \bar{N}_x \sum_{pq}^{P Q} W_{pq} W_{p_2 q_2} \int \int \frac{1}{2} X_p' Y_q X_{p_2}' Y_{q_2} dx dy \\
& + \lambda \sum_{klpq p_2 q_2}^{K L P Q P Q} W_{pq} W_{p_2 q_2} F_{kl} \int \int \frac{1}{2} \begin{pmatrix} X_k Y_l'' \\ X_k'' Y_l \\ -X_k' Y_l' \end{pmatrix}^T \begin{pmatrix} X_p' X_{p_2}' Y_q Y_{q_2} \\ X_p X_{p_2} Y_q' Y_{q_2}' \\ X_p' Y_q X_{p_2} Y_{q_2}' + X_p Y_q' X_{p_2}' Y_{q_2} \end{pmatrix} dx dy \\
& - \lambda \sum_{klpq}^{K L P Q} F_{kl} W_{pq} \int \int \frac{1}{R} X_k'' Y_l X_p Y_q dx dy
\end{aligned} \tag{4.126}$$

First, making the total energy functional stationary with respect to W_{pq} ,

$$\frac{\partial \Pi}{\partial W_{pq}} = 0 \quad (p = 1 \dots P, q = 1 \dots Q) \tag{4.127}$$

a set of linear equations is obtained, which can be expressed in the matrix form as

$$[\mathbf{C}_D + \lambda(\mathbf{C}_N + \mathbf{C}_F)] \mathbf{w}_{pq} + \lambda \mathbf{C}_R \mathbf{f}_{kl} = \mathbf{0} \tag{4.128}$$

where, \mathbf{C}_R is a $P \times Q$ by $K \times L$ matrix, each element of which is

$$-\int \int \frac{1}{R} X_k'' Y_l X_p Y_q dx dy \tag{4.129}$$

Notice that the difference between equation 4.116 for plates and above equation for shells is the extra term with \mathbf{C}_R . This new term is coupled with the parameter \mathbf{f}_{kl} , which means the buckling factor λ cannot be solved from the above equation by solving the eigenvalues. It is reasonable because these equations are actually the equilibrium equations, which in principle cannot be used for determining buckling initiation. Thus the stability equations should be derived.

Second, making the total energy functional stationary with respect to F_{kl} ,

$$\frac{\partial \Pi}{\partial F_{kl}} = 0 \quad (k = 1 \dots K, l = 1 \dots L) \tag{4.130}$$

a set of linear equations is obtained, which can be expressed in matrix form as

$$-\lambda(\bar{N}_x \mathbf{c}_{kl} + \mathbf{C}_a \mathbf{f}_{kl}) + \mathbf{C}_W \mathbf{w}_{pq} \mathbf{w}_{pq} + \mathbf{C}_R^T \mathbf{w}_{pq} = \mathbf{0} \quad (4.131)$$

Where, \mathbf{C}_W is a $K \times L$ by $P \times Q$ by $P \times Q$ three dimensional matrix (tensor), each element of which is

$$\int \int \frac{1}{2} \begin{pmatrix} X_k Y_l'' \\ X_k'' Y_l' \\ -X_k' Y_l' \end{pmatrix}^T \begin{pmatrix} X_p' X_{p2}' Y_q Y_{q2} \\ X_p X_{p2}' Y_q' Y_{q2}' \\ X_p' Y_q X_{p2} Y_{q2}' + X_p Y_q' X_{p2}' Y_{q2} \end{pmatrix} dx dy \quad (4.132)$$

This matrix equation is actually the counterpart of equation 4.120 for prebuckling analysis from which the prebuckling in-plane loads distribution are obtained. If the assumption 1 and 2 are applied here, the above equation will be reduced to equation 4.120. However, the assumptions cannot be applied to stability analysis. So the equation here actually describes the in-plane loads distribution in the buckling and post-buckling state, which is equivalent to the non-linear compatibility equation of shells in previous chapter. However, this equation is coupled with the first equilibrium equation 4.128. Therefore, for post-buckling analysis, these two equations should be solved together.

Stability Analysis: Adjacent-Equilibrium Criterion

As already mentioned, the equations derived from making the total energy functional stationary are the equilibrium equations. So in this section, the stability equations for shells will be derived from the equilibrium equations by applying the adjacent-equilibrium criterion [1]. Then the stability equation for shells can easily reduce to the stability equation for plates by assuming the curvatures are zero.

Since the only unknowns are the parameters F_{kl} and W_{pq} , infinitesimal increments are added to them as the perturbation to the system,

$$F_{kl} \rightarrow F_{kl} + F_{kl}^1 \quad (4.133)$$

$$W_{pq} \rightarrow W_{pq} + W_{pq}^1 \quad (4.134)$$

where, F_{kl}^1 and W_{pq}^1 are the increments of F_{kl} and W_{pq} .

They are equivalent to the following process

$$F(x, y) = \lambda \left[\frac{1}{2} \bar{N}_x y^2 + \sum_{kl}^{KL} (F_{kl} + F_{kl}^1) X_k(x) Y_l(y) \right] \quad (4.135)$$

$$w(x, y) = \sum_{pq}^{PQ} (W_{pq} + W_{pq}^1) X_p(x) Y_q(y) \quad (4.136)$$

However, the number of terms K and L used for the increments F_{kl}^1 can be different than the number of terms K and L used for F , which will be discussed later in the section of Trefftz buckling criterion.

Substituting the expressions (4.133,4.134) into equations 4.128 and 4.131, the following equations are obtained.

$$-\lambda[\bar{N}_x \mathbf{c}_{kl} + \mathbf{C}_a (\mathbf{f}_{kl} + \mathbf{f}_{kl}^1)] + \mathbf{C}_W (\mathbf{w}_{pq} + \mathbf{w}_{pq}^1) (\mathbf{w}_{pq} + \mathbf{w}_{pq}^1) + \mathbf{C}_R^T (\mathbf{w}_{pq} + \mathbf{w}_{pq}^1) = \mathbf{0} \quad (4.137)$$

$$[\mathbf{C}_D + \lambda(\mathbf{C}_N + \mathbf{C}_F)] (\mathbf{w}_{pq} + \mathbf{w}_{pq}^1) + \lambda \mathbf{C}_R (\mathbf{f}_{kl} + \mathbf{f}_{kl}^1) = \mathbf{0} \quad (4.138)$$

where, \mathbf{f}_{kl}^1 and \mathbf{w}_{pq}^1 are vector of F_{kl}^1 and W_{pq}^1 , respectively.

After truncating the original equations (equation 4.128 and 4.131) from above equations, the above equations become

$$-\lambda \mathbf{C}_a \mathbf{f}_{kl}^1 + \mathbf{C}_W (2\mathbf{w}_{pq}^1 \mathbf{w}_{pq} + \mathbf{w}_{pq}^1 \mathbf{w}_{pq}^1) + \mathbf{C}_R^T \mathbf{w}_{pq}^1 = \mathbf{0} \quad (4.139)$$

$$[\mathbf{C}_D + \lambda (\mathbf{C}_N + \mathbf{C}_F)] \mathbf{w}_{pq}^1 + \lambda \mathbf{C}_R \mathbf{f}_{kl}^1 = \mathbf{0} \quad (4.140)$$

Ignoring the higher order terms, they become

$$-\lambda \mathbf{C}_a \mathbf{f}_{kl}^1 + \mathbf{C}_W (2\mathbf{w}_{pq}^1 \mathbf{w}_{pq}) + \mathbf{C}_R^T \mathbf{w}_{pq}^1 = \mathbf{0} \quad (4.141)$$

$$[\mathbf{C}_D + \lambda (\mathbf{C}_N + \mathbf{C}_F)] \mathbf{w}_{pq}^1 + \lambda \mathbf{C}_R \mathbf{f}_{kl}^1 = \mathbf{0} \quad (4.142)$$

Since \mathbf{w}_{pq} are a vector of the parameters of w in the prebuckling state, it can be assumed to be zero according to the assumption 1 and 2. So

$$-\lambda \mathbf{C}_a \mathbf{f}_{kl}^1 + \mathbf{C}_R^T \mathbf{w}_{pq}^1 = \mathbf{0} \quad (4.143)$$

$$[\mathbf{C}_D + \lambda (\mathbf{C}_N + \mathbf{C}_F)] \mathbf{w}_{pq}^1 + \lambda \mathbf{C}_R \mathbf{f}_{kl}^1 = \mathbf{0} \quad (4.144)$$

Therefore, the stability equations for shells are derived . They can be further simplified in following process.

$$\mathbf{f}_{kl}^1 = \frac{1}{\lambda} \mathbf{C}_a^{-1} \mathbf{C}_R^T \mathbf{w}_{pq}^1 \quad (4.145)$$

$$[\mathbf{C}_D + \lambda (\mathbf{C}_N + \mathbf{C}_F)] \mathbf{w}_{pq}^1 + \lambda \mathbf{C}_R \frac{1}{\lambda} \mathbf{C}_a^{-1} \mathbf{C}_R^T \mathbf{w}_{pq}^1 = \mathbf{0} \quad (4.146)$$

Thus, substituting the first one into the second one, only one equation is left

$$\left[\mathbf{C}_D + \mathbf{C}_R \mathbf{C}_a^{-1} \mathbf{C}_R^T + \lambda (\mathbf{C}_N + \mathbf{C}_F) \right] \mathbf{w}_{pq}^1 = \mathbf{0} \quad (4.147)$$

With this equation, the buckling factor can be solved by solving the generalized eigenvalues of matrix $[\mathbf{C}_D + \mathbf{C}_R \mathbf{C}_a^{-1} \mathbf{C}_R^T]$ and $[\mathbf{C}_N + \mathbf{C}_F]$.

If the curvature $\frac{1}{R}$ is zero, the matrix \mathbf{C}_R will be zero, as shown in the expression 4.129. The stability equation 4.147 will reduce to

$$[\mathbf{C}_D + \lambda (\mathbf{C}_N + \mathbf{C}_F)] \mathbf{w}_{pq}^1 = \mathbf{0} \quad (4.148)$$

Since a shell with zero curvature is exactly a plate, so the above equation is exactly the stability equation for a plate. As mentioned before, the equilibrium equation for plates is similar to the stability equation. For plates, the equilibrium equation 4.116 is shown below for convenience.

$$[\mathbf{C}_D + \lambda (\mathbf{C}_N + \mathbf{C}_F)] \mathbf{w}_{pq} = \mathbf{0} \quad (4.149)$$

Obviously, the only difference of above two equations is the parameter vectors, \mathbf{w}_{pq}^1 and \mathbf{w}_{pq} . Solving the buckling load of plates from equilibrium equations is not theoretically correct [5], because the parameter vector $\mathbf{w}_{pq} = \mathbf{0}$ according the assumption 2 in Chapter 3. However, still many researchers [2, 3, 7, 11, 19, 26] adopted the equilibrium equation (however, not the same as equation 4.149) to solve the buckling load because the eigenvalues solved from the equilibrium equation is exactly the same as these solved from the stability equation, since they

are solved from the same matrices. Nevertheless, solving the buckling load from equilibrium equation is not theoretically correct, which can only be regarded as a simplified method for plates (and any other linear structure, such as beams).

However, for shells, obviously the buckling load can only be solved from the stability equation (equation 4.147) not from the equilibrium equation (equation 4.128).

Stability Analysis: Second variation of total energy functional

The same stability equations for shells and plates can be derived using the principle of minimum potential energy (or as in the current case it is the total energy functional).

The total energy functional can be varied, or expanded in a Taylor's series, about an equilibrium state [5]:

$$\Pi + \Delta\Pi = \Pi + \delta\Pi + \frac{1}{2!}\delta^2\Pi + \frac{1}{3!}\delta^3\Pi + \dots \quad (4.150)$$

The equilibrium state is derived from the first variation of the energy functional, which is also known as the principle of stationary potential energy [5]:

$$\delta\Pi = 0 \quad (4.151)$$

The stability of the equilibrium state is determined from the second variation of the total energy functional at the equilibrium state according to the principle of minimum potential energy [5]:

$$\bar{\delta}^2\Pi = \delta^2\Pi \Big|_{\delta\Pi=0} > 0 \quad (4.152)$$

The total energy functional is firstly discretized through discretizing the Airy stress function F and displacement w using the series expressed in equations 4.91 and 4.90. The final expression for the total energy functional is shown in equation 4.126.

Therefore, if directly taking the second variation of the total energy functional (equation 4.126) with respect to the unknown parameters F_{kl} and W_{pq} , the following equation in matrix form will be obtained,

$$\delta^2\Pi = \begin{pmatrix} \delta\mathbf{f}_{kl} \\ \delta\mathbf{w}_{pq} \end{pmatrix}^T \begin{bmatrix} -\lambda^2\mathbf{C}_a & \lambda\mathbf{C}_W\mathbf{w}_{pq} - \lambda\mathbf{C}_R^T \\ \lambda(\mathbf{C}_W\mathbf{w}_{pq})^T - \lambda\mathbf{C}_R & \mathbf{C}_D + \lambda\mathbf{C}_N + \lambda\mathbf{C}_F \end{bmatrix} \begin{pmatrix} \delta\mathbf{f}_{kl} \\ \delta\mathbf{w}_{pq} \end{pmatrix} \quad (4.153)$$

which is a quadratic form in $\delta\mathbf{f}_{kl}$ and $\delta\mathbf{w}_{pq}$, where $\delta\mathbf{f}_{kl}$ and $\delta\mathbf{w}_{pq}$ are the variations of \mathbf{f}_{kl} and \mathbf{w}_{pq} .

However, the total energy functional can also be discretized after taking the second variation. The same equations will be obtained as these shown above.

At equilibrium state, the out-of-plane displacement is zero according to the assumption 1 and 2. Thus the parameters \mathbf{w}_{pq} in equilibrium state is zero. The above equation will reduce to

$$\bar{\delta}^2\Pi = \delta^2\Pi \Big|_{W_{pq}=0} = \begin{pmatrix} \delta\mathbf{f}_{kl} \\ \delta\mathbf{w}_{pq} \end{pmatrix}^T \begin{bmatrix} -\lambda^2\mathbf{C}_a & -\lambda\mathbf{C}_R^T \\ -\lambda\mathbf{C}_R & \mathbf{C}_D + \lambda\mathbf{C}_N + \lambda\mathbf{C}_F \end{bmatrix} \begin{pmatrix} \delta\mathbf{f}_{kl} \\ \delta\mathbf{w}_{pq} \end{pmatrix} \quad (4.154)$$

For stability, above quadratic form should be always larger than zero, in other words, positive definite [1] for all possible variations of \mathbf{f}_{kl} and \mathbf{w}_{pq} . Otherwise, the system is unstable. So

buckling occurs once $\bar{\delta}^2\Pi$ ceases to be positive definite as increasing the value of the buckling factor. According to the algebraic theory of quadratic form, the limit of positive-definiteness of a quadratic form is the determinate of the following coefficient matrix is zero [1].

$$\begin{vmatrix} -\lambda^2\mathbf{C}_a & -\lambda\mathbf{C}_R^T \\ -\lambda\mathbf{C}_R & \mathbf{C}_D + \lambda\mathbf{C}_N + \lambda\mathbf{C}_F \end{vmatrix} = 0 \quad (4.155)$$

Therefore, the buckling factor can be solved from above equation, which is equivalent to solve the generalized eigenvalue of the matrix in equation 4.147, as shown below.

$$\left[\mathbf{C}_D + \mathbf{C}_R\mathbf{C}_a^{-1}\mathbf{C}_R^T + \lambda(\mathbf{C}_N + \mathbf{C}_F) \right] \mathbf{w}_{pq}^1 = \mathbf{0} \quad (4.156)$$

Stability Analysis: Trefftz Buckling Criterion

Another buckling criterion is based on the Trefftz buckling criterion, which is to make the second variation of the total energy functional, $\bar{\delta}^2\Pi$, stationary [1, 5].

$$\delta(\bar{\delta}^2\Pi) = 0 \quad (4.157)$$

A short description of the Trefftz buckling criterion is given in the section 2.1 in the literature review. The reader is referred to the literature for more details [1, 5].

The total energy functional (equation 4.123) is rewritten as follows,

$$\begin{aligned} \Pi = & -\frac{1}{2} \int \int \begin{pmatrix} F_{,yy} \\ F_{,xx} \\ -F_{,xy} \end{pmatrix}^T \mathbf{A}^{-1} \begin{pmatrix} F_{,yy} \\ F_{,xx} \\ -F_{,xy} \end{pmatrix} dx dy + \frac{1}{2} \int \int \begin{pmatrix} -w_{,xx} \\ -w_{,yy} \\ -2w_{,xy} \end{pmatrix}^T \mathbf{D} \begin{pmatrix} -w_{,xx} \\ -w_{,yy} \\ -2w_{,xy} \end{pmatrix} dx dy \\ & + \frac{1}{2} \int \int (F_{,yy}w_{,x}^2 + F_{,xx}w_{,y}^2 - 2F_{,xy}w_{,x}w_{,y}) dx dy \\ & - \int \int F_{,xx} \frac{w}{R} dx dy \end{aligned} \quad (4.158)$$

The second variation of the above total energy functional is

$$\begin{aligned} \delta^2\Pi = & - \int \int \begin{pmatrix} \delta F_{,yy} \\ \delta F_{,xx} \\ -\delta F_{,xy} \end{pmatrix}^T \mathbf{A}^{-1} \begin{pmatrix} \delta F_{,yy} \\ \delta F_{,xx} \\ -\delta F_{,xy} \end{pmatrix} dx dy + \int \int \begin{pmatrix} -\delta w_{,xx} \\ -\delta w_{,yy} \\ -2\delta w_{,xy} \end{pmatrix}^T \mathbf{D} \begin{pmatrix} -\delta w_{,xx} \\ -\delta w_{,yy} \\ -2\delta w_{,xy} \end{pmatrix} dx dy \\ & + \int \int (F_{,yy}\delta w_{,x}^2 + F_{,xx}\delta w_{,y}^2 - 2F_{,xy}\delta w_{,x}\delta w_{,y}) dx dy \\ & + \int \int [\delta F_{,yy}\delta w_{,x}w_{,x} + \delta F_{,xx}\delta w_{,y}w_{,y} - 2\delta F_{,xy}(\delta w_{,x}w_{,y} + w_{,x}\delta w_{,y})] dx dy \\ & - \int \int \delta F_{,xx} \frac{\delta w}{R} dx dy \end{aligned} \quad (4.159)$$

According to assumption 1 and 2, in the equilibrium state (prebuckling)

$$w = w_{,x} = w_{,y} = 0 \quad (4.160)$$

So the second variation of the total energy functional in equilibrium state is

$$\begin{aligned}
\bar{\delta}^2\Pi &= \delta^2\Pi |_{w,x=w,y=0} \\
&= - \int \int \begin{pmatrix} \delta F_{,yy} \\ \delta F_{,xx} \\ -\delta F_{,xy} \end{pmatrix}^T \mathbf{A}^{-1} \begin{pmatrix} \delta F_{,yy} \\ \delta F_{,xx} \\ -\delta F_{,xy} \end{pmatrix} dx dy + \int \int \begin{pmatrix} -\delta w_{,xx} \\ -\delta w_{,yy} \\ -2\delta w_{,xy} \end{pmatrix}^T \mathbf{D} \begin{pmatrix} -\delta w_{,xx} \\ -\delta w_{,yy} \\ -2\delta w_{,xy} \end{pmatrix} dx dy \\
&\quad + \int \int (F_{,yy}\delta w_{,x}^2 + F_{,xx}\delta w_{,y}^2 - 2F_{,xy}\delta w_{,x}\delta w_{,y}) dx dy \\
&\quad - \int \int \delta F_{,xx} \frac{\delta w}{R} dx dy
\end{aligned} \tag{4.161}$$

According to Trefftz buckling criterion, buckling initiation is determined through

$$\delta(\bar{\delta}^2\Pi) = 0 \tag{4.162}$$

The variation of $\bar{\delta}^2\Pi$ can be implemented through Ritz method since Ritz method always tries to make a functional stationary with respect to the unknown parameters.

In this case, δF and δw can be approximated using following series,

$$\delta F = \sum_{kl}^{K_2 L_2} F_{kl}^1 X_k(x) Y_l(y) \tag{4.163}$$

$$\delta w = \sum_{pq}^{PQ} W_{pq}^1 X_p(x) Y_q(y) \tag{4.164}$$

where, K_2 and L_2 are numbers of terms used for δF , which does not necessarily equal to K and L used for F .

Making $\bar{\delta}^2\Pi$ stationary with respect to the undetermined parameters F_{kl}^1 and W_{pq}^1 , respectively,

$$\frac{\partial \bar{\delta}^2\Pi}{\partial F_{kl}^1} = 0 \tag{4.165}$$

$$\frac{\partial \bar{\delta}^2\Pi}{\partial W_{pq}^1} = 0 \tag{4.166}$$

then the same equations as what derived from the adjacent-equilibrium approach (equation 4.143 and 4.144) are obtained,

$$-\lambda \mathbf{C}_a \mathbf{f}_{kl}^1 + \mathbf{C}_R^T \mathbf{w}_{pq}^1 = \mathbf{0} \tag{4.167}$$

$$[\mathbf{C}_D + \lambda(\mathbf{C}_N + \mathbf{C}_F)] \mathbf{w}_{pq}^1 + \lambda \mathbf{C}_R \mathbf{f}_{kl}^1 = \mathbf{0} \tag{4.168}$$

They can reduce to one equation (the same as equation 4.147),

$$\left[\mathbf{C}_D + \mathbf{C}_R \mathbf{C}_a^{-1} \mathbf{C}_R^T + \lambda(\mathbf{C}_N + \mathbf{C}_F) \right] \mathbf{w}_{pq}^1 = \mathbf{0} \tag{4.169}$$

The last issue is related to number of terms used for discretizing Airy stress function F and its variation δF . Clearly, in this section the number of terms used for δF are K_2 and L_2 , rather than K and L which are used for F . According to the definition, the variation δF is a arbitrary infinitesimal value, which is independent from F . So not only the number of terms of δF can be different from F , but also can the shape functions of δF be different from F as long as the shape function of δF satisfy the homogeneous form of the boundary conditions.

4.6.2 Prescribed Displacement

Shells under prescribed end-shortening Δu_1 and Δu_2 on edges $x = 0, a$ are discussed. The same derivations can be easily extended to these accounting for the prescribed displacements on the edges $y = 0, b$.

Prebuckling Analysis

Based on the assumption 2 in Chapter 3, the out-of-plane displacement of shallow cylindrical shell panel is zero in the prebuckling state. So the strain-displacement relations for plates and shells should be the same, as shown in equation 4.7. Then, the prebuckling analysis for plates and shells should be the same. For convenience, the same equations as these for plates are shown as follows.

The Airy stress function is assumed the same as ,

$$F(x, y) = \sum_e^E F_e \int \int Y_e(y) dy dy + \sum_{kl}^{KL} F_{kl} X_k(x) Y_l(y) \quad (4.170)$$

The equilibrium equations for solving in-plane loads distribution is .

$$\begin{bmatrix} \mathbf{C}_a & \mathbf{E}_1 \\ \mathbf{E}_1^T & \mathbf{E}_3 \end{bmatrix} \begin{pmatrix} \mathbf{f}_{kl} \\ \mathbf{f}_e \end{pmatrix} = \Delta u_1 \begin{pmatrix} \mathbf{i}_{kl_1} \\ \mathbf{i}_{e_1} \end{pmatrix} + \Delta u_2 \begin{pmatrix} \mathbf{i}_{kl_2} \\ \mathbf{i}_{e_2} \end{pmatrix} \quad (4.171)$$

Buckling Analysis

If only the end-shortening Δu_1 and Δu_2 are prescribed on the edges ($x = 0, a$), the total energy functional (equation 4.76) reduces into

$$\begin{aligned} \Pi = & -\frac{1}{2} \int \int (\mathbf{f}^T \mathbf{A}^{-1} \mathbf{f}) dx dy + \frac{1}{2} \int \int \begin{pmatrix} -w_{,xx} \\ -w_{,yy} \\ -2w_{,xy} \end{pmatrix}^T \mathbf{D} \begin{pmatrix} -w_{,xx} \\ -w_{,yy} \\ -2w_{,xy} \end{pmatrix} dx dy \\ & + \frac{1}{2} \int \int (F_{,yy} w_{,x}^2 + F_{,xx} w_{,y}^2 - 2F_{,xy} w_{,x} w_{,y}) dx dy \\ & - \int \int F_{,xx} \frac{w}{R} dx dy \\ & + \int_{S_2} F_{,yy} (-\Delta u_2)_{x=a} - F_{,yy} (\Delta u_1)_{x=0} dy \end{aligned} \quad (4.172)$$

Again it is noted that the extra energy term with $\frac{w}{R}$ is added to the total energy functional for shells.

The out-of-plane displacement is approximated using the same series as plates, as

$$w = \sum_{pq}^{PQ} W_{pq} X_p(x) Y_q(y) \quad (4.173)$$

and the buckling factor is introduced to the Airy stress function as (equation 4.112),

$$F(x, y) = \lambda \left[\sum_e^E F_e \int \int Y_e(y) dy dy + \sum_{kl}^{KL} F_{kl} X_k(x) Y_l(y) \right] \quad (4.174)$$

The equilibrium equations are derived by making the total energy functional stationary with respect to the undetermined parameters W_{pq} , F_{kl} and F_e , respectively.

$$\frac{\partial \Pi}{\partial F_{kl}} = 0 \quad (k = 1 \dots K, l = 1 \dots L) \quad (4.175)$$

$$\frac{\partial \Pi}{\partial F_e} = 0 \quad (e = 1 \dots E) \quad (4.176)$$

$$\frac{\partial \Pi}{\partial W_{pq}} = 0 \quad (p = 1 \dots P, q = 1 \dots Q) \quad (4.177)$$

Then applying the adjacent-equilibrium criterion, small increments are added to the parameters, as

$$F_{kl} \rightarrow F_{kl} + F_{kl}^1 \quad (4.178)$$

$$W_{pq} \rightarrow W_{pq} + W_{pq}^1 \quad (4.179)$$

$$F_e \rightarrow F_e + F_e^1 \quad (4.180)$$

After replacing the parameters in the equilibrium equations by above expressions, truncating the equilibrium equations, ignoring the higher order term and assuming the out-of-plane displacement in prebuckling state is zero (assumption 2 in Chapter 3), the following stability equations are obtained.

$$-\lambda(\mathbf{C}_a \mathbf{f}_{kl}^1 + \mathbf{E}_1 \bar{F}_e^1) + \mathbf{C}_R^T \mathbf{w}_{pq}^1 = \mathbf{0} \quad (4.181)$$

$$-\mathbf{E}_1^T \mathbf{f}_{kl}^1 - \mathbf{E}_3 \bar{F}_e^1 = \mathbf{0} \quad (4.182)$$

$$[\mathbf{C}_D + \lambda(\mathbf{C}_F + \mathbf{C}_e)] \mathbf{w}_{pq}^1 + \lambda \mathbf{C}_R \mathbf{f}_{kl}^1 = \mathbf{0} \quad (4.183)$$

\mathbf{f}_{kl}^1 can be solved from the first two equations, then the third equation is rewritten as

$$[\mathbf{C}_D + \mathbf{C}_R(\mathbf{C}_a - \mathbf{E}_1 \mathbf{E}_3^{-1} \mathbf{E}_1^T)^{-1} \mathbf{C}_R^T + \lambda(\mathbf{C}_F + \mathbf{C}_e)] \mathbf{w}_{pq}^1 = \mathbf{0} \quad (4.184)$$

The buckling factor λ can be solved from the above equation by solving the generalized eigenvalues of matrix $[\mathbf{C}_D + \mathbf{C}_R(\mathbf{C}_a - \mathbf{E}_1 \mathbf{E}_3^{-1} \mathbf{E}_1^T)^{-1} \mathbf{C}_R^T]$ and $[\mathbf{C}_F + \mathbf{C}_e]$

For plates, the matrix \mathbf{C}_R is zero, thus the above equation reduces into

$$[\mathbf{C}_D + \lambda(\mathbf{C}_F + \mathbf{C}_e)] \mathbf{w}_{pq}^1 = \mathbf{0} \quad (4.185)$$

The stability equations can also be derived by applying the method of second variation of total energy functional or Trefftz buckling criterion as introduced in section 4.6.1.

4.7 Summary

In this chapter, the energy functionals for prebuckling analysis and stability analysis have been derived for both plates and shallow cylindrical shell panels. Then Ritz method has

been applied to the energy functional for prebuckling analysis in order to obtain the linear compatibility equation, from which the in-plane loads distribution is solved. The stability equations are obtained from the total energy functional for stability analysis using adjacent-equilibrium criterion or minimum potential energy approach (second variation of the total energy functional and Trefftz buckling criterion), from which the buckling factor is solved. However, the specific shape functions used for Airy stress function (F) and its variation (or increment, δF), out-of-plane displacement (w) and its variation (or increment, δw) have not been shown in this chapter, which will be discussed in the next two chapters as well as the predictions of the in-plane loads and buckling loads (or factors).

Prebuckling Analysis: in-plane loads distribution

5.1 Introduction

In this chapter, the in-plane loads distribution of a panel in the prebuckling state is investigated. Firstly, the panel has been considered only under a constant load \bar{N}_x on the edges $x = 0, a$. Then, constant shear \bar{N}_{xy} is applied to the panel. In the last section, the panel has been considered under constant end-shortenings on the edges of $x = 0, a$.

According to the assumption 2, the out-of-plane displacement of shallow cylindrical shell panel is zero in the prebuckling state. Therefore, the in-plane loads distribution is the same for plates and shallow cylindrical shell panels in the prebuckling state. So the in-plane loads distribution will be directly given without specifically indicating it is for plates or shells.

5.1.1 Material Property

The material property used in this chapter is shown in Table 5.1

Table 5.1: Material Property of AS4/3501-6 graphite epoxy laminate obtained from literature [35]

E_{11} (Gpa)	$E_{22} = E_{33}$ (Gpa)	$G_{12} = G_{13}$ (Gpa)	G_{23} (Gpa)	$\nu_{12} = \nu_{13}$	ν_{23}	t_{ply} (mm)
141.4	11.5	6	3.4	0.28	0.43	0.1397

where, E_{11} is the ply Young's modulus along the fiber orientation, E_{22} and E_{33} are the ply Young's modulus transverse to the fiber orientation; G_{12} , G_{13} and G_{23} are the ply shear modulus; ν_{12} , ν_{13} and ν_{23} are the ply Poisson's ratios; t_{ply} is the thickness of each ply.

5.1.2 Model

As shown in Figure 3.3, the variation of stiffness in this thesis is simplified to a few sections each having their own constant stiffness defined by fiber direction. In practice, the stiffness of a variable stiffness panel is normally continuous, instead of a piecewise function based on the sections. The reason for the simplicity is that the variation of fiber orientation is not easy to be assigned to the model in Abaqus, especially to the models of shells. Due to the limitation of time, this simplification has been adopted.

The layup of each section is considered to be symmetric, but the stretching-shearing couplings (A_{16} and A_{26}) and the bend-twist couplings (D_{16} and D_{26}) are not necessarily to be zero.

Moreover, the dimension of the panel is chosen as

$$a = b = 100 \text{ mm} \quad (5.1)$$

5.1.3 Verification

The in-plane loads distributions of variable stiffness panels are predicted using Ritz method, and the results are compared to the results obtained from commercial Finite element analysis (FEA) package, Abaqus 6.11.

The material properties used in Abaqus is the same as what used in Ritz method, as shown in Table 5.1. The S4 element, which is a 4-node quadrilateral conventional shell element with full integration, was chosen for discretizing the panels in Abaqus. According to a convergence study, the mesh density of 25×25 was chosen for each section to achieve the required accuracy. The examples of the mesh density are shown in Figure 5.1. The convergence studies for the mesh density are shown in Figure 6.4 and 6.9 in next chapter, where the convergences of buckling loads are investigated.

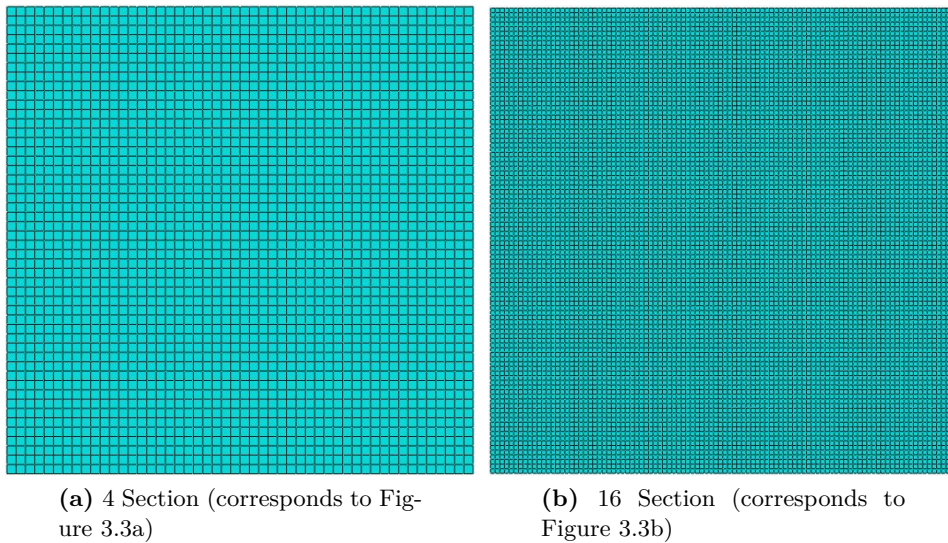


Figure 5.1: Mesh Density (25×25 per section)

5.2 Prescribed Compression (\bar{N}_x)

In this section, the prediction of in-plane loads of a panel under prescribed compression load is investigated. First, the boundary conditions of Airy stress function are discussed. Then sine function, beam characteristic function, polynomial function, sine and cosine function with Lagrange multiplier method are applied as the shape function in approximating the Airy stress function, respectively, and the predictions using these functions are compared to the predictions of FEM.

5.2.1 Boundary Condition

For a panel under the prescribed load \bar{N}_x , the Airy stress function is approximated by equation 4.80 in previous chapter, which is shown below for convenience.

$$F(x, y) = \frac{1}{2}\bar{N}_x y^2 + \sum_{kl} F_{kl} X_k(x) Y_l(y) \quad (5.2)$$

So the in-plane loads are

$$N_x = \bar{N}_x + \sum_{kl} F_{kl} X_k(x) Y_l''(y) \quad (5.3)$$

$$N_y = \sum_{kl} F_{kl} X_k''(x) Y_l(y) \quad (5.4)$$

$$N_{xy} = - \sum_{kl} F_{kl} X_k'(x) Y_l'(y) \quad (5.5)$$

Since only the load \bar{N}_x is prescribed on the panel, the mechanical boundary conditions are:

$$N_x = \bar{N}_x, N_{xy} = 0 \text{ on } x=0, a \quad (5.6)$$

$$N_y = 0, N_{xy} = 0 \text{ on } y=0, b \quad (5.7)$$

To satisfy the above boundary conditions, there are two options for the shape functions:

Option 1: The shape functions X_k and Y_l must held the following conditions term by term.

$$X_k(x) = X_k'(x) = 0 \text{ on } x=0, a \quad (k = 1 \cdots K) \quad (5.8)$$

$$Y_l(y) = Y_l'(y) = 0 \text{ on } y=0, b \quad (l = 1 \cdots L) \quad (5.9)$$

Option 2: The sum of a set of shape functions with the corresponding parameters must held the following conditions.

$$\sum_k F_{kl} X_k(x) = \sum_k F_{kl} X_k'(x) = 0 \text{ on } x=0, a \quad (l = 1 \cdots L) \quad (5.10)$$

$$\sum_l F_{kl} Y_l(y) = \sum_l F_{kl} Y_l'(y) = 0 \text{ on } y=0, b \quad (k = 1 \cdots K) \quad (5.11)$$

In the second option, the boundary conditions are satisfied by the sum of a set of functions, instead by the shape function term by term. This will be accomplished by manipulating the values of their parameters F_{kl} . A possible approach was introduced by Budiansky and Hu [36] where they introduced the Lagrange Multiplier method to hold these conditions during the minimization of total complementary energy. The detail of this approach will be discussed later in section 5.2.5 and 5.2.6.

In the section 5.2.2 5.2.3 and 5.2.4, sine function, beam characteristic function and polynomial function will be discussed corresponding to the option 1. Both the beam characteristic function and polynomial function shows satisfactory predictions of the in-plane loads, compared to Abaqus. However, the sine function that cannot exactly satisfy all the boundary conditions in the option 1, gives unsatisfactory predictions, which is reported in section 5.2.2 as an example to show the importance of satisfying all boundary conditions. Then the Lagrange multiplier is introduced to 'force' the sine function to satisfy the conditions of the option 2 in section 5.2.5, which shows significant improvements in the prediction of in-plane loads. However, the sine function still overly constrains in-plane loads at the boundaries, which is solved by the cosine function as shown in section 5.2.6.

5.2.2 Sine Function

Shape Function

In this section, the sine function has been adopted for both X_k and Y_l as

$$X_k(x) = \sin\left(\frac{k\pi x}{a}\right) \quad (5.12)$$

$$Y_l(y) = \sin\left(\frac{l\pi y}{b}\right) \quad (5.13)$$

Then the Airy stress function can be written as

$$F(x, y) = \frac{1}{2}\bar{N}_x y^2 + \sum_{kl} F_{kl} \sin\left(\frac{k\pi x}{a}\right) \sin\left(\frac{l\pi y}{b}\right) \quad (5.14)$$

However, the derivatives of the shape functions are not zero at the boundaries, as the following shows

$$X'_k(x) = \frac{k\pi}{a} \cos\left(\frac{k\pi x}{a}\right) \neq 0 \text{ on } x=0, a \quad (5.15)$$

$$Y'_l(y) = \frac{l\pi}{b} \cos\left(\frac{l\pi y}{b}\right) \neq 0 \text{ on } y=0, b \quad (5.16)$$

Thus, the shear load is not zero at the four edges,

$$N_{xy} = - \sum_{kl} F_{kl} X'_k(x) Y'_l(y) \neq 0 \text{ on } x=0, a; y=0, b \quad (5.17)$$

Although the boundary conditions of N_x and N_y can be exactly satisfied, the sine function is not expected to predict the in-plane loads correctly. A variable stiffness panel shown in

Figure 5.2 has been used as an example, where the four sections are labeled for convenience and the corresponding fiber directions in each section are given.

1	2
3	4

Layup 1 ($A_{16} = A_{26} = D_{16} = D_{26} = 0$)

- Section 1: $[90\ 0\ 0\ 90]$
- Section 2: $[0\ 0\ 0\ 0]$
- Section 3: $[0\ 90\ 90\ 0]$
- Section 4: $[90\ 90\ 90\ 90]$

Figure 5.2: Layup 1

Verification

The prediction in Ritz method is carried out by using $K = 10$ and $L = 10$ terms in x and y direction. The prescribed load \bar{N}_x is 1N/mm in both Ritz method and Finite element method (FEM). In the following section, if not specifically indicated, the prescribed load is always set to be $\bar{N}_x = 1\text{N/mm}$. Figure 5.3 shows the prediction of in-plane stresses compared to FEM. The force resultants N_x , N_y , N_{xy} are averaged on the thickness corresponding to the results of Abaqus, so the stresses are given in the figure, where t is the thickness of the panel. Moreover, the results of FEM are given at the integration points to show the exact values of stresses.

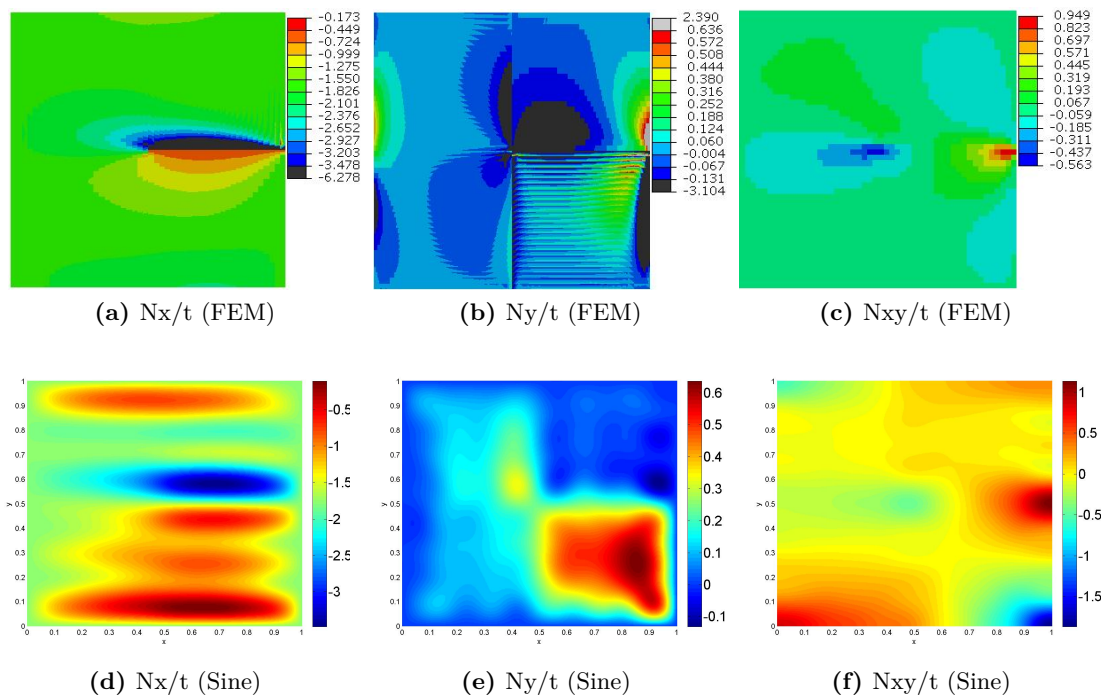


Figure 5.3: In-plane stress of Layup 1 (Mpa, $K=L=10$, $\bar{N}_x = 1\text{ N/mm}$)

Since the maximum and minimum stresses obtained from FEM are higher and lower than the maximum and minimum stresses obtained from Ritz method, the values in FEM are scaled according to the values in Ritz method. In the pictures for FEM, the areas with gray color are where the stresses higher than the maximum stress obtained from Ritz method; the areas with dark color are where the stresses lower than the minimum stress obtained from Ritz method. In the following sections, whenever the stress distributions in FEM are compared to these obtained from Ritz method, the maximum and minimum value displayed in FEM are limited by the maximum and minimum value in Ritz method, for the purpose of better comparison of the stresses distributions.

Clearly, the prediction of in-plane stresses distribution is substantially far away from the results obtained in FEM. The reason is the that the boundary condition of N_{xy} has not been satisfied by the sine function.

The sine function in this section has been shown as an example of the importance of exactly satisfying all the boundary condition of the in-plane loads. However, it does not declare that the sine function is of no usefulness in predicting the in-plane loads. Later, in the section 5.2.5 the Lagrange multiplier method will be introduced to improve the predictions of sine function.

5.2.3 Beam Characteristic Function

Shape Function

Instead of the sine function, another shape function that is a linear combination of sine, cosine, sine hyperbolic and cosine hyperbolic functions is introduced [3], which is known as the beam characteristic function.

The general form of the beam characteristic function is given as

$$X(x) = c_1 \sin \mu x + c_2 \cos \mu x + c_3 \sinh \mu x + c_4 \cosh \mu x \quad (5.18)$$

where, c_i ($i = 1 \cdots 4$) are the undetermined parameters which can be solved from the boundary conditions.

This equation is actually the general solution of the fourth order governing differential equation for beams under natural vibration. For the detail of this equation, please refer to the chapter 4.2.4 of Reddy's book [3]. The specific form of the beam characteristic function will be derived to satisfy the boundary conditions expressed in option 1 term by term.

The boundary conditions for the general form of the beam characteristic function corresponding to the conditions in option 1 are

$$X(x) = X'(x) = 0 \text{ on } x=0, a \quad (5.19)$$

The beam characteristic function is subjected to the above boundary conditions, and then the following equations are obtained.

$$X(0) = c_2 + c_4 = 0 \quad (5.20)$$

$$X(a) = c_1 \sin \mu a + c_2 \cos \mu a + c_3 \sinh \mu a + c_4 \cosh \mu a = 0 \quad (5.21)$$

$$X'(0) = \mu(c_1 + c_3) = 0 \quad (5.22)$$

$$X'(a) = \mu[c_1 \cos \mu a - c_2 \sin \mu a + c_3 \cosh \mu a + c_4 \sinh \mu a] = 0 \quad (5.23)$$

Since $c_4 = -c_2$ and $c_1 = -c_3$, they can further reduce to

$$c_1(\sin \mu a - \sinh \mu a) + c_2(\cos \mu a - \cosh \mu a) = 0 \quad (5.24)$$

$$c_1(\cos \mu a - \cosh \mu a) - c_2(\sin \mu a + \sinh \mu a) = 0 \quad (5.25)$$

which written in matrix form is

$$\begin{bmatrix} \sin \mu a - \sinh \mu a & \cos \mu a - \cosh \mu a \\ \cos \mu a - \cosh \mu a & -\sin \mu a - \sinh \mu a \end{bmatrix} \begin{pmatrix} c_1 \\ c_2 \end{pmatrix} = \begin{pmatrix} 0 \\ 0 \end{pmatrix} \quad (5.26)$$

To get the non-zero solution of c_1 and c_2 , the determinate of the coefficient matrix must be zero.

$$\begin{vmatrix} \sin \mu a - \sinh \mu a & \cos \mu a - \cosh \mu a \\ \cos \mu a - \cosh \mu a & -\sin \mu a - \sinh \mu a \end{vmatrix} = 2 \cos \mu a \cosh \mu a - 2 = 0 \quad (5.27)$$

So μ can be solved from above equation as

$$\mu = \frac{k + \frac{1}{2}\pi}{a} \quad (5.28)$$

where, k is a positive integer.

Then $-\frac{c_1}{c_2}$ can be solved from equation 5.26 as

$$-\frac{c_1}{c_2} = \frac{\sin \mu a + \sinh \mu a}{\cosh \mu a - \cos \mu a} = \frac{\cos \mu a - \cosh \mu a}{\sin \mu a - \sinh \mu a} \quad (5.29)$$

where, the above two expressions for $-\frac{c_1}{c_2}$ are equivalent to each other.

The equation 5.18 can then be written as

$$X(x) = -c_2[\cosh \mu x - \cos \mu x - r(\sinh \mu x - \sin \mu x)] \quad (5.30)$$

where, r is given as

$$r = -\frac{c_1}{c_2} = \frac{\sin \mu a + \sinh \mu a}{\cosh \mu a - \cos \mu a} \quad (5.31)$$

or

$$r = -\frac{c_1}{c_2} = \frac{\cos \mu a - \cosh \mu a}{\sin \mu a - \sinh \mu a} \quad (5.32)$$

Therefore, there is only one unknown parameter c_2 left in the beam characteristic function.

Since the boundary conditions of X_k , the shape function of Airy stress function in x direction, are the same as the boundary conditions of X as shown in equation 5.19, the shape function for X_k can be assumed as

$$X_k(x) = \cosh \mu_k x - \cos \mu_k x - r_x(\sinh \mu_k x - \sin \mu_k x) \quad (5.33)$$

where,

$$r_k = \frac{\cos \mu_k a - \cosh \mu_k a}{\sin \mu_k a - \sinh \mu_k a} \quad (5.34)$$

and

$$\mu_k = \frac{k + \frac{1}{2}\pi}{a} \quad (5.35)$$

The unknown parameter c_2 in equation 5.30 is not shown in the equation for X_k . The reason is that c_2 can be regarded as the undetermined parameter (F_{kl}) of the shape function as shown in equation 5.2, which will be solved using Ritz method.

Similarly, the shape function for Y_l , which is the shape function of Airy stress function in y direction, can be assumed as

$$Y_l(y) = \cosh \mu_l y - \cos \mu_l y - r_l(\sinh \mu_l x - \sin \mu_l y) \quad (5.36)$$

where,

$$r_l = \frac{\cos \mu_l b - \cosh \mu_l b}{\sin \mu_l b - \sinh \mu_l b} \quad (5.37)$$

and

$$\mu_l = \frac{l + \frac{1}{2}}{b} \pi \quad (5.38)$$

These shape functions for X_k and Y_l are directly derived from the boundary conditions 5.8 and 5.9, so they satisfy these conditions term by term. Moreover, if the boundary conditions change into

$$X_k(x) = X_k''(x) = 0 \text{ on } x=0, a \quad (5.39)$$

$$Y_l(y) = Y_l''(y) = 0 \text{ on } y=0, b \quad (5.40)$$

the beam characteristic function subjected to above boundary conditions is actually the sine function because the parameters of cosine, sine hyperbolic and cosine hyperbolic functions are zero. So the sine function is a special case of the beam characteristic function.

Verification

The panel with the layup 1 shown in Figure 5.2 is studied by applying the beam characteristic function (equation 5.33 5.36), and compared to the results obtained from FEM and sine function in Figure 5.4. The prediction in Ritz method is carried out by using $K = 10$ and $L = 10$ terms in x and y direction, respectively. Clearly, the prediction has been improved significantly, because the boundary condition of N_{xy} has been satisfied in the beam characteristic functions.

However, the peak stresses (the minimum or the maximum stresses) in FEM are extremely lower or higher than the minimum and maximum stresses obtained in Ritz method by using the beam characteristic function. This is due to the discontinuity of stiffness at the boundaries of the neighboring sections since the panel has been divided into sections with different stiffness. Due to the discontinuity of stiffness, the stresses in FEM are discontinuous and the peak stresses only appear at the boundaries, as seen in Figure 5.4a. Moreover, the results in FEM are given at the integration points, so FEM can only exactly show the stresses by points which are discontinuous. While, in Ritz method, the in-plane stresses are approximated by finite number of continuous shape functions. Since the shape functions are continuous, the in-plane stresses obtained from Ritz method are continuous over the panel. So the extreme discontinuity of stresses in FEM cannot be predicted by Ritz method using finite number of continuous shape functions unless infinite number of shape functions are used. This can also explain why the locations of the peak stresses in Ritz method are slight away from the

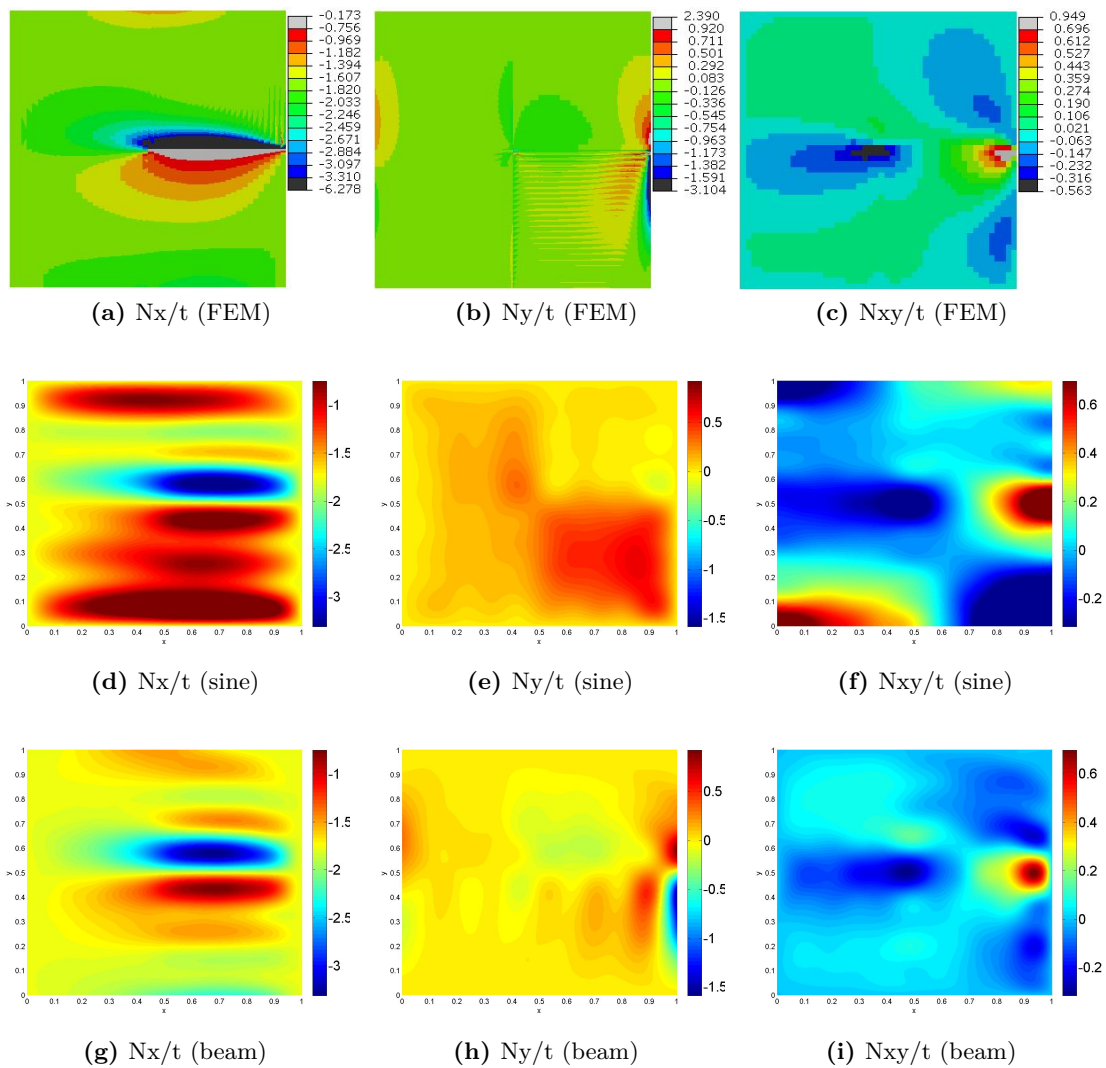


Figure 5.4: In-plane Stress of Layup 1 (Mpa, $K=L=10$, $\bar{N}_x = 1$ N/mm)

boundaries of the neighboring sections, while the peak stresses in FEM are located closely at the boundaries, as shown in 5.4a.

Although the stresses in Ritz method are always continuous, the discontinuity of the stresses can be approximated through increasing the number of terms used in Ritz method. As shown in Figure 5.5, the stresses in Ritz method are obtained at $K = L = 18$ and compared to FEM; in Figure 5.6, the stresses in Ritz method are obtained at $K = L = 50$ and compared to FEM. It is clearly shown in these figures that as increasing the number of terms, the predictions of in-plane loads distribution in the Ritz method become increasingly closer to these in FEM, as well as the peak stresses and their locations.

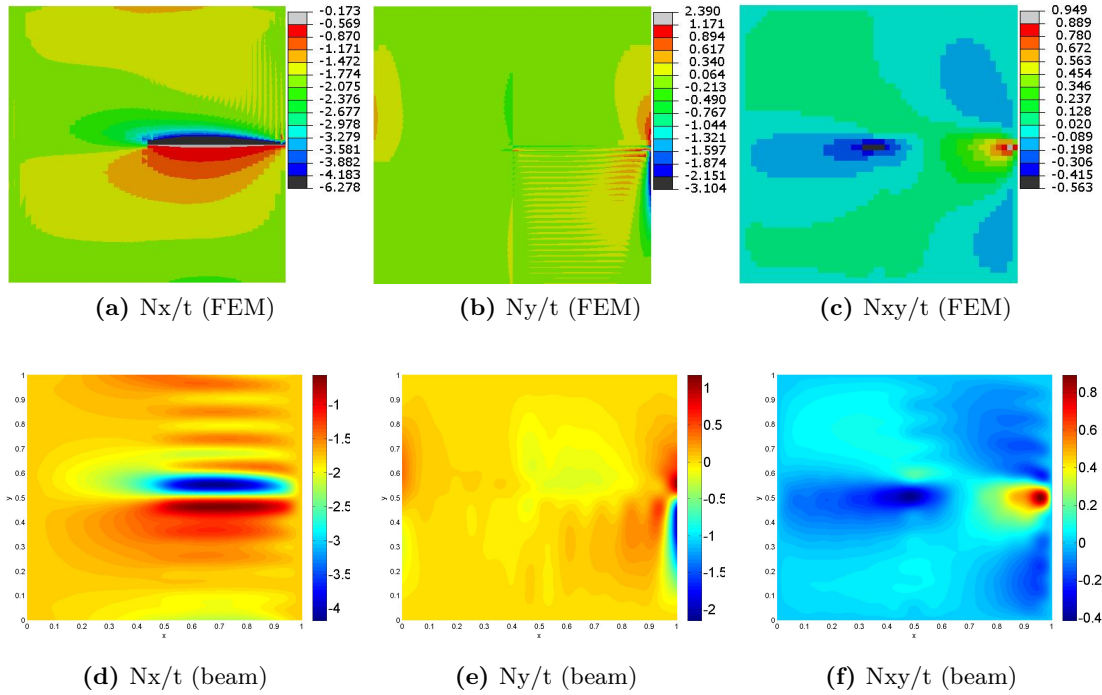


Figure 5.5: In-plane Stress of Layup 1 (Mpa, $K=L=18$, $\bar{N}_x = 1$ N/mm)

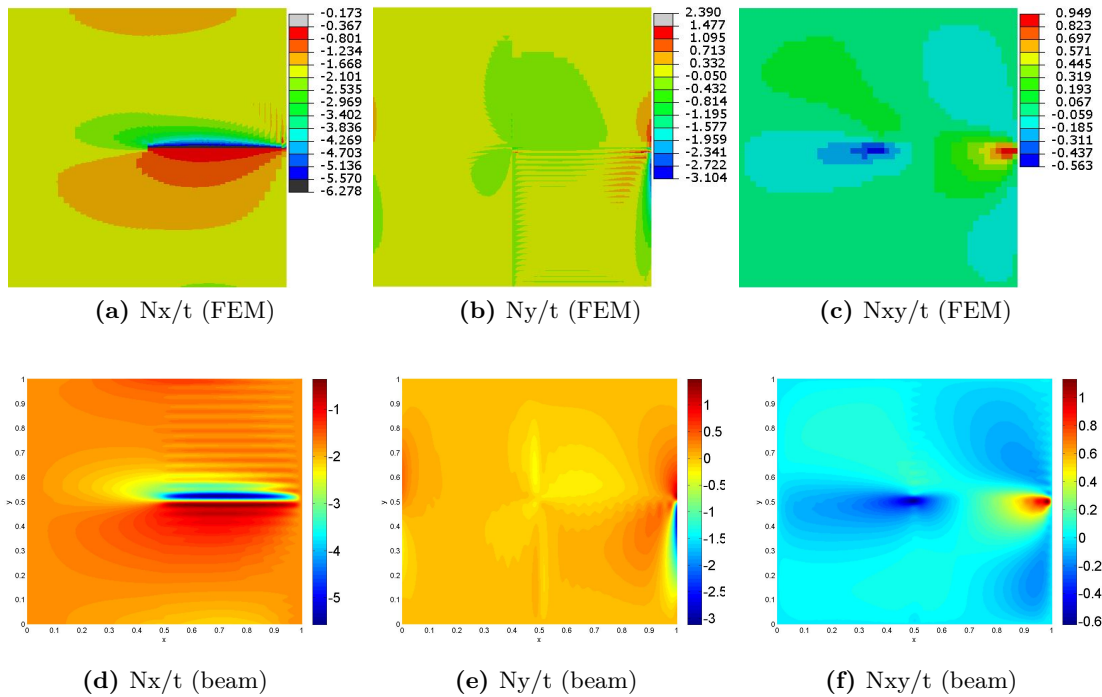
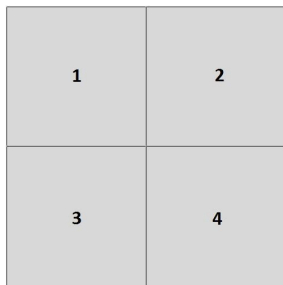


Figure 5.6: In-plane Stress of Layup 1 (Mpa, $K=L=50$, $\bar{N}_x = 1$ N/mm)

The stretching-shearing couplings (A_{16} and A_{26}) of Layup 1 shown in Figure 5.2 are both

zero, since the layup is balanced. The second layup is shown in Figure 5.7, where A_{16} and A_{26} are non-zero, to verify that Ritz method can also predict the in-plane stresses of this kind of panels. The stresses distributions are shown in Figure 5.8, where $K = L = 18$ in Ritz method. Clearly, the stress distributions have been satisfactorily predicted by the Ritz method using beam characteristic functions. However, the peak stresses in FEM still cannot be exactly predicted which are shown in gray and black colors in the pictures. Again these peak stresses only appear at the boundaries of the neighboring sections since they are caused by the stiffness discontinuity.



Layup 2 ($A_{16}, A_{26}, D_{16}, D_{26} \neq 0$)

- Section 1: [45 45 45 45]
- Section 2: [0 -45 -45 0]
- Section 3: [-45 -45 -45 -45]
- Section 4: [90 45 45 90]

Figure 5.7: Layup 2

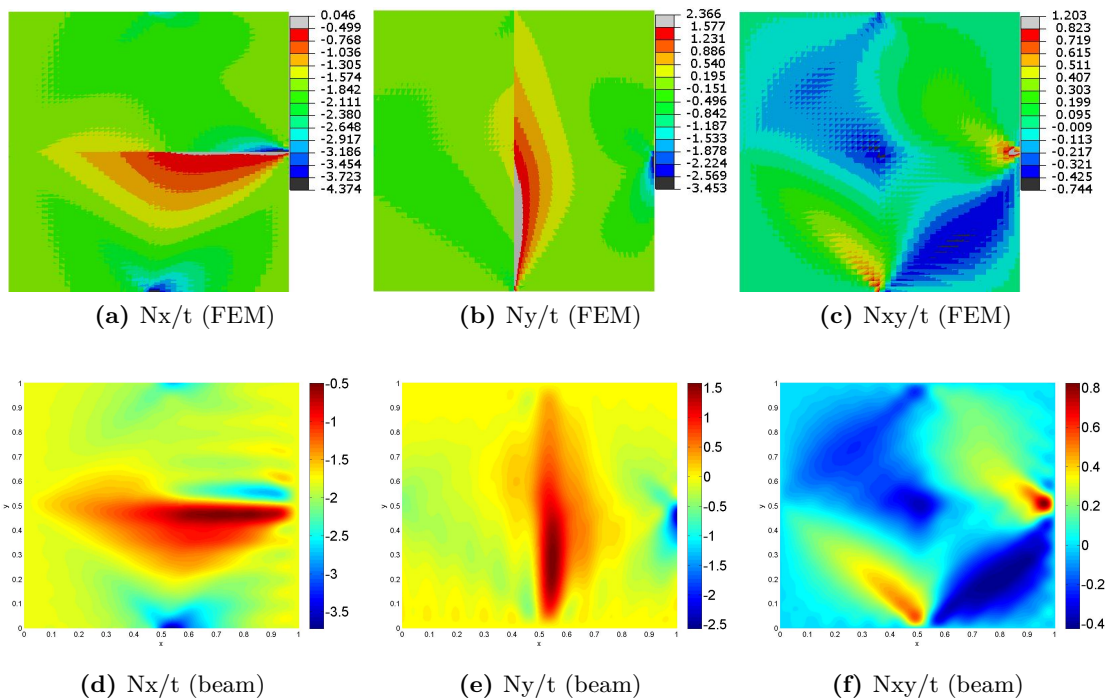


Figure 5.8: In-plane Stress of Layup 2 (Mpa, $K=L=18, \bar{N}_x = 1$ N/mm)

Since the peaks stresses of layup 1 and 2 shown in FEM are caused by the stiffness discontinuity, another example is used to show the prediction of in-plane stress distributions and the peak stresses will be improved if reducing the discontinuity of stiffness. The layup of this example is shown in Figure 5.9, where both A_{16} and A_{26} are non-zero in section 2 and 3. The

stiffness is still discontinuous in layup 3, however, the transition of discontinuous stiffness in neighboring sections is smoother than layup 1 and 2 since the difference of fiber orientations is only 5 degree. The stress distributions are shown in Figure 5.10, where $K = L = 18$ in Ritz method. Clearly, the prediction of in-plane loads and the peak stresses obtained in Ritz method become closer to these in FEM. Therefore, one can expect that if a panel whose stiffness is variable but continuous has been considered here, the prediction of in-plane loads will be even better than what are shown in Figure 5.5, 5.8 and 5.10.

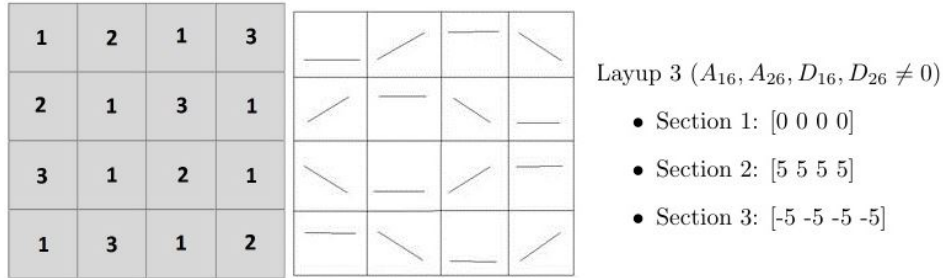


Figure 5.9: Layup 3

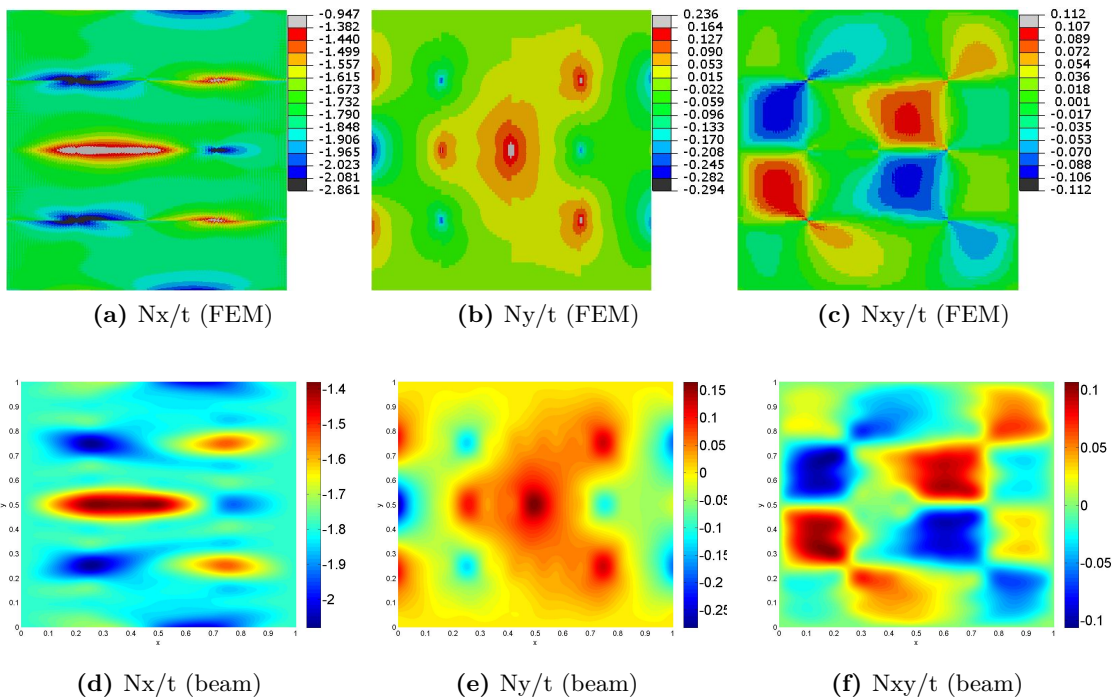


Figure 5.10: In-plane Stress of Layup 3 (Mpa, $K=L=18$, $\bar{N}_x = 1$ N/mm)

Numerical Issue

During the implementation in numerical software (such as Matlab, Maple), the numerical problems were observed using the beam characteristic function. Similar numerical issues

were also reported by Zhang and Matthews [12] that the values of r_k (equation 5.34) and r_l (equation 5.37) must have as many significant figures as possible. They noticed that six significant figures are not enough to get good orthogonality of the shape functions and some error (6.4%) in prediction of buckling load may be expected. They compared the values of r_k obtained using more than six significant figures with these obtained using only six significant figures, which are shown in Figure 2.2, where r_i in the figure is the r_k here. Clearly, after three terms, the value of r_k (or r_i) is exactly 1 if only six significant figures are used. However, it is r_k equals to 1 that leads to the numerical problem, which can be explained using the following equation.

$$X_k = \frac{1 - r_k}{2} e^{\mu_k x} + \frac{1 + r_k}{2} e^{-\mu_k x} - \cos \mu_k x + r_k \sin \mu_k x \quad (5.41)$$

Above equation is equivalent to the beam characteristic equation (equation 5.33) since the hyperbolic functions can be written in terms of exponential functions. r_k equals 1 implies that the first term on the right-hand side of the equation disappears. While, $e^{\mu_k x}$ may be very large which cannot be ignored. So r_k cannot be exactly 1. Thus, enough significant figures should be used for r_k , and as well as r_l .

Their observation is correct, the exact value of r_k has important influence on the orthogonality of the shape function and thus on the accuracy of the prediction. However, even though the most significant figures are used for r_k , r_k still equals to 1 when $k > 11$ as shown in Table 5.2. In the third column of Table 5.2, $r_k - 1$ is exactly 0 after $k = 11$, which implies r_k is exactly 1 in numerical software (Maple or Matlab).

Table 5.2: The value of r_k and $r_k - 1$

k	r_k	$r_k - 1$	$r_k - 1$ (rewrite)
1	0,982507682528266	-0,017492317	-0,017492317
2	1,000777311438030	0,000777311	0,000777311
3	0,999966450125447	-3,35E-05	-3,35E-05
4	1,000001449897660	1,45E-06	1,45E-06
5	0,999999937344383	-6,27E-08	-6,27E-08
6	1,000000002707600	2,71E-09	2,71E-09
7	0,99999999882994	-1,17E-10	-1,17E-10
8	1,00000000005060	5,06E-12	5,06E-12
9	0,9999999999782	-2,18E-13	-2,19E-13
10	1,00000000000010	9,55E-15	9,44E-15
11	1,00000000000000	-4,44E-16	-4,08E-16
12	1,00000000000000	0	1,76E-17
13	1,00000000000000	0	-7,62E-19
14	1,00000000000000	0	3,29E-20
15	1,00000000000000	0	-1,42E-21

The reason for this problem is that both the denominator and numerator of r_k will be infinite large when $k > 11$ due to the hyperbolic functions in the denominator and numerator. Then the quotient of these two infinite large values is exactly 1 in numerical software. In addition, the values of sine and cosine function will be truncated when added to cosine and sine hyperbolic functions since they are too small. If plot the shape function $X_k(x)$ from $\frac{x}{a} = 0$ to $\frac{x}{a} = 1$

as increasing the value of k , the numerical error is clearly shown in Figure 5.11. Especially when $k = 15$, the half-waves near $\frac{x}{a} = 1$ are truncated due to the numerical error.

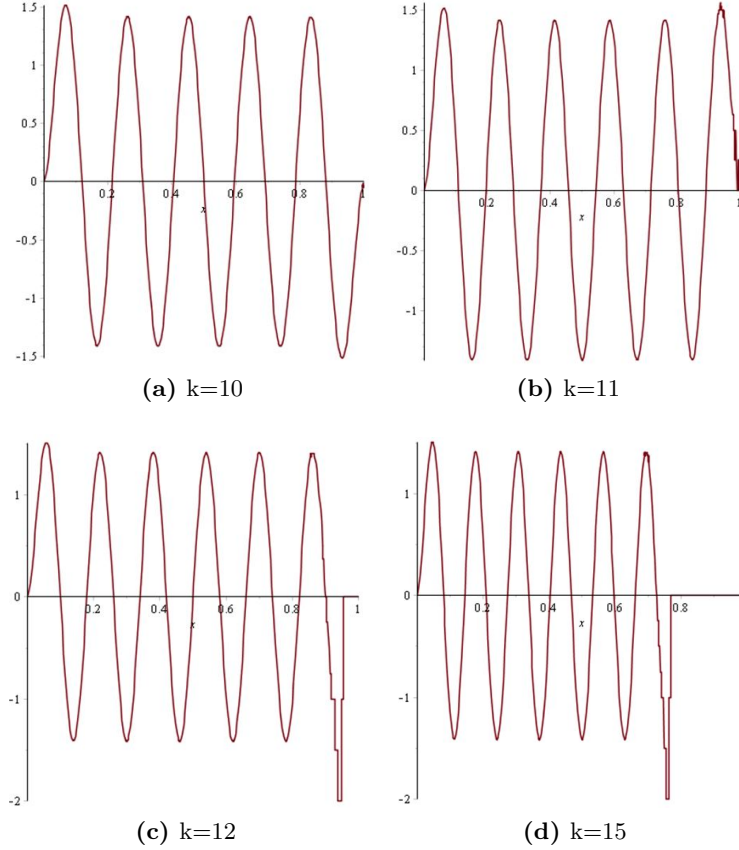


Figure 5.11: Plot of X_k with Numerical Error as Increasing k ($\frac{x}{a} = 0 \dots 1$)

Therefore the solution proposed by Zhang and Matthews [12] is not valid when $k > 11$. However, the problem has been solved through rewriting the expressions of r_k and the beam characteristic function.

Since the numerical error is originally from r_k , to solve the problem it can be rewritten as

$$r_k - 1 = \frac{\cos \mu_k a - \cosh \mu_k a}{\sin \mu_k a - \sinh \mu_k a} - 1 = \frac{\cos \mu_k a - \sin \mu_k a - e^{-\mu_k a}}{\sin \mu_k a - \sinh \mu_k a} \quad (5.42)$$

As increasing k , the absolute value of the denominator will be extremely large due to the sine hyperbolic function, while the numerator is always relatively small. Consequently, the value of $r_k - 1$ is extremely close to 0, but never be 0, as shown in the fourth column of Table 5.2. The reason is the numerical software can always store it with enough digits. Although the sine function in the denominator will be truncated since the sine hyperbolic function is extremely large, but the error of the truncation is relatively small. To keep this beneficial property of $r_k - 1$, it is replaced by r_{k1} as

$$r_{k1} = r_k - 1 = \frac{\cos \mu_k a - \sin \mu_k a - e^{-\mu_k a}}{\sin \mu_k a - \sinh \mu_k a} \quad (5.43)$$

Correspondingly, the equation 5.33 of X_k can be rewritten as

$$X_k(x) = e^{-\mu_k x} + \sin \mu_k x - \cos \mu_k x + r_{k1} \sin \mu_k x - r_{k1} \sinh \mu_k x \quad (5.44)$$

or a more computational efficient way,

$$X_k(x) = e^{-\mu_k x} + \sin \mu_k x - \cos \mu_k x + r_{k1} \sin \mu_k x - r_{k1} \frac{e^{\mu_k x} - e^{-\mu_k x}}{2} \quad (5.45)$$

Similarly, Y_l can be rewritten as

$$Y_l(y) = e^{-\mu_l y} + \sin \mu_l y - \cos \mu_l y + r_{l1} \sin \mu_l y - r_{l1} \frac{e^{\mu_l y} - e^{-\mu_l y}}{2} \quad (5.46)$$

where,

$$r_{l1} = r_l - 1 = \frac{\cos \mu_l b - \sin \mu_l b - e^{-\mu_l b}}{\sin \mu_l b - \sinh \mu_l b} \quad (5.47)$$

Then, the correct plots of X_k are shown in Figure 5.12, which are substantially improved compared to Figure 5.11. In Figure 5.13, the in-plane stress distribution with numerical errors are compared to these without numerical error obtained using the modified version of shape functions. Furthermore, all the in-plane stresses distributions in this section (section 5.2.3) were obtained with the modified version of shape functions.

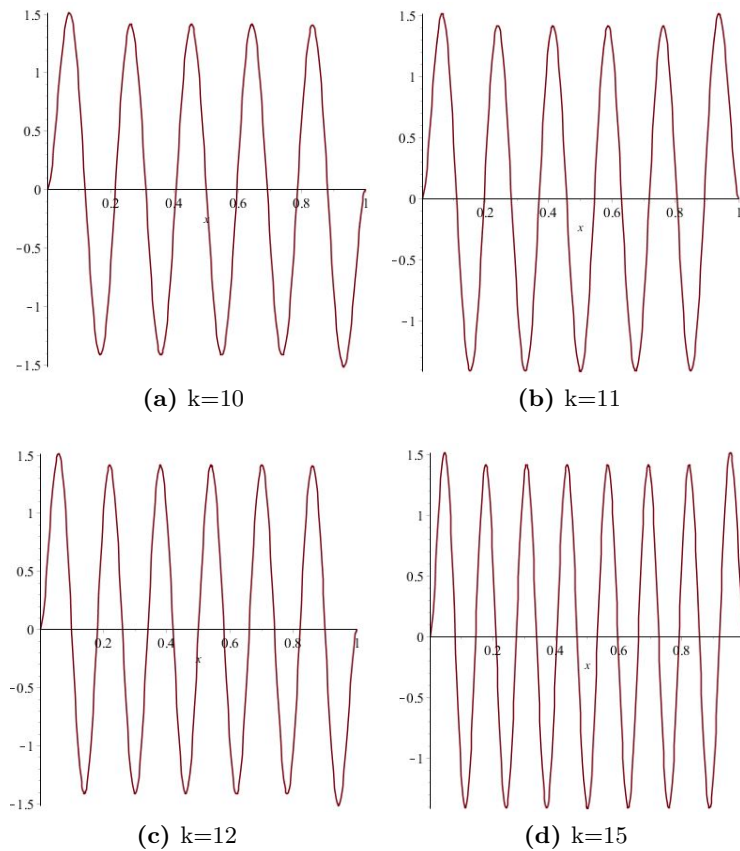


Figure 5.12: Plot of X_k as Increasing k ($\frac{x}{a} = 0 \dots 1$)

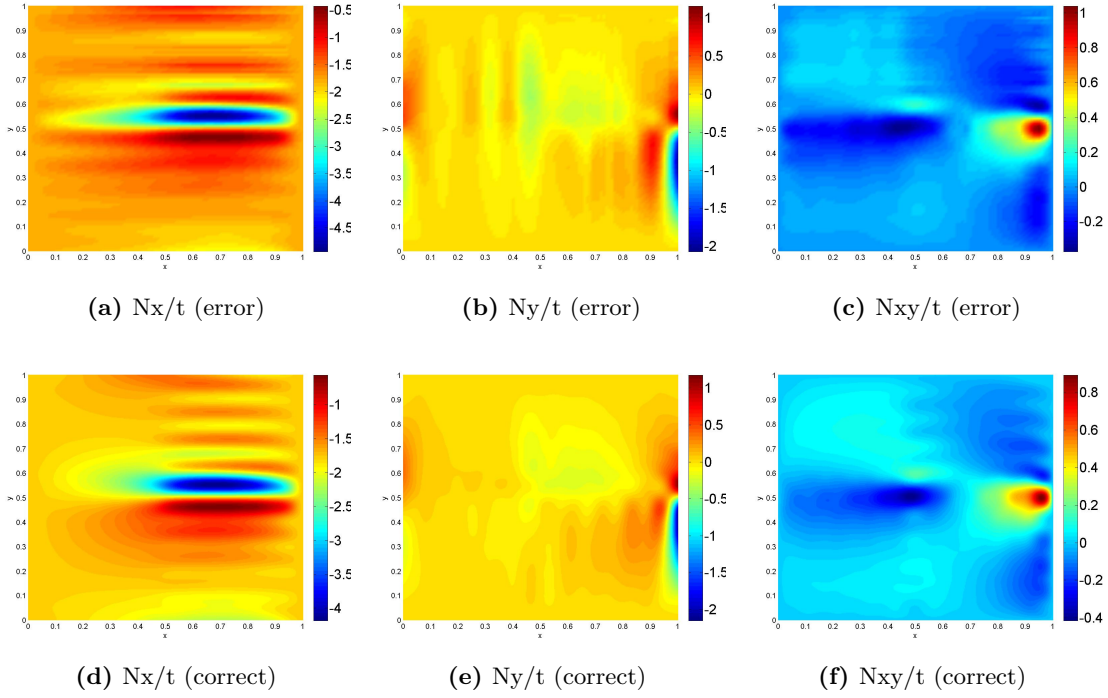


Figure 5.13: Numerical Error of In-plane Stress of Beam Characteristic Function (Mpa, K=L=18)

5.2.4 Polynomial Function

Shape Function

Besides the beam characteristic function, the algebraic polynomial function can exactly satisfy the boundary conditions of the option 1 term by term.

The boundary conditions X_k has to satisfy term by term is shown as follows (equation 5.8)

$$X_k(x) = X'_k(x) = 0 \text{ on } x=0, a \quad (k = 1 \cdots K) \quad (5.48)$$

If an algebraic polynomial is to be selected, one may begin with the five-term complete polynomial, as

$$X(x) = k_0 + k_1x + k_2x^2 + k_3x^3 + k_4x^4 \quad (5.49)$$

where, k_0 to k_4 are undetermined parameters.

The fourth order polynomial is chosen to correspond to the four conditions in the boundary condition of X_k . Similarly, the boundary conditions of $X(x)$ is

$$X(x) = X'(x) = 0 \text{ on } x=0, a \quad (5.50)$$

With four boundary conditions for X in above equation, the four of five undetermined parameters can be solved. The rest parameter is arbitrary, thus it may be set as unity. Then, the shape function of $X(x)$ has been solved as

$$X(x) = \left(\frac{x}{a}\right)^2 \left(\frac{x}{a} - 1\right)^2 \quad (5.51)$$

The k^{th} function of $X(x)$ can be assumed as

$$X_k(x) = \left(\frac{x}{a}\right)^{k+1} \left(\frac{x}{a} - 1\right)^2 \quad (5.52)$$

Similarly, the shape function Y_l can be assumed as

$$Y_l(y) = \left(\frac{y}{b}\right)^{l+1} \left(\frac{y}{b} - 1\right)^2 \quad (5.53)$$

However, these functions are not orthogonal, which means they do not satisfy the following conditions.

$$\int_0^a X_i(x)X_j(x)dx = 0 \quad i \neq j \quad (5.54)$$

$$\int_0^b Y_i(y)Y_j(y)dy = 0 \quad i \neq j \quad (5.55)$$

To avoid possible numerical problem (for examples, some matrices may not be positive definite) and achieve numerical accuracy and convenience, it is advantages to orthogonalize the shape functions [15]. The orthogonalization of the polynomial functions (equation 5.52 5.53) are implemented through the Gram-Schmidt process. Furthermore, to avoid the numerical unstable problem after Gram-Schmidt process, the shape functions are transformed to the nondimensional form spanning the interval $[-1, 1]$.

$$X_k(\xi) = (\xi - 1)^{k+1}(\xi + 1)^2 \quad (\xi \in [-1, 1]) \quad (5.56)$$

$$Y_l(\eta) = (\eta - 1)^{l+1}(\eta + 1)^2 \quad (\eta \in [-1, 1]) \quad (5.57)$$

where, $\xi = \frac{2x-a}{a}$ and $\eta = \frac{2y-b}{b}$.

After the Gram-Schmidt process, the orthogonalized polynomial function X_k can be written as

$$X_1(\xi) = \frac{3\sqrt{35}}{16}(\xi^2 - 1)^2 \quad (5.58)$$

$$X_2(\xi) = \frac{3\sqrt{385}}{16}\xi(\xi^2 - 1)^2 \quad (5.59)$$

$$X_3(\xi) = \frac{3\sqrt{91}}{32}(\xi^2 - 1)^2(11\xi^2 - 1) \quad (5.60)$$

$$X_4(\xi) = \frac{3\sqrt{385}}{32}\xi(\xi^2 - 1)^2(13\xi^2 - 3) \quad (5.61)$$

$$\vdots \quad (5.62)$$

Similarly, the orthogonalized Y_l is given as

$$Y_1(\eta) = \frac{3\sqrt{35}}{16}(\eta^2 - 1)^2 \quad (5.63)$$

$$Y_2(\eta) = \frac{3\sqrt{385}}{16}\eta(\eta^2 - 1)^2 \quad (5.64)$$

$$Y_3(\eta) = \frac{3\sqrt{91}}{32}(\eta^2 - 1)^2(\eta^2 - 1) \quad (5.65)$$

$$Y_4(\eta) = \frac{3\sqrt{385}}{32}\eta(\eta^2 - 1)^2(\eta^2 - 3) \quad (5.66)$$

$$\vdots \quad (5.67)$$

Correspondingly, the total complementary energy functional (equation 4.81) has to be rewritten as

$$\begin{aligned} \Pi_{pre}^c = & \frac{1}{2} \frac{ab}{4} \int_{-1}^1 \int_{-1}^1 [a_{11} \bar{N}_x^2 + 2\bar{N}_x \sum_{kl}^{KL} F_{kl} \begin{pmatrix} a_{11} \\ a_{12} \\ a_{16} \end{pmatrix}^T \begin{pmatrix} (\frac{2}{b})^2 X_k Y_l'' \\ (\frac{2}{a})^2 X_k'' Y_l \\ -(\frac{4}{ab}) X_k' Y_l' \end{pmatrix} \\ & + \sum_{klk_2l_2}^{KLLK} F_{kl} F_{k_2l_2} \begin{pmatrix} (\frac{2}{b})^2 X_k Y_l'' \\ (\frac{2}{a})^2 X_k'' Y_l \\ -(\frac{4}{ab}) X_k' Y_l' \end{pmatrix}^T \mathbf{A}^{-1} \begin{pmatrix} (\frac{2}{b})^2 X_{k_2} Y_{l_2}'' \\ (\frac{2}{a})^2 X_{k_2}'' Y_{l_2} \\ -(\frac{4}{ab}) X_{k_2}' Y_{l_2}' \end{pmatrix}] d\xi d\eta \end{aligned} \quad (5.68)$$

Verification

The prediction in Ritz method is carried out by using $K = 18$ and $L = 18$ terms in x and y direction. Figure 5.14, 5.15 and 5.16 show the prediction of in-plane stresses of Layup 1, Layup 2 and Layup 3, respectively. The maximum and minimum limits in FEM are constrained by the maximum and minimum values of the predictions using polynomial functions. The predictions using beam characteristic functions are also shown there for comparison.

It is noted that the predictions using these two shape functions are more or less the same which proves that both shape functions are sufficient to predict the in-planes loads.

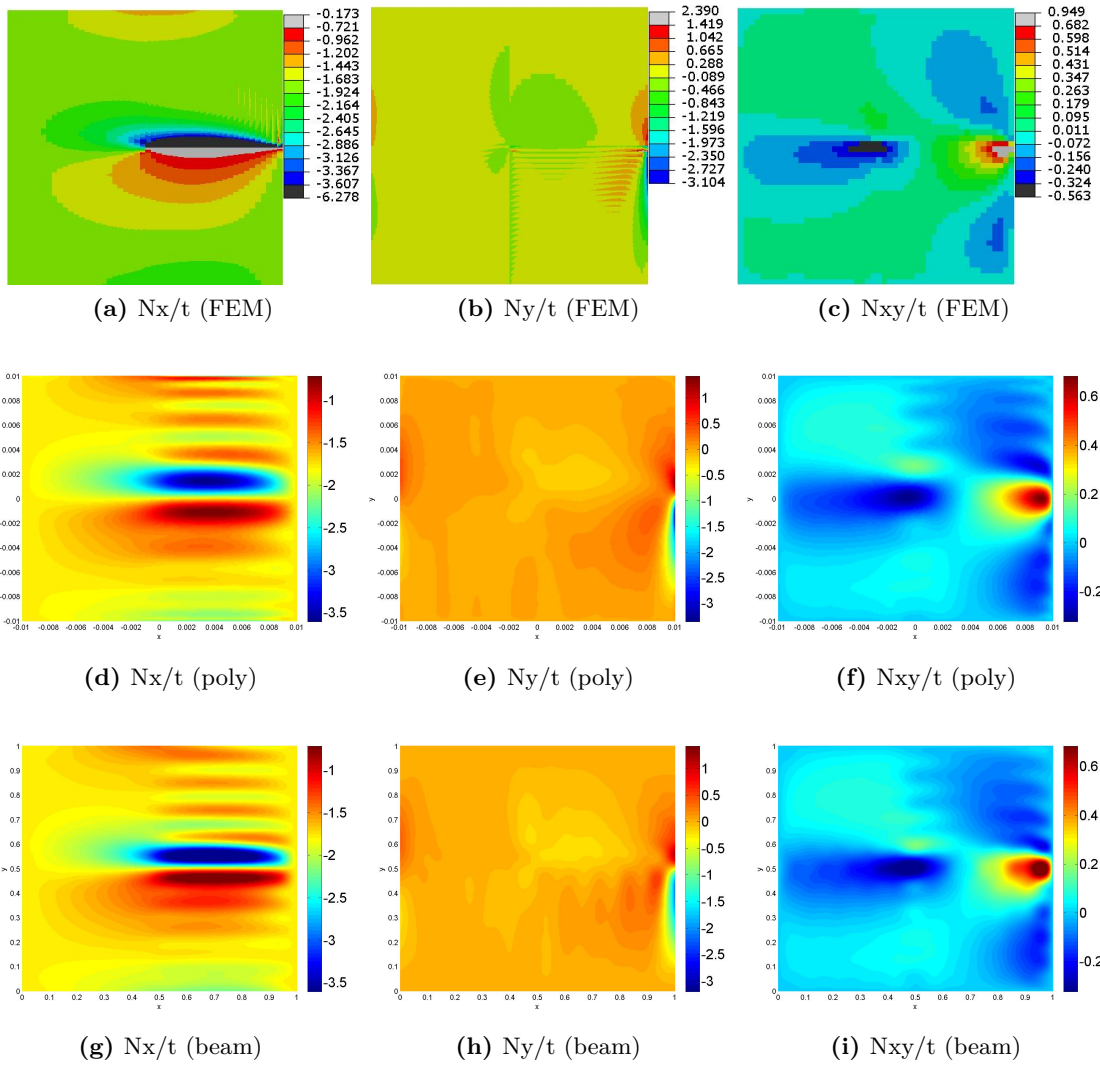


Figure 5.14: In-plane Stress of Layup 1 (Mpa, $K=L=18$, $\bar{N}_x = 1$ N/mm)

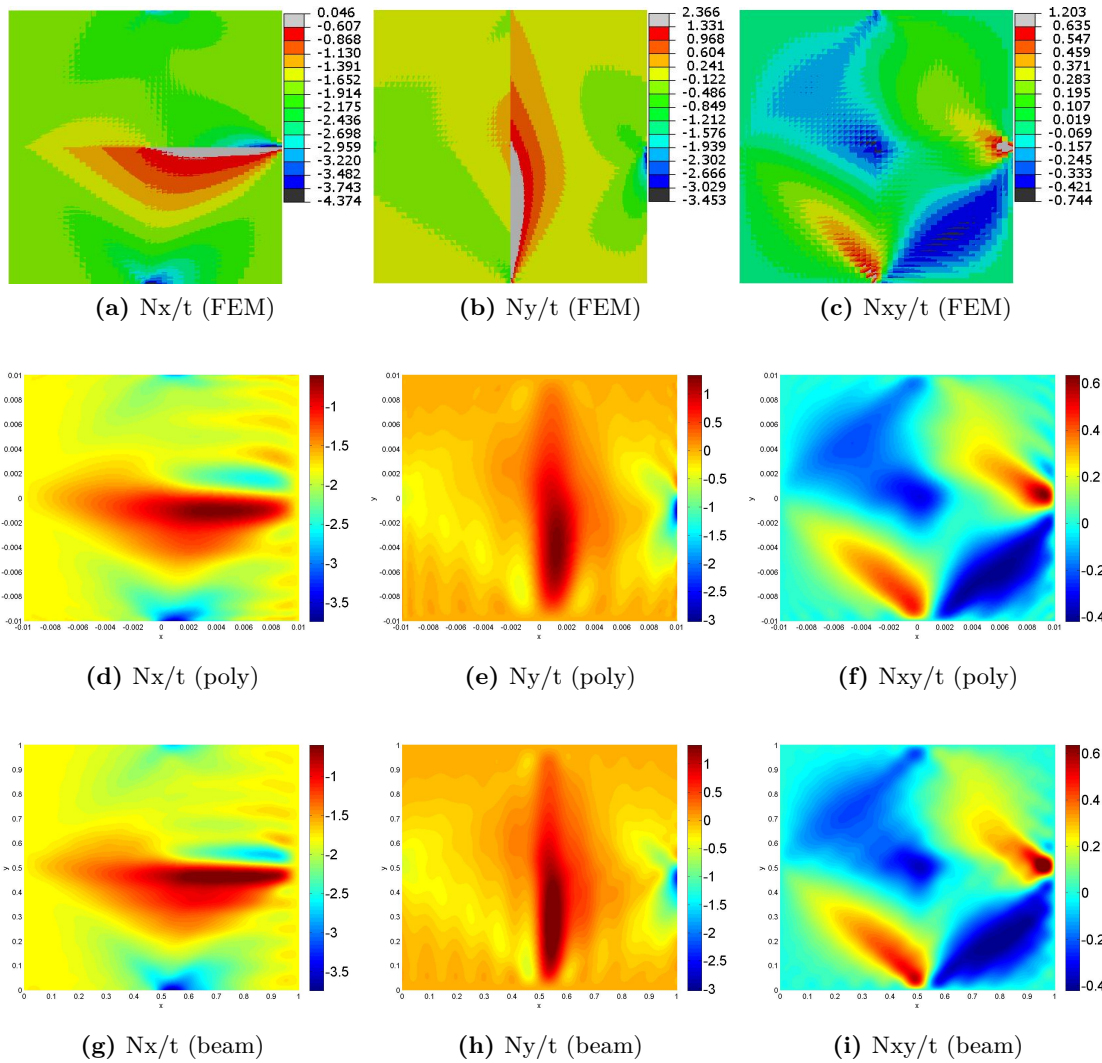


Figure 5.15: In-plane Stress of Layup 2 (Mpa, $K=L=18$, $\bar{N}_x = 1$ N/mm)

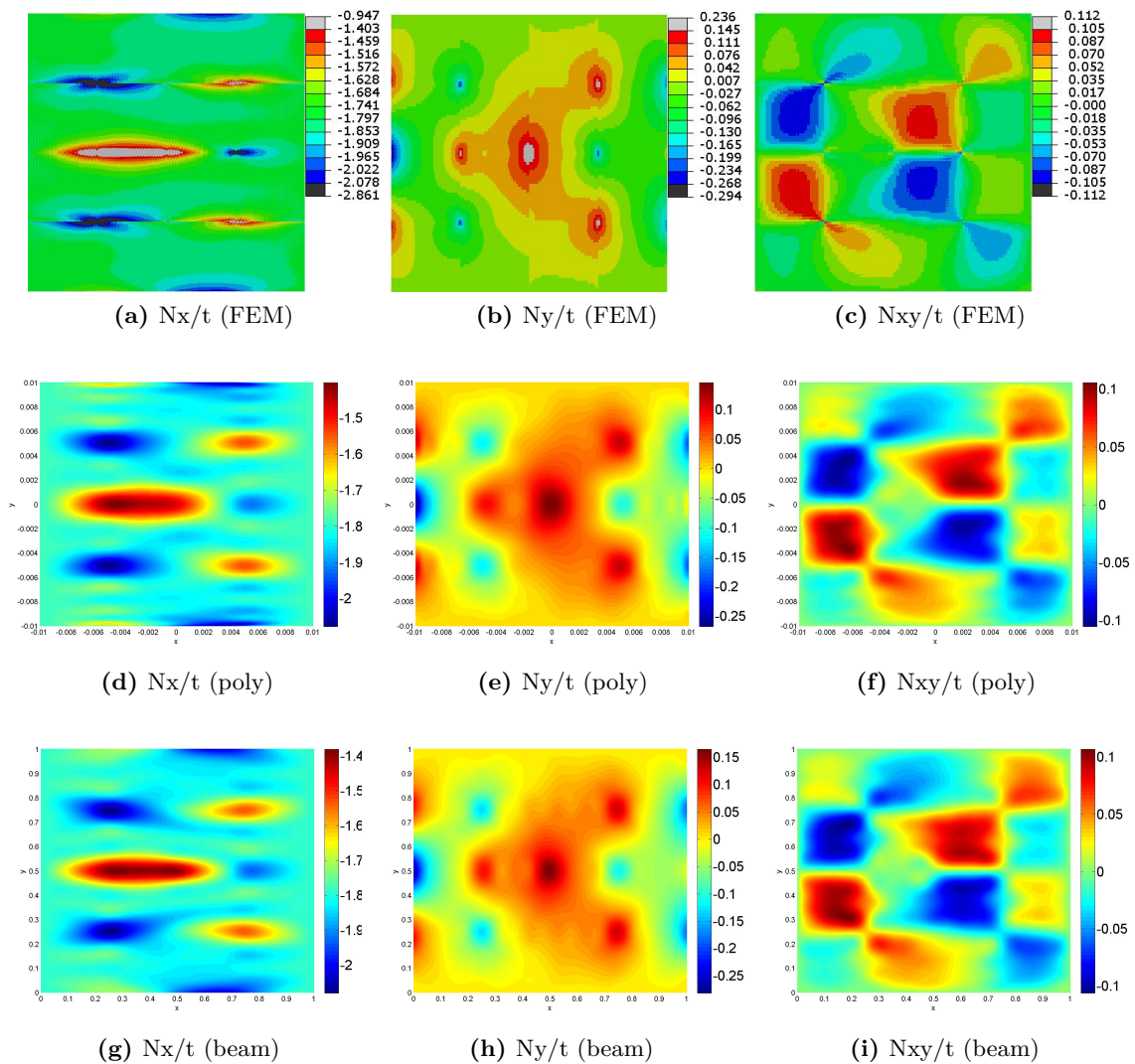


Figure 5.16: In-plane Stress of Layup 3 (Mpa, $K=L=18$, $\bar{N}_x = 1$ N/mm)

5.2.5 Sine Function with Lagrange Multiplier

Shape Function

As indicated in the conditions of option 2, the boundary conditions are satisfied by the shape function in a set, instead of term by term. This will be accomplished by introducing the Lagrange Multiplier to the total complementary energy.

Taking the sine function for example, the problem of the sine function is that it cannot satisfy the boundary condition of shear stress term by term, as indicated in equation 5.15 5.16 5.17. However, the method of Lagrange multiplier will make the sum of a set of sine functions with parameters to be zero at the boundaries by manipulating the values of the parameters.

Since the sine function does not satisfy the boundary conditions of N_{xy} term by term, following conditions must be applied to the sine function such that it can satisfy the boundary conditions

in a set, as what required by the option 2.

$$\sum_k^K F_{kl} X'_k(x) = 0 \text{ on } x=0, a \quad (l = 1 \cdots L) \quad (5.69)$$

$$\sum_l^L F_{kl} Y'_l(y) = 0 \text{ on } y=0, b \quad (k = 1 \cdots K) \quad (5.70)$$

If the above conditions are satisfied, the boundary conditions of shear loads will be exactly satisfied, as shown below.

$$N_{xy} = - \sum_l^L \left[\sum_k^K F_{kl} X'_k(x) \right] Y'_l(y) = 0 \text{ on } x=0, a \quad (5.71)$$

$$N_{xy} = - \sum_k^K \left[\sum_l^L F_{kl} Y'_l(y) \right] X'_k(x) = 0 \text{ on } y=0, b \quad (5.72)$$

The conditions in equation 5.69 and 5.70 are implemented in Ritz method by introducing the Lagrange multipliers into the total complementary energy (equation 4.23), as

$$\begin{aligned} \Pi_{pre}^c = & \frac{1}{2} \int \int (\mathbf{f}^T \mathbf{A}^{-1} \mathbf{f}) dx dy + \sum_{j_1}^{J_1} \Lambda_{j_1} \left[\sum_k^K F_{kl} X'_k(0) \right] + \sum_{j_2}^{J_2} \Lambda_{j_2} \left[\sum_k^K F_{kl} X'_k(a) \right] \\ & + \sum_{i_1}^{I_1} \Lambda_{i_1} \left[\sum_l^L F_{kl} Y'_l(0) \right] + \sum_{i_2}^{I_2} \Lambda_{i_2} \left[\sum_l^L F_{kl} Y'_l(b) \right] \end{aligned} \quad (5.73)$$

where, Λ_{j_1} , Λ_{j_2} , Λ_{i_1} and Λ_{i_2} are Lagrange multipliers; I_1 , I_2 , J_1 , J_2 are numbers of Lagrange multipliers and $I_1 \leq K$, $I_2 \leq K$, $J_1 \leq L$, $J_2 \leq L$.

By making the total energy functional Π_{pre}^c stationary with respect to Λ_{j_1} , Λ_{j_2} , Λ_{i_1} and Λ_{i_2} , respectively,

$$\frac{\partial \Pi_{pre}^c}{\partial \Lambda_{j_1}} = 0 \quad (j_1 = 1 \dots J_1) \quad (5.74)$$

$$\frac{\partial \Pi_{pre}^c}{\partial \Lambda_{j_2}} = 0 \quad (j_2 = 1 \dots J_2) \quad (5.75)$$

$$\frac{\partial \Pi_{pre}^c}{\partial \Lambda_{i_1}} = 0 \quad (i_1 = 1 \dots I_1) \quad (5.76)$$

$$\frac{\partial \Pi_{pre}^c}{\partial \Lambda_{i_2}} = 0 \quad (i_2 = 1 \dots I_2) \quad (5.77)$$

the same conditions as in equation 5.69 and 5.70 will be obtained.

Then making the total energy functional Π_{pre}^c stationary with respect to F_{kl} ,

$$\frac{\partial \Pi_{pre}^c}{\partial F_{kl}} = 0 \quad (k = 1 \dots K, l = 1 \dots L) \quad (5.78)$$

a set of equations, expressed in matrix form, will be obtained as following,

$$\bar{N}_x \mathbf{c}_{kl} + \mathbf{C}_a \mathbf{f}_{kl} + \mathbf{H}_1 \boldsymbol{\lambda}_{ij} = \mathbf{0} \quad (5.79)$$

where, $\boldsymbol{\lambda}_{ij}$ is a vector of dimension $(I_1 + I_2 + J_1 + J_2)$ that contains all Lagrange multipliers, \mathbf{H}_1 is a $K \times L$ by $(I_1 + I_2 + J_1 + J_2)$ matrix.

These conditions in equation 5.69 and 5.70 can be written in matrix form as

$$\mathbf{H}_1^T \mathbf{f}_{kl} = \mathbf{0} \quad (5.80)$$

The two matrix equations can be written together as

$$\begin{pmatrix} \mathbf{C}_a & \mathbf{H}_1 \\ \mathbf{H}_1^T & \mathbf{O} \end{pmatrix} \begin{pmatrix} \mathbf{f}_{kl} \\ \boldsymbol{\lambda}_{ij} \end{pmatrix} = -\bar{N}_x \begin{pmatrix} \mathbf{c}_{kl} \\ \mathbf{0} \end{pmatrix} \quad (5.81)$$

By solving the parameter vector \mathbf{f}_{kl} from above equation, the conditions in equation 5.69 and 5.70 will be automatically satisfied.

Verification

The verification is done for layup 1 and layup 2, where $K = 18$ and $L = 18$ terms are used in x and y direction, respectively, in Ritz method. Figure 5.17 and 5.18 show the comparison of the predictions obtained from sine function, sine function (with Lagrange multiplier) and beam characteristic function. Clearly, the predictions obtained using sine function (with Lagrange multiplier) is significantly better than those obtained using only sine function, since the boundary conditions of the shear stresses are exactly satisfied.

However, by comparison with the beam characteristic function, the sine function with Lagrange multiplier overly constrains the stress N_x on the edges of $y = 0, b$ and N_y on the edges of $x = 0, a$. Because, as shown in the equations of N_x and N_y below, N_x is exactly \bar{N}_x at $y = 0, b$ and N_y is exactly zero at $x = 0, a$.

$$N_x = F_{,yy} = \bar{N}_x - \sum_{kl}^{KL} F_{kl} \left(\frac{l\pi}{b}\right)^2 \sin \frac{k\pi x}{a} \sin \frac{l\pi y}{b} = \bar{N}_x \quad (y=0, b) \quad (5.82)$$

$$N_y = F_{,xx} = - \sum_{kl}^{KL} F_{kl} \left(\frac{k\pi}{a}\right)^2 \sin \frac{k\pi x}{a} \sin \frac{l\pi y}{b} = 0 \quad (x=0, a) \quad (5.83)$$

However, N_x (or N_y) does not have to be \bar{N}_x at $y = 0, b$ (or be zero at $x = 0, a$), as shown in the predictions of the beam characteristic function or FEM. The additional constraints from the sine function are due to that the second derivative of sine function is actually zero at the boundaries, as shown in the equations below.

$$X_k''(x) = -\left(\frac{k\pi}{a}\right)^2 \sin \frac{k\pi x}{a} = 0 \quad \text{on } x=0, a \quad (5.84)$$

$$Y_l''(y) = -\left(\frac{l\pi}{b}\right)^2 \sin \frac{l\pi y}{b} = 0 \quad \text{on } y=0, b \quad (5.85)$$

which are not the conditions of option 1 shown in equation 5.8.

Therefore, the predictions of N_x and N_y obtained using the sine function (with Lagrange multiplier) are not as accurate as the beam characteristic function (and also the polynomial functions) at the edges, due to the overly constrained boundary conditions of N_x and N_y inherently existing in sine function. However the predictions have been improved significantly by introducing the Lagrange multiplier to sine function compared to the pure sine function.

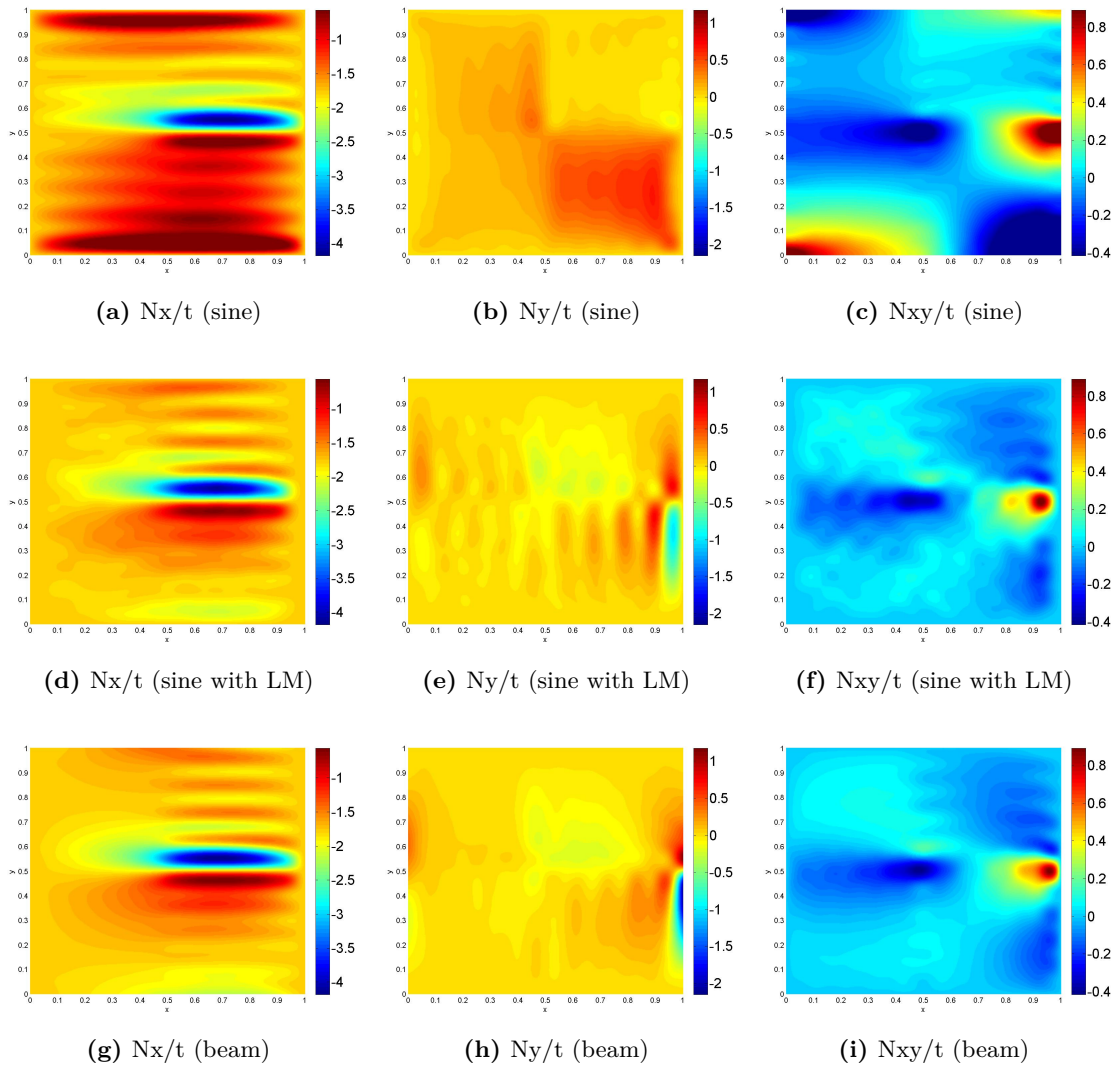


Figure 5.17: In-plane Stress of Layup 1 (Mpa, $K=L=18$, $\bar{N}_x = 1$ N/mm)

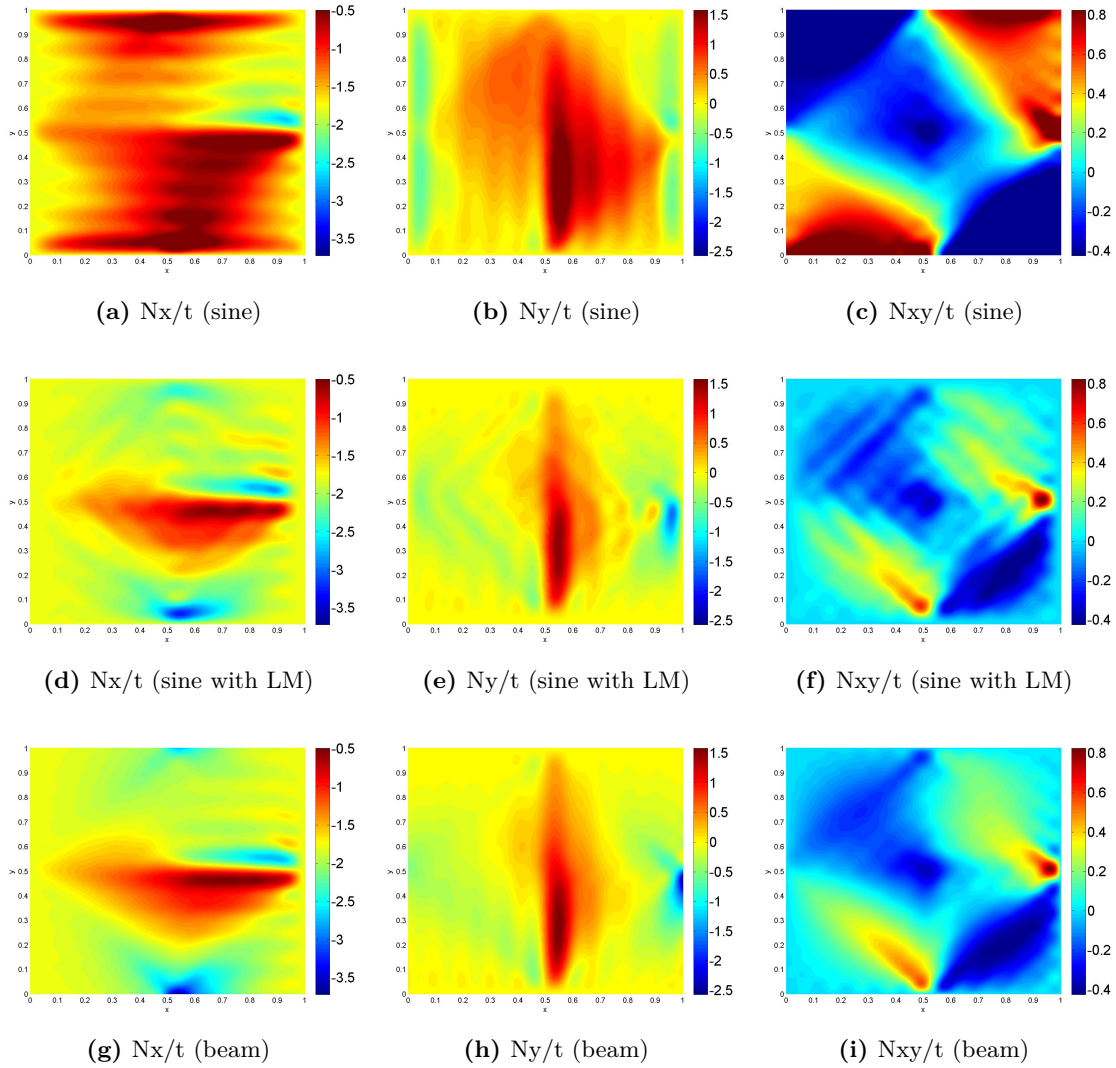


Figure 5.18: In-plane Stress of Layup 2 (Mpa, $K=L=18$, $\bar{N}_x = 1$ N/mm)

5.2.6 Cosine Function with Lagrange Multiplier

Shape Function

The cosine function can be introduced to solve the problem of sine function described in previous section, since the second derivative of cosine function is not zero at the boundary. Moreover, the cosine function can satisfy the boundary condition of N_{xy} term by term. However, the cosine function itself is not zero at the boundaries, so it does not satisfy the boundary condition of N_x and N_y term by term. This problem can be solved by introducing the Lagrange multiplier, which is similar to what did for the sine function.

Since the cosine function does not satisfy the boundary conditions of N_x and N_y term by term, the following conditions must be applied to the cosine function to ensure the boundary

conditions of N_x and N_y are satisfied in a set, as required in the option 2.

$$\sum_k^K F_{kl} X_k(x) = 0 \text{ on } x=0, a \quad (l = 1 \cdots L) \quad (5.86)$$

$$\sum_l^L F_{kl} Y_l(y) = 0 \text{ on } y=0, b \quad (k = 1 \cdots K) \quad (5.87)$$

If the above conditions are satisfied, the boundary conditions of N_x and N_y will be exactly satisfied, as shown below.

$$N_x = \bar{N}_x + \sum_l^L \left[\sum_k^K F_{kl} X_k(x) \right] Y_l(y) = \bar{N}_x \text{ on } x=0, a \quad (5.88)$$

$$N_y = \sum_k^K \left[\sum_l^L F_{kl} Y_l(y) \right] X_k(x) = 0 \text{ on } y=0, b \quad (5.89)$$

The conditions in equation 5.86 and 5.87 are implemented in Ritz method by introducing the Lagrange multipliers into the total complementary energy (equation 4.23), as

$$\begin{aligned} \Pi_{pre}^c = & \frac{1}{2} \int \int (\mathbf{f}^T \mathbf{A}^{-1} \mathbf{f}) dx dy + \sum_{j_1}^{J_1} \Lambda_{j_1}^c \left[\sum_k^K F_{kl} X_k(0) \right] + \sum_{j_2}^{J_2} \Lambda_{j_2}^c \left[\sum_k^K F_{kl} X_k(a) \right] \\ & + \sum_{i_1}^{I_1} \Lambda_{i_1}^c \left[\sum_l^L F_{kl} Y_l(0) \right] + \sum_{i_2}^{I_2} \Lambda_{i_2}^c \left[\sum_l^L F_{kl} Y_l(b) \right] \end{aligned} \quad (5.90)$$

where, $\Lambda_{j_1}^c$, $\Lambda_{j_2}^c$, $\Lambda_{i_1}^c$ and $\Lambda_{i_2}^c$ are Lagrange multipliers; I_1 , I_2 , J_1 , J_2 are numbers of Lagrange multipliers and $I_1 \leq K$, $I_2 \leq K$, $J_1 \leq L$, $J_2 \leq L$.

However, it is noted that a complete set of cosine functions is given as

$$1, \cos \frac{\pi x}{a}, \cos \frac{2\pi x}{a}, \cos \frac{3\pi x}{a}, \cos \frac{4\pi x}{a} \cdots \quad (5.91)$$

So the shape functions assumed for X_k and Y_l should start from $k = l = 0$ as shown below,

$$X_k = \cos \frac{k\pi x}{a} \quad (k = 0 \cdots K) \quad (5.92)$$

$$Y_l = \cos \frac{l\pi y}{b} \quad (l = 0 \cdots L) \quad (5.93)$$

Thus the Airy stress function is

$$F(x, y) = \frac{1}{2} \bar{N}_x y^2 + \sum_{k=0, l=0}^{KL} F_{kl} \cos \frac{k\pi x}{a} \cos \frac{l\pi y}{b} \quad (5.94)$$

If making the total energy functional stationary with respect to $\Lambda_{j_1}^c$, $\Lambda_{j_2}^c$, $\Lambda_{i_1}^c$, $\Lambda_{i_2}^c$ and F_{kl} , respectively, two sets of equations will be obtained which are expressed in matrix form as below.

$$\begin{pmatrix} \mathbf{C}_a & \mathbf{H}_2 \\ \mathbf{H}_2^T & \mathbf{O} \end{pmatrix} \begin{pmatrix} \mathbf{f}_{kl} \\ \boldsymbol{\lambda}_{ij}^c \end{pmatrix} = -\bar{N}_x \begin{pmatrix} \mathbf{c}_{kl} \\ \mathbf{0} \end{pmatrix} \quad (5.95)$$

where, $\boldsymbol{\lambda}_{ij}^c$ is a vector of dimension $I_1 + I_2 + J_1 + J_2$ that contains all Lagrange multipliers, \mathbf{H}_2 is a $K \times L$ by $I_1 + I_2 + J_1 + J_2$ matrix.

By solving the parameter vector \mathbf{f}_{kl} from above equation, the conditions in equation 5.86 and 5.87 will be automatically satisfied.

Verification

The verification is done for layup 1, layup 2 and layup 3, where $K = 18$ and $L = 18$ terms are used in x and y direction, respectively, in Ritz method. Figure 5.19, 5.20 and 5.21 show the comparisons of the predictions obtained using cosine function (with Lagrange multiplier), sine function (with Lagrange multiplier) and beam characteristic function. Clearly, the predictions using cosine function (with Lagrange multiplier) are slightly better compared to the predictions using sine function (with Lagrange multiplier), since the stresses on the boundaries are not overly constrained.

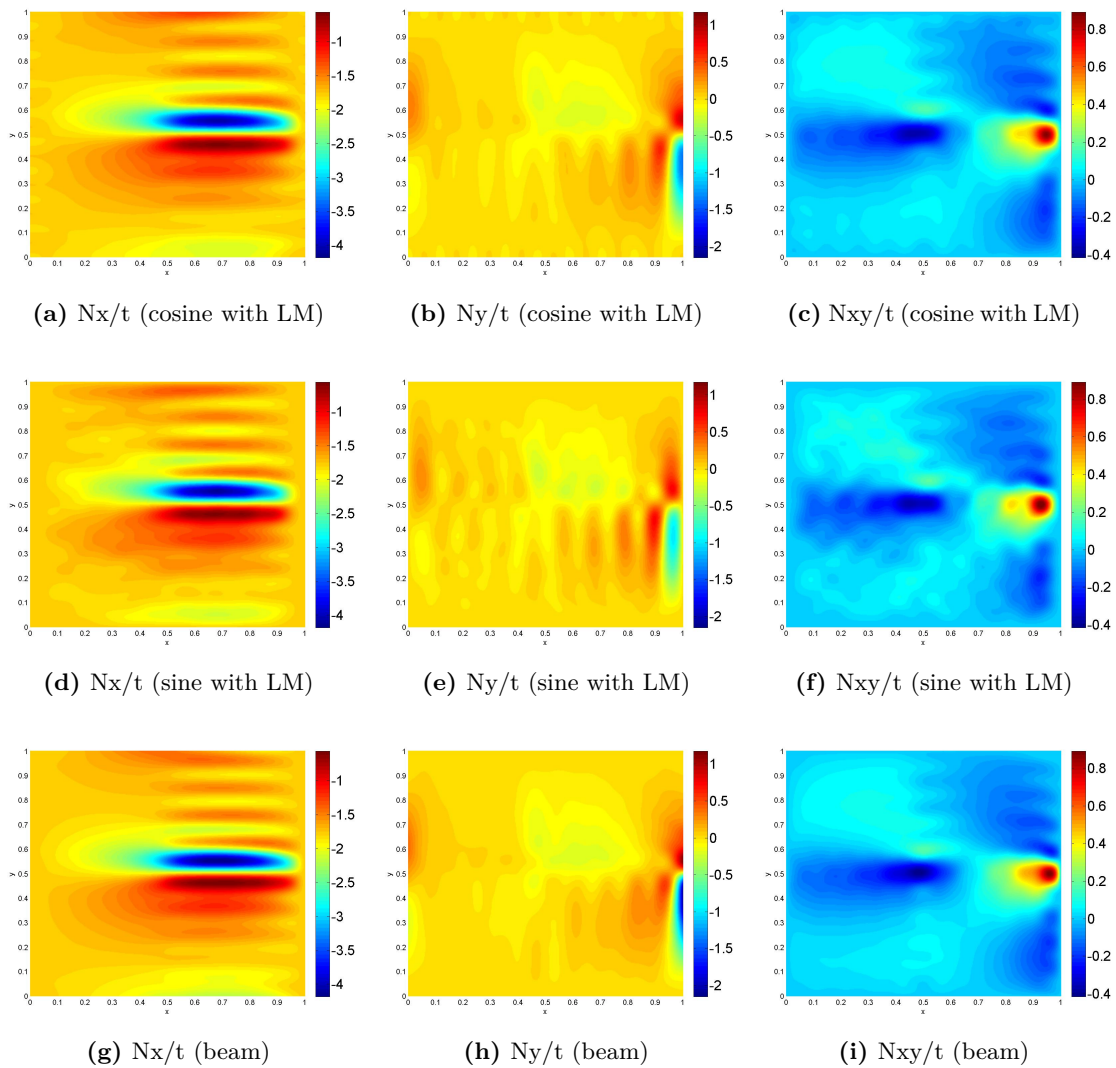


Figure 5.19: In-plane Stress of Layup 1 (Mpa, $K=L=18$, $\bar{N}_x = 1$ N/mm)

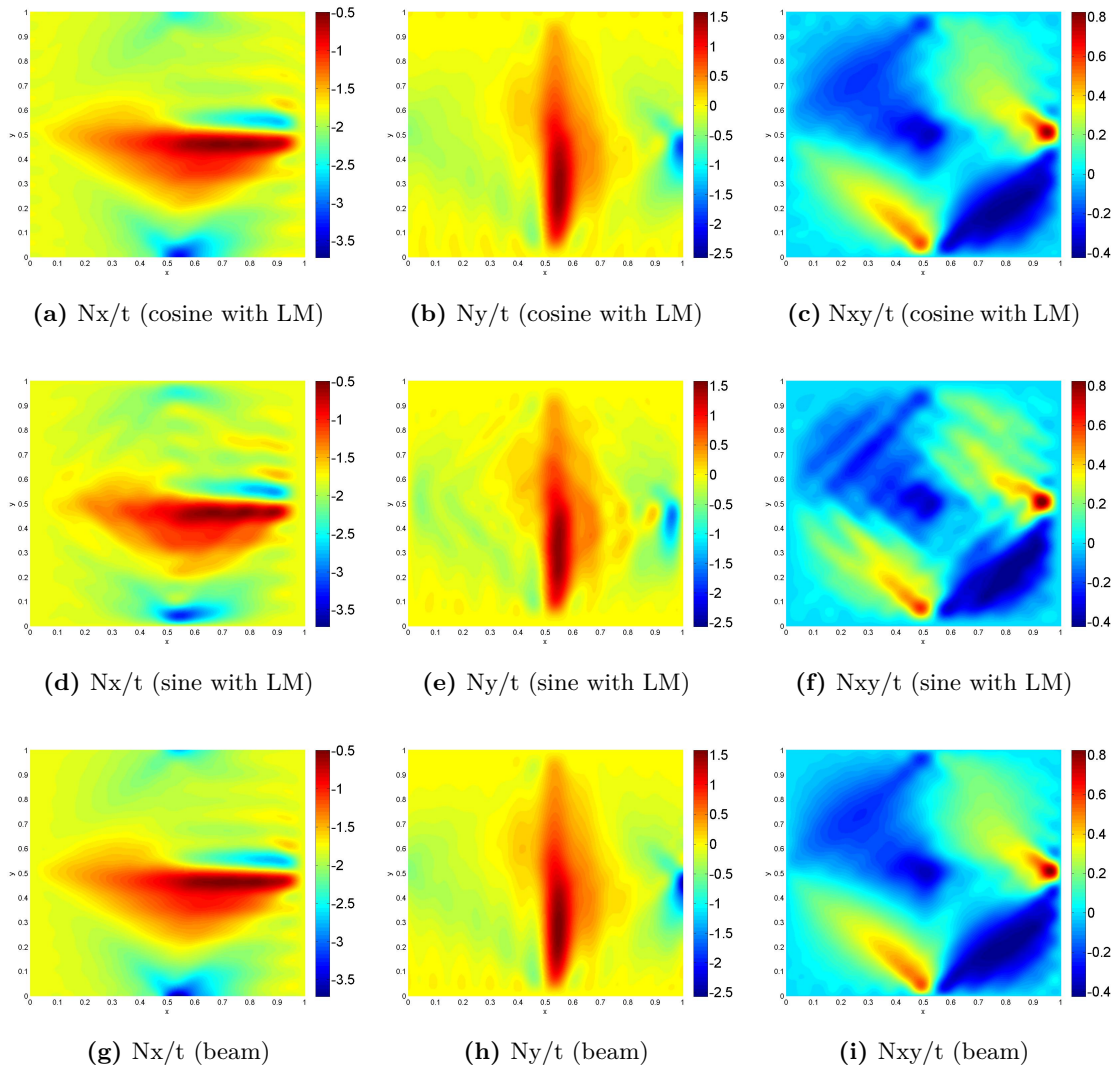


Figure 5.20: In-plane Stress of Layup 2 (Mpa, $K=L=18$, $\bar{N}_x = 1$ N/mm)

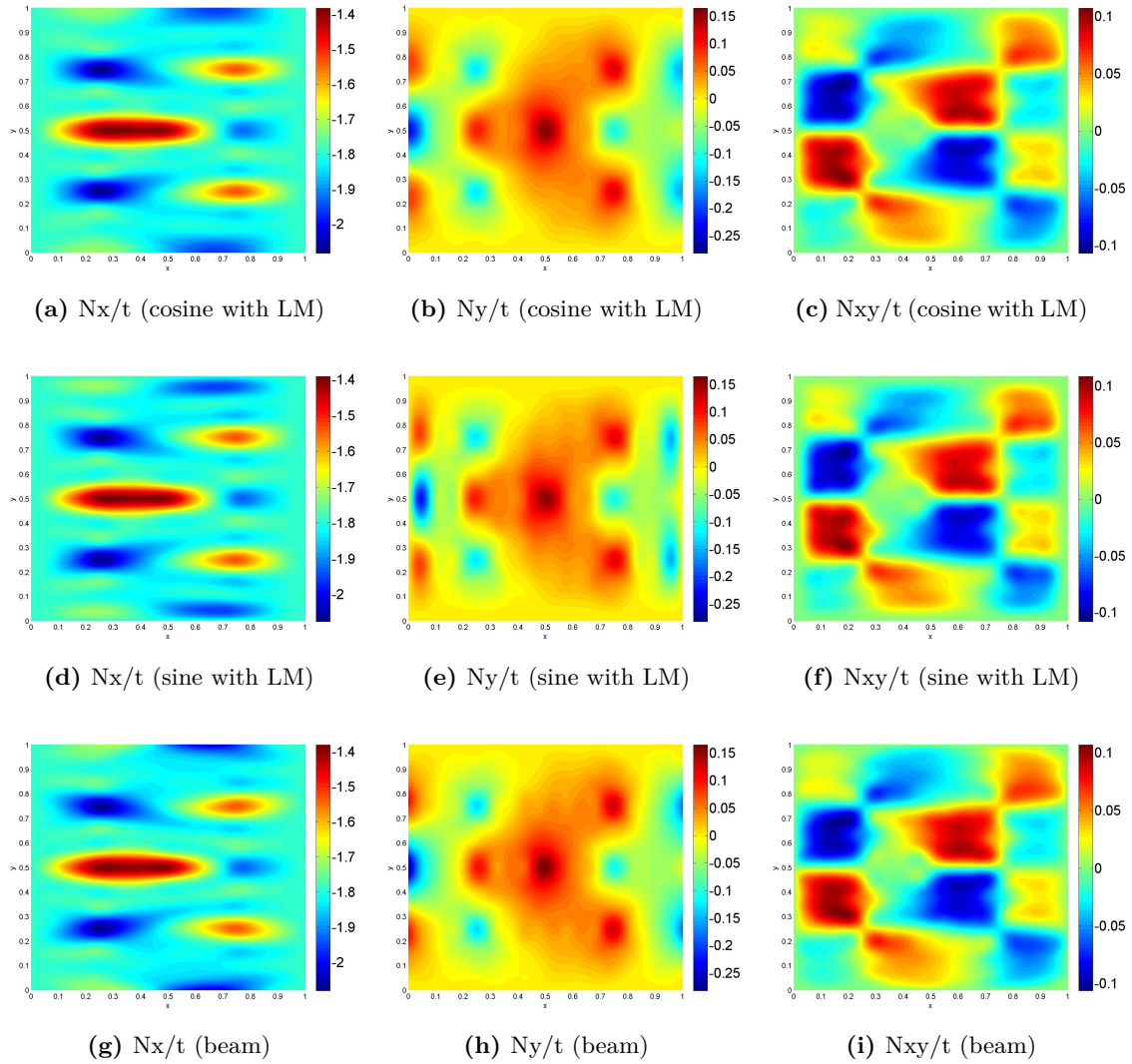


Figure 5.21: In-plane Stress of Layup 3 (Mpa, $K=L=18$, $\bar{N}_x = 1$ N/mm)

Budiansky and Hu [36] introduced the Lagrange multiplier method to find the upper and lower limits to the critical buckling loads of clamped plates in 1946. The boundary conditions of clamping requires that the deflection and the slope (first derivative of deflection) are zero at the boundaries, which are similar to the boundary conditions of the shape functions used for Airy stress function where N_{xy} corresponds to the slope and N_x and N_y correspond to the deflection. Budiansky and Hu indicated that the Lagrange multiplier method is preferably used to satisfy the zero-deflection condition rather than the zero-slope condition to obtain more rapid convergence, since the slope is the derivative of deflection and in general the differentiation of a Fourier series makes it more slowly convergent [36]. So the cosine function was preferably used to satisfy the condition of slope in their case, while the conditions of deflection was satisfied by Lagrange multiplier method. Similarly, in the prediction of in-plane loads, the cosine function is preferably used since it satisfied the condition of N_{xy} and thus having more rapid convergence compared to the sine function. This can be observed in

Figure 5.19 and 5.20, where the predictions of cosine function (with Lagrange multiplier) is slightly better than the sine function (with Lagrange multiplier) when using the same number of terms ($K = L = 18$) in Ritz method.

5.3 Prescribed Shear (\bar{N}_{xy})

The prediction of the in-plane stresses of a panel under prescribed shear is investigated in this section by using the polynomial functions. However, other shape functions discussed in previous section can also be applied here. The prescribed shear is set to be $\bar{N}_{xy} = 1$ N/mm, which is applied to all edges.

5.3.1 Pure Shear

The stretching-shearing couplings, A_{16} and A_{26} , of the layups dramatically influence the in-plane loads distribution for panels under pure shear. If A_{16} and A_{26} are zero, the panels' shear deformation is not coupled with the stretches. So applying shear load to the panel will not lead to stretches in x and y direction. Thus, the in-plane loads N_x and N_y will be zero when the panel is under pure shear. Moreover, the in-plane shear load N_{xy} will be constant even though the stiffness is variable. Figure 5.22 shows the prediction of in-plane loads of layup 1 whose A_{16} and A_{26} are zero. Both N_x and N_y obtained from FEM and Ritz method are zero, and N_{xy} is constant.

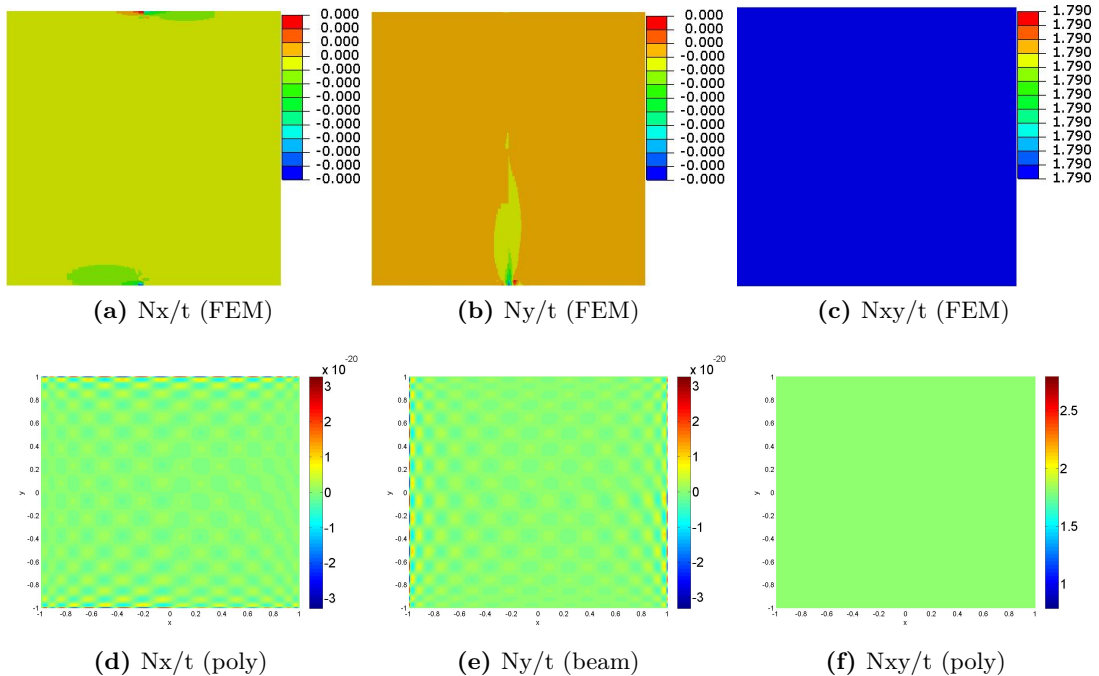


Figure 5.22: In-plane Stress of Layup 1 (Mpa, $K=L=18$, $\bar{N}_{xy} = 1$ N/mm)

On the contrary, if A_{16} and A_{26} are not zero, the panels' shear deformation is coupled with

stretches. So applying shear load to the panel will lead to stretches in x and y direction. Thus the in-plane loads N_x and N_y will not be zero and N_{xy} will not be constant neither, as shown in Figure 5.23 and 5.24 where the layup 2 and layup 3 are used whose A_{16} and A_{26} are not zero.

However, the stresses in FEM are discontinuous at the boundaries of the neighboring sections which cannot be predicted in Ritz method using finite number of continuous shape functions. Moreover, the peak stresses cannot be predicted correctly. These are similar to what observed when compression is applied in previous section. But besides these, the predictions of the in-plane stress distributions are satisfactory.

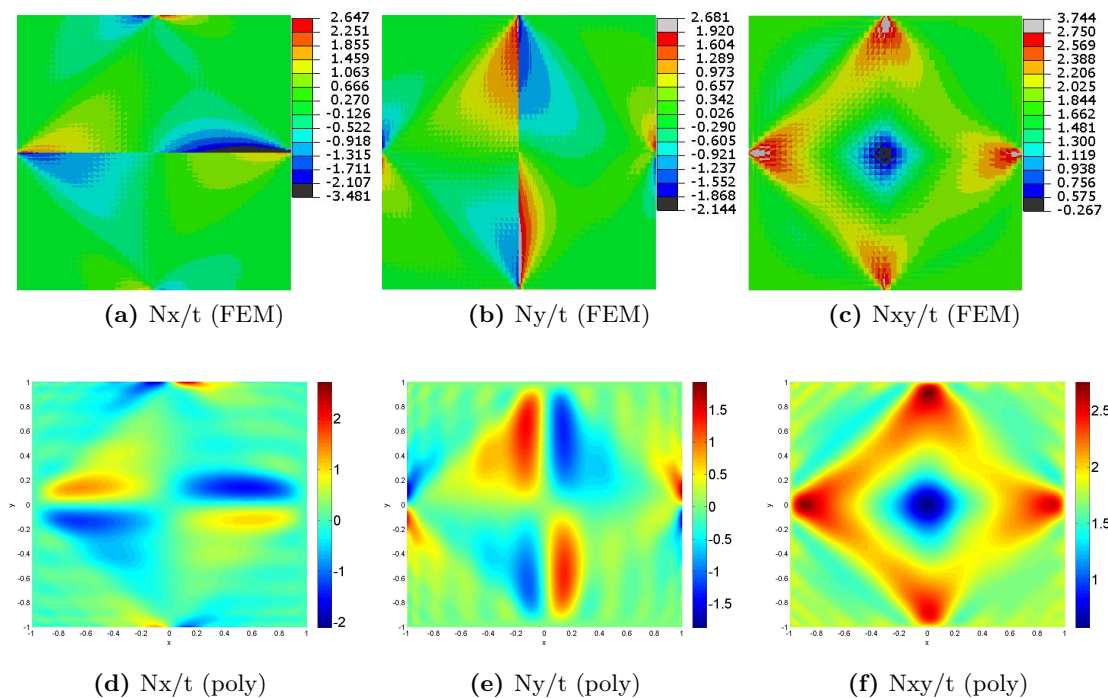


Figure 5.23: In-plane Stress of Layup 2 (Mpa, $K=L=18$, $\bar{N}_{xy} = 1$ N/mm)

5.3.2 Shear and Compression

Besides pure shear, it is more practical to consider a panel under combined loads, for instance a combination of \bar{N}_x and \bar{N}_{xy} . The predictions of in-plane stresses of layup 1 and 2 are shown in Figure 5.25 and 5.26, where $\bar{N}_x = \bar{N}_{xy} = 1$ N/mm. Clearly the predictions are as good as the prediction of panels under pure shear or compression. The discontinuity of peaks of the stresses are still cannot be predicted exactly neither.

It is interesting to noted that the in-plane loads of a panel under combined loads are just a linear combination of the in-plane loads of the panel under pure shear and pure compression separately. An example is clearly shown in Figure 5.25, which is the combination of Figure 5.14 and 5.22.

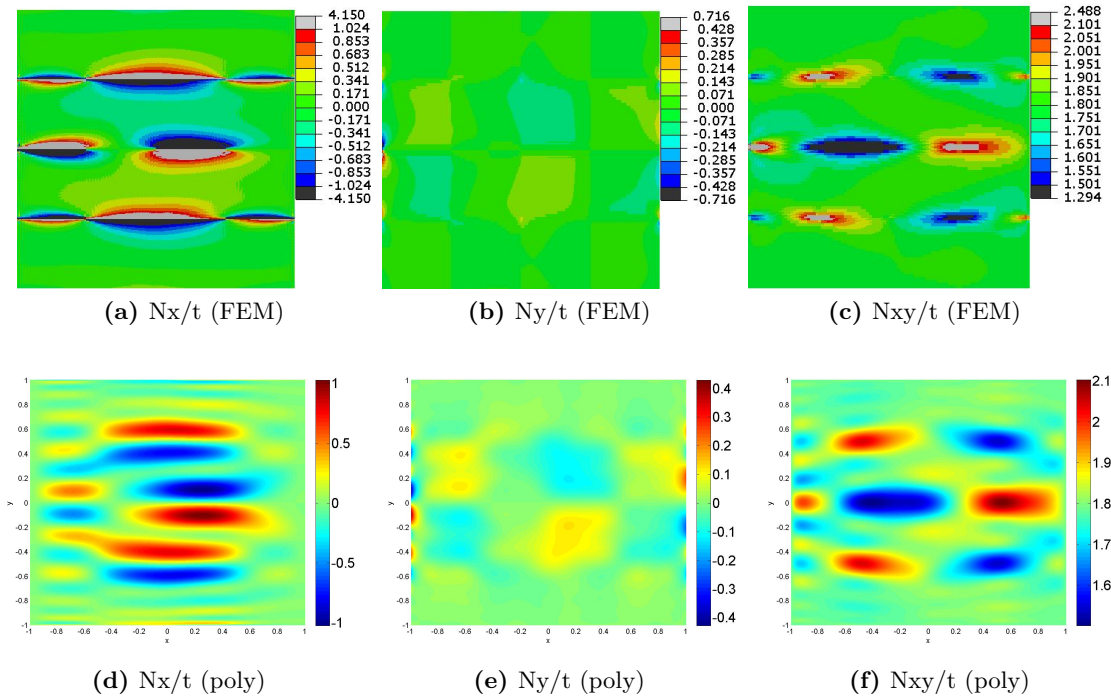


Figure 5.24: In-plane Stress of Layup 3 (Mpa, $K=L=18$, $\bar{N}_{xy} = 1$ N/mm)

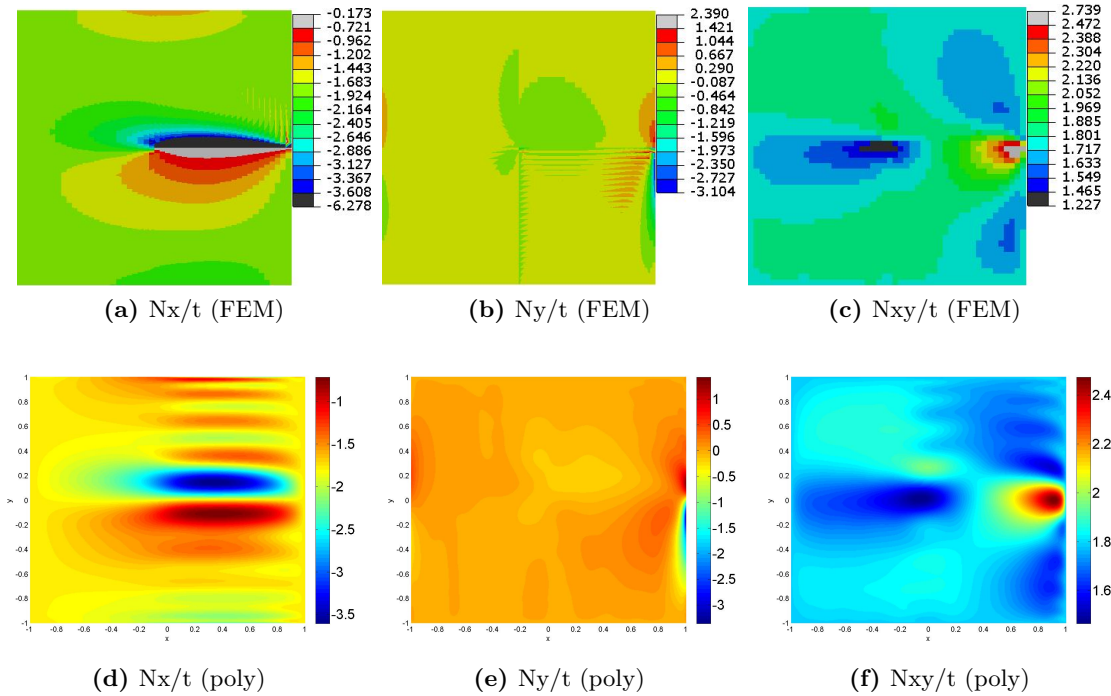


Figure 5.25: In-plane Stress of Layup 1 (Mpa, $K=L=18$, $\bar{N}_x = \bar{N}_{xy} = 1$ N/mm)

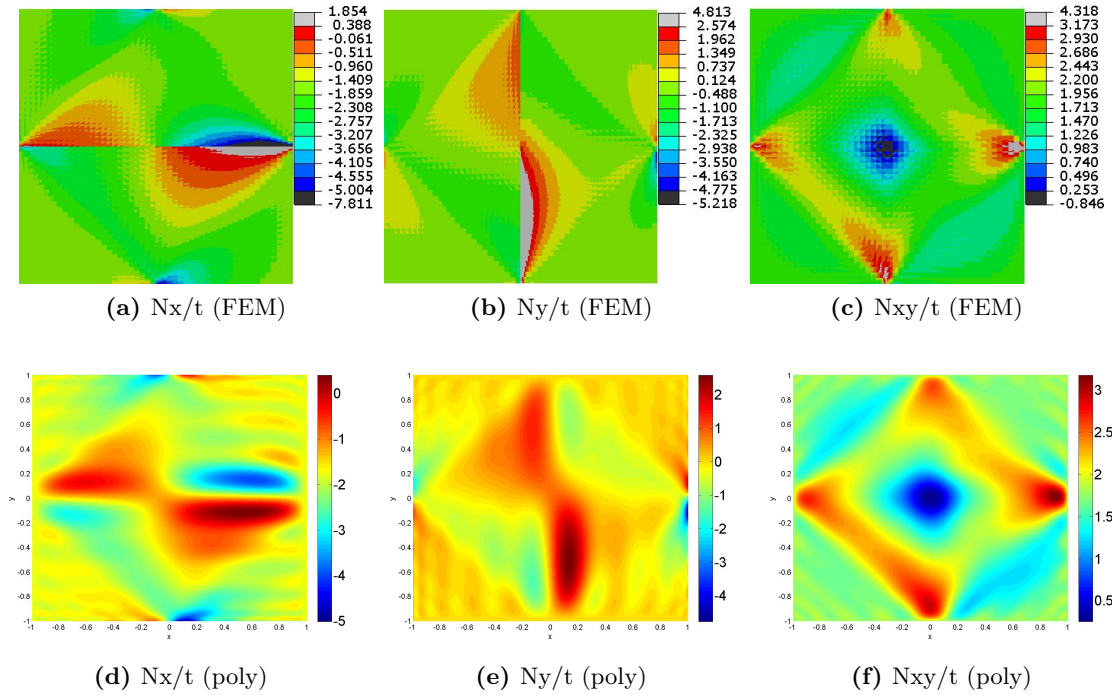


Figure 5.26: In-plane Stress of Layup 2 (Mpa, $K=L=18$, $\bar{N}_x = \bar{N}_{xy} = 1$ N/mm)

5.4 Prescribed Displacement

In this section, the in-plane loads of panels under prescribed displacement are investigated using Ritz method and verified with Abaqus.

5.4.1 Boundary Condition

The panel is simply-supported at all the edges and subjected to uniform end-shortenings on both sides ($x = 0, a$). The boundary conditions have been split into the geometrical boundary condition (prescribed displacement) and the mechanical boundary condition.

As the geometry constraints are only the prescribed end-shortenings on the edges of $x = 0, a$, the edges of $y = 0, b$ are free to move. It is convenient to assume that the end-shortenings prescribed on the edges of $x = 0$ and $x = a$ are Δu_1 and Δu_2 , respectively. Then the geometrical boundary conditions become

$$u = \Delta u_1 \text{ on } x = 0 \quad (5.96)$$

$$u = -\Delta u_2 \text{ on } x = a \quad (5.97)$$

$$v = \text{free on } y = 0, b \quad (5.98)$$

Since the plate is free to move in y direction and no extra loads prescribed on all the edges,

the mechanical boundary conditions are

$$N_x \neq 0, N_{xy} = 0 \text{ on } x = 0, a \quad (5.99)$$

$$N_y = 0, N_{xy} = 0 \text{ on } y = 0, b \quad (5.100)$$

5.4.2 Shape function

The stress resultant N_x is not constant on the edges of $x = 0, a$ due to the stiffness variation along the edges. Therefore, the Airy stress function is assumed to have two components (also shown in equation 4.103)

$$F(x, y) = \sum_e^E F_e \int \int Y_e(y) dy dy + \sum_{kl}^{KL} F_{kl} X_k(x) Y_l(y) \quad (5.101)$$

Then the in-plane loads can be derived from the Airy stress function as

$$N_x = F_{,yy} = \sum_e^E F_e Y_e + \sum_{kl}^{KL} F_{kl} X_k Y_l'' \quad (5.102)$$

$$N_y = F_{,xx} = \sum_{kl}^{KL} F_{kl} X_k'' Y_l \quad (5.103)$$

$$N_{xy} = -F_{,xy} = - \sum_{kl}^{KL} F_{kl} X_k' Y_l' \quad (5.104)$$

The first term in equation 5.101 describes the stress variation in y direction on the edge of $x = 0, a$, so it is only a function of y . The second term describes the stress variation inside of the panel. Compared to the case of prescribing loads in previous sections, the first term is similar to the prescribed load \bar{N}_x (equation 5.2) on the edges. The only difference is that in previous sections the prescribed load is constant but here it is a function of y . However, the second term used here is slightly different from that used in previous sections. In previous sections, X_k is required to be zero at $x = 0, a$, because the stresses on the edges are exactly the applied load \bar{N}_x which are not determined by X_k . But here X_k cannot be zero, because the stresses on the edges of $x = 0, a$ are determined by both the first term and the second term of equation 5.101. So compared to the case of prescribed loads, different shape functions have to be selected for X_k in this case.

Therefore, the conditions that each shape function should satisfy are

$$Y_e(y) = \text{free (on } y = 0 \dots b) \quad (5.105)$$

$$X_k(x) \neq 0, X_k'(x) = 0 \text{ (on } x = 0, a) \quad (5.106)$$

$$Y_l(y) = 0, Y_l'(y) = 0 \text{ (on } y = 0, b) \quad (5.107)$$

The shape functions selected for Y_e , X_k and Y_l are all polynomial functions. The advantage of the polynomial functions is that they can be easily manipulated to satisfy most of the required boundary conditions through simply changing their coefficients. However, other shape functions can also be applied here.

For $Y_e(y)$, a set of polynomial functions can be selected as

$$Y_e(y) = 1, \frac{y}{b}, \left(\frac{y}{b}\right)^2, \left(\frac{y}{b}\right)^3, \dots \quad (e = 1, 2, 3, 4, \dots) \quad (5.108)$$

For $X_k(x)$,

$$X_k(x) = \int \left(\frac{x}{a}\right)^k \left(\frac{x}{a} - 1\right) dx \quad (x = 1 \dots K) \quad (5.109)$$

For $Y_l(y)$,

$$Y_l(y) = \left(\frac{y}{b}\right)^{l+1} \left(\frac{y}{b} - 1\right)^2 \quad (5.110)$$

where, $Y_l(y)$ is still the same as that in the case of prescribed loads.

Similar to what did in the case of prescribed loads, these polynomials functions are transformed to the nondimensional form spanning the interval $[-1, 1]$, and orthogonalized through Gram-Schmidt process.

The final expressions for $Y_e(y)$ are

$$Y_1(\eta) = \frac{\sqrt{2}}{2} \quad (5.111)$$

$$Y_2(\eta) = \frac{\sqrt{6}}{2} \eta \quad (5.112)$$

$$Y_3(\eta) = \frac{3\sqrt{10}}{4} \eta^2 - \frac{\sqrt{10}}{4} \quad (5.113)$$

$$\vdots \quad (5.114)$$

The final expressions for $X_k(x)$ are

$$X_1(\xi) = \frac{\sqrt{1190}}{68} \xi^3 - \frac{3\sqrt{1190}}{68} \xi \quad (5.115)$$

$$X_2(\xi) = \frac{3\sqrt{7490}}{214} (\xi^4 - 2\xi^2) \quad (5.116)$$

$$X_3(\xi) = \frac{9\sqrt{17017}}{208} (\xi^5 - \frac{290}{153} \xi^3 - \frac{35}{51} \xi) \quad (5.117)$$

$$\vdots \quad (5.118)$$

The final expressions for $Y_l(y)$ are the same as equation 5.63.

It is noted the shape functions of $Y_e(\eta)$, which is obtained from $Y_e(y)$ through Gram-Schmidt process, are similar to the Legendre polynomials. Because both of them are obtained from the same set of polynomials (equation 5.108) through Gram-Schmidt process. However, they are normalized in a different way, because for Legendre polynomials,

$$\int_{-1}^1 P_e(\eta) P_e(\eta) d\eta = \frac{2}{2e+1} \quad (5.119)$$

but for $Y_e(\eta)$,

$$\int_{-1}^1 Y_e(\eta) Y_e(\eta) d\eta = 1 \quad (5.120)$$

where, $P_e(\eta)$ are Legendre polynomials.

The total complementary energy functional (equation 4.107) has to be transformed in the nondimensional form spanning the interval $[-1, 1]$, similar to what did in equation 5.68. After making it stationary with respect to the undetermined parameters F_e and F_{kl} , respectively, a set of linear equations can be obtained, as shown below for convenience (the same as equation 4.108).

$$\begin{pmatrix} C_a & E_1 \\ E_1^T & E_3 \end{pmatrix} \begin{pmatrix} f_{kl} \\ f_e \end{pmatrix} = \Delta u_1 \begin{pmatrix} i_{kl_1} \\ i_{e_1} \end{pmatrix} + \Delta u_2 \begin{pmatrix} i_{kl_2} \\ i_{e_2} \end{pmatrix} \quad (5.121)$$

5.4.3 Verification

The prescribed displacements on edges of $x = 0$ and $x = a$ are set as

$$\Delta u_1 = 0.001\text{mm} \quad (5.122)$$

$$\Delta u_2 = 0.001\text{mm} \quad (5.123)$$

The layup 1, 2 and 3 are used to compared the predictions of Ritz method with these of FEM. The number of terms used in Ritz method are $K = L = E = 18$. The predictions of layup 1, 2 and 3 are shown in Figure 5.27 5.28 and 5.29, respectively.

Clearly, only the discontinuity and peaks of the stresses in FEM are not exactly predicted by Ritz method using polynomial functions, as shown in Figure 5.27 and 5.28. However, the predictions are improved through reducing the stiffness discontinuity, as shown in Figure 5.29.

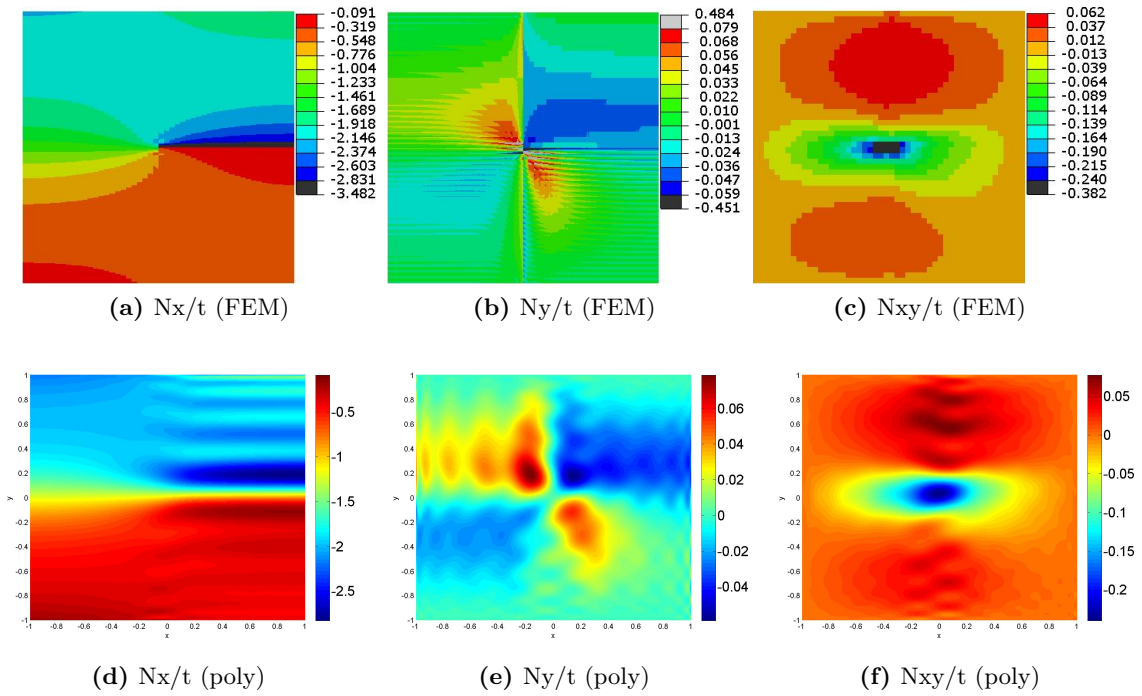


Figure 5.27: In-plane Stress of Layup 1 (Mpa, $K=L=18$, $\Delta u_1 = 0.001\text{mm}$, $\Delta u_2 = 0.001\text{mm}$)

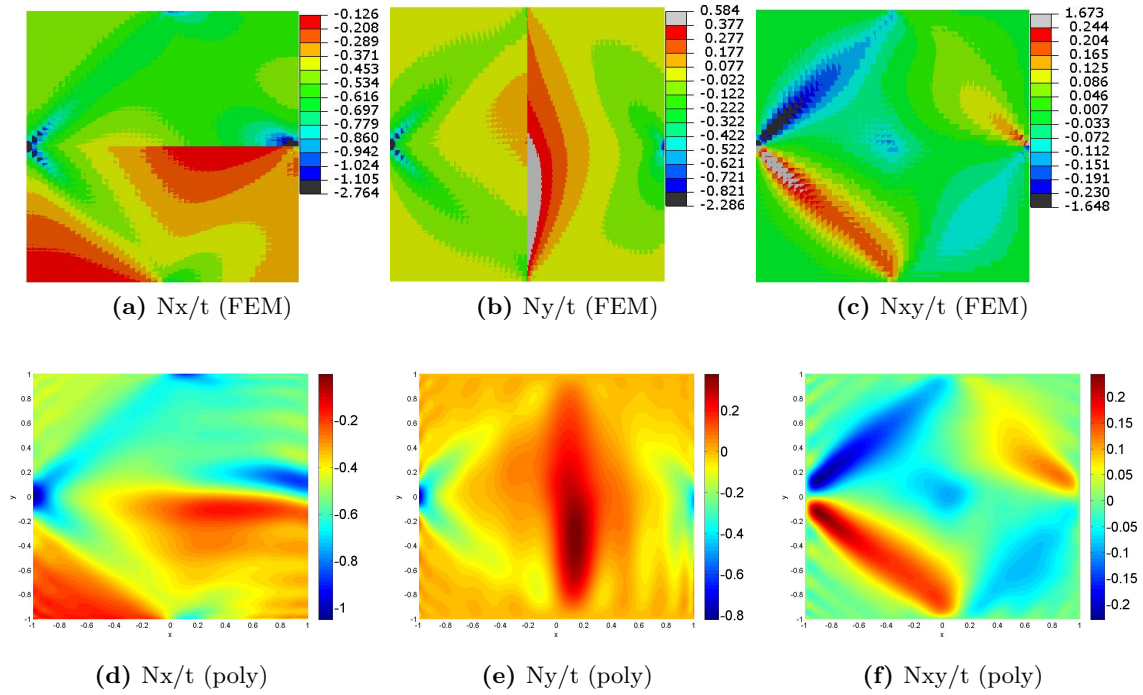


Figure 5.28: In-plane Stress of Layup 2 (Mpa, $K=L=18$, $\Delta u_1 = 0.001\text{mm}$, $\Delta u_2 = 0.001\text{mm}$)

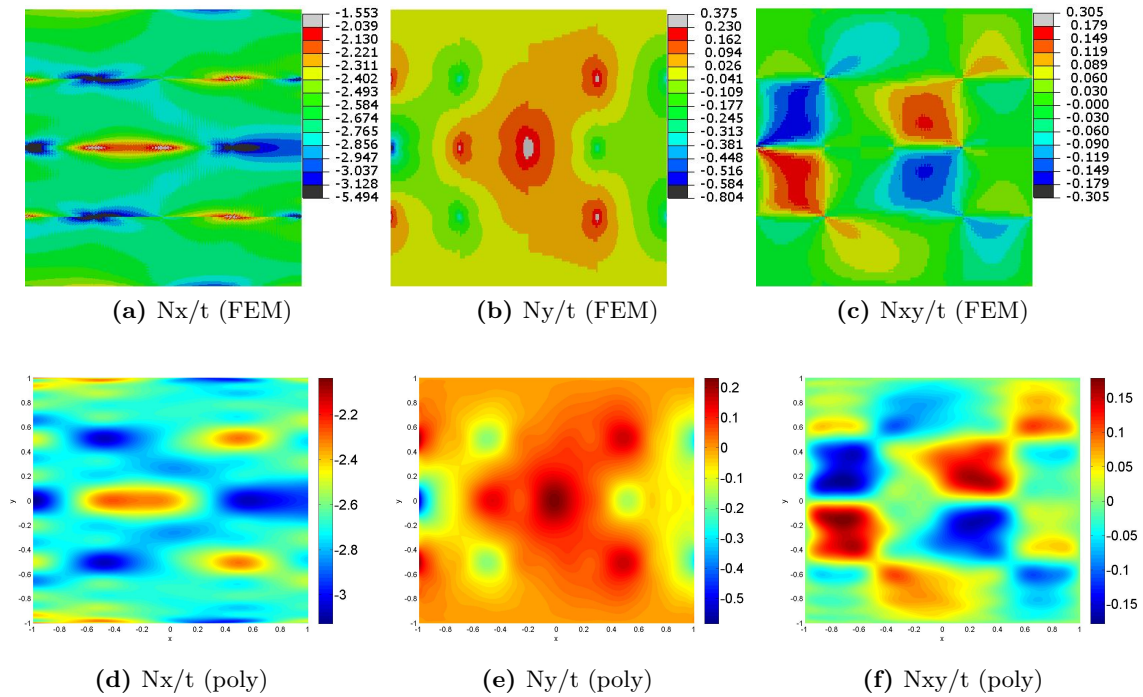


Figure 5.29: In-plane Stress of Layup 3 (Mpa, $K=L=18$, $\Delta u_1 = 0.001\text{mm}$, $\Delta u_2 = 0.001\text{mm}$)

5.5 Summary

In this chapter, the in-plane loads distributions of panels under either prescribed loads (compression and shear) or prescribed end-shortenings are investigated using Ritz method. Different shape functions (beam characteristic function, polynomial function, sine and cosine functions) are applied to approximate the Airy stress function, the accuracy of the predictions using these functions are investigated. Although the extreme stresses in FEM cannot be predicted using Ritz method as accurate as FEM due to the stiffness discontinuity in the examples of the layups (layup 1, 2 and 3), the predictions of the peak stresses are improved by reducing the stiffness discontinuity as shown in the predictions for layup 3. Since the stiffness discontinuity in these layups are extreme examples which are unlikely to be encountered in practice, one can expect that if the same method would be applied to a panel with continuous stiffness the prediction would be much better. The examples shown in this chapter have demonstrated that the Ritz method is a suitable approach to predicting the in-plane loads distributions of variable-stiffness panels.

Stability Analysis

6.1 Introduction

In this chapter, the stability of plates and shallow cylindrical shells under prescribed loads (compression and shear) and prescribed end-shortenings is investigated. For stability analysis, the out-of-plane deflection is no longer zero when buckling occurs. Therefore, the stability behavior of plates and shells is different, and has to be discussed separately.

In this section, the boundary conditions of the out-of-plane displacement of panels under in-plane load cases (prescribed loads and prescribed displacements) are discussed. Then the curvature of shallow cylindrical shell considered in the thesis is discussed based on the curvature of the airfoil of NACA 0012. The buckling loads of panels under compression are investigated using Ritz method in Section 6.2 where the shape functions of the out-of-plane displacement are selected as sine functions and polynomial functions. In Section 6.3 and 6.4, the panels under shear and end-shortenings are investigated using Ritz method, respectively, where the polynomial functions are selected as the shape functions.

6.1.1 Boundary Condition

For panels with simply-support boundary conditions, the essential boundary conditions are the out-of-plane deflections are zero at the edges of the panel,

$$w = 0 \text{ (on } x = 0, a \text{ and } y = 0, b) \quad (6.1)$$

and the natural boundary conditions are the moments at the edges are zero.

$$M_x = -D_{11}w_{,xx} - D_{12}w_{,yy} - 2D_{16}w_{,xy} = 0 \text{ (on } x = 0, a) \quad (6.2)$$

$$M_y = -D_{12}w_{,xx} - D_{22}w_{,yy} - 2D_{26}w_{,xy} = 0 \text{ (on } y = 0, b) \quad (6.3)$$

where, D_{ij} ($i, j = 1, 2, 6$) are variables.

As discussed in Chapter 4, the out-of-plane displacement w is approximated by a combination of series of the form

$$w = \sum_{pq}^{PQ} W_{pq} X_p(x) Y_q(y) \quad (6.4)$$

If the shape functions satisfy the following conditions term by term, the essential boundary conditions are satisfied exactly.

$$X_p(x) = 0 \quad (\text{on } x = 0, a) \quad (6.5)$$

$$Y_q(y) = 0 \quad (\text{on } y = 0, b) \quad (6.6)$$

However, the shape functions can also satisfy the essential boundary conditions in a set, similar to what discussed in the condition of option 2 for Airy stress function in Chapter 5.

Since D_{ij} ($i, j = 1, 2, 6$) are variables, to satisfy the natural boundary conditions the only choice for the shape functions is to satisfy following conditions term by term

$$X_p(x) = 0 \quad (\text{on } x = 0, a) \quad (6.7)$$

$$Y_q(y) = 0 \quad (\text{on } y = 0, b) \quad (6.8)$$

$$X'_p(x) = 0 \quad (\text{on } x = 0, a) \quad (6.9)$$

$$Y'_q(y) = 0 \quad (\text{on } y = 0, b) \quad (6.10)$$

$$X''_p(x) = 0 \quad (\text{on } x = 0, a) \quad (6.11)$$

$$Y''_q(y) = 0 \quad (\text{on } y = 0, b) \quad (6.12)$$

Among above conditions, that the first derivatives of X_p and Y_q are zero implies the slopes are zero at the boundaries

$$w_{,x} = \sum_{pq}^{PQ} W_{pq} X'_p(x) Y_q(y) = 0 \quad (\text{on } x = 0, a) \quad (6.13)$$

$$w_{,y} = \sum_{pq}^{PQ} W_{pq} X_p(x) Y'_q(y) = 0 \quad (\text{on } y = 0, b) \quad (6.14)$$

However, for simply-support conditions the slopes should not be zero at boundaries. Because both deflections and slopes are zero implies that the panel is clamped at the boundaries. Therefore, the essential boundary conditions and the natural boundary conditions cannot be satisfied by the shape functions term by term in the same time. However, if the bending-twisting couplings D_{16} and D_{26} are both zero, the natural boundary conditions reduce to

$$M_x = -D_{11}w_{,xx} - D_{12}w_{,yy} = 0 \quad (\text{on } x = 0, a) \quad (6.15)$$

$$M_y = -D_{12}w_{,xx} - D_{22}w_{,yy} = 0 \quad (\text{on } y = 0, b) \quad (6.16)$$

Then the shape functions only have to satisfy following conditions term by term

$$X_p(x) = 0 \quad (\text{on } x = 0, a) \quad (6.17)$$

$$Y_q(y) = 0 \quad (\text{on } y = 0, b) \quad (6.18)$$

$$X''_p(x) = 0 \quad (\text{on } x = 0, a) \quad (6.19)$$

$$Y''_q(y) = 0 \quad (\text{on } y = 0, b) \quad (6.20)$$

where, the conditions of the first derivatives of X_p and Y_q do not exist.

Therefore, the slopes at the boundaries are not constrained by the above conditions. In this case, it is possible to find a shape function which satisfies the essential boundary condition and natural boundary in the same time. However, only the specially orthotropic laminates' bending-twisting couplings are exactly zero; most laminates' bending-twisting couplings are non-zero. So in the following sections, the discussion will focus on these two kinds of laminates.

6.1.2 Curvature

Since the skins of aircraft wings are normally shallow shell panels, it is of great interests to predict the buckling loads of this kind of panels. However, the curvatures of the skins are variables which are the curvatures of airfoils. For example, the NACA 0012 airfoil's radius is plotted along the chord direction as shown in Figure 6.2a. Clearly the radius is not constant. In the current thesis, the Ritz method has been applied to predict the buckling load of shallow shells with variable curvatures. An good example is the panels with the curvature of NACA 0012 airfoil.

The equation of the NACA 0012 is given as [37]

$$\begin{aligned} \frac{y_t}{c} = & 0.594689181(0.298222773\sqrt{\frac{x}{c}} - 0.127125232\frac{x}{c} \\ & - 0.357907906(\frac{x}{c})^2 + 0.291984971(\frac{x}{c})^3 - 0.105174606(\frac{x}{c})^4 \end{aligned} \quad (6.21)$$

where, y_t is the half thickness of the airfoil, c is the chord length and x is the position along the chord from 0 to c .

The NACA 0012 airfoil is plotted in Figure 6.1. The nondenominational radius ($\frac{R}{c}$) of the airfoil along the chord direction is calculated and plotted in Figure 6.2a, where R is the radius.

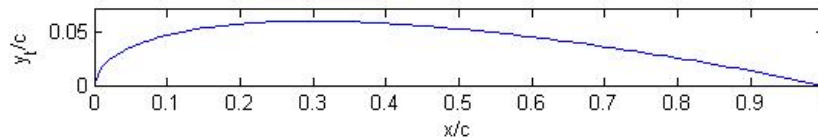


Figure 6.1: NACA 0012

A wing box is located in the section approximately between $x = 0.3c$ and $x = 0.6c$. The smallest radius (largest curvature) in this section is $2.2245c$ at $x = 0.3c$. Assuming that the shells used in current thesis is located exactly in the section between $x = 0.3c$ and $x = 0.6c$, the length of the shells will be $b \approx 0.3c$. So the ratio of the radius (R) to the length of the section ($b \approx 0.3c$) can be plotted along the chord direction as shown in Figure 6.2b. The smallest radius of the panel is $7.3883b$ and the largest radius is $20.2368b$. Since the dimension of the panel considered in this chapter is still $a = b = 100$ mm, so the smallest and largest radius of the shells is 738.83 mm and 2023.68 mm, respectively.

However, in this chapter the panels with constant radius will be discussed first. The panel with variable radius will be discussed later. Moreover, the arc angle of a cylindrical shell with

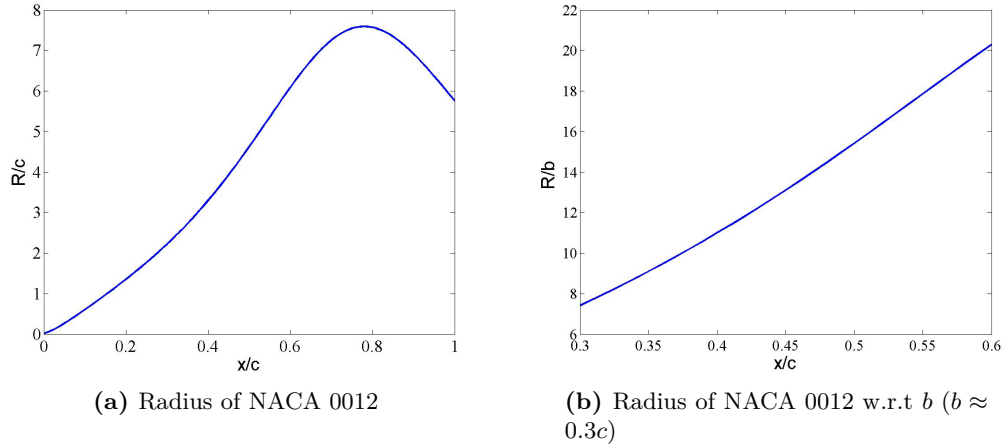


Figure 6.2: Non-dimensional radius of NACA 0012

constant radius is selected as 10 degrees resulting in a radius of 572.9578 mm, so

$$R = 572.9578 \text{ mm} \quad (6.22)$$

which is even smaller than required.

Since a shell with larger radius is closer to a plate and vice versa, a shell with smaller radius can be a better example of shells. Another reason is that it is more convenient to build the FEM model of a shell with an arc angle of 10° than other angles with non-integer value in Abaqus.

6.2 Stability Analysis: prescribed compression

In this section, the compression loads are applied on the edges of $x = 0, a$. The buckling behaviors of panels are discussed based on two kinds of laminates where the bending-twisting couplings (D_{16} and D_{26}) are zero and non-zero, respectively. The sine functions and polynomial functions are used as the shape functions of out-of-plane displacement, the convergences of the buckling loads obtained using these functions is investigated in section 6.2.1 and 6.2.2. In the section 6.2.3, the buckling of shallow cylindrical shells with variable curvatures is investigated.

The prediction of buckling load of variable stiffness panels is comprised of two steps: prebuckling analysis and stability analysis, as discussed in Chapter 4. In the first step, the in-plane loads distributions of the panel in prebuckling state are predicted, as shown in Chapter 5.

The Airy stress function has been approximated as

$$F(x, y) = \frac{1}{2} \bar{N}_x y^2 + \sum_{kl}^{KL} F_{kl} X_k(x) Y_l(y) \quad (6.23)$$

However, it is noted that in the prediction of buckling loads some negligible parameters of Airy stress function (F_{kl}) can be truncated and the error due to the truncation is less than 1%. The detail of the truncation will be shown in the end of section 6.2.1.

The out-of-plane displacement w in the first step has been approximated as

$$w = \sum_{pq}^{PQ} W_{pq} X_p(x) Y_q(y) \quad (6.24)$$

However, according to the in Chapter 3 it is zero before buckling occurring. So

$$w = \sum_{pq}^{PQ} W_{pq} X_p(x) Y_q(y) = 0 \quad (6.25)$$

Once the in-plane loads are predicted in the first step, they can be used to determine the buckling initiation in the second step. In the second step, as shown in the section 4.6.1 of Chapter 4 the variations of Airy stress function and out-of-plane deflection have been approximated as

$$\delta F = \sum_{kl}^{K_2 L_2} F_{kl}^1 X_k(x) Y_l(y) \quad (6.26)$$

$$\delta w = \sum_{pq}^{PQ} W_{pq}^1 X_p(x) Y_q(y) \quad (6.27)$$

where, K_2 and L_2 are numbers of terms used for δF .

As indicated in section 4.6.1 of Chapter 4, the number of terms used for δF are K_2 and L_2 , rather than K and L that are used for F . In calculus of variation, the variation of Airy stress function (δF) is an arbitrary infinitesimal value, which is independent of F . So not only the numbers of terms used for δF can be different from the number of terms used for F , but also can the shape functions of δF be different from the shape functions of F as long as the shape functions of δF satisfy the homogeneous form of boundary conditions. So a more general form of δF can be written as

$$\delta F = \sum_{kl}^{K_2 L_2} F_{kl}^1 X_k^1(x) Y_l^1(y) \quad (6.28)$$

where, X_k^1 and Y_l^1 are the shape functions of δF .

However, for simplicity the shape functions of δF and F are assumed to be the same in this chapter. So the equation 6.26 has been used instead of equation 6.28, but the K_2 and L_2 are still different from K and L . Similarly, the shape functions of δw can be different from these of w as well, since δw is just the variation of w . However, for convenience, the shape functions of δw are assumed as the same as w , as shown in equation 6.27.

Since the out-of-plane displacement w is zero before buckling occurs according to the in Chapter 3, its variation (δw) is the actual displacement during buckling. So the out-of-plane displacement during buckling is

$$w + \delta w = \delta w = \sum_{pq}^{PQ} W_{pq}^1 X_p(x) Y_q(y) \quad (6.29)$$

Then the equations 4.167 and 4.168 in section 4.6.1 of Trefftz method of Chapter 4 can be directly used, which are shown below.

$$-\lambda \mathbf{C}_a \mathbf{f}_{kl}^1 + \mathbf{C}_R^T \mathbf{w}_{pq}^1 = \vec{0} \quad (6.30)$$

$$[\mathbf{C}_D + \lambda(\mathbf{C}_N + \mathbf{C}_F)] \mathbf{w}_{pq}^1 + \lambda \mathbf{C}_R \mathbf{f}_{kl}^1 = \mathbf{0} \quad (6.31)$$

They can reduce to one equation (the same as equation 4.147),

$$[\mathbf{C}_D + \mathbf{C}_R \mathbf{C}_a^{-1} \mathbf{C}_R^T + \lambda(\mathbf{C}_N + \mathbf{C}_F)] \mathbf{w}_{pq}^1 = \mathbf{0} \quad (6.32)$$

For plates the equation can further reduce to

$$[\mathbf{C}_D + \lambda(\mathbf{C}_N + \mathbf{C}_F)] \mathbf{w}_{pq}^1 = \mathbf{0} \quad (6.33)$$

6.2.1 Buckling of Specially Orthotropic Laminate ($D_{16} = D_{26} = 0$)

For specially orthotropic laminates, the bending-twisting couplings are zero

$$D_{16} = D_{26} = 0 \quad (6.34)$$

The natural boundary conditions in equation 6.2 and 6.3 reduce to

$$M_x = -D_{11}w_{,xx} - D_{12}w_{,yy} = 0 \quad (\text{on } x = 0, a) \quad (6.35)$$

$$M_y = -D_{12}w_{,xx} - D_{22}w_{,yy} = 0 \quad (\text{on } y = 0, b) \quad (6.36)$$

Shape Function

Though Ritz method only requires that the essential boundary conditions to be satisfied by the shape functions, if the natural boundary conditions can be satisfied as well the prediction will be substantial better [15]. So to satisfy both boundary conditions, the sine function has been selected as

$$X_p(x) = \sin \frac{p\pi x}{a} \quad (p= 1, 2, \dots, P) \quad (6.37)$$

$$Y_q(y) = \sin \frac{q\pi y}{b} \quad (q= 1, 2, \dots, Q) \quad (6.38)$$

Then the out-of-plane displacement δw becomes

$$\delta w = \sum_{pq}^{PQ} W_{pq}^1 X_p(x) Y_q(y) = \sum_{pq}^{PQ} W_{pq}^1 \sin \frac{p\pi x}{a} \frac{q\pi y}{b} \quad (6.39)$$

which exactly satisfies both essential and natural boundary conditions term by term.

Since the selected shape functions do not have to satisfy the natural boundary condition, polynomial functions can be selected as the shape function which, though, only satisfy the essential boundary conditions.

$$X_p(x) = \left(\frac{x}{a}\right)^p \left(\frac{x}{a} - 1\right) \quad (p= 1, 2, \dots, P) \quad (6.40)$$

$$Y_q(y) = \left(\frac{y}{b}\right)^q \left(\frac{y}{b} - 1\right) \quad (q= 1, 2, \dots, Q) \quad (6.41)$$

Similar to what did in previous chapter, these polynomials should be transformed into in the nondimensional form as

$$X_p(\xi) = (\xi - 1)^p(\xi + 1) \quad (p= 1, 2, \dots, P) \quad (6.42)$$

$$Y_q(\eta) = (\eta - 1)^q(\eta + 1) \quad (q= 1, 2, \dots, Q) \quad (6.43)$$

where, $\xi = \frac{2x-a}{a}$ and $\eta = \frac{2y-b}{b}$.

Applying the Gram-Schmidt process, the shape function $X_p(\xi)$ and $Y_q(\eta)$ become

$$X_1(\xi) = \frac{\sqrt{15}}{4}(\xi^2 - 1) \quad (6.44)$$

$$X_2(\xi) = \frac{\sqrt{105}}{4}\xi(\xi^2 - 1) \quad (6.45)$$

$$X_3(\xi) = \frac{\sqrt{45}}{8}(7\xi^2 - 1)(\xi^2 - 1) \quad (6.46)$$

$$\vdots \quad (6.47)$$

$$Y_1(\eta) = \frac{\sqrt{15}}{4}(\eta^2 - 1) \quad (6.48)$$

$$Y_2(\eta) = \frac{\sqrt{105}}{4}\eta(\eta^2 - 1) \quad (6.49)$$

$$Y_3(\eta) = \frac{\sqrt{45}}{8}(\eta^2 - 1)(\eta^2 - 1) \quad (6.50)$$

$$\vdots \quad (6.51)$$

Verification

Two sets shape functions are used in Ritz method for in-plane loads prediction and stability analysis. The first set is a combination of beam characteristic function (equation 5.33, 5.36) and sine function (equation 6.37, 6.38), which are used as the shape functions of Airy stress function (F , and its variation δF) and the out-of-plane deflection (δw), respectively. The second set is a combination of polynomial functions (equation 5.52 5.53 and equation 6.40 6.41) which are used for the Airy stress function (F , and its variation δF) and out-of-plane deflection (δw). The results of Ritz method using these two sets of shape functions will be compared with FEM.

Panels with two kinds of layups are considered in the verification. The first kind of layups are the ones with constant stiffness. The second kind of layups are the ones with variable stiffness. The panels with the second kind of layups are assumed to have four or sixteen sections, as shown in Figure 3.3. The reason for considering the panels with constant stiffness is to prove Ritz method and the selected shape functions can exactly predict the buckling loads of panels with constant stiffness.

Constant Stiffness

For panels with constant stiffness, the in-plane loads are uniform and equal to the applied loads. Then the prebuckling analysis is not necessary, so the approximation of Airy stress

function using a set of series is not necessary. Thus the number of terms used for Airy stress function F is zero,

$$K = L = 0 \quad (6.52)$$

However, the variation δF is independent of F , which still has to be approximated by a set of series as shown in equation 6.26.

The layups with constant stiffness considered in this section are shown as follows

- Layup 4: [90 90 90 90]
- Layup 5: [0 0 0 0]
- Layup 6: [90 0 0 90]

Table 6.1, 6.2 and 6.3 show the predicted buckling loads compared to FEM, respectively, as increasing the number of terms used for the approximation of δw in x and y direction. The variation of Airy stress function (δF) is approximated by 18 terms in both x and y direction to achieve convergent predictions. The predictions of FEM are placed in the tables as columns with constant values since they are independent of K and L . The buckling modes of the plate and shell with layup 4 predicted by FEM and Ritz methods are compared in Figure 6.3.

Table 6.1: Buckling load of Layup 4

P=Q* (K=L=0)* (K ₁ =L ₁ =18)*(N/mm)	Plate					Shell				
	Ritz ₁ * (N/mm)	Ritz ₂ † (N/mm)	FEM (N/mm)	error ₁ ‡ (%)	error ₂ * (%)	Ritz ₁ (N/mm)	Ritz ₂ (N/mm)	FEM (N/mm)	error ₁ (%)	error ₂ (%)
2	1.612	2.044	1.610	0.162	26.984	5.063	5.296	4.696	7.821	12.774
4	1.612	1.617	1.610	0.162	0.439	4.922	4.745	4.696	4.805	1.049
6	1.612	1.612	1.610	0.162	0.163	4.810	4.736	4.696	2.429	0.845
8	1.612	1.612	1.610	0.162	0.162	4.764	4.684	4.696	1.442	-0.258
10	1.612	1.612	1.610	0.162	0.162	4.748	4.680	4.696	1.103	-0.346
12	1.612	1.612	1.610	0.162	0.162	4.742	4.680	4.696	0.981	-0.346

* Number of terms used for δw , F and δF , respectively

* The prediction of beam characteristic function (F , δF) and sine function (δw)

† The prediction of polynomial functions (F , δF and δw)

‡ Difference between Ritz₁ and FEM ($\frac{Ritz_1 - FEM}{FEM} \times 100\%$)

* Difference between Ritz₂ and FEM ($\frac{Ritz_2 - FEM}{FEM} \times 100\%$)

Table 6.2: Buckling load of Layup 5

P=Q (K=L=0) (K ₁ =L ₁ =18)	Plate					Shell				
	Ritz ₁	Ritz ₂	FEM	error ₁	error ₂	Ritz ₁	Ritz ₂	FEM	error ₁	error ₂
	(N/mm)	(N/mm)	(N/mm)	(%)	(%)	(N/mm)	(N/mm)	(N/mm)	(%)	(%)
2	2.646	3.128	2.643	0.126	18.384	5.064	5.169	4.913	3.060	5.202
4	2.646	2.647	2.643	0.126	0.173	4.994	4.936	4.913	1.635	0.464
6	2.646	2.646	2.643	0.126	0.126	4.990	4.915	4.913	1.555	0.039
8	2.646	2.646	2.643	0.126	0.126	4.989	4.915	4.913	1.544	0.039
10	2.646	2.646	2.643	0.126	0.126	4.989	4.915	4.913	1.541	0.039
12	2.646	2.646	2.643	0.126	0.126	4.989	4.915	4.913	1.541	0.039

Table 6.3: Buckling load of Layup 6

P=Q (K=L=0) (K ₁ =L ₁ =18)	Plate					Shell				
	Ritz ₁	Ritz ₂	FEM	error ₁	error ₂	Ritz ₁	Ritz ₂	FEM	error ₁	error ₂
	(N/mm)	(N/mm)	(N/mm)	(%)	(%)	(N/mm)	(N/mm)	(N/mm)	(%)	(%)
2	2.492	3.128	2.490	0.091	25.654	7.166	7.018	6.180	15.958	13.566
4	2.492	2.503	2.490	0.091	0.546	6.462	6.532	6.180	4.559	5.705
6	2.492	2.492	2.490	0.091	0.093	6.289	6.216	6.180	1.759	0.586
8	2.492	2.492	2.490	0.091	0.091	6.255	6.181	6.180	1.214	0.021
10	2.492	2.492	2.490	0.091	0.091	6.246	6.181	6.180	1.076	0.021
12	2.492	2.492	2.490	0.091	0.091	6.244	6.181	6.180	1.032	0.021

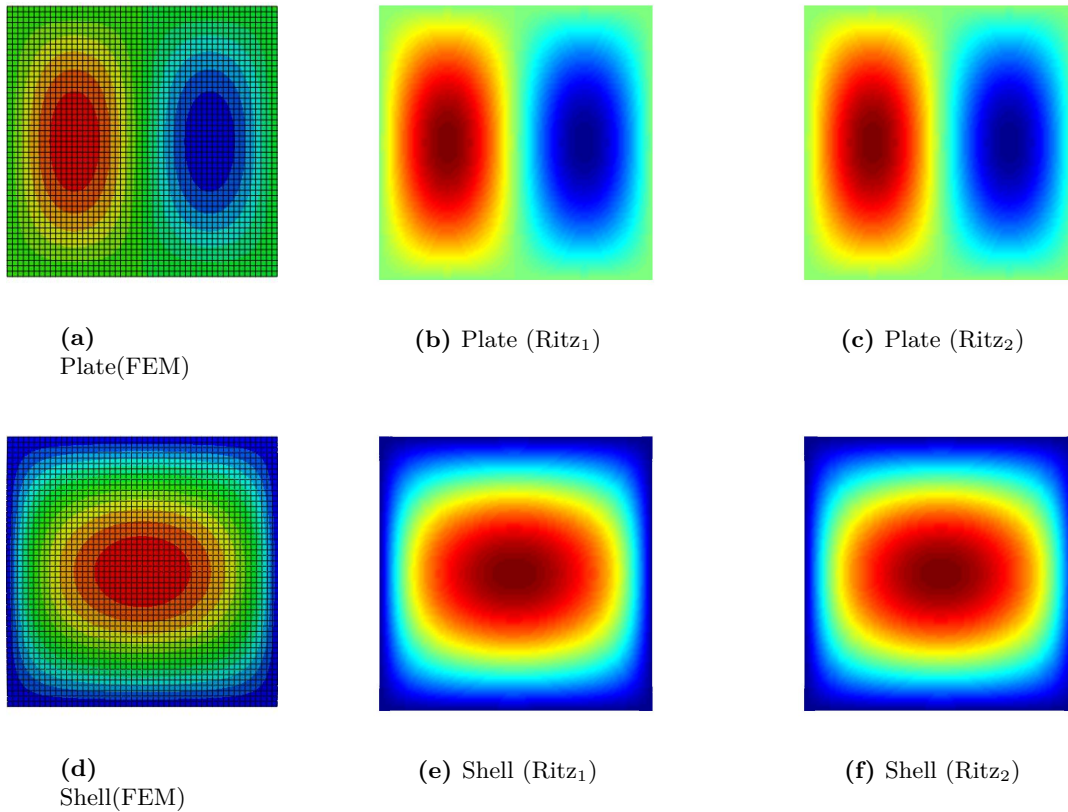


Figure 6.3: First Buckling Mode of Layup 4

The verification in FEM was implemented by using 25×25 elements in each section, as mentioned in section 5.1.3 of previous chapter. A convergence study was carried out for layup 4, as shown in Figure 6.4. As shown in the figures, the results obtained by using 40×40 elements in each section are only improved by 0.3% (plate) and 0.8% (shell) as compared to the results obtained using 25×25 elements in each section. The convergence criterion in FEM is set to be that the difference of the last loads are less than 1%. So the mesh density of 25×25 elements in each section is enough.

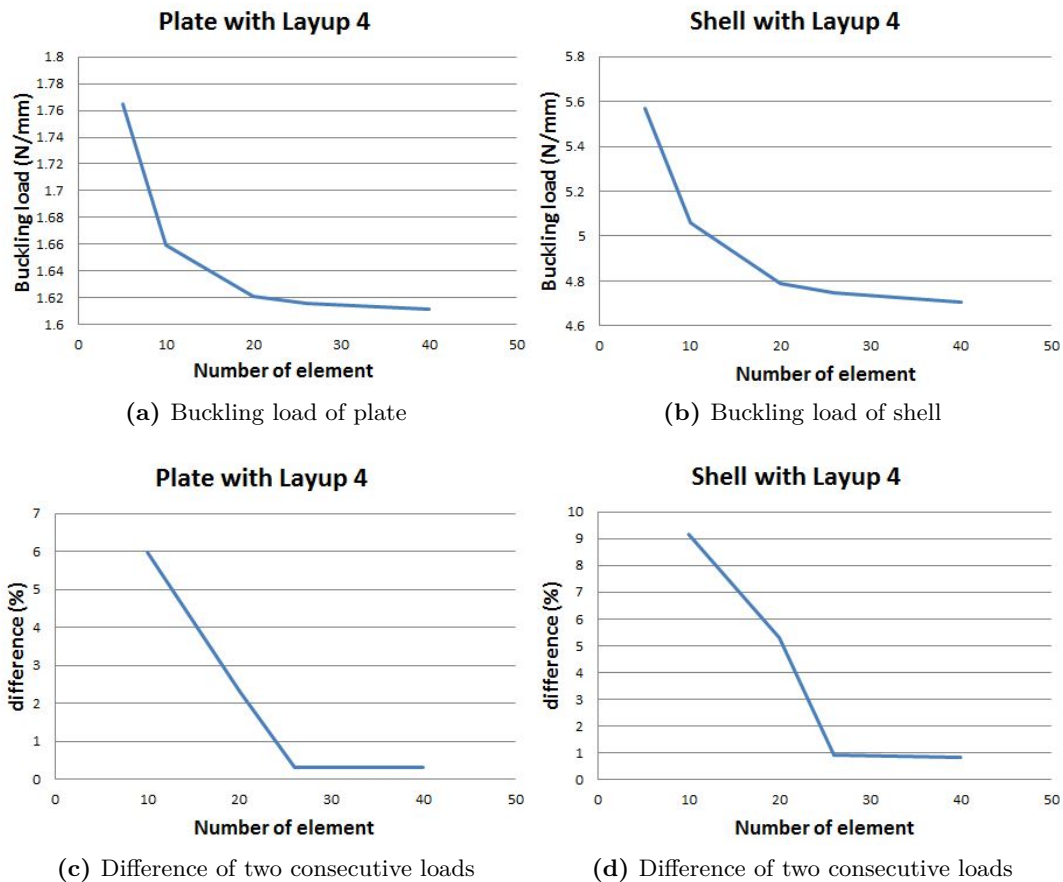


Figure 6.4: Convergence study of Layup 4 in FEM

Clearly, the predictions of plates and shells with all the layups obtained from Ritz method are converged within a few terms. For plates, the predictions obtained by using sine functions have been converged within two terms, while the predictions obtained by using the polynomials only have been converged in six terms for these layups. It is reasonable because the sine functions represent the exact eigenmodes of plates with constant stiffness. So the predictions converge to the exact value once the number of terms used in sine functions reach the exact number of half waves of a buckled plate. While polynomial functions do not exactly represent the eigenmodes of plates with constant stiffness, so they need more terms than sine functions to converge to the exact buckling mode. However, once both of them have been converged, the first buckling modes predicted by them will match well with FEM, as shown in Figure 6.3.

For shells, it is noticed that the predictions for layup 4 have converged to be lower than FEM. For plates, it is impossible because the predictions of Ritz method always converge from a higher value down to the exact value. In other words, the predictions are always larger or equal to the exact value, which provide upper-bound approximation [2–4, 15]. If the predictions of FEM have been converged, the prediction of Ritz method for plates will never be lower than FEM. For shells, as increasing number of terms used for out-of-plane deflection δw , the predictions also converge from a higher value down to a lower value similar to plates.

However, for layup 4 the predictions converge to be lower than FEM. This is due to the variation of Airy stress function (δF) which is coupled with the out-of-plane deflection (δw) for shells, as shown in equation 6.30. The coupling leads to that additional number of terms (K_1 and L_1) are needed to approximate δF . By contrast to δw , as increasing K_1 and L_1 , the predictions converge from a lower value up to the exact value. It can be explained by the plots shown in Figure 6.5. In Table 6.1, 6.2 and 6.3, K_1 and L_1 are set to be 18, however, in Figure 6.5 K_1 and L_1 are increasing. Clearly, as increasing K_1 and L_1 the buckling load will increase and converge to a higher value, which is opposite to what is observed in increasing P and Q . Besides the plots, this can also be explained analytically. In the section of the Trefftz buckling criterion (section 4.6.1), the second variation of the total energy functional (equation 4.161) is stationary with respect to the unknowns, δF and δw , respectively. When making it stationary with respect to δF , the first term, which is the negative of the second variation of the membrane complementary energy, is maximized since it is the negative of a quadratic form. However, when making it stationary with respect to δw , the second term, which is the second variation of the bending strain energy, is minimized since a quadratic form is normally minimized. The maximization makes the predictions converge from below up to the exact value; the minimization makes the predictions converge from upper down to the exact value. Ideally, if P and Q are infinite (the approximation of δw is exact), the predictions for shells using finite K_1 and L_1 are always smaller or equal to the exact value, which are the lower-bound. Only when P , Q , K_1 and L_1 are all infinite, the prediction will be the exact value. Therefore, as K_1 and L_1 increasing to certain values, the predictions for shells with layup 4 will become larger than FEM (if FEM is converged).

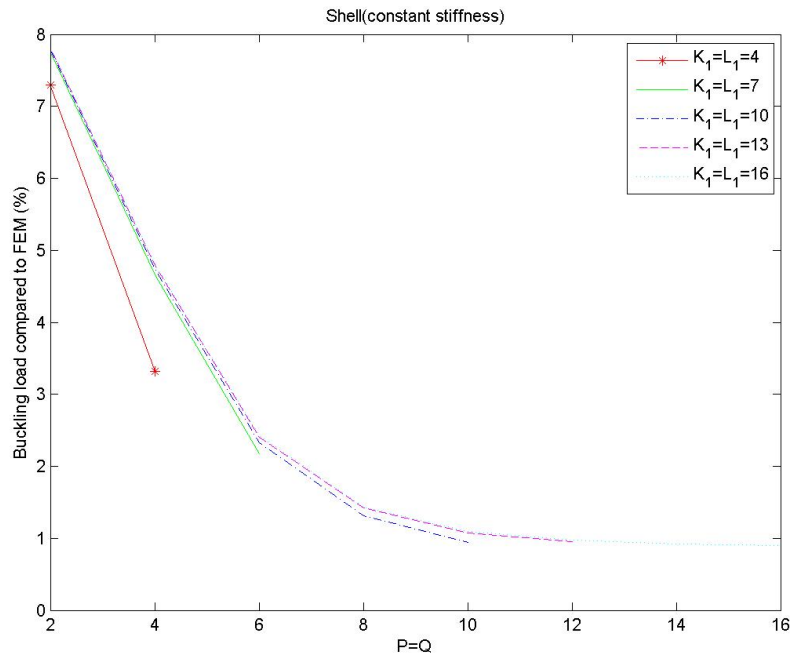
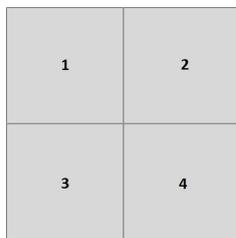


Figure 6.5: Buckling Load as increasing K_1 and L_1

Variable Stiffness

For the panels with variable stiffness, the in-plane loads are not uniform, which have to be predicted before starting the stability analysis. The details are shown in Chapter 5, so in this section only the influence of in-plane loads on the prediction of buckling loads will be investigated. In stability analysis of shells, the coupling of δw and δF will affect the buckling loads as discussed in section 6.2 and previous section. Therefore, all the number of terms (P , Q , K , L , K_1 and L_1) have influence on the convergence of predictions of buckling loads.

The layups with variable stiffness considered in this section are layup 1 (Figure 5.2) and layup 7 as shown in Figure 6.6.



Layup 7 ($A_{16} = A_{26} = D_{16} = D_{26} = 0$)

- Section 1: [90 0 0 90]
- Section 2: [90 90 90 90]
- Section 3: [0 90 90 0]
- Section 4: [0 0 0 0]

Figure 6.6: Layup 7

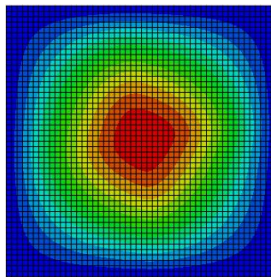
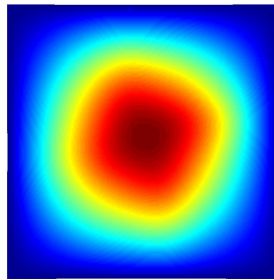
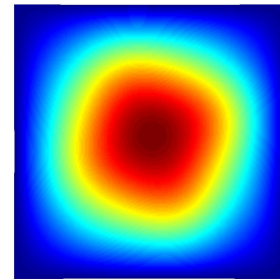
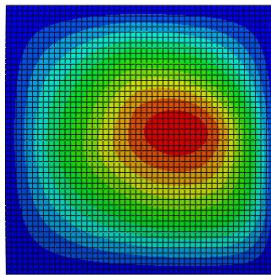
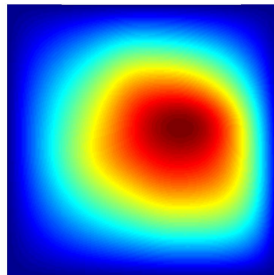
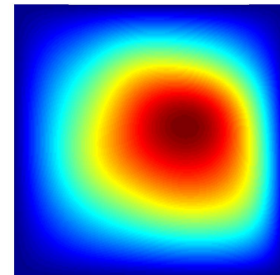
Table 6.4 and 6.5 show the predicted buckling loads compared to FEM, respectively, as increasing the number of terms used for the approximation of δw in x and y direction. The Airy stress function F and its variation (δF) are both approximated by using 18 terms in both x and y direction to achieve convergent predictions. The corresponding first buckling modes predicted by FEM and Ritz methods are compared in Figure 6.7 and 6.8.

Table 6.4: Buckling Load of Layup 1

P=Q (K=L=18) (K ₁ =L ₁ =18)	Plate					Shell				
	Ritz ₁	Ritz ₂	FEM	error ₁	error ₂	Ritz ₁	Ritz ₂	FEM	error ₁	error ₂
	(N/mm)	(N/mm)	(N/mm)	(%)	(%)	(N/mm)	(N/mm)	(N/mm)	(%)	(%)
2	2.566	3.059	2.166	18.444	41.208	5.703	5.900	5.128	11.214	15.056
4	2.484	2.554	2.166	14.643	17.888	5.447	5.428	5.128	6.232	5.860
6	2.428	2.509	2.166	12.095	15.835	5.358	5.342	5.128	4.496	4.183
8	2.387	2.467	2.166	10.182	13.903	5.306	5.292	5.128	3.472	3.203
10	2.357	2.432	2.166	8.804	12.244	5.279	5.258	5.128	2.950	2.536
12	2.335	2.402	2.166	7.785	10.899	5.257	5.231	5.128	2.532	2.021

Table 6.5: Buckling Load of Layup 7

P=Q (K=L=18) (K ₁ =L ₁ =18)	Plate					Shell				
	Ritz ₁	Ritz ₂	FEM	error ₁	error ₂	Ritz ₁	Ritz ₂	FEM	error ₁	error ₂
	(N/mm)	(N/mm)	(N/mm)	(%)	(%)	(N/mm)	(N/mm)	(N/mm)	(%)	(%)
2	2.298	2.695	2.088	10.056	29.086	5.396	5.499	4.896	10.223	12.316
4	2.225	2.297	2.088	6.564	10.022	5.100	5.118	4.896	4.167	4.550
6	2.188	2.241	2.088	4.807	7.333	5.028	4.990	4.896	2.705	1.933
8	2.168	2.206	2.088	3.852	5.673	4.993	4.943	4.896	1.992	0.968
10	2.156	2.184	2.088	3.265	4.633	4.976	4.917	4.896	1.633	0.430
12	2.148	2.170	2.088	2.877	3.940	4.964	4.899	4.896	1.406	0.067

**(a)** Plate
(FEM)**(b)** Plate (Ritz₁)**(c)** Plate (Ritz₂)**(d)** Shell
(FEM)**(e)** Shell (Ritz₁)**(f)** Shell (Ritz₂)**Figure 6.7:** First Buckling Mode of Layup 1

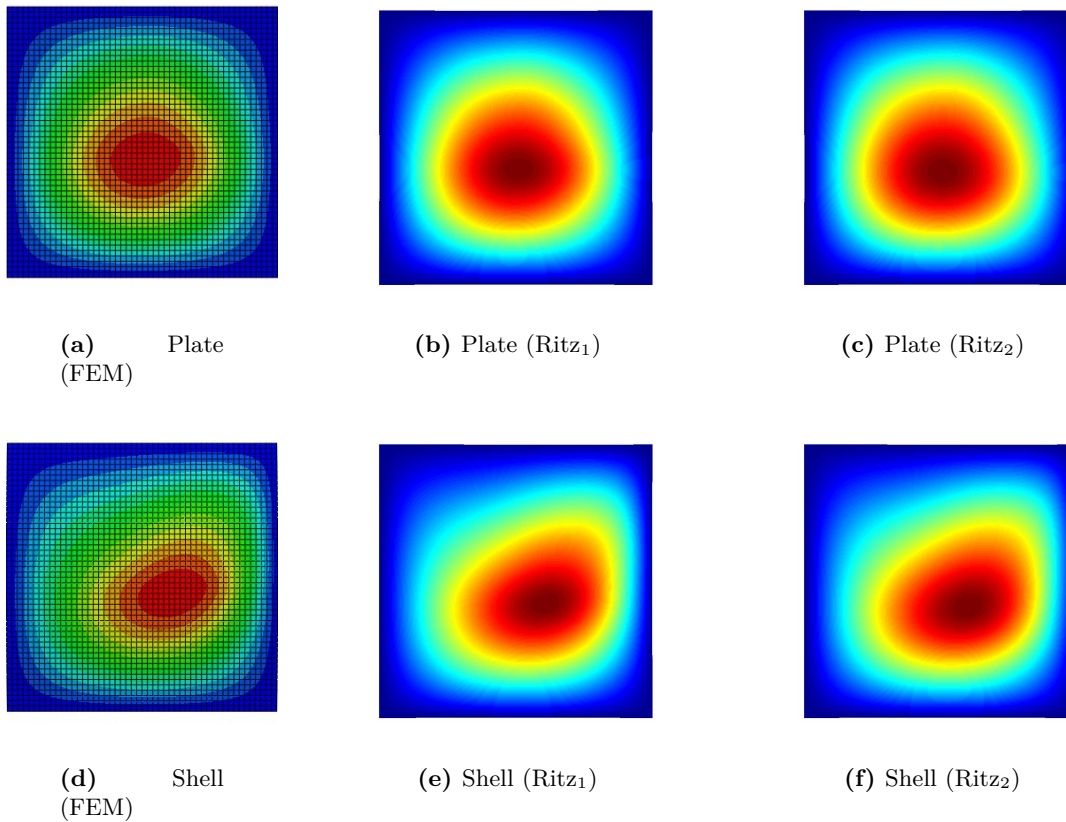


Figure 6.8: First Buckling Mode of Layup 7

The verification in FEM was implemented by using 25×25 elements in each section as well. Since the layup 1 and 7 have four sections, there are 50×50 elements in the whole panel, as shown in Figure 5.1a. A convergence study was carried out for layup 1, as shown in Figure 6.9. As shown in the figures, the results obtained by using 40×40 elements in each section are only improved by 0.11% (plate) and 0.24% (shell) as compared to the results obtained using 25×25 elements in each section. So the mesh density of 25×25 in each section is enough.

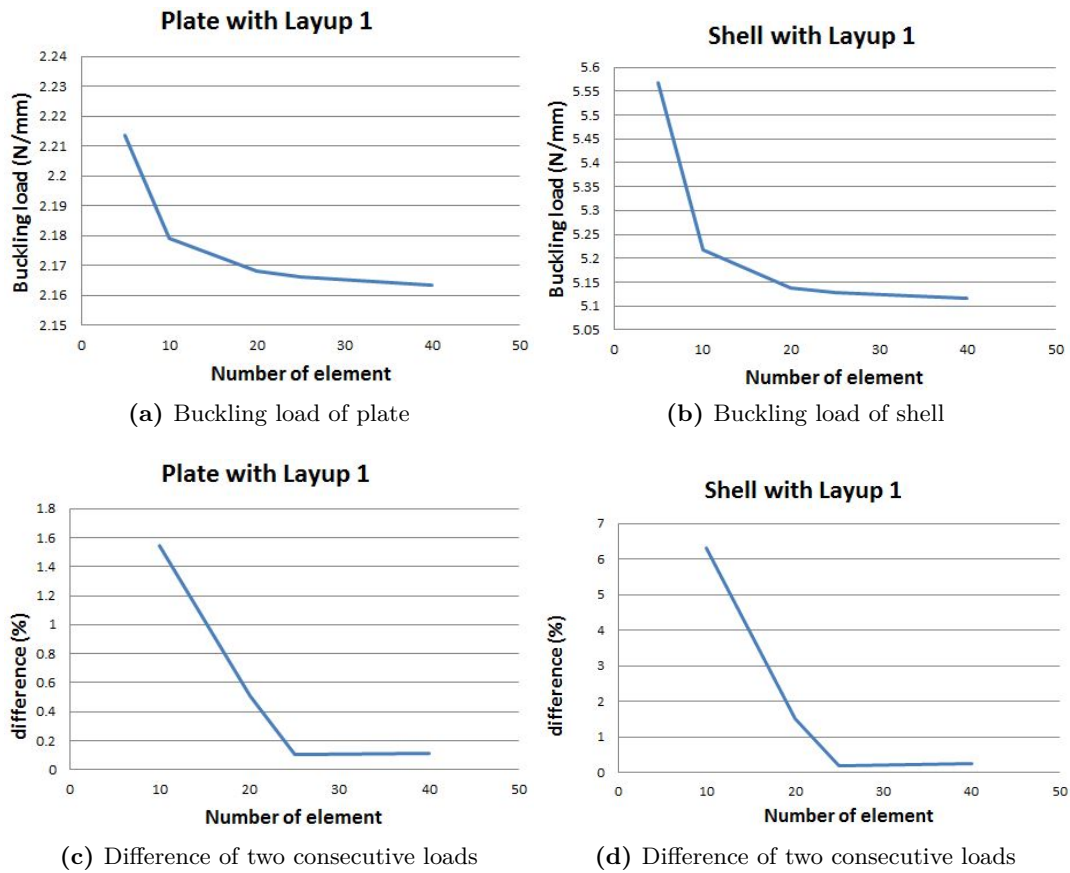
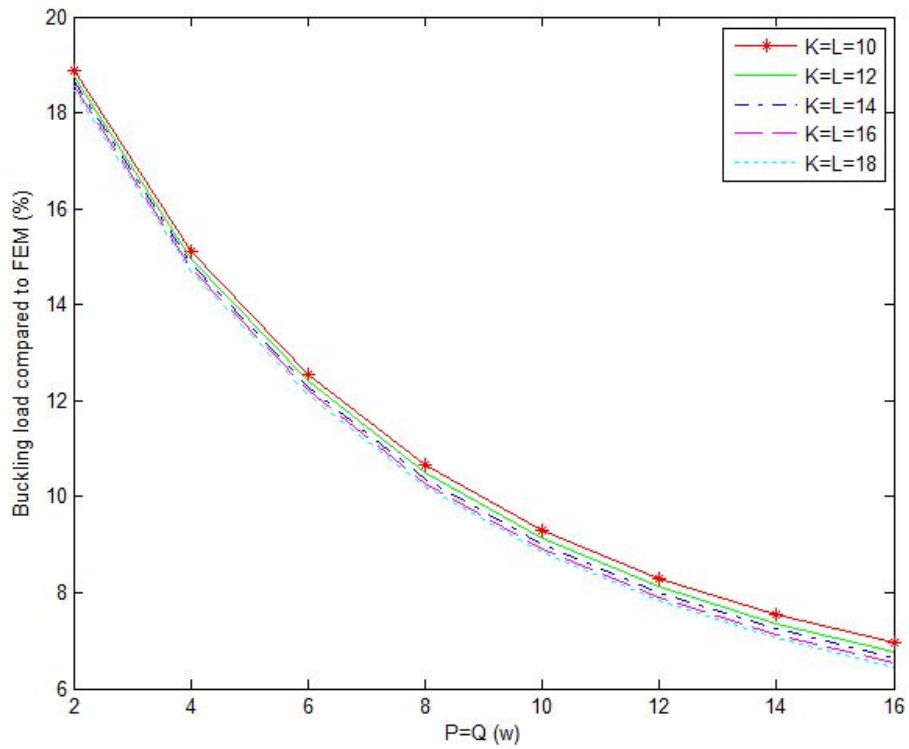
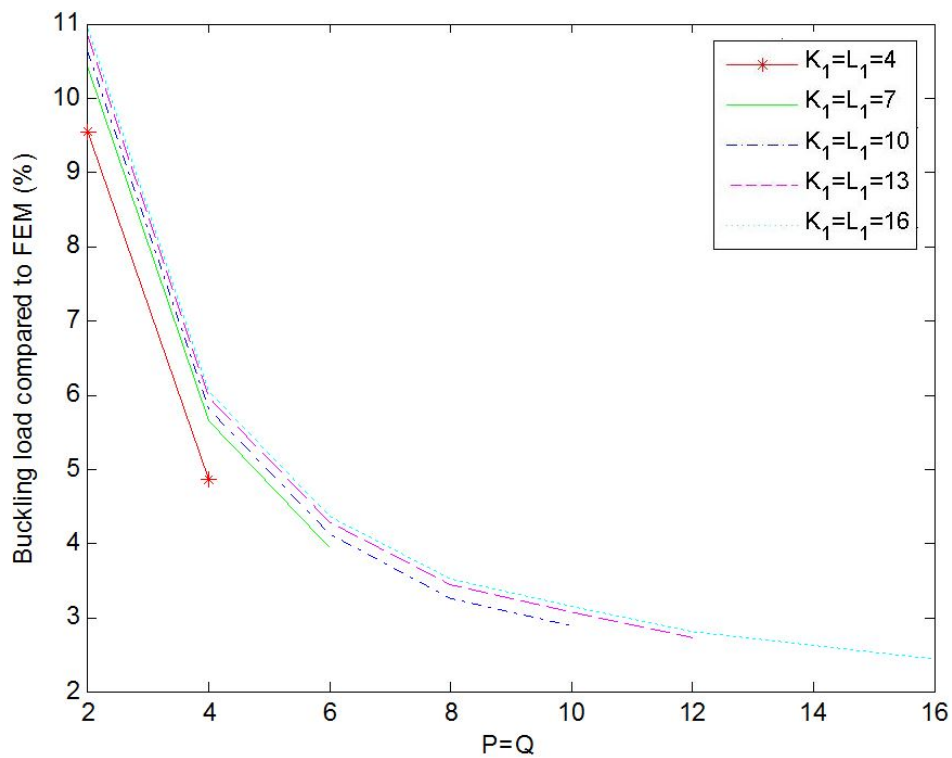


Figure 6.9: Convergence study of Layup 4 in FEM

Clearly, the buckling modes are correctly predicted by both shape functions. However, the predicted buckling loads of the plate with layup 1 obtained using both shape functions are not good. After 12 terms, the differences compared to FEM are still 7.785% and 10.899%, respectively. There are two possible reasons for it. Firstly, the number of terms (in both x and y direction) used to approximate the in-plane loads are not enough to capture a converged prediction. Secondly, the number of terms used for δw are not enough. However, the number of terms used for δF has no effect on the buckling of plates since δw is not coupled with δF for plates. So in Figure 6.10a, the predicted buckling load using the first set of shape functions (beam character function and sine function) are compared to FEM as increasing numbers of terms used for both δF and δw . Clearly, the effect of in-plane loads on the predictions of buckling load is very small and 18 terms used for F is nearly enough. As increasing number of terms used for δw to $P = Q = 16$, the predictions are increasingly better. However, the error is still above 6%. Therefore, these are not the main reasons why the predictions are not so good.



(a) Buckling load as increasing K and L (plate with Layup 1)



(b) Buckling Load as increasing K_1 and L_1 (shell with Layup 1, $K = L = 18$)

Figure 6.10: convergence of the buckling load (Layup 1)

Another reason might be the discontinuity of stiffness of the panels used in this section. Since for both layup 1 and layup 7 the panels have four section each having their own stiffness, the stiffness is discontinuous at the boundaries of the neighboring sections. However, the moments on boundaries are continuous due to the moment equilibrium, as shown in Figure 6.11. Since the moments are continuous and stiffness is discontinuous, the curvatures have to be discontinuous over the boundary. However, the curvatures are the second derivative of out-of-plane displacement,

$$\kappa_x = -w_{,xx} \quad (6.53)$$

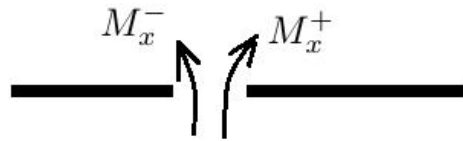


Figure 6.11: Bending moment equilibrium on the boundary of sections

Since the out-of-plane displacement is approximated by a set of continuous shape functions, such as the sine functions or polynomial functions, the curvatures calculated from the second derivative of the continuous shape functions are still continuous. Thus the shape functions used for δw are impossible to exactly capture the discontinuous curvatures, unless infinite number of terms are used. To approximately capture the discontinuous curvatures, a large number of terms are needed. So the prediction of buckling load will be better as increasing the number of terms used for dw , as shown in Figure 6.10a.

Since the layup 1 and 7 are extreme cases with stiffness discontinuity, if the stiffness discontinuity is reduced the predictions can be improved within small number of terms. This will be discussed and shown in the section 6.2.2 where layup 3 and 11 are used (the results are shown in Table 6.14 and 6.15).

For shells, it seems that the predictions using both shape functions are much better than the predictions for plates. However, similar to what discussed in previous section, as increasing the number of terms used for δF , the prediction will converge to higher values which means the errors compared FEM will be larger. This is also shown in the plots in Figure 6.10b. So it is meaningless to compare the predictions for plates and shells.

Truncation of Negligible Parameters

It is interesting to notice that only a few biggest parameters (F_{kl}) of the Airy stress function (F) are needed to predict the buckling load. While, the other negligible parameters can be truncated and the error due to the truncation is less than 1%. The benefit of the truncation is that the efficiency can be significantly improved since less number of terms of Airy stress functions are used in the prediction of buckling loads.

As shown in previous chapter, a large number of terms are needed to exactly predict the in-plane loads. Moreover, with more number of terms used for Airy stress function, the prediction of buckling load becomes closer to FEM, as shown in Figure 6.10a. However, even though lots of terms are required, only a few parameters (F_{kl}) are needed to predict

the buckling load. Taking the layup 1 for example, the parameters (F_{kl}) obtained in the prebuckling analysis when 10 terms are used in both x any direction ($K = L = 10$) are plotted in Figure 6.12a. The largest parameter occurs when $k \times l = 2$, which is -15.56. After $k \times l = 30$, most parameters are extremely close to 0. Since they are close to 0, they might have negligible influence on the prediction of buckling load (which will be shown in Table 6.6 and 6.7). Thus in the prediction, these negligible parameters might be truncated. To truncate these parameters quantitatively, following formula can be used.

$$f = \sum_{kclc} F_{kclc}^2 \geq \sum_{kl} F_{kl}^2 \times 99.8\% \quad (6.54)$$

where, F_{kclc} are the larger parameters still retained after truncating the smaller parameters, and the percentage of 99.8 % is used to select the largest parameters which can be changed to other values.

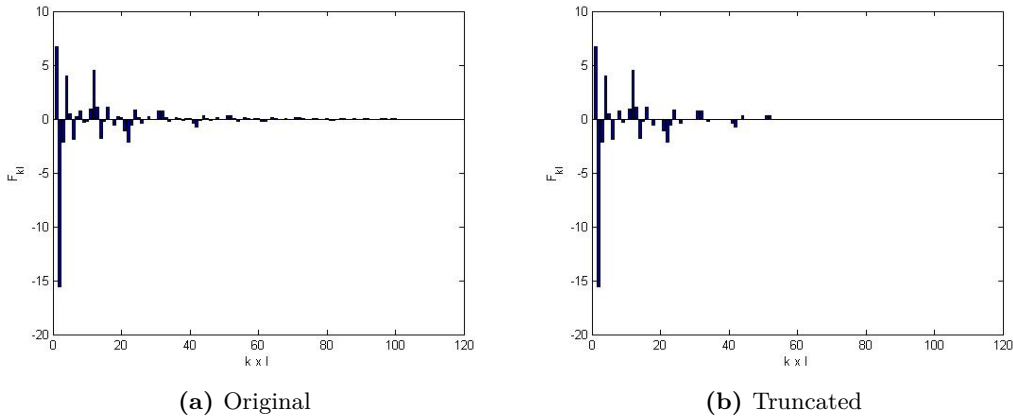


Figure 6.12: Plot of F_{kl} (Layup 1)

After applying this formula, only the largest the parameters whose sum of the square of themselves is over 99.8% have been retained. The other parameters are truncated. For example, after truncating the smallest parameters of layup 1, only 28 parameters left (when the percentage is 99.8%), which are plotted in Figure 6.12b.

The buckling loads of layup 1 are re-predicted using this idea and compared to the original predictions, as shown in Table 6.6. The original predictions are obtained by setting $K = L = 18$, thus in total there are 324 parameters. By setting the percentage in equation 6.54 as 99.8%, only 33 parameters left. So nearly 90% of the parameters are truncated from the prediction. However, as shown in Table 6.6, the errors due to the truncation are nearly zero. Similar observation has been found for layup 7, as shown in Table 6.7. Clearly, the errors of the predictions due to the truncation are negligible for these two layups. Similarly, the prediction of in-plane loads of layup 1, after truncation nearly 90% percent of parameters, are still closed to the original prediction (however, not as closed as the prediction of buckling load), as shown in Figure 6.13.

Since nearly 10% percent of the parameters are used in the prediction of buckling load, the efficiency of the predictions is improved nearly 900%. However, the formula and the

percentage used for truncating the small parameters still have to be investigated in the future. Here they are only examples to show how negligible these small parameters are.

Table 6.6: Buckling load of Layup 1 after truncating the negligible parameters

P=Q	Plate						Shell					
	Ritz ₁ (N/mm)	Ritz ₁ ^t (N/mm)	error ₁ ^c (%)	Ritz ₂ (N/mm)	Ritz ₂ ^t (N/mm)	error ₂ ^c (%)	Ritz ₁ (N/mm)	Ritz ₁ ^t (N/mm)	error ₁ ^c (%)	Ritz ₂ (N/mm)	Ritz ₂ ^t (N/mm)	error ₂ ^c (%)
2	2.566	2.566	0.011	3.059	3.059	-0.002	5.703	5.703	0.014	5.900	5.900	0.001
4	2.484	2.484	0.011	2.554	2.554	0.003	5.447	5.448	0.015	5.428	5.428	0.002
6	2.428	2.429	0.011	2.509	2.509	0.006	5.358	5.359	0.013	5.342	5.342	0.006
8	2.387	2.387	0.011	2.467	2.468	0.004	5.306	5.306	0.008	5.292	5.292	-0.003
10	2.357	2.357	0.011	2.432	2.432	0.000	5.279	5.279	0.008	5.258	5.257	-0.009
12	2.335	2.335	0.012	2.402	2.402	-0.003	5.257	5.258	0.013	5.231	5.231	-0.007

^t prediction after truncating the negligible parameters

^c error of the prediction due to the truncation $\frac{Ritz_1^t - Ritz_1}{Ritz_1} \times 100\%$

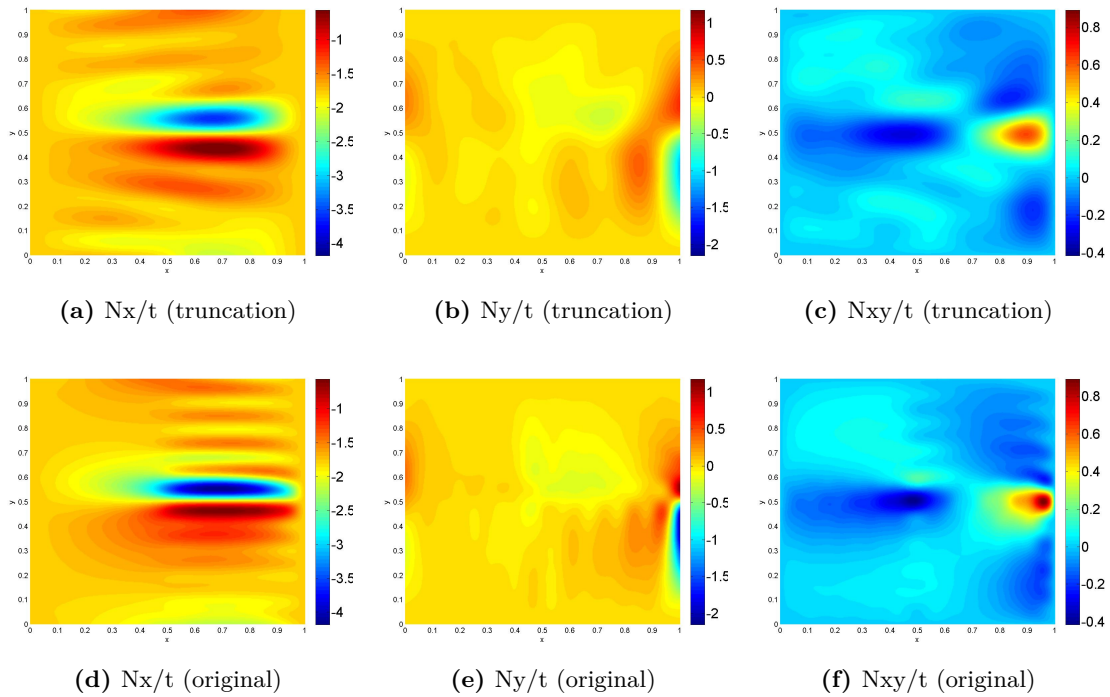


Figure 6.13: Comparison of in-plane stresses of layup 1 before and after truncation (Mpa, K=L=18, $\bar{N}_x = 1$ N/mm)

Table 6.7: Buckling load of Layup 7 after truncating the negligible parameters

P=Q	Plate						Shell					
	Ritz ₁ (N/mm)	Ritz ₁ ^t (N/mm)	error ₁ ^c (%)	Ritz ₂ (N/mm)	Ritz ₂ ^t (N/mm)	error ₂ ^c (%)	Ritz ₁ (N/mm)	Ritz ₁ ^t (N/mm)	error ₁ ^c (%)	Ritz ₂ (N/mm)	Ritz ₂ ^t (N/mm)	error ₂ ^c (%)
2	2.298	2.298	0.008	2.697	2.695	-0.071	5.396	5.397	0.021	5.499	5.498	-0.004
4	2.225	2.225	0.007	2.299	2.297	-0.077	5.100	5.101	0.023	5.118	5.118	-0.002
6	2.188	2.188	0.006	2.242	2.241	-0.064	5.028	5.029	0.012	4.990	4.990	0.002
8	2.168	2.168	0.002	2.207	2.206	-0.041	4.993	4.993	-0.003	4.943	4.942	-0.011
10	2.156	2.156	0.001	2.185	2.184	-0.033	4.976	4.975	-0.005	4.917	4.916	-0.018
12	2.148	2.148	0.005	2.171	2.170	-0.047	4.964	4.965	0.004	4.899	4.898	-0.017

^t prediction after truncating the negligible parameters

^c error of the prediction due to the truncation $\frac{Ritz_1^t - Ritz_1}{Ritz_1} \times 100\%$

6.2.2 Buckling of General Symmetric Laminate ($D_{16}, D_{26} \neq 0$)

Since the bending-twisting couplings are not zero, the natural boundary conditions are the same as equation 6.2 and 6.3.

$$M_x = -D_{11}w_{,xx} - D_{12}w_{,yy} - 2D_{16}w_{,xy} = 0 \quad (\text{on } x = 0, a) \quad (6.55)$$

$$M_y = -D_{12}w_{,xx} - D_{22}w_{,yy} - 2D_{26}w_{,xy} = 0 \quad (\text{on } y = 0, b) \quad (6.56)$$

Shape Function

Due to the existence of the bending-twisting couplings, the natural boundary conditions cannot be exactly satisfied by the sine functions and polynomial functions term by term. Moreover, as indicated in section 6.1.1, the shape function which can satisfy the natural boundary conditions term by term will force the slope fixed at boundaries. Therefore, there is no such a shape function which satisfies both essential and natural boundary conditions term by term (to the best knowledge of the author). However, in Ritz method the natural boundary condition does not need to be satisfied, the sine function and polynomial function are sufficient to predict the buckling load if enough terms are used in the approximations. The effect of not satisfying the natural boundary conditions on the predictions of buckling loads will be discussed in this section.

Verification

Similarly, panels with two kinds of layups are considered in the verification. The first kind of layups are the ones with constant stiffness. The second kind of layups are the ones with variable stiffness, which are assumed to have four or sixteen sections. The reason for considering the layups with constant stiffness is to investigate whether the Ritz method and the selected shape functions can exactly predict the buckling load of panels when bending-twisting couplings exist ignoring the influence of variable stiffness.

Constant Stiffness

For the panel with constant stiffness, the in-plane loads are uniform and equal to the applied loads. Then the prebuckling analysis is not necessary. However, the variation δF is independent of F , which is still approximated by a set of series as shown in equation 6.26.

The layups with constant stiffness considered in this section are shown as follows

- Layup 8: [45 45 45 45]
- Layup 9: [15 15 15 15]

Table 6.8 and 6.9 show the predicted Buckling Load compared to FEM, respectively, as increasing the number of terms used for the approximation of δw in x and y direction. The variation of Airy stress function (δF) is approximated by 18 terms in both x and y direction to achieve convergent predictions. The buckling modes of the plate and shell with layup 8 predicted by FEM and Ritz methods are compared in Figure 6.14.

Table 6.8: Buckling load of Layup 8

P=Q* (K=L=0)* (K ₁ =L ₁ =18)*	Plate					Shell				
	Ritz ₁ * (N/mm)	Ritz ₂ † (N/mm)	FEM (N/mm)	error ₁ ‡ (%)	error ₂ * (%)	Ritz ₁ (N/mm)	Ritz ₂ (N/mm)	FEM (N/mm)	error ₁ (%)	error ₂ (%)
2	3.605	3.868	2.459	46.594	57.302	6.352	6.094	4.958	5.190	22.922
4	2.990	2.651	2.459	21.608	7.795	5.870	5.473	4.958	8.013	10.385
6	2.867	2.564	2.459	16.593	4.286	5.622	5.083	4.958	10.884	2.522
8	2.802	2.539	2.459	13.942	3.258	5.500	5.041	4.958	9.265	1.675
10	2.759	2.525	2.459	12.200	2.691	5.428	5.024	4.958	8.150	1.330
12	2.728	2.516	2.459	10.941	2.340	5.379	5.014	4.958	7.369	1.124

* Number of terms used for δw , F and δF , respectively

* The prediction of beam characteristic function (F , δF) and sine function (δw)

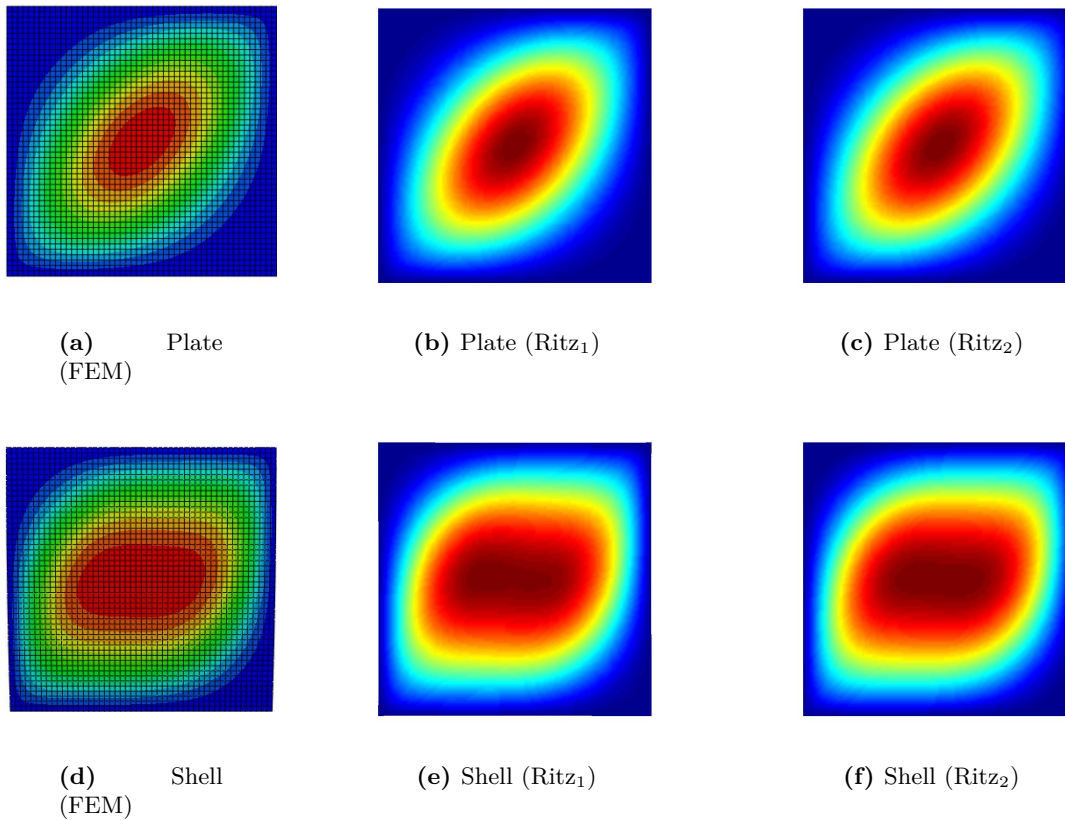
† The prediction of polynomial functions (F , δF and δw)

‡ Difference between Ritz₁ and FEM ($\frac{Ritz_1 - FEM}{FEM} \times 100\%$)

* Difference between Ritz₂ and FEM ($\frac{Ritz_2 - FEM}{FEM} \times 100\%$)

Table 6.9: Buckling load of Layup 9

P=Q (K=L=0) (K ₁ =L ₁ =18)	Plate					Shell				
	Ritz ₁ (N/mm)	Ritz ₂ (N/mm)	FEM (N/mm)	error ₁ (%)	error ₂ (%)	Ritz ₁ (N/mm)	Ritz ₂ (N/mm)	FEM (N/mm)	error ₁ (%)	error ₂ (%)
2	2.790	3.251	2.581	8.082	25.950	5.228	5.292	4.914	-1.318	7.692
4	2.689	2.610	2.581	4.179	1.101	5.105	4.955	4.914	3.047	0.834
6	2.657	2.596	2.581	2.940	0.552	5.070	4.922	4.914	3.013	0.145
8	2.642	2.593	2.581	2.330	0.450	5.051	4.918	4.914	2.704	0.083
10	2.632	2.592	2.581	1.961	0.404	5.040	4.917	4.914	2.504	0.056
12	2.626	2.591	2.581	1.710	0.380	5.033	4.916	4.914	2.364	0.042

**Figure 6.14:** First Buckling Mode of Layup 8

It is noted that the predictions of layup 8 are substantial worse than the predictions of layup 9 for both shape functions. The reason is the layup 8 has bigger bending-twisting couplings than layup 9. In previous section, when the bending-twisting couplings are zero, the predictions are converged very fast, as shown Table 6.1, 6.2 and 6.3. So one can expect that when the bending-twisting couplings are smaller, the convergence will be faster for most layups.

Among all the layups with constant stiffness, the layup 8 is the one with largest bending-twisting couplings since the fiber orientations are all 45 degree. Therefore, the predictions converge slowest. The discussion will focus on this layup.

It is also noted that the predictions using polynomial functions are significant better than these using sine function, which is contrary to what observed in layup 4, 5 and 6 whose bending-twisting couplings are zero in section 6.2.1. In section 6.2.1, the natural boundary condition is satisfied by the sine function, so the predictions using sine function are better than polynomial function. However, in this section the sine functions cannot satisfy the natural boundary conditions, either. So in principle, these two shape functions should have more or less the same predictions. However, here the polynomial functions have shown to be better than the sine functions. As indicated by Wu, Raju and Weaver [32], the polynomial functions which are nonperiodic can better capture the localized features, such as strong gradients in the buckling mode shape, than the periodic sine functions. This can explain why polynomial functions are better in predictions of buckling loads. But polynomial functions still cannot capture the exact buckling load. Except the natural boundary condition not being satisfied, another reason is the differentiation on the approximated out-of-plane displacement will lead to further errors in the evaluation of moments and slopes [32].

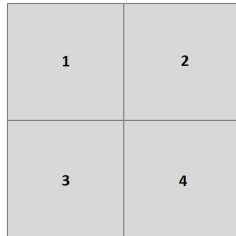
The Legendre polynomials were used as the shape functions of the out-of-plane displacement by Wu, Raju and Weaver [32], where the buckling load of a square laminated plate with completely 45 degree plies was investigated. Since the Legendre polynomial functions can satisfy neither the essential nor the natural boundary condition, the Lagrange multiplier was introduced to force the Legendre polynomials to satisfy the essential boundary condition set by set. It is similar to what did in Chapter 5, where the sine and cosine functions were forced to satisfy the boundary conditions of stresses set by set, instead of term by term. The error of the buckling loads predicted using Legendre polynomials reduced to 2.4% when only 13 by 13 terms are used. In this thesis, the polynomial shape functions can exactly satisfy the essential boundary term by term. For a laminated square plate with all 45 degree plies (layup 8), the error reduces to 2.34% when 12 by 12 terms are used, as shown in Table 6.8 . Although the dimensions and the material properties used for these two square plates are different, it is still reasonable to say the polynomial functions used in the thesis are proper choices.

For shells, similar to what observed in section 6.2.1 the buckling loads predicted by both shape functions seem to be better than these for plates. However, as increasing the number of terms used for δF , the predictions will converge to higher value thus leading to bigger errors. So unless δF of shells converges to the exact value it is meaningless to compare the predictions between plates and shells.

Variable Stiffness

For the panels with variable stiffness, the in-plane loads are not uniform , which have to be predicted before predicting the buckling loads. The details are shown in Chapter 4 and 5, so in this section only the influence of in-plane loads on the predictions of buckling loads are investigated. In stability analysis of shells, the coupling of deflection δw and δF will affect the buckling loads as discussed in section 6.2. Therefore, all the number of terms (P , Q , K , L , K_1 and L_1) have influence on the predictions of buckling loads.

The layups with variable stiffness considered in this section are layup 2 (Figure 5.7) and layup 10 as shown in Figure 6.15.



Layup 10 ($D_{16}, D_{26} \neq 0$)

- Section 1: [60 45 -45 90 -60 0 0 -60 90 -45 45 60]
- Section 2: [45 30 -45 -45 -30 90 90 -30 -45 -45 30 45]
- Section 3: [90 45 75 90 0 -75 -75 0 90 75 45 90]
- Section 4: [0 15 45 -45 -15 90 90 -15 -45 45 15 0]

Figure 6.15: Layup 10

Table 6.10 and 6.11 show the predicted buckling loads compared to FEM, respectively, as increasing the number of terms used for the approximation of δw in x and y direction. The Airy stress function F and its variation (δF) are both approximated by 18 terms in both x and y direction to achieve convergent predictions. The corresponding first buckling modes predicted by FEM and Ritz methods are compared in Figure 6.16 and 6.17.

Table 6.10: Buckling Load of Layup 2

P=Q (K=L=18) ($K_1=L_1=18$)	Plate					Shell				
	Ritz ₁	Ritz ₂	FEM	error ₁	error ₂	Ritz ₁	Ritz ₂	FEM	error ₁	error ₂
	(N/mm)	(N/mm)	(N/mm)	(%)	(%)	(N/mm)	(N/mm)	(N/mm)	(%)	(%)
2	4.934	5.633	4.012	22.987	40.398	9.022	8.793	6.530	38.160	34.653
4	4.569	4.508	4.012	13.896	12.355	7.718	7.919	6.530	18.193	21.264
6	4.367	4.258	4.012	8.863	6.136	7.354	7.021	6.530	12.620	7.522
8	4.332	4.173	4.012	7.987	4.007	7.255	6.879	6.530	11.102	5.350
10	4.271	4.140	4.012	6.463	3.203	7.170	6.846	6.530	9.792	4.831
12	4.255	4.122	4.012	6.050	2.752	7.127	6.830	6.530	9.147	4.598

Table 6.11: Buckling Load of Layup 10

P=Q (K=L=18) ($K_1=L_1=18$)	Plate					Shell				
	Ritz ₁	Ritz ₂	FEM	error ₁	error ₂	Ritz ₁	Ritz ₂	FEM	error ₁	error ₂
	(N/mm)	(N/mm)	(N/mm)	(%)	(%)	(N/mm)	(N/mm)	(N/mm)	(%)	(%)
2	90.739	100.267	79.176	14.604	26.638	110.115	116.501	99.981	10.136	16.523
4	88.066	87.437	79.176	11.228	10.434	106.901	105.546	99.981	6.922	5.566
6	87.470	86.472	79.176	10.475	9.214	106.330	104.312	99.981	6.350	4.332
8	87.043	86.199	79.176	9.936	8.870	105.871	104.168	99.981	5.891	4.188
10	86.851	86.062	79.176	9.694	8.697	105.675	104.078	99.981	5.696	4.098
12	86.673	85.977	79.176	9.469	8.590	105.491	104.019	99.981	5.511	4.038

Similar to what was observed in section 6.2.2, the predictions obtained from the polynomial

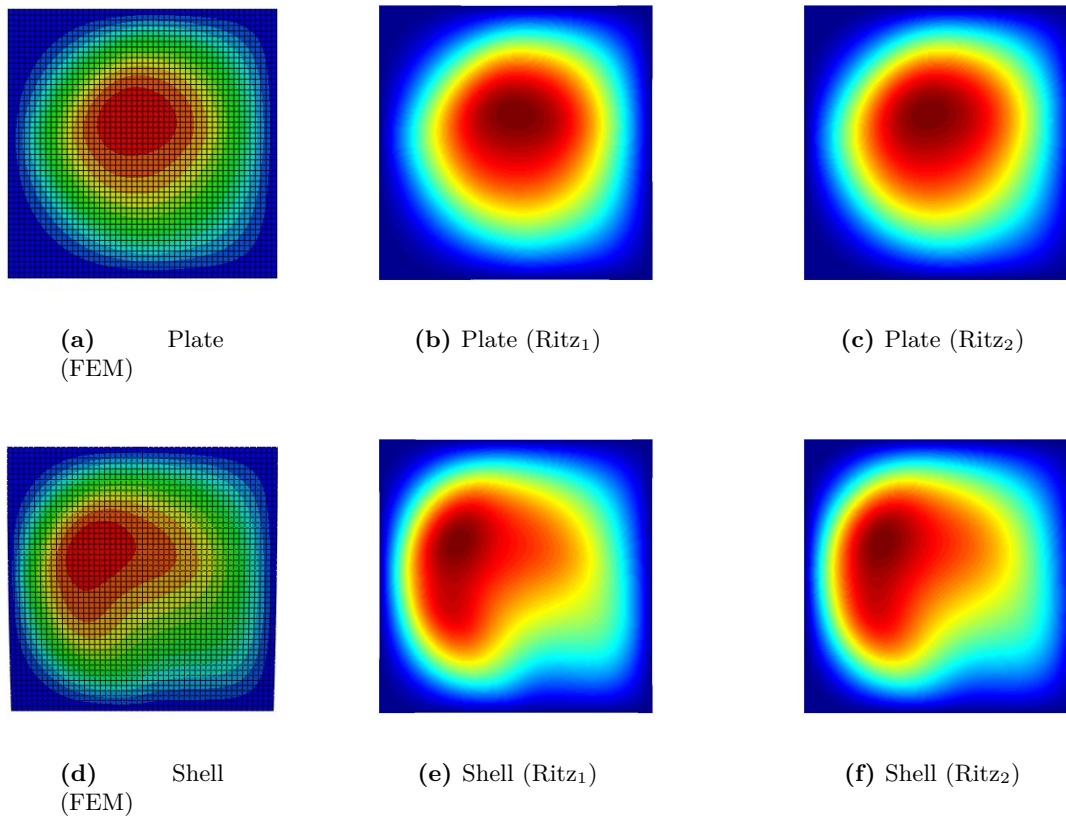


Figure 6.16: First Buckling Mode of Layup 2

functions are better than these obtained from the sine function for plates and shells with both layups. The reason is the same that the nonperiodic polynomial function can better capture the localized features, such as strong gradients in the buckling mode shape [32].

It is noted that the predictions for plate with layup 10 are worse than these for plate with layup 2 whatever shape functions are used. Especially for polynomial functions, the predictions obtained for plate with layup 10 are substantially worse than these obtained for plate with layup 2. The reason is that the difference of stiffness in the neighboring sections of layup 10 are more evident than that of layup 2. For layup 2, the difference of the stiffness is small because the layup is primary made up of 45-degree plies. While for layup 10, the layup is randomly made up of various plies so the differences of the stiffness in the sections are not small. The differences of stiffness in the sections, which, in other words, are the discontinuity of stiffness, will lead to discontinuous curvatures, as discussed in section 6.2.1. A large number of terms is needed to approximate the discontinuity of curvatures. The larger the differences of stiffness are, the more terms are needed to approximate the curvatures. Therefore, the prediction of plate with layup 10 converge to FEM slower since more terms are needed than layup 2. The same ideal of truncating small parameters from Airy stress function are applied to the two layups, the errors of the truncation are found to be negligible, as shown in Table 6.12 and 6.13. However, for shell with layup 2, the errors are over 1%, which are dramatically bigger than others. Therefore, this ideal needs to be further investigated, and as well as the

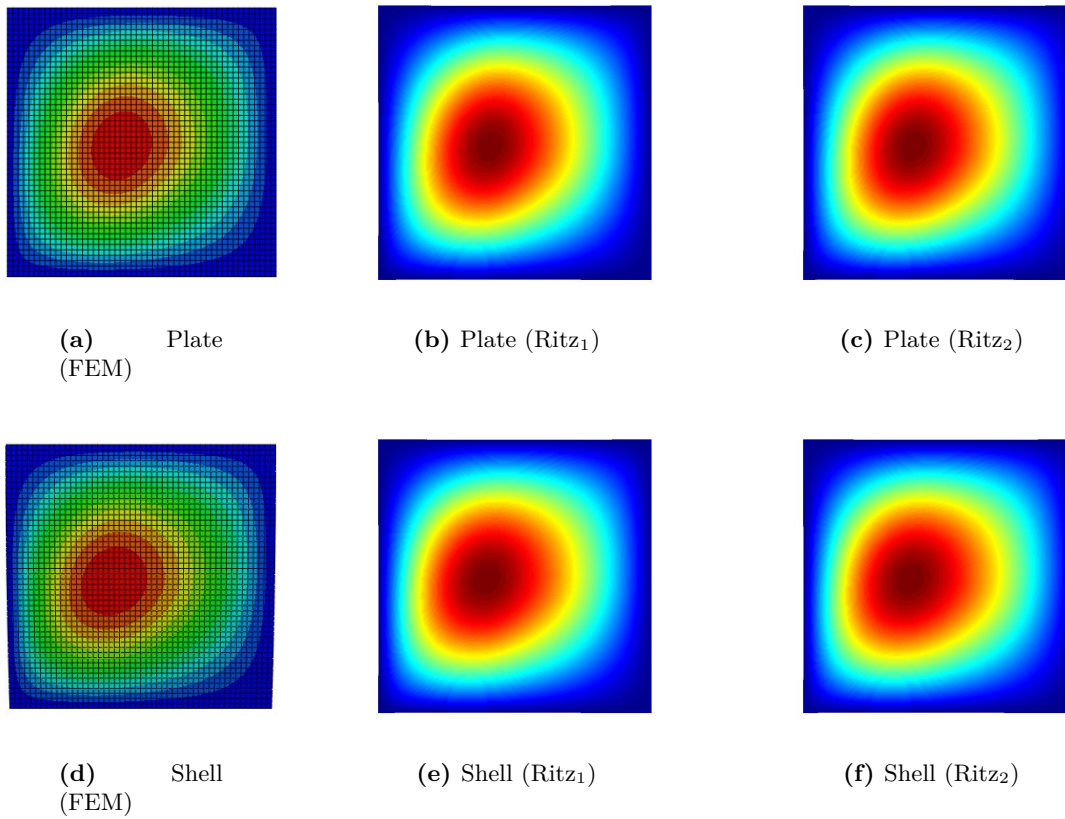


Figure 6.17: First Buckling Mode of Layup 10

formula and percentage used for truncation.

Table 6.12: Buckling load of Layup 2 after truncating the negligible parameters

P=Q	Plate						Shell					
	Ritz ₁ (N/mm)	Ritz ₁ ^t (N/mm)	error ₁ ^c (%)	Ritz ₂ (N/mm)	Ritz ₂ ^t (N/mm)	error ₂ ^c (%)	Ritz ₁ (N/mm)	Ritz ₁ ^t (N/mm)	error ₁ ^c (%)	Ritz ₂ (N/mm)	Ritz ₂ ^t (N/mm)	error ₂ ^c (%)
2	4.934	4.941	0.144	5.621	5.635	0.241	9.022	9.032	0.111	8.772	8.797	0.284
4	4.569	4.578	0.181	4.471	4.510	0.877	7.718	7.727	0.114	7.913	7.919	0.076
6	4.367	4.377	0.210	4.243	4.260	0.412	7.354	7.359	0.068	7.103	7.028	-1.064
8	4.332	4.341	0.210	4.167	4.176	0.228	7.255	7.261	0.086	6.983	6.894	-1.283
10	4.271	4.280	0.216	4.136	4.145	0.210	7.170	7.177	0.106	6.953	6.862	-1.307
12	4.255	4.264	0.213	4.117	4.127	0.224	7.127	7.135	0.107	6.939	6.848	-1.308

^t prediction after truncating the negligible parameters

^c error of the prediction due to the truncation

Table 6.13: Buckling load of Layup 10 after truncating the negligible parameters

P=Q	Plate						Shell					
	Ritz ₁ (N/mm)	Ritz ₁ (N/mm)	error ₁ (%)	Ritz ₂ (N/mm)	Ritz ₂ (N/mm)	error ₂ (%)	Ritz ₁ (N/mm)	Ritz ₁ (N/mm)	error ₁ (%)	Ritz ₂ (N/mm)	Ritz ₂ (N/mm)	error ₂ (%)
2	90.739	90.730	-0.010	100.267	100.262	-0.005	110.115	110.105	-0.010	116.501	116.495	-0.005
4	88.066	88.060	-0.006	87.437	87.428	-0.010	106.901	106.895	-0.006	105.546	105.535	-0.010
6	87.470	87.462	-0.010	86.472	86.462	-0.011	106.330	106.321	-0.008	104.312	104.299	-0.012
8	87.043	87.033	-0.011	86.199	86.190	-0.011	105.871	105.861	-0.009	104.168	104.155	-0.013
10	86.851	86.842	-0.011	86.062	86.053	-0.011	105.675	105.666	-0.009	104.078	104.065	-0.012
12	86.673	86.663	-0.012	85.977	85.967	-0.011	105.491	105.481	-0.009	104.019	104.005	-0.013

Due to the stiffness discontinuity, the prediction of buckling loads of panels with layup 2 and 10 are converged slower than these with constant stiffness (layup 8 and 9). Similar observations had been discussed in section 6.2.1, where the panels' bending-twisting coupling s are zero. Since the problems are from the stiffness discontinuity, it is of great interests to show that the problems will be solved if the stiffness is continuous. An example of continuous stiffness is the panels with constant stiffness, where the predictions are converged very fast. Another examples can be the panels with variable stiffness where the fibers are curved. However, due to the difficulty in modeling the panels (especially for shells) with variable stiffness in Abaqus, these examples are reduced to which have more sections but less difference of stiffness in the neighboring sections.

Therefore another two layups have been investigated, which are layup 3 (Figure 5.9) and layup 11 (Figure 6.18). As shown in Figure 5.10 in previous chapter, the prediction of in-plane loads have been improved by reducing the stiffness discontinuity for the same reason. The predictions of the buckling loads are also improved for these two layups compared to other layups (layup 1, 2, 7 10), as shown in Table 6.14 and 6.15 . The predictions converge to FEM substantially faster than layups 2 and 10 (and also layup 1 and 7). For polynomial functions, the errors reduce to be less than 1 % after a few terms. However, for sine functions the errors are slightly bigger than polynomial function since the polynomial functions are better in prediction when bending-twisting couplings are not zero. The first buckling modes of these two layups are also compared to FEM in Figure 6.19 and 6.20, all of which coincide with FEM very well. Therefore, one can expect if the stiffness of the panels are continuous the prediction obtained from Ritz method will converge to the FEM much faster than these examples.

1	2	3	4
2	3	4	5
3	4	5	6
4	5	6	7

- Layup 11
- Section 4: [15]₄
 - Section 1: [0]₄
 - Section 2: [5]₄
 - Section 3: [10]₄
 - Section 5: [20]₄
 - Section 6: [25]₄
 - Section 7: [30]₄

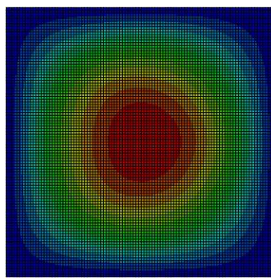
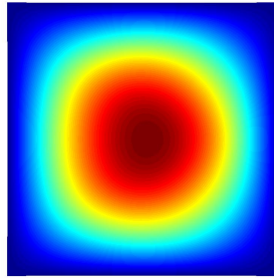
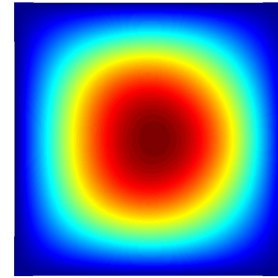
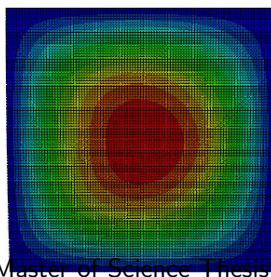
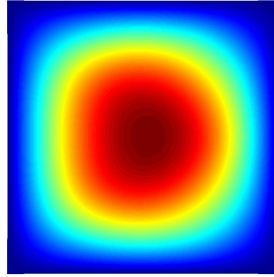
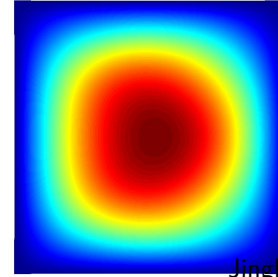
Figure 6.18: Layup 11

Table 6.14: Buckling Load of Layup 3

P=Q (K=L=18) (K ₁ =L ₁ =18)	Plate					Shell				
	Ritz ₁	Ritz ₂	FEM	error ₁	error ₂	Ritz ₁	Ritz ₂	FEM	error ₁	error ₂
	(N/mm)	(N/mm)	(N/mm)	(%)	(%)	(N/mm)	(N/mm)	(N/mm)	(%)	(%)
2	2.874	3.399	2.821	1.893	20.488	5.354	5.477	5.088	5.227	7.635
4	2.850	2.855	2.821	1.015	1.216	5.243	5.205	5.088	3.033	2.297
6	2.840	2.843	2.821	0.666	0.786	5.230	5.159	5.088	2.786	1.388
8	2.838	2.836	2.821	0.610	0.548	5.228	5.150	5.088	2.751	1.219
10	2.838	2.834	2.821	0.592	0.474	5.228	5.148	5.088	2.743	1.176
12	2.836	2.834	2.821	0.546	0.447	5.227	5.147	5.088	2.717	1.163

Table 6.15: Buckling Load of Layup 11

P=Q (K=L=18) (K ₁ =L ₁ =18)	Plate					Shell				
	Ritz ₁	Ritz ₂	FEM	error ₁	error ₂	Ritz ₁	Ritz ₂	FEM	error ₁	error ₂
	(N/mm)	(N/mm)	(N/mm)	(%)	(%)	(N/mm)	(N/mm)	(N/mm)	(%)	(%)
2	2.780	3.216	2.522	10.237	27.517	5.187	5.238	4.854	6.847	7.909
4	2.657	2.566	2.522	5.342	1.741	5.055	4.893	4.854	4.139	0.797
6	2.617	2.547	2.522	3.777	1.014	5.011	4.855	4.854	3.222	0.010
8	2.597	2.545	2.522	2.988	0.902	4.987	4.851	4.854	2.739	-0.069
10	2.587	2.543	2.522	2.570	0.827	4.975	4.849	4.854	2.485	-0.114
12	2.579	2.541	2.522	2.260	0.760	4.966	4.847	4.854	2.304	-0.156

**(a)** Plate (FEM)**(b)** Plate (Ritz₁)**(c)** Plate (Ritz₂)**(d)** Shell (FEM)**(e)** Shell (Ritz₁)**(f)** Shell (Ritz₂)

Master of Science Thesis

Jinghua Tang

Figure 6.19: First Buckling Mode of Layup 3

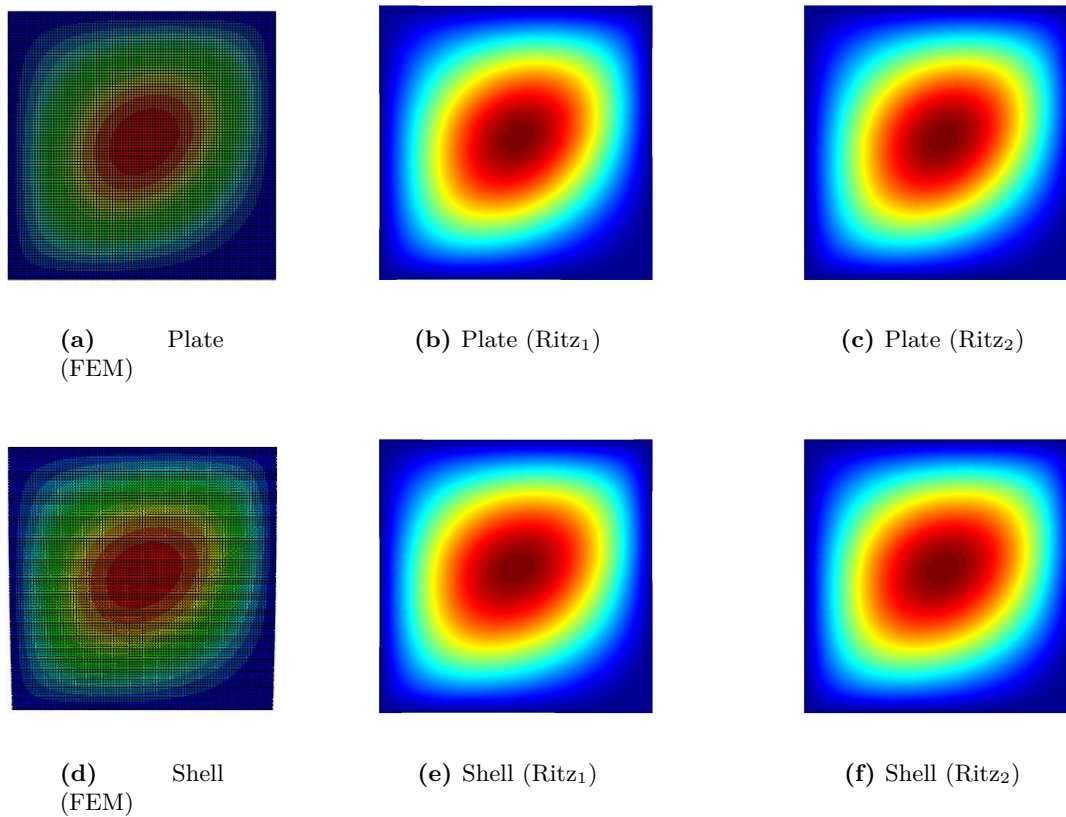


Figure 6.20: First Buckling Mode of Layup 11

6.2.3 Buckling of Shallow Cylindrical Shells with Variable Curvature

In the previous sections, the curvature of the shells were set as a constant. In this section, the shells with variable curvature are investigated. Ideally, the buckling load of shells with any variable curvature can be predicted by the Ritz method. So the shell with the same curvature as NACA00112 is of most interests in current thesis. However, due to the difficulty in building the FEM model with variable curvature and variable stiffness in Abaqus, the variable curvature is modeled as a combination of two different curvatures, as shown in Figure 6.21.

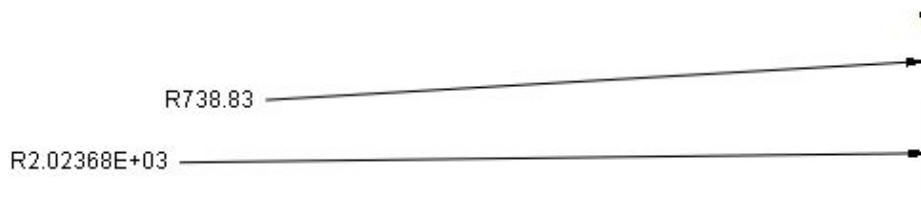


Figure 6.21: Shell with two different radii

The radius $R = 738.83\text{mm}$ is obtained from the smallest radius of NACA 0012 at $x/c = 0.3$, as shown in Figure 6.2b; the radius $R = 2023.68\text{mm}$ is obtained from the biggest radius of

NACA 0012 at $x/c = 0.6$. This is an extreme example to show the Ritz method can predict the buckling load of shells with variable curvatures similar to NACA 0012.

For simplicity, the beam characteristic function and the sine function have been applied here to approximate the in-plane loads and the out-of-plane displacement, respectively. The shells with constant stiffness (layup 4) and variable stiffness (layup 1, 3) are investigated in this section as examples. The polynomial functions can also be applied here. But they only have advantages when the bending-twisting couplings are not zero, so it is not necessary to repeat the same works.

It is seen from Table 6.16 that the predictions for all three layups are good enough. For layup 4 where the stiffness is constant, the predictions converge to FEM fastest. While the predictions for layup 1 with four sections converge to FEM slowest due to the biggest differences of stiffness existing in neighboring sections. Once the differences of stiffness are reduced, such as layup 3, the predictions converge to FEM much faster. The first buckling modes of all three layups are compared to FEM in Figure 6.22, all of which coincide with FEM very well.

Table 6.16: Buckling load of shells with variable curvatures

Layup	1*			3†			4‡		
	Ritz ₁	FEM	error ₁	Ritz ₁	FEM	error ₁	Ritz ₁	FEM	error ₁
P=Q (K=L=18) (K ₁ =L ₁ =18)	(N/mm)(N/mm)(%)			(N/mm)(N/mm)(%)			(N/mm)(N/mm)(%)		
2	3.564	3.234	10.211	3.552	3.487	1.874	2.775	2.738	1.371
4	3.486	3.234	7.783	3.520	3.487	0.961	2.738	2.738	0.034
6	3.433	3.234	6.148	3.510	3.487	0.678	2.728	2.738	-0.334
8	3.390	3.234	4.806	3.509	3.487	0.635	2.725	2.738	-0.443
10	3.361	3.234	3.923	3.508	3.487	0.622	2.724	2.738	-0.480
12	3.339	3.234	3.239	3.507	3.487	0.584	2.724	2.738	-0.495

* 4 sections with variable stiffness

† 16 sections with variable stiffness

‡ 1 section with constant stiffness

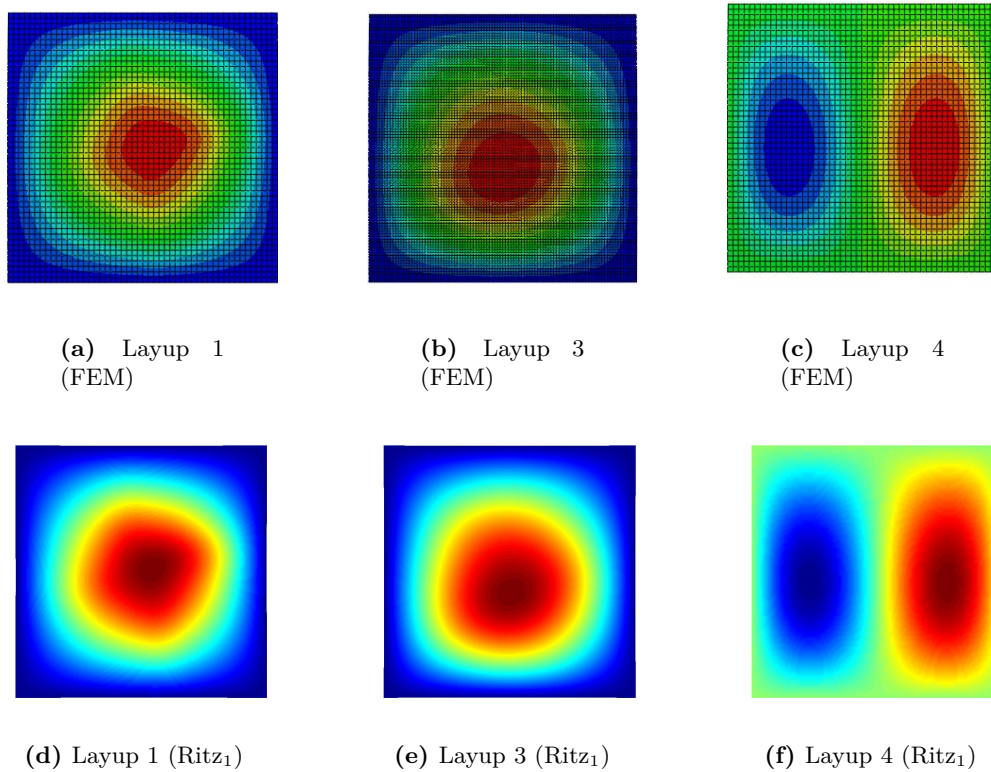


Figure 6.22: First buckling mode of shells with variable curvature

6.3 Stability Analysis: prescribed shear

In the previous sections, the panel under constant compression load \bar{N}_x were investigated. In this section the panels under shear load are discussed.

The layup investigated are layup 1 (Figure 5.2) , 2 (Figure 5.7) and 3 (Figure 5.9). The shape functions used for both Airy stress function and out-of-plane displacement are polynomial functions.

First, a pure shear is applied to the four edges of panels under simply-support boundary conditions. Then, a combined load with shear and compression, where the compression is only applied on the edges of $x = 0, a$, is applied to panels under the same boundary condition. The prediction of the in-plane loads under the two load cases are already shown in section 5.3 of previous chapter.

6.3.1 Pure Shear

In this section, only shear load is applied to the panel. The predicted buckling loads for these three layups are shown in Table 6.17 and 6.18. The convergence behavior of the predictions for the panels with first two layups is similar to what observed in panels with the same layup under compression. The convergences are not fast because the stiffness discontinuity of these

two layups is very large where the stiffness of their four sections are different from each other. The predictions for last layup are much better due to the reduced stiffness discontinuity where the stiffness of its sixteen sections increase slowly. The corresponding buckling modes are shown in Figure 6.23 and 6.24, all of which coincide with the buckling modes obtained from FEM.

Table 6.17: Buckling load of plates under shear

Layup	1*			2†			3‡		
	Ritz ₂	FEM	error ₂	Ritz ₂	FEM	error ₂	Ritz ₂	FEM	error ₂
P=Q (K=L=18) (K ₁ =L ₁ =18)	(N/mm)(N/mm)(%)			(N/mm)(N/mm)(%)			(N/mm)(N/mm)(%)		
2	10.088	5.363	88.085	12.431	5.733	116.838	10.415	5.555	87.488
4	6.365	5.363	18.677	7.398	5.733	29.054	6.243	5.555	12.375
6	5.933	5.363	10.622	6.632	5.733	15.693	5.619	5.555	1.143
8	5.856	5.363	9.185	6.207	5.733	8.266	5.599	5.555	0.782
10	5.791	5.363	7.978	6.058	5.733	5.667	5.587	5.555	0.583
12	5.741	5.363	7.045	5.994	5.733	4.564	5.582	5.555	0.488

Table 6.18: Buckling load of shells under shear

Layup	1*			2†			3‡		
	Ritz ₂	FEM	error ₂	Ritz ₂	FEM	error ₂	Ritz ₂	FEM	error ₂
P=Q (K=L=18) (K ₁ =L ₁ =18)	(N/mm)(N/mm)(%)			(N/mm)(N/mm)(%)			(N/mm)(N/mm)(%)		
2	14.544	8.037	80.962	16.131	7.987	101.956	13.520	6.184	118.617
4	9.397	8.037	16.919	10.497	7.987	31.417	6.990	6.184	13.030
6	8.603	8.037	7.039	9.320	7.987	16.682	6.250	6.184	1.055
8	8.510	8.037	5.877	8.650	7.987	8.298	6.225	6.184	0.650
10	8.433	8.037	4.917	8.399	7.987	5.150	6.212	6.184	0.450
12	8.377	8.037	4.224	8.287	7.987	3.754	6.206	6.184	0.356

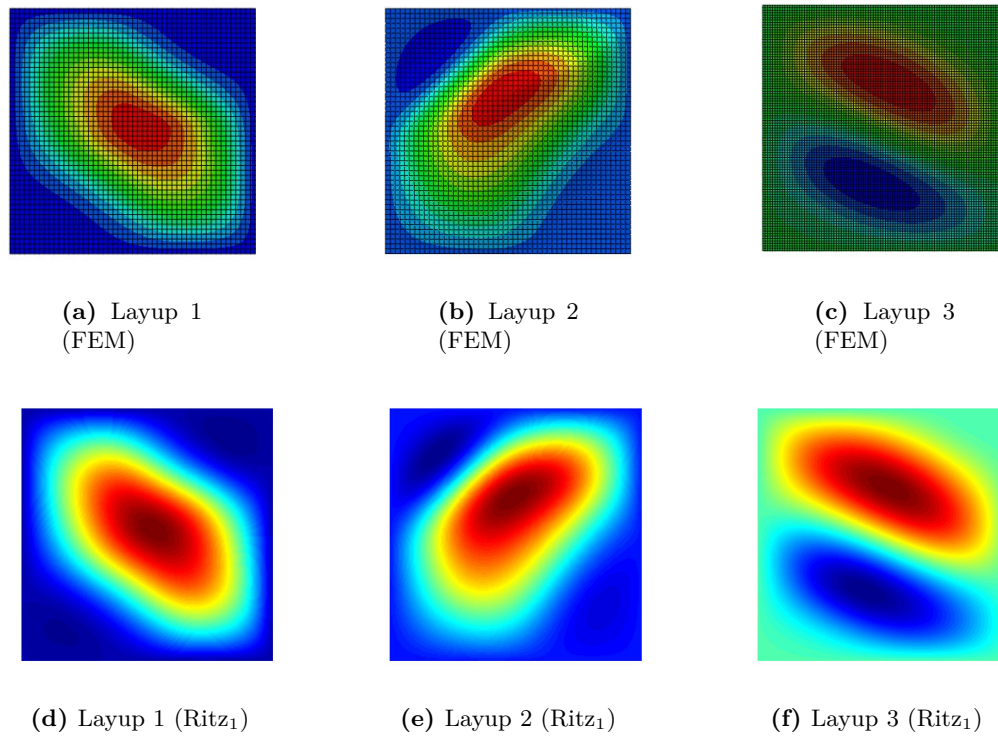


Figure 6.23: First buckling mode of plates under shear

6.3.2 Shear and Compression

In this section, the stability of panels under combined compression and shear is discussed. The examples with the same layups as previous section are shown. The ratio of compression load and shear is set to be

$$\frac{\bar{N}_x}{\bar{N}_{xy}} = -1 \quad (6.57)$$

The ratio affects the buckling load and has been selected to be 1 in this case. Because the purpose of this section is just to prove the effectiveness of the Ritz method and selected shape functions, not to study the topic of shear buckling in deep.

The predicted in-plane loads are shown in Table 6.19 and 6.20 for plates and shells, respectively. For predictions of both plate and shell with layup 3 are converged fastest due to the reduced stiffness discontinuity of layup 3. The corresponding buckling modes are shown in Figure 6.25 and 6.26.

Clearly, the predictions are still good. Especially when the stiffness discontinuity is reduced

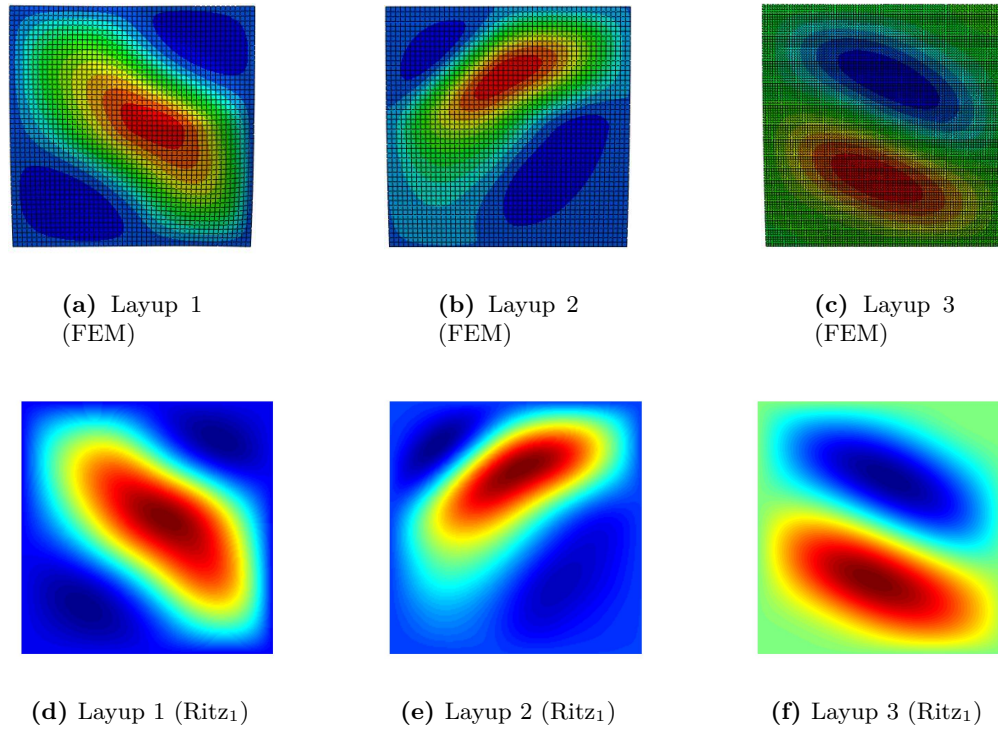


Figure 6.24: First buckling mode of shells under shear

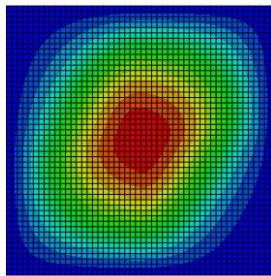
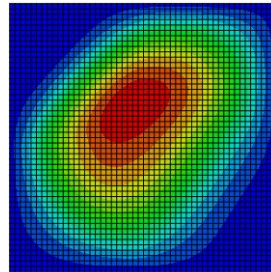
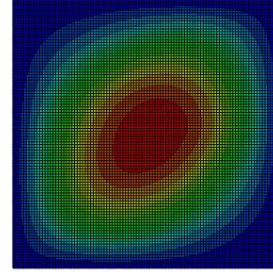
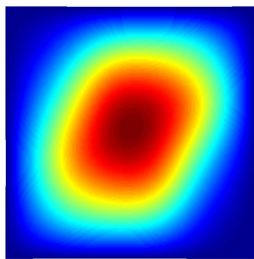
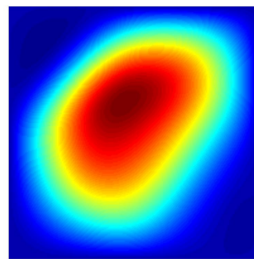
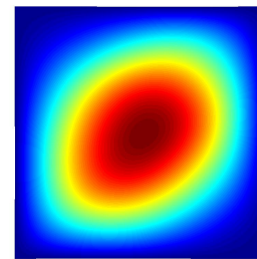
the predictions converge in a few terms.

Table 6.19: Buckling load of plates under shear and compression

Layup	1*			2†			3‡		
	Ritz ₂	FEM	error ₂	Ritz ₂	FEM	error ₂	Ritz ₂	FEM	error ₂
P=Q (K=L=18) (K ₁ =L ₁ =18)	(N/mm)(N/mm)(%)			(N/mm)(N/mm)(%)			(N/mm)(N/mm)(%)		
2	2.768	1.892	46.313	4.687	2.820	66.216	3.038	2.400	26.583
4	2.193	1.892	15.940	3.329	2.820	18.056	2.437	2.400	1.546
6	2.127	1.892	12.449	3.085	2.820	9.417	2.420	2.400	0.861
8	2.093	1.892	10.634	2.980	2.820	5.665	2.414	2.400	0.575
10	2.064	1.892	9.093	2.939	2.820	4.231	2.412	2.400	0.495
12	2.041	1.892	7.870	2.919	2.820	3.532	2.411	2.400	0.464

Table 6.20: Buckling load of shells under shear and compression

Layup	1*			2†			3‡		
	Ritz ₂	FEM	error ₂	Ritz ₂	FEM	error ₂	Ritz ₂	FEM	error ₂
P=Q (K=L=18) (K ₁ =L ₁ =18)	(N/mm)(N/mm)(%)			(N/mm)(N/mm)(%)			(N/mm)(N/mm)(%)		
2	4.928	4.089	20.517	6.501	4.502	44.387	4.590	3.810	20.475
4	4.292	4.089	4.973	5.271	4.502	17.082	3.955	3.810	3.812
6	4.228	4.089	3.392	4.971	4.502	10.412	3.868	3.810	1.525
8	4.198	4.089	2.667	4.828	4.502	7.247	3.860	3.810	1.305
10	4.173	4.089	2.050	4.777	4.502	6.110	3.856	3.810	1.205
12	4.154	4.089	1.587	4.756	4.502	5.628	3.854	3.810	1.160

(a) Layup 1
(FEM)(b) Layup 2
(FEM)(c) Layup 3
(FEM)(d) Layup 1 (Ritz₁)(e) Layup 2 (Ritz₁)(f) Layup 3 (Ritz₁)**Figure 6.25:** First buckling mode of plates under shear and compression

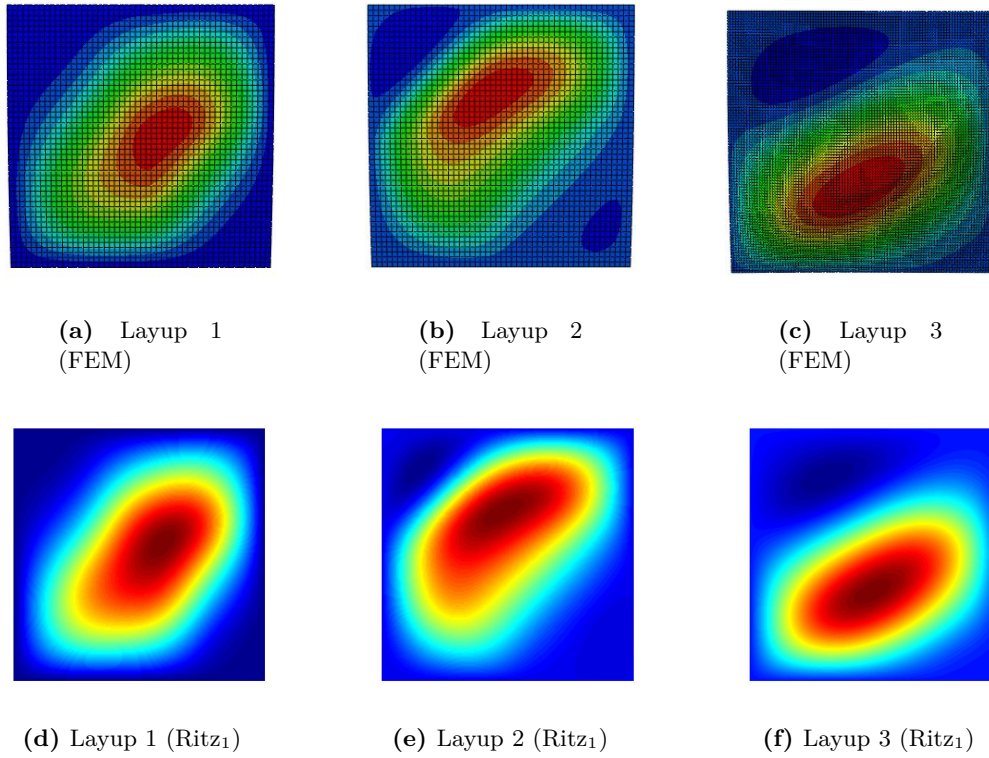


Figure 6.26: First buckling mode of shells under shear and compression

6.4 Stability Analysis: prescribed displacement

In this section, the stability of plates and shallow cylindrical shells under prescribed displacement are investigated using Ritz method and verified with Abaqus. The polynomial functions are used for the approximations of Airy stress function (F) and its variation (δF) and the out-of-plane displacement (δw).

The panel is assumed to be subjected to uniform end-shortenings (Δu_1 and Δu_2) on both sides ($x = 0, a$). The boundary condition is simply-supported at all the edges. The essential boundary condition can be satisfied by the shape function of out-of-plane displacement (δw). However, natural boundary conditions cannot be satisfied since the polynomial functions are used.

To determine buckling initiation, buckling factor λ can be introduced as

$$\Delta u_1^{critical} = \lambda \Delta u_1 \quad (6.58)$$

$$\Delta u_2^{critical} = \lambda \Delta u_2 \quad (6.59)$$

Then the Airy stress function at the critical point can be assumed as (same as equation 4.112)

$$F(x, y) = \lambda \left[\sum_e^E F_e \int \int Y_e(y) dy dy + \sum_{kl}^{KL} F_{kl} X_k(x) Y_l(y) \right] \quad (6.60)$$

So in this section the buckling factor is used instead of buckling load, as a factor of determining the buckling initiation.

6.4.1 Verification

Panels with two kinds of layups are considered in the verification. The first kind of layups are the ones with constant stiffness. The second kind of layups are the ones with variable stiffness. The panels with the second kind of layups are assumed to have four or sixteen sections, as shown in Figure 3.3. The reason for considering the panels with constant stiffness layups is to show Ritz method and the selected shape functions can exactly predict the buckling load of panels with constant stiffness. In both kinds of layups, the bending-twisting couplings can be either zero or non-zero.

Constant Stiffness

The layups considered in this section are layup 4, 8 and 9. Since the in-plane loads distributions are uniform, the prebuckling analysis is not necessary. The variation of Airy stress function (δF) is approximated by 18 terms in both x and y direction to achieve convergent predictions. Table 6.21 and 6.22 show the predicted buckling load compared to FEM, respectively, as increasing the number of terms used for the approximation of δw in x and y direction. The predictions obtained from FEM are placed in the tables as columns with constant values since they are independent of P and Q .

Table 6.21: Buckling factors of plates with constant stiffness (prescribed displacement)

Layup	4*			8 [†]			9 [‡]		
	Ritz ₂	FEM	error ₂ (%)	Ritz ₂	FEM	error ₂ (%)	Ritz ₂	FEM	error ₂ (%)
P=Q (K ₁ =L ₁ =18)									
2	15.905	12.492	27.323	22.213	14.009	58.565	4.863	3.850	26.308
4	12.580	12.492	0.706	15.222	14.009	8.661	3.903	3.850	1.389
6	12.546	12.492	0.430	14.727	14.009	5.123	3.882	3.850	0.838
8	12.546	12.492	0.429	14.581	14.009	4.087	3.878	3.850	0.736
10	12.546	12.492	0.429	14.501	14.009	3.515	3.877	3.850	0.690
12	12.546	12.492	0.429	14.452	14.009	3.162	3.876	3.850	0.666

Table 6.22: Buckling factors of shells with constant stiffness (prescribed displacement)

Layup	4*			8 [†]			9 [‡]		
	Ritz ₂	FEM	error ₂ (%)	Ritz ₂	FEM	error ₂ (%)	Ritz ₂	FEM	error ₂ (%)
P=Q (K ₁ =L ₁ =18)									
2	43.215	40.809	5.896	41.599	32.672	27.324	8.318	7.781	6.896
4	42.286	40.809	3.620	38.225	32.672	16.996	7.851	7.781	0.900
6	40.988	40.809	0.438	33.353	32.672	2.085	7.789	7.781	0.102
8	40.567	40.809	-0.594	33.081	32.672	1.253	7.785	7.781	0.043
10	40.564	40.809	-0.599	32.991	32.672	0.975	7.783	7.781	0.017
12	40.564	40.809	-0.600	32.937	32.672	0.811	7.782	7.781	0.004

* Layup 4: [90 90 90 90]

† Layup 8: [45 45 45 45]

‡ Layup 9: [15 15 15 15]

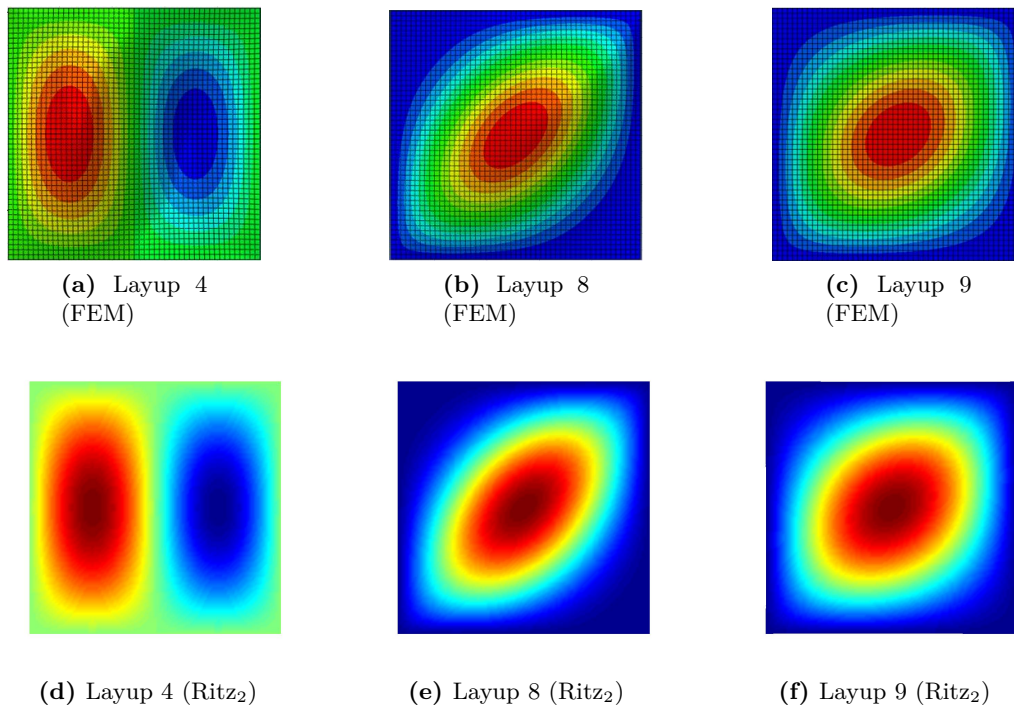


Figure 6.27: First buckling mode of plates with constant stiffness (prescribed displacement)

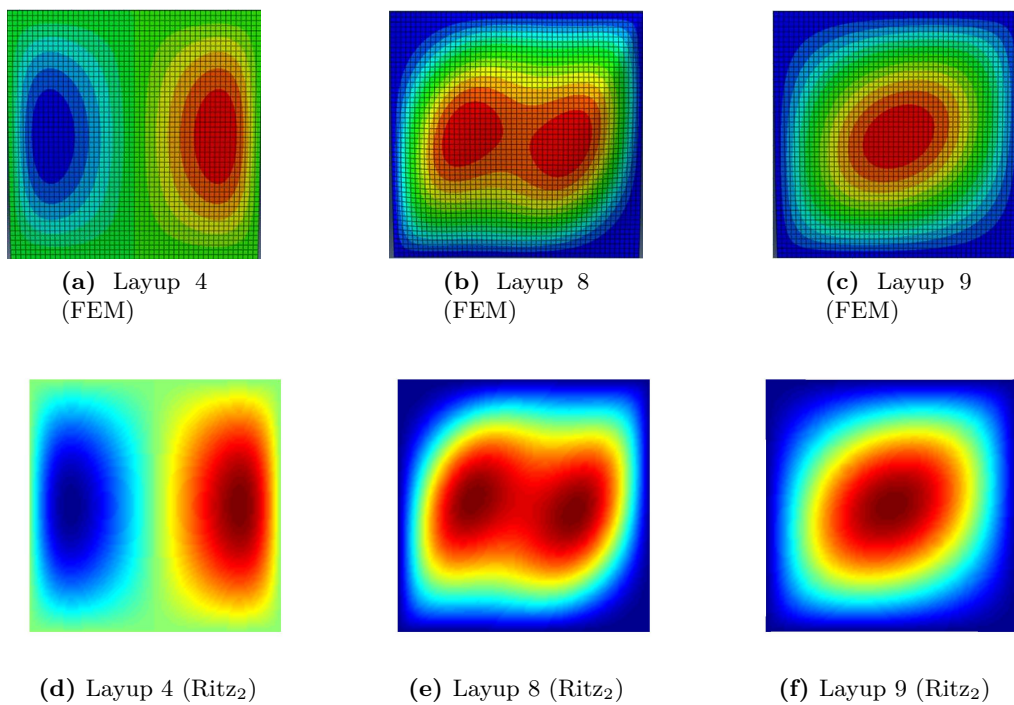


Figure 6.28: First buckling mode of shells with constant stiffness (prescribed displacement)

It is seen from Table 6.21 and 6.22 that the predictions for all three layups are good enough.

As reducing the bending-twisting couplings (in the order of layup 8, layup 9 and layup 4), the predictions for both plates and shells are increasingly better. However, it is noted that the predictions for the shell with layup 4 converge to be lower than FEM, similar to what observed in Table 6.1. The reason is the same that the δF , which is coupled with δw , makes the predictions converge to the exact value from a lower value. The first buckling modes of all three layups are compared to FEM in Figure 6.27 and 6.28, all of which coincide with FEM very well.

Variable stiffness

In this section, the stability of panels with variable stiffness is considered. The layups considered here are layup 1 (Figure 5.2), layup 2 (Figure 5.7), layup 3 (Figure 5.9) and layup 11 (Figure 6.18). Among these layups only the the bending-twisting couplings of layup 1 are zero.

Since the stiffness is variable for these layups, the in-plane loads have to be predicted before the stability analysis, which are shown in section 5.4.3, where the Airy stress function (F) is approximated by 18 terms in both x and y direction. In stability analysis, the variation of Airy stress function (δF) is also approximated by 18 terms in both x and y direction to achieve convergent predictions. Table 6.23 and 6.24 show the predicted buckling load of plates and shells with these layups compared to FEM, respectively, as increasing the number of terms used for the approximation of δw in x and y direction. The first buckling modes of the plate and shell predicted by FEM and Ritz methods are compared in Figure 6.29 and 6.30.

The tables show that for panels with small stiffness discontinuity, the predictions are close to FEM, such as the panels with layup 3 and 11. When the stiffness discontinuity increases, the prediction of plate with layup 1 has 13.49 % difference compared to FEM even 12 terms are used in both x and y direction. It is similar to what observed in Table 6.4 for the same plate under prescribed compression, where the difference is 10.899% when the same number of terms were used. However, the buckling modes predicted by Ritz method are similar FEM.

As long as enough terms are used, the predictions will converge to the exact values.

Table 6.23: Buckling factors of plates with variable stiffness (prescribed displacement)

Layup	1			2			3			11		
	Ritz ₂	FEM	error ₂	Ritz ₂	FEM	error ₂	Ritz ₂	FEM	error ₂	Ritz ₂	FEM	error ₂
P=Q (K=L=18) (K ₁ =L ₁ =18)			(%)			(%)			(%)			(%)
2	4.361	3.028	43.998	20.352	14.014	45.228	2.229	1.844	20.859	4.605	3.645	26.351
4	3.631	3.028	19.909	16.269	14.014	16.092	1.870	1.844	1.402	3.718	3.645	1.997
6	3.569	3.028	17.858	15.115	14.014	7.857	1.862	1.844	0.994	3.696	3.645	1.391
8	3.515	3.028	16.088	14.792	14.014	5.553	1.858	1.844	0.762	3.691	3.645	1.270
10	3.472	3.028	14.642	14.688	14.014	4.812	1.857	1.844	0.688	3.688	3.645	1.190
12	3.437	3.028	13.490	14.631	14.014	4.401	1.856	1.844	0.659	3.686	3.645	1.124

Table 6.24: Buckling factors of shells with variable stiffness (prescribed displacement)

Layup	1			2			3			11		
	Ritz ₂	FEM	error ₂	Ritz ₂	FEM	error ₂	Ritz ₂	FEM	error ₂	Ritz ₂	FEM	error ₂
P=Q (K=L=18) (K ₁ =L ₁ =18)			(%)			(%)			(%)			(%)
2	9.249	7.591	21.848	36.182	25.977	39.286	3.687	3.452	6.800	7.780	7.176	8.418
4	8.115	7.591	6.912	30.785	25.977	18.507	3.512	3.452	1.744	7.275	7.176	1.382
6	7.956	7.591	4.808	26.153	25.977	0.678	3.482	3.452	0.863	7.188	7.176	0.169
8	7.899	7.591	4.054	25.434	25.977	-2.089	3.476	3.452	0.700	7.180	7.176	0.049
10	7.873	7.591	3.711	25.235	25.977	-2.857	3.475	3.452	0.656	7.176	7.176	-0.007
12	7.857	7.591	3.508	25.146	25.977	-3.198	3.474	3.452	0.641	7.173	7.176	-0.048

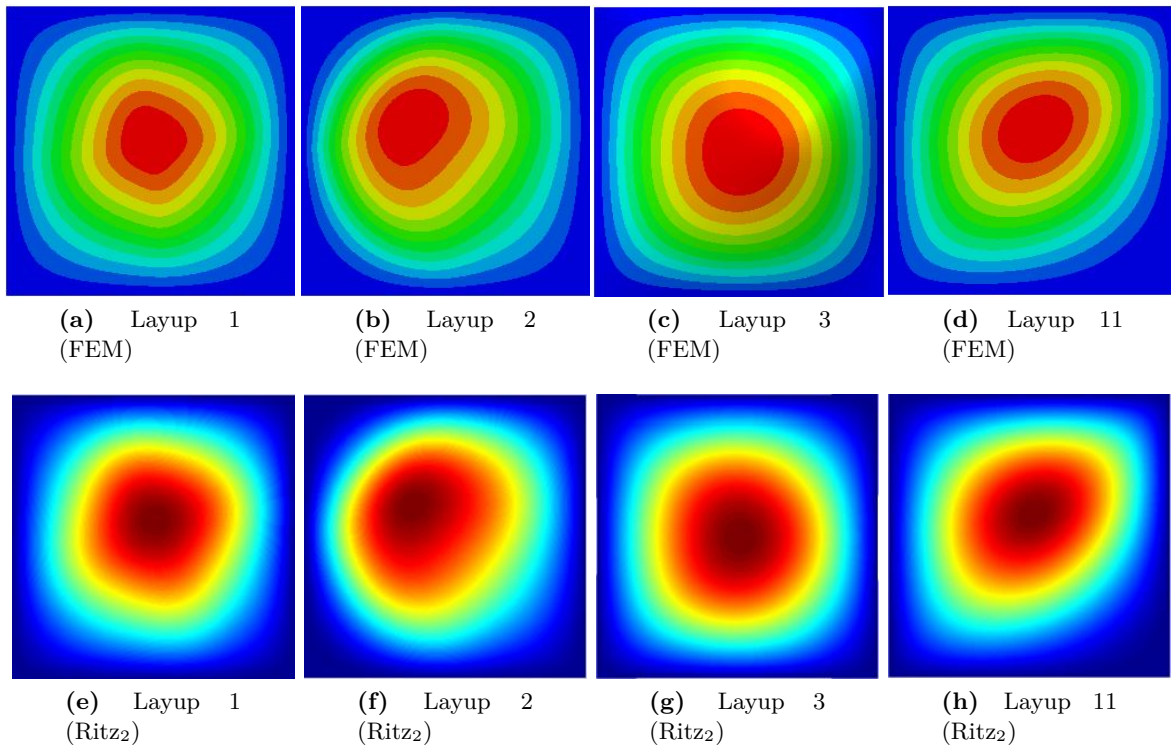


Figure 6.29: First buckling mode of plates with variable stiffness (prescribed displacement)

6.5 Summary

In this chapter, the buckling loads of panels under prescribed loads (compression and shear) and under prescribed end-shortenings are investigated using Ritz method.

In general, the convergences of predictions become faster when the stiffness discontinuity of the panel is reduced. For plates with constant stiffness and zero bending-twisting couplings (layup 4, 5, 6), the predictions, using sine function as the shape function of out-of-plane displacement, converge to the exact buckling load when the number of terms used in x and y direction reach the exact number of half waves of the buckling mode in x and y direction. Because for such plates the buckling modes can be analytically described by half waves of sine function in x and y direction. (For simply-support shallow cylindrical shell panel, the buckling modes cannot which is different from a complete cylindrical shell.) For panels with variable stiffness but reduced stiffness discontinuity (layup 3, 11), the prediction converged to exact value slightly slower. Because the buckling mode of these layups cannot be analytically described by a single shape function (such as sine function) in x and y direction. So more number of terms of shape functions are required to achieve a converged prediction. For panels with large stiffness discontinuity (layup 2, 7, 10), a large number of terms of shape functions are needed. So the convergence of the predictions of these layups are slowest. However, these layups are used as extreme examples, which are unlikely to be encountered in practice.

When the bending-twisting couplings are not zero, it is found that the exact buckling load

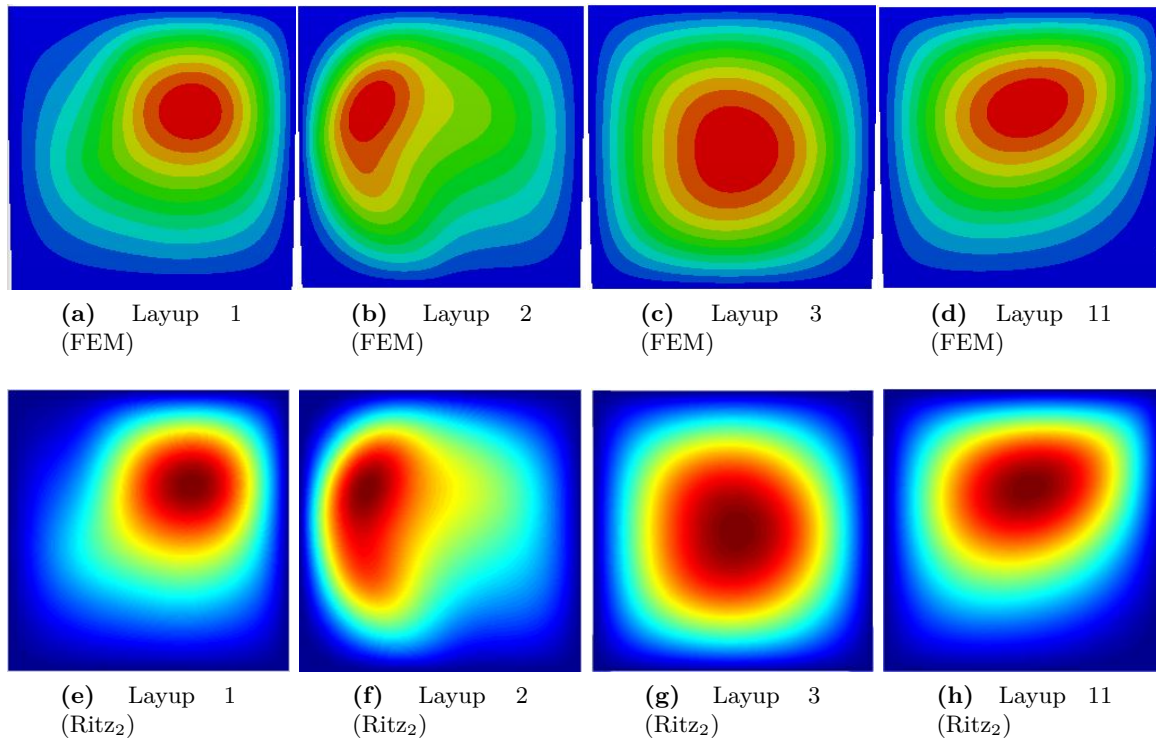


Figure 6.30: First buckling mode of shells with variable stiffness (prescribed displacement)

cannot be obtained in finite number of terms even when the stiffness is constant. The reason is that the natural boundary conditions cannot be exactly satisfied. However, by comparison, the polynomial functions have greater advantages than sine functions in the convergence of prediction due to their better capability to capture the localized features, such as strong gradients in the buckling mode shape [32].

Shallow cylindrical shells with variable curvature are also discussed. The prediction shows the Ritz method can be applied to predict the buckling load of such panels.

Conclusion and Recommendation

7.1 Thesis Review and Conclusion

The main goal of the thesis was to build a semi-analytical model for solving the buckling problem of variable stiffness composite panels (plates and shallow cylindrical shells). A literature review was conducted in the beginning of the thesis and summarized in Chapter 2. Then two semi-analytical models were built for solving the problem.

The first model based on solving the governing differential equations using Galerkin method was presented in Chapter 3. The differential equations governing the membrane and buckling behaviours of variable stiffness composite panels were derived and compared to the available equations in existing literature. Due to the complexity of these equations, the closed form solution is not possible. Thus, the Galerkin method was applied to obtain an approximate solution. In principle, this is a suitable solution to the panels with continuous stiffness that can be exactly described by a continuous function. However, for simplicity, the stiffness variation considered in the thesis was reduced to sections of constant stiffness. Consequently, a continuous approximation of stiffness variation across the panel using a series expansion had to be employed in the Galerkin method, which reduced its efficiency and accuracy with respect to the Ritz method.

The second model, based on the Ritz method and the variational statement of total energy functionals that are equivalent to the governing differential equations derived in Chapter 3, was presented in Chapter 4. The advantage of this approach in comparison to the Galerkin method is that no series approximation to the stiffness variation is required which proved to be more efficient and more accurate than the Galerkin method. The detailed derivations of the energy functional which had been rarely shown in literature were presented as well.

The accuracy of the model based on the Ritz method was investigated in Chapter 5 and 6. In-plane loads distributions resulting from either prescribed loads or prescribed displacements in the prebuckling state were solved and compared to FEM in Chapter 4. Moreover the effect of the selected shape function on the quality of the solution was examined. In general, the predictions of in-plane loads are satisfactory, compared to the prediction of FEM. However,

the stiffness discontinuity existing in the example layups led to the peak stresses and stress discontinuities over the boundaries of neighbouring sections which can only be captured using large number of terms in Ritz method. However, if the stiffness is continuous or at least the discontinuity is reduced, the predictions are significantly improved. Similar observations were noticed in the buckling loads prediction in Chapter 6. As the stiffness discontinuity was reduced, the convergence of the predicted buckling loads was significantly increased.

Furthermore the effect of the bending-twisting couplings of the composite layups on the buckling load prediction was also investigated. It was found out that compared to the sine function the polynomial function proved to be more efficient in predicting the buckling loads of the panels with large bending-twisting couplings. This was attributed to their capability to better capture the localized features, such as strong gradients in the buckling mode shape.

Various load cases were applied to the panels which can be divided into the case of prescribed loads, including compression and shear, and the case of prescribed displacements (end-shortenings). The model based on the Ritz method proved to be capable of predicting both in-plane loads and buckling loads of the panels (plates and shallow cylindrical shells) under either of the two load cases. Moreover, the shallow cylindrical shell with variable curvatures were also investigated, where the Ritz method again proved to be able to predict the buckling loads very well as long as the pertinent assumptions concerning the shallow shells are obeyed.

Based on the work presented in the thesis, the research questions proposed in Chapter 1 are answered as follows:

- Closed form solution is neither available in literature nor obtained in the thesis due to two main reasons. The first one is the existence of bending-twisting couplings; the second one is the variation of stiffness.
- Two semi-analytical models have been developed based on Galerkin method and Ritz method. Both methods are able to solve the buckling problems of variable-stiffness composite panels. However, the Ritz method is more efficient and accurate in solving the buckling problems of the panels with discontinuous stiffness considered in this thesis.

7.2 Recommendation

Considering the problems encountered in the thesis, the following recommendations and improvements are proposed:

- Avoiding the stiffness discontinuity. In practice, the variable stiffness of the composite panel is achieved by steering the fibre directions. This way, the stiffness is a function of the fiber orientations which is continues over the panel. The predictions of in-plane loads and buckling loads are expected to be significantly improved compared to these investigated in the thesis.
- Using sine function with the Lagrange multiplier method as the shape function of the Airy stress function (and its variation) proved to be most efficient in predicting both the in-plane loads and buckling loads among all the shape functions investigated in the

thesis. The predictions of the buckling loads using sine function with the Lagrange multiplier method appear to be more conservative than FEM, which, however, needs further investigation in future and thus was not shown in current thesis. The cosine function, which is better than sine function in predicting the in-plane loads, is also expected to better predict the buckling loads. This is also suggested to do in further. The reason to consider these two shape functions is the possibility to dramatically increase the efficiency of the semi-analytical model.

- The criterion used to truncate the negligible parameters of Airy stress function should be further studied since the formula used in the thesis is just an example. In addition, it was noted that the in-plane loads distribution might have little effect on the prediction of buckling load for some layups (layup 3 and 11), which, however, was not presented in the thesis. It seems that in these cases the buckling load primarily depends on the bending stiffness distribution. If so, the prediction of in-plane loads in the prebuckling state can be skipped and therewith significantly improving the efficiency of the model, while causing only a negligible error in the buckling load prediction. However, for post-buckling analysis the in-plane loads redistribution is always important and must be considered. It is noteworthy that the equations derived in this thesis can also be used for the future post-buckling analysis.
- Due to the bending-twisting couplings, the natural boundary conditions of simply-supported composite panels cannot be satisfied, in the past a mixed variational principles, Hellinger-Reissner variational principle, were proposed in order to overcome this problem. In this variational principles, the bending complementary energy expressed in terms of bending moments is used, instead of bending strain energy. Then bending moments can then be approximated by series, which are similar to the out-of-plane deflection. The natural (moment) boundary conditions can be satisfied through the selected shape functions for the moments. Consequently the convergence of buckling load is improved since both natural and essential boundary conditions are exactly satisfied. Therefore, it is of great interest to investigate this approach in the model.
- Buckling of stiffened panels hasn't been considered yet. Extending the existing model to stiffened variable stiffness panels would be of great interest in future.
- Previous research revealed that imperfections dramatically affect the buckling resistance of shells. Hence it would be of interest to add the imperfection analysis (for instance, analysis of geometrical imperfection) to the model.
- Introducing the Bessel function, which presents the exact eigenmode of beams with linearly varying stiffness, to the shape function of the out-of-plane displacement. In principle, if the buckling mode can be exactly presented by the shape functions the convergence is the fastest. For example, for plates with constant stiffness where bending-twisting couplings are zero, the exact buckling mode is described by a trigonometric function. The prediction converge to the exact value when the number of terms reach the number of half waves of the buckling mode. When the bending-twisting couplings are not zero, both polynomial and sine functions can not represent the exact buckling modes. However, the convergence of predictions using polynomial function is faster since the polynomial function can better capture the localized features (such as strong gradients in buckling mode shape). In the case of beams with linearly varying stiffness,

the Bessel function presents the exact eigenmode (for example buckling mode). For variable-stiffness panels, the Bessel function might also present the exact eigenmode. If not, it still might better capture the localized features than the polynomial functions used in this thesis.

Appendix A

Total Potential Energy for Prebuckling Analysis

In this section, the panel (plate and shallow cylindrical shell) is assumed prescribed by loads on boundary S_1 and displacements on boundary S_2 . The detailed descriptions of the boundary conditions are given in section 4.3.1. In this section, the total potential energy of a panel before buckling occurring will be proved to be the negative of the total complementary energy of the panel under the same boundary conditions.

As shown in section 4.3.1, the total potential energy of both plates and shells (using assumption 2) for prebuckling analysis is given as [33]

$$\Pi_{pre} = U_m + V_{S_1} \quad (\text{A.1})$$

where, Π_{pre} is the total potential energy for prebuckling analysis, V_{S_1} is the work done by the prescribed loads on boundary S_1 in stretching.

The membrane strain energy U_m is given as (equation 4.8)

$$U_m = \frac{1}{2} \int \int [(A_{11}(u,x)^2 + 2A_{12}(u,x)(v,y) + 2A_{16}(u,x)(v_x + u_y) + A_{22}(v,y)^2 + 2A_{26}(v,y)(v_x + u_y) + A_{66}(v_x + u_y)^2] dx dy \quad (\text{A.2})$$

and the external work done on the boundary S_1 is given as (equation 4.14)

$$V_{S_1} = - \int_{S_1} (\bar{N}_y v + \bar{N}_{xy} u)_{y=b} - (\bar{N}_y v + \bar{N}_{xy} u)_{y=0} dx - \int_{S_1} (\bar{N}_x u + \bar{N}_{xy} v)_{x=a} - (\bar{N}_x u + \bar{N}_{xy} v)_{x=0} dy \quad (\text{A.3})$$

For small displacements, the displacements u, v are related to the mid-plane strains through

$$\epsilon_{xo} = u_{,x}, \epsilon_{yo} = v_{,y}, \gamma_{xyo} = v_{,x} + u_{,y} \quad (\text{A.4})$$

So the membrane strain energy (equation A.2) can be written in terms of the mid-plane strains, instead of displacements, as

$$U_m = \frac{1}{2} \int \int [(A_{11}(\epsilon_{xo})^2 + 2A_{12}(\epsilon_{xo})(\epsilon_{yo}) + 2A_{16}(\epsilon_{xo})(\gamma_{xyo}) + A_{22}(\epsilon_{yo})^2 + 2A_{26}(\epsilon_{yo})(\gamma_{xyo}) + A_{66}(\gamma_{xyo})^2] dx dy \quad (\text{A.5})$$

Then the total potential energy will be

$$\begin{aligned} \Pi_{pre} = & \frac{1}{2} \int \int [(A_{11}(\epsilon_{xo})^2 + 2A_{12}(\epsilon_{xo})(\epsilon_{yo}) + 2A_{16}(\epsilon_{xo})(\gamma_{xyo}) + A_{22}(\epsilon_{yo})^2 \\ & + 2A_{26}(\epsilon_{yo})(\gamma_{xyo}) + A_{66}(\gamma_{xyo})^2] dx dy \\ & - \int_{S_1} (\bar{N}_y v + \bar{N}_{xy} u)_{y=b} - (\bar{N}_y v + \bar{N}_{xy} u)_{y=0} dx - \int_{S_1} (\bar{N}_x u + \bar{N}_{xy} v)_{x=a} - (\bar{N}_x u + \bar{N}_{xy} v)_{x=0} dy \end{aligned} \quad (\text{A.6})$$

By the introduction of mid-plane strains, the total potential energy (equation A.6) becomes a functional of mid-plane strains, instead of the displacements. However, during variation (or minimization) of the total potential energy with respect to the mid-plane strains, the strain-displacement relations defined by equation A.4 must always be hold [33]. Therefore, the Lagrange multipliers are used in order to enforce the strain-displacement relations as

$$\begin{aligned} \Pi_{pre} = & \frac{1}{2} \int \int [(A_{11}(\epsilon_{xo})^2 + 2A_{12}(\epsilon_{xo})(\epsilon_{yo}) + 2A_{16}(\epsilon_{xo})(\gamma_{xyo}) + A_{22}(\epsilon_{yo})^2 \\ & + 2A_{26}(\epsilon_{yo})(\gamma_{xyo}) + A_{66}(\gamma_{xyo})^2] \\ & - [(\epsilon_{xo} - u_{,x})\Lambda_x + (\epsilon_{yo} - v_{,y})\Lambda_y + (\gamma_{xyo} - v_{,x} - u_{,y})\Lambda_{xy}] dx dy \\ & - \int_{S_1} (\bar{N}_y v + \bar{N}_{xy} u)_{y=b} - (\bar{N}_y v + \bar{N}_{xy} u)_{y=0} dx - \int_{S_1} (\bar{N}_x u + \bar{N}_{xy} v)_{x=a} - (\bar{N}_x u + \bar{N}_{xy} v)_{x=0} dy \end{aligned} \quad (\text{A.7})$$

where, Λ_x , Λ_y and Λ_{xy} are the Lagrange multipliers.

It is noted that the second term of above equation which is related to the Lagrange multipliers is zero if the strain-displacement relations hold. So as long as the strain-displacement relations hold, the total potential energy will not change.

For convenience, the above equation can be written in matrix form as

$$\begin{aligned} \Pi_{pre} = & \int \int \frac{1}{2} \boldsymbol{\epsilon}^T \mathbf{A} \boldsymbol{\epsilon} - \boldsymbol{\lambda}^T \left[\boldsymbol{\epsilon} - \begin{pmatrix} u_{,x} \\ v_{,y} \\ v_{,x} + u_{,y} \end{pmatrix} \right] dx dy \\ & - \int_{S_1} (\bar{N}_y v + \bar{N}_{xy} u)_{y=b} - (\bar{N}_y v + \bar{N}_{xy} u)_{y=0} dx - \int_{S_1} (\bar{N}_x u + \bar{N}_{xy} v)_{x=a} - (\bar{N}_x u + \bar{N}_{xy} v)_{x=0} dy \end{aligned} \quad (\text{A.8})$$

where, the strain vector is defined as

$$\boldsymbol{\epsilon} = \begin{pmatrix} \epsilon_{xo} & \epsilon_{yo} & \gamma_{xyo} \end{pmatrix}^T \quad (\text{A.9})$$

and the Lagrange multiplier vector $\boldsymbol{\lambda}$ is defined as

$$\boldsymbol{\lambda} = \begin{pmatrix} \Lambda_x & \Lambda_y & \Lambda_{xy} \end{pmatrix}^T \quad (\text{A.10})$$

If making the energy Π_{pre} stationary with respect to the strains, ϵ_{xo} , ϵ_{yo} and γ_{xyo} , respectively, the following conditions expressed in matrix form will be obtained,

$$\frac{\partial \Pi_{pre}}{\partial \boldsymbol{\epsilon}} = \int \int (\mathbf{A}\boldsymbol{\epsilon} - \boldsymbol{\lambda}) dx dy = \mathbf{0} \quad (\text{A.11})$$

which implies,

$$\boldsymbol{\lambda} = \mathbf{A}\boldsymbol{\epsilon} \quad (\text{A.12})$$

Moreover, notice that the in-plane force resultants are given as

$$\mathbf{n} = \begin{pmatrix} N_x \\ N_y \\ N_{xy} \end{pmatrix} = \begin{pmatrix} A_{11}\epsilon_{xo} + A_{12}\epsilon_{yo} + A_{16}\gamma_{xyo} \\ A_{12}\epsilon_{xo} + A_{22}\epsilon_{yo} + A_{26}\gamma_{xyo} \\ A_{16}\epsilon_{xo} + A_{26}\epsilon_{yo} + A_{66}\gamma_{xyo} \end{pmatrix} = \mathbf{A}\boldsymbol{\epsilon} \quad (\text{A.13})$$

where, \mathbf{n} is a vector contains the in-plane force resultants as shown in above equation.

Thus

$$\mathbf{n} = \mathbf{A}\boldsymbol{\epsilon} = \boldsymbol{\lambda} \quad (\text{A.14})$$

So the physical meanings of Lagrange multipliers applied above are actually the in-plane force resultants. Hence,

$$\boldsymbol{\epsilon} = \mathbf{A}^{-1}\boldsymbol{\lambda} = \mathbf{A}^{-1}\mathbf{n} \quad (\text{A.15})$$

Substituting the above two equations back to the total potential energy (equation A.8), the following energy functional will be obtained.

$$\begin{aligned} \Pi_{pre} = & -\frac{1}{2} \int \int \mathbf{n}^T \mathbf{A}^{-1} \mathbf{n} dx dy + \int \int \mathbf{n}^T \begin{pmatrix} u_{,x} \\ v_{,y} \\ v_{,x} + u_{,y} \end{pmatrix} dx dy \\ & - \int_{S_1} (\bar{N}_y v + \bar{N}_{xy} u)_{y=b} - (\bar{N}_y v + \bar{N}_{xy} u)_{y=0} dx - \int_{S_1} (\bar{N}_x u + \bar{N}_{xy} v)_{x=a} - (\bar{N}_x u + \bar{N}_{xy} v)_{x=0} dy \end{aligned} \quad (\text{A.16})$$

Furthermore,

$$\int \int \mathbf{n}^T \begin{pmatrix} u_{,x} \\ v_{,y} \\ v_{,x} + u_{,y} \end{pmatrix} dx dy = \int \int [N_x u_{,x} + N_y v_{,y} + N_{xy}(v_{,x} + u_{,y})] dx dy \quad (\text{A.17})$$

After integration by parts,

$$\begin{aligned} \int \int \mathbf{n}^T \begin{pmatrix} u_{,x} \\ v_{,y} \\ v_{,x} + u_{,y} \end{pmatrix} dx dy = & \oint_{C_x} (N_x u + N_{xy} v) dy - \oint_{C_y} (N_{xy} u + N_y v) dx \\ & - \int \int [(N_{x,x} + N_{xy,y})u + (N_{xy,x} + N_{y,y})v] dx dy \end{aligned} \quad (\text{A.18})$$

For rectangular plates or cylindrical shells,

$$\begin{aligned} \int \int \mathbf{n}^T \begin{pmatrix} u_{,x} \\ v_{,y} \\ v_{,x} + u_{,y} \end{pmatrix} dx dy = & \int_S (N_y v + N_{xy} u)_{y=b} - (N_y v + N_{xy} u)_{y=0} dx \\ & + \int_S (N_x u + N_{xy} v)_{x=a} - (N_x u + N_{xy} v)_{x=0} dy \\ & - \int \int [(N_{x,x} + N_{xy,y})u + (N_{xy,x} + N_{y,y})v] dx dy \end{aligned} \quad (\text{A.19})$$

Note that, on the boundary $S1$, $N_x = \bar{N}_x, N_y = \bar{N}_y, N_{xy} = \bar{N}_{xy}$; on boundary $S2$, $u = \bar{u}, v = \bar{v}$. So

$$\begin{aligned} \iint \mathbf{n}^T \begin{pmatrix} u,x \\ v,y \\ v,x + u,y \end{pmatrix} dx dy &= \int_{S1} (\bar{N}_y v + \bar{N}_{xy} u)_{y=b} - (\bar{N}_y v + \bar{N}_{xy} u)_{y=0} dx \\ &+ \int_{S1} (\bar{N}_x u + \bar{N}_{xy} v)_{x=a} - (\bar{N}_x u + \bar{N}_{xy} v)_{x=0} dy \\ &+ \int_{S2} (N_y \bar{v} + N_{xy} \bar{u})_{y=b} - (N_y \bar{v} + N_{xy} \bar{u})_{y=0} dx \\ &+ \int_{S2} (N_x \bar{u} + N_{xy} \bar{v})_{x=a} - (N_x \bar{u} + N_{xy} \bar{v})_{x=0} dy \\ &- \iint [(N_{x,x} + N_{xy,y})u + (N_{xy,x} + N_{y,y})v] dx dy \end{aligned} \quad (\text{A.20})$$

In addition, according to the in-plane equilibrium equations,

$$N_{x,x} + N_{xy,y} = 0 \quad (\text{A.21})$$

$$N_{xy,x} + N_{y,y} = 0 \quad (\text{A.22})$$

Equation A.20 can further reduce into

$$\begin{aligned} \iint \mathbf{n}^T \begin{pmatrix} u,x \\ v,y \\ v,x + u,y \end{pmatrix} dx dy &= \int_{S1} (\bar{N}_y v + \bar{N}_{xy} u)_{y=b} - (\bar{N}_y v + \bar{N}_{xy} u)_{y=0} dx \\ &+ \int_{S1} (\bar{N}_x u + \bar{N}_{xy} v)_{x=a} - (\bar{N}_x u + \bar{N}_{xy} v)_{x=0} dy \\ &+ \int_{S2} (N_y \bar{v} + N_{xy} \bar{u})_{y=b} - (N_y \bar{v} + N_{xy} \bar{u})_{y=0} dx \\ &+ \int_{S2} (N_x \bar{u} + N_{xy} \bar{v})_{x=a} - (N_x \bar{u} + N_{xy} \bar{v})_{x=0} dy \end{aligned} \quad (\text{A.23})$$

It is noted that the first two terms on the right of above equation is canceled with V_{S1} (equation A.3)

$$\begin{aligned} \iint [\mathbf{n}^T \begin{pmatrix} u,x \\ v,y \\ v,x + u,y \end{pmatrix}] dx dy + V_{S1} &= \int_{S2} (N_y \bar{v} + N_{xy} \bar{u})_{y=b} - (N_y \bar{v} + N_{xy} \bar{u})_{y=0} dx \\ &+ \int_{S2} (N_x \bar{u} + N_{xy} \bar{v})_{x=a} - (N_x \bar{u} + N_{xy} \bar{v})_{x=0} dy \end{aligned} \quad (\text{A.24})$$

Then, the total potential energy (equation A.16) becomes

$$\begin{aligned} \Pi_{pre} &= -\frac{1}{2} \iint (\mathbf{n}^T \mathbf{A}^{-1} \mathbf{n}) dx dy \\ &+ \int_{S2} (N_y \bar{v} + N_{xy} \bar{u})_{y=b} - (N_y \bar{v} + N_{xy} \bar{u})_{y=0} dx \\ &+ \int_{S2} (N_x \bar{u} + N_{xy} \bar{v})_{x=a} - (N_x \bar{u} + N_{xy} \bar{v})_{x=0} dy \end{aligned} \quad (\text{A.25})$$

which is the negative of the total complementary energy (equation 4.15).

So far the total potential energy (equation A.1) has been transformed into the negative of the total complementary energy step by step.

In addition, since the in-plane equilibrium equations (equation A.21, A.22) were introduced during the derivation, they must be the subsidiary conditions for the equation A.25. In other words, only when the in-plane equilibrium equations are hold, the total potential energy is the negative of the total complementary energy. These in-plane equilibrium equations can be simply hold by introducing the Airy stress function into the in-plane loads as

$$N_x = F_{,yy}, \quad N_y = F_{,xx}, \quad N_{xy} = -F_{,xy} \quad (\text{A.26})$$

Then the total complementary energy or potential energy can be written in terms of Airy stress function.

Bibliography

- [1] D. O. Brush and B. O. Almroth, “Buckling of bars, plates, and shells,” 1975.
- [2] J. Ashton and J. M. Whitney, *Theory of laminated plates*, vol. 4. CRC Press, 1970.
- [3] J. N. Reddy, *Mechanics of laminated composite plates and shells: theory and analysis*. CRC press, 2004.
- [4] J. M. Whitney, *Structural analysis of laminated anisotropic plates*. CRC Press, 1987.
- [5] R. M. Jones, *Buckling of bars, plates, and shells*. Bull Ridge Corporation, 2006.
- [6] C. H. Yoo and S. Lee, *Stability of structures: principles and applications*. Elsevier, 2011.
- [7] C. Kassapoglou, *Design and analysis of composite structures: with applications to aerospace structures*. John Wiley & Sons, 2013.
- [8] J.-H. Kang and A. W. Leissa, “Exact solutions for the buckling of rectangular plates having linearly varying in-plane loading on two opposite simply supported edges,” *International Journal of Solids and Structures*, vol. 42, no. 14, pp. 4220–4238, 2005.
- [9] C. Bisagni and R. Vescovini, “Analytical formulation for local buckling and post-buckling analysis of stiffened laminated panels,” *Thin-Walled Structures*, vol. 47, no. 3, pp. 318–334, 2009.
- [10] C. Bisagni and R. Vescovini, “Fast tool for buckling analysis and optimization of stiffened panels,” *Journal of Aircraft*, vol. 46, no. 6, pp. 2041–2053, 2009.
- [11] Z. Gürdal, B. F. Tatting, and C. Wu, “Variable stiffness composite panels: effects of stiffness variation on the in-plane and buckling response,” *Composites Part A: Applied Science and Manufacturing*, vol. 39, no. 5, pp. 911–922, 2008.
- [12] Y. Zhang and F. Matthews, “Initial buckling of curved panels of generally layered composite materials,” *Composite Structures*, vol. 1, no. 1, pp. 3–30, 1983.

- [13] Y. Zhang and F. Matthews, "Postbuckling behaviour of curved panels of generally layered composite materials," *Composite structures*, vol. 1, no. 2, pp. 115–135, 1983.
- [14] F. Matthews, "Large deflection behavior of simply supported laminated panels under in-plane loading," *Journal of applied mechanics*, vol. 52, p. 553, 1985.
- [15] Z. P. Bazant and L. Cedolin, *Stability of structures: elastic, inelastic, fracture and damage theories*. World Scientific, 2010.
- [16] B. Geier, H.-R. Meyer-Piening, and R. Zimmermann, "On the influence of laminate stacking on buckling of composite cylindrical shells subjected to axial compression," *Composite structures*, vol. 55, no. 4, pp. 467–474, 2002.
- [17] C. Chia and M. Prabhakara, "Postbuckling behavior of unsymmetrically layered anisotropic rectangular plates," *Journal of Applied Mechanics*, vol. 41, no. 1, pp. 155–162, 1974.
- [18] R. Vescovini and C. Bisagni, "Buckling analysis and optimization of stiffened composite flat and curved panels," *AIAA journal*, vol. 50, no. 4, pp. 904–915, 2012.
- [19] J. Ashton and M. Waddoups, "Analysis of anisotropic plates," *Journal of composite materials*, vol. 3, no. 1, pp. 148–165, 1969.
- [20] P. Qiao, F. Chen, J. Xu, and Z. Lu, "Local buckling analysis of restrained orthotropic plates under generic in-plane loading," *Journal of Engineering Mechanics*, vol. 139, no. 8, pp. 936–951, 2013.
- [21] S. T. IJsselmuiden, M. M. Abdalla, and Z. Gürdal, "Optimization of variable-stiffness panels for maximum buckling load using lamination parameters," *AIAA journal*, vol. 48, no. 1, pp. 134–143, 2010.
- [22] S. T. IJsselmuiden, M. M. Abdalla, and Z. Gürdal, "Maximising buckling loads of variable stiffness shells using lamination parameters," in *50th AIAA/ASME/ASCE/AHS/ASC Structures, Structural Dynamics, and Materials Conference 17th AIAA/ASME/AHS Adaptive Structures Conference 11th AIAA No*, 2009.
- [23] Z. Gurdal and R. Olmedo, "In-plane response of laminates with spatially varying fiber orientations-variable stiffness concept," *AIAA journal*, vol. 31, no. 4, pp. 751–758, 1993.
- [24] Z. Guerdal and R. Olmedo, "Composite laminates with spatially varying fiber orientations: variable stiffness panel concept," in *Proceedings of the AIAA/ASME/ASCE/AHS/ASC 33rd structures, structural dynamics and materials conference*, vol. 2, pp. 798–808, 1992.
- [25] J. R. Rice and R. F. Boisvert, "Solving elliptic problems using ellpack," *Springer Series in Computational Mathematics, New York: Springer, 1985*, vol. 1, 1985.
- [26] R. Olmedo and Z. Gurdal, "Buckling response of laminates with spatially varying fiber orientations," in *AIAA/ASME/ASCE/AHS/ASC 34th Structures, Structural Dynamics, and Materials Conference*, vol. 1, pp. 2261–2269, 1993.

-
- [27] Z. Wu, G. Raju, and P. M. Weaver, "Buckling of vat plates using energy methods," in *53rd AIAA/ASME/ASCE/AHS/ASC Structures, Structural Dynamics and Materials Conference 20th AIAA/ASME/AHS Adaptive Structures Conference 14th AIAA*, 2012.
- [28] Z. Wu, P. M. Weaver, G. Raju, and B. C. Kim, "Buckling analysis and optimisation of variable angle tow composite plates," *Thin-walled structures*, vol. 60, pp. 163–172, 2012.
- [29] B. H. Coburn, Z. Wu, and P. M. Weaver, "Local buckling of blade stiffened variable angle tow panels," in *55th AIAA/ASMe/ASCE/AHS/SC Structures, Structural Dynamics, and Materials Conference*, pp. 13–17, 2014.
- [30] B. H. Coburn, Z. Wu, and P. M. Weaver, "Buckling analysis of stiffened variable angle tow panels," *Composite Structures*, vol. 111, pp. 259–270, 2014.
- [31] B. H. Coburn, Z. Wu, and P. M. Weaver, "Buckling analysis and optimization of blade stiffened variable stiffness panels,"
- [32] Z. Wu, G. Raju, and P. M. Weaver, "Comparison of variational, differential quadrature, and approximate closed-form solution methods for buckling of highly flexurally anisotropic laminates," *Journal of Engineering Mechanics*, vol. 139, no. 8, pp. 1073–1083, 2012.
- [33] K. Washizu, *Variational methods in elasticity and plasticity*, vol. 3. Pergamon press Oxford, 1975.
- [34] Z. Wu, G. Raju, and P. M. Weaver, "Postbuckling analysis of variable angle tow composite plates," *International Journal of Solids and Structures*, vol. 50, no. 10, pp. 1770–1780, 2013.
- [35] K. Rhee, "Evaluation of elastic work factor for a double cantilever beam specimen," *Journal of materials science letters*, vol. 13, no. 8, pp. 613–614, 1994.
- [36] B. Budiansky and P. C. Hu, "The lagrangian multiplier method of finding upper and lower limits to critical stresses of clamped plates," 1946.
- [37] E. N. Jacobs, K. E. Ward, and R. M. Pinkerton, "The characteristics of 78 related airfoil sections from tests in the variable-density wind tunnel," 1933.

Glossary

List of Acronyms

FEM Finite element method

FEA Finite element analysis

Latin Symbols

a, b	Length and width of the panel along x and y direction, respectively[mm]
a_{ij} ($i, j = 1, 2, 6$)	Compliance of \mathbf{A}
A_{ij} ($i, j = 1, 2, 6$)	Laminate membrane stiffness[N/mm]
\mathbf{A}	Matrix of laminate membrane stiffness
\mathbf{B}	Matrix of laminate membrane-bending coupling stiffness
\mathbf{c}_{kl}	Vector of length $K \times L$
C_{kl}	Element of vector \mathbf{c}_{kl}
$C_{klk_2l_2}$	Element of matrix \mathbf{C}_a
\mathbf{C}_a	$K \times L$ by $K \times L$ matrix
\mathbf{C}_D	Matrix of dimension $P \times Q$ by $P \times Q$
\mathbf{C}_F	Matrix of dimension $P \times Q$ by $P \times Q$
\mathbf{C}_N	Matrix of dimension $P \times Q$ by $P \times Q$
\mathbf{C}_R	Matrix of dimension $P \times Q$ by $K \times L$
D_{ij} ($i, j = 1, 2, 6$)	Laminate bending stiffness[N]
\mathbf{D}	Matrix of laminate bending stiffness
\mathbf{e}	Vector of mid-plane strains for large deflection
\mathbf{e}_t	First part of \mathbf{e} relates to the in-plane displacements
\mathbf{e}_n	Second part of \mathbf{e} relates to the out-of-plane displacement
E	Number of terms used to describe the stress variation on edge $x = 0, a$ when displacements are prescribed
\mathbf{f}	Vector of Airy stress function $\mathbf{f} = (F_{,yy} \quad F_{,xx} \quad -F_{,xy})^T$
\mathbf{f}_{kl}	Vector of length $K \times L$
F	Airy stress function
F_e	Undetermined parameters of Airy stress function to describe the stress variation on edge $x = 0, a$ when displacements are prescribed
F_{kl}	Undetermined parameters of Airy stress function
F_{kl}^1	Undetermined parameters of the increment of Airy stress function
\mathbf{H}_1	Matrix of dimension $K \times L$ by $(I_1 + I_2 + J_1 + J_2)$
\mathbf{H}_2	Matrix of dimension $K \times L$ by $(I_1 + I_2 + J_1 + J_2)$
I_1, I_2, J_1, J_2	Number of Lagrange multiplier $\Lambda_{j_1}, \Lambda_{j_2}, \Lambda_{i_1}, \Lambda_{i_2}$, respectively
K, L	Number of terms used for the shape functions of Airy stress function (F) in x and y direction, respectively
K_1, L_1	Number of terms used for the shape functions of the increment of Airy stress function (F_1) in x and y direction, respectively
\mathbf{m}	Vector of moment resultants per unit width [N] $\mathbf{m} = (M_x \quad M_y \quad M_{xy})^T$
M_x, M_y, M_{xy}	Moment resultants per unit width [N]
\mathbf{n}	Vector of force resultants per unit width [N/mm] $\mathbf{n} = (N_x \quad N_y \quad N_{xy})^T$
$\bar{N}_x, \bar{N}_y, \bar{N}_{xy}$	In-plane loads: force resultants per unit width [N/mm]
$\bar{N}_x, \bar{N}_y, \bar{N}_{xy}$	Prescribed in-plane loads: force resultants per unit width [N/mm]

P, Q	Number of terms used for the shape functions of out-of-plane displacement (w) and its increment (or variation) (w_1 or δw) in x and y direction, respectively
R	Radius of cylindrical shells
t	Thickness of panels
u, v, w	Displacement along x, y, z direction [mm]
\bar{u}, \bar{v}	Prescribed displacement along x, y direction [mm]
$\delta u, \delta v, \delta w$	Variation of u, v, w
U_m	Membrane energy
U_m^c	Membrane complementary energy
U_b	Bending energy
V_{S1}	External work done by the prescribed external loads
V_{S2}	External complementary work done by the prescribed displacements
\mathbf{w}_{pq}	Vector of length $P \times Q$
W_{pq}	Undetermined parameters of the shape functions of w
W_{pq}^1	Undetermined parameters of the shape functions of w_1
X_k, Y_l	Shape functions used for Airy stress function (F) and its increment (or variation) (F_1 or δF) in x and y direction, respectively
X_p, Y_q	Shape functions used for out-of-plane displacement (w) and its increment (or variation) (w_1 or δw) in x and y direction, respectively
Y_e	Shape functions used for Airy stress function to describe the stress variation on edge $x = 0, a$ when displacements are prescribed

Greek Symbols

$\epsilon_x, \epsilon_y, \gamma_{xy}$	Strain along x, y, z direction
$\epsilon_{xo}, \epsilon_{yo}, \gamma_{xyo}$	Mid-plane strain along x, y, z direction
$\boldsymbol{\epsilon}$	Vector of mid-plane strains $\boldsymbol{\epsilon} = (\epsilon_{xo} \quad \epsilon_{yo} \quad \gamma_{xyo})^T$
$\kappa_x, \kappa_y, \kappa_{xy}$	curvatures
$\sigma_x, \sigma_y, \gamma_{xy}$	In-plane stresses [MPa]
ν	Poisson's ratio for isotropic material
Π_{pre}	Total potential energy for prebuckling analysis
Π_{pre}^c	Total complementary energy for prebuckling analysis
$\Lambda_x, \Lambda_y, \Lambda_{xy}$	Lagrange multipliers
$\boldsymbol{\lambda}$	Vector of Lagrange multipliers $\boldsymbol{\lambda} = (\Lambda_x \quad \Lambda_y \quad \Lambda_{xy})^T$
$\Lambda_{j1}, \Lambda_{j2}, \Lambda_{i1}, \Lambda_{i2}$	Lagrange multipliers
$\boldsymbol{\lambda}_{ij}$	Vector of Lagrange multipliers ($\boldsymbol{\lambda}_{ij} = (\Lambda_{j1}, \Lambda_{j2}, \Lambda_{i1}, \Lambda_{i2})^T$)
λ	Buckling factor
$\boldsymbol{\kappa}$	Vector of curvatures $\boldsymbol{\kappa} = (-w_{,xx} \quad -w_{,yy} \quad -2w_{,xy})^T$
∇	Laplace operator in two dimensions

Superscripts

- ' prime indicates derivative with respect to length coordinate (e.g. x, y)
- ¹ incremental quantity denotes the increment of a variable
(used in adjacent buckling criterion)

Subscripts

- $,i$ ($i = x, y, z$) a subscript (e.g. x, y, z) preceded by a comma indicates a partial derivative
(with respect to coordinate x, y, z)
- ₁ incremental quantity denotes the increment of a variable
(used in adjacent buckling criterion)